ADVANCING BALEEN WHALE ACOUSTIC AND HABITAT MONITORING IN THE NORTHWEST ATLANTIC

by

Hansen Dalmasse Johnson

Submitted in partial fulfillment of the requirements
for the degree of Doctor of Philosophy

at

Dalhousie University
Halifax, Nova Scotia
April 2022

To my parents

TABLE OF CONTENTS

LIST OF TABLES

LIST OF FIGURES

ABSTRACT

Baleen whales of the Northwest Atlantic live in an urbanized ocean. They attempt a slow recovery from commercial whaling amid threats from the infrastructure, pollution, and shifting environmental baseline associated with human exploitation of the natural world. Current risk mitigation strategies all rely on a comprehensive knowledge of whale distribution, which is difficult to obtain given limited resources, a vast ocean, and the cryptic nature of whale behaviour. This thesis strives to advance baleen whale monitoring with passive acoustics, habitat ecology, and new technology. Chapters 2 and 3 use several different approaches to improve the quality and interpretation of data derived from passive acoustic monitoring. Chapter 4 introduces 'WhaleMap', a tool for rapidly collating and displaying whale survey results to inform dynamic research and management activities. Chapters 5 and 6 characterize associations among baleen whale species and their oceanographic habitat to identify priority areas and times for increased monitoring and/or risk mitigation. Particular focus is paid to the North Atlantic right whale because their dire conservation status motivates much of this work, but in many cases the results apply to other baleen whale species. It is our hope that the monitoring advancements put forward by this thesis lead directly to improved conservation outcomes that help preserve these species for generations to come.

ACKNOWLEDGEMENTS

I am indebted to many colleagues whose help and support made this work possible. They are mentioned explicitly in each chapter, but include: Kimberley Davies, Delphine Durette-Morin, Meg Carr, Christoph Renkl, Keith Thompson, Kim Franklin, Valentina Ceballos, Daniel Morrison, Mark Merrimen, Todd Hart, Richard Cheel, Walter Judge, Matt Hatcher, Marcia Pearson, Gina Lonati, Moira Brown, Philip Hamilton, Amy Knowlton, Kelsey Howe, Heather Pettis, Monica Zani, Marianna Hagbloom, Megan McOsker, Pete Duley, Tim Cole, Danielle Cholewiak, Leah Crowe, Gen Davis, Richard Davis, Adam Comeau, Jude Van der Meer, Fred Whoriskey, Pam Emery, Stephanie Ratelle, Angelia Vanderlaan, Kevin Sorochan, YT Lin, Art Newhall, Julien Bonnel, Dan Zitterbart, and Phil Alatalo. I am grateful to Hilary Moors-Murphy and David Barclay for their guidance as members of my committee. I could not have asked for a better supervisory team than Chris Taggart and Mark Baumgartner. Together they struck a seemingly impossible balance of patience and drive, wisdom and ingenuity, freedom and direction, and support and challenge that somehow always delivered exactly what I needed. Finally, I owe the greatest debt of gratitude to my friends, family, and, above all, my parents for their enduring love and strength that keeps me going. Thank you.

CHAPTER 1

INTRODUCTION

1.1 Motivation

Large whales in the Northwest Atlantic live under constant threat. They are acutely subjected to risk of ship strike and entanglement in fishing gear (*Vanderlaan et al.*, 2011; *Vanderlaan and Taggart*, 2007), and chronically exposed to anthropogenic noise and other pollution from shipping- or industry-related activities (e.g., *Rolland et al.*, 2012). Critically endangered North Atlantic right whales (*Eubalaena glacialis*, hereafter 'right whales') are especially vulnerable as their migration corridors run the length of the highly urbanized eastern seaboard of the USA and Canada (e.g., *Davis et al.*, 2017), and their population of approximately 336 individuals (*Pettis et al.*, 2021) is so fragile that the loss of a single breeding female could influence the survival of the species (e.g., *Fujiwara and Caswell*, 2001; *Kraus et al.*, 2005). Other species such as fin (*Balaenoptera physalus*), humpback (*Megaptera novaeangliea*), sei (*Balaenoptera borealis*), and blue (*Balaenoptera musculus*) whales face the same threats with more poorly understood outcomes. Furthermore, large whales present both a physical and public image hazard to maritime commerce if they are injured or killed by vessels, and whale-vessel collisions are likely to increase as vessel traffic intensifies (*Pirotta et al.*, 2019). Both Atlantic Canadians and Americans demand sustainable maritime practices that minimize risk to whales without compromising safety of navigation or social, cultural, ethical, and economic priorities.

There is a large and growing body of evidence to suggest that right whales, as well as other baleen whale species, have altered their patterns of habitat use, particularly at the northern end of their distribution (e.g., *Davis et al.*, 2017; *Simard et al.*, 2019; *Davis et al.*, 2020). Right whales no longer predictably aggregate in well-described habitats like Grand

Manan Basin in the Bay of Fundy and Roseway Basin on the Scotian Shelf (e.g., *Davies et al.*, 2019), and are occurring with numbers and regularity in previously un-surveyed areas like the southern Gulf of St Lawrence (*Simard et al.*, 2019; *Crowe et al.*, 2021). This poses a significant problem to conservation efforts that have come to rely on particular habitats to both monitor the health of and mitigate risk to the population. The gravity of this issue was underscored in 2017 when 17 right whales were found dead, signalling the start of a devastating and ongoing mortality event, the magnitude of which has not been documented since these whales were actively hunted over a century ago (*Daoust et al.*, 2017; *NOAA*, 2021).

Nearly all risk mitigation and management strategies rely on knowledge of whale distribution. Traditional visual survey methods provide the critically important information used for population and health assessment, but they alone cannot cover the time and space scales required to resolve range-scale distribution patterns, particularly when these patterns appear to be changing. The dire status of right whales and other large whale species compels us to look beyond traditional tools and take up new, complimentary approaches to meet conservation goals.

1.2 Outline

This thesis addresses this need by providing novel advancements in passive acoustic monitoring (PAM), habitat ecology, and technology. Chapters 2 and 3 are dedicated to improving passive acoustics as a tool for monitoring right whales. The goal of Chapter 2 is to design an experiment that allows us to empirically measure the range over which our near real-time acoustic monitoring platforms can effectively detect calling right whales. Chapter 3 addresses concerns in the use of passive acoustics for right whale management by modeling the uncertainty in acoustically- and visually-detected whales following detection. Chapter 4 introduces a novel tool, called 'WhaleMap', designed to advance conservation outcomes by collating and disseminating survey results in near real-time. Chapters 5 and 6 focus on characterizing habitat associations between baleen whales and their ocean environments so that we may identify times and places to focus monitoring and risk mitigation efforts. Chapter 5 is a characterization of right whale habitat in the southern Gulf of St Lawrence informed by multi-year, vessel-based oceanographic sampling and visual surveys. Chapter 6 uses concurrent environmental and whale acoustic presence

data from Slocum glider deployments to evaluate how baleen whale species associate with oceanographic habitat in the Northwest Atlantic.

1.3 Note

Several chapters have been accepted for publication (Chapter 2; accepted to the Journal of the Acoustical Society of America), or have already been published (Chapter 3, *Johnson et al.* 2020a; Chapter 4, *Johnson et al.* 2021). As a result, each thesis chapter has been written as an independent manuscript. This introduces some redundancy, especially in the introductory material of each chapter, and some minor inconsistencies arising from the information available at the time a chapter was written, but is necessary to keep the content of these chapters consistent with the submitted and/or published versions.

CHAPTER 2

ACOUSTIC DETECTION RANGE OF RIGHT WHALE UPCALLS IDENTIFIED IN NEAR-REAL TIME FROM A MOORED BUOY AND A SLOCUM GLIDER

2.1 Abstract

The goal of this study was to characterize the detection range of a near real-time baleen whale detection system, the DMON/LFDCS, equipped on a Slocum glider and a moored buoy. As a reference, a hydrophone array was deployed alongside the glider and buoy at a shallow-water site southwest of Marthas Vineyard, Massachusetts, USA over a 4-week period in spring 2017. A call-by-call comparison between North Atlantic right whale upcalls localized with the array (n = 541) and those detected by the glider or buoy was used to estimate the detection function for each DMON/LFDCS platform. The probability of detection was influenced by range, ambient noise level, platform depth, detection process, review protocol, and calling rate. The conservative analysis of near real-time pitch tracks suggested that, under typical conditions, a 0.33 probability of detection of a single call occurred at 6.2 km for the buoy and $8.6 - 13.4$ km for the glider (depending on glider depth), while a 0.10 probability of detection of a single call occurred at 14.4 km for the buoy and $22.6 - 27.5$ km for the glider. Probability of detection is predicted to increase substantially at all ranges if more than one call is available for detection.

2.2 Introduction

Mitigation of anthropogenic impacts on North Atlantic right whales (*Eubalaena glacialis*; hereafter 'right whales') and other at-risk species is critical for effective conservation but challenging given limited survey resources and the cryptic nature of whale behavior. Nearly all risk mitigation and management strategies rely on knowledge of whale distribution collected by monitoring surveys (e.g. *Vanderlaan et al.*, 2011). Conventional visual survey methods provide important information for population and health assessment, but they alone cannot cover the time and space scales required to resolve range-wide distribution patterns. Passive acoustic monitoring (PAM) can complement visual survey methods by offering the ability to autonomously monitor remote areas persistently for months to years at a time (e.g., *Davis et al.*, 2017).

Numerous efforts have demonstrated the efficacy of PAM for right whales. *Clark et al.* (2010) conducted an extensive comparison between aerial and acoustic surveys for right whales in Cape Cod Bay and demonstrated that visual surveys detected right whales on two-thirds of the days for which they were detected acoustically. The same authors concluded that PAM is more reliable than visual methods for determining right whale presence over daily timescales in Cape Cod Bay and strongly recommended that PAM be used to inform management decisions. In a similar comparison on the southwestern Scotian Shelf, *DuretteMorin et al.* (2019) reached similar conclusions and highlighted the capacity of PAM to extend monitoring beyond visual surveys constrained by limited resources and poor sighting conditions. *Davis et al.* (2017) collated and analyzed an acoustic dataset spanning 35,600 days over 2004-2014 on 324 recorders located in the western North Atlantic from the Caribbean to the Davis Strait and Iceland. Their analyses documented shifts in the range-wide distribution pattern of right whales since 2010 as well as persistent wintertime presence in most regions; observations that would not have been possible if reliant on sporadic visual survey effort expended over the last decade.

Archival PAM data are rich in information but typically not available on timescales required to inform risk-mitigation strategies and dynamic management of industrial activities that affect whales. The Woods Hole Oceanographic Institution (WHOI) developed a PAM system comprised of the low-power digital acoustic monitoring instrument (DMON; *Johnson and Hurst*, 2007) and an on-board detection algorithm (low-frequency detection

and classification system; LFDCS; *Baumgartner and Mussoline*, 2011) that detects, classifies and reports the sounds of baleen whales (right, fin, sei, blue, and humpback) in near real-time from autonomous platforms (*Baumgartner et al.*, 2013, 2019, 2020). The LFDCS algorithm produces spectrograms of the audio data, removes spurious broadband noise and continuous tonal noise and then uses a contour-following algorithm to create pitch tracks of tonal sounds from the spectrogram. Each pitch track is classified by comparing attributes of the pitch track to a library of call types using quadratic discriminate function analysis. The DMON/LFDCS then sends a subset of the pitch tracks and classifications to a land station via Iridium satellite every 2 hours where they are divided into 15-minute analysis (tally) periods that are manually reviewed by a trained analyst for the acoustic presence of several species, including right whales (*Baumgartner et al.*, 2013, 2019, 2020)

The DMON/LFDCS is fully operational on Slocum gliders (*Baumgartner et al.*, 2013, 2020) and moored buoys (*Baumgartner et al.*, 2019). These platforms are particularly useful for management applications as they can monitor persistently for days to years at a time, regardless of weather conditions, at no risk to human operators, and at a relatively low cost compared to conventional visual surveys. Since 2013, the DMON/LFDCS system has been deployed on at least 50 Slocum glider and 10 moored buoy missions in the Northwest Atlantic, amassing over 4500 days at sea, and recording over 1,500 validated right whale detections. All of these data are made available in near real-time in a variety of ways, including email and text messages, websites (robots4whales.whoi.edu, whalemap.org, whalesafe.com) and a mobile app (Whale Alert). The system has demonstrated its effectiveness in several monitoring initiatives with the National Oceanic and Atmospheric Administration (NOAA) Northeast Fisheries Science Center (NEFSC), the US Navy, US Coast Guard, Fisheries and Oceans Canada (DFO), Transport Canada (TC), and the Department of National Defense Canada (DND).

The LFDCS detector and validation protocol have been extensively used and quantitatively evaluated for right whales. *Davis et al.* (2017) used the LFDCS for their analysis of archival recordings, and *Baumgartner et al.* (2019, 2020) recently evaluated the accuracy of the LFDCS on the DMON for near real-time detections from moored buoys and Slocum gliders. *Baumgartner et al.* (2019) found that the false positive rate for moored buoys was 0%, meaning that right whales were never detected in near real-time when they were not acoustically present, and that the system missed right whale occurrence 27% of the time on

daily time scales. Using the same near real-time review protocol, *Baumgartner et al.* (2020) found a 0% false positive rate and an 18% missed occurrence rate for Slocum gliders on daily time scales. The near real-time review protocol was designed to be conservative in recognition of the high operational costs of a false detection, but it can be adjusted depending on the application (*Baumgartner et al.*, 2019).

As with visual surveys, PAM detection performance depends on a variety of species-, site-, and platform-specific factors. Sound source level, background noise, propagation conditions, receiver characteristics and detection processes all influence the probability of detecting a call. A challenge when using detection information from many PAM systems (including the DMON/LFDCS for science, conservation, and mitigation applications) is the uncertainty in the relationship between the probability of detecting a whale call and the range to a calling animal, which can lead to misinterpretation of PAM results (e.g., *Helble et al.*, 2013a). The platforms on which the DMON/LFDCS has been integrated currently relay only the position of the platform when a sound is detected, not the position of the sound source. Determining whether positional uncertainty is tolerable for a particular application depends on the acoustic detection range for a species of concern; for short detection ranges (e.g., hundreds of meters), the position of the platform may be an acceptable proxy for the position of the animal, but for large detection ranges (e.g., tens of kilometers), lack of location specificity may limit mitigation options over short response time scales (see Chapter 3).

The acoustic detection range of a PAM system is best described by a detection function, which refers to the continuous relationship between the probability of detection and the horizontal distance between a sound source and the acoustic receiver. Estimating the site- and species-specific detection function is necessary to properly interpret and compare PAM results (*Helble et al.*, 2013a) and is a prerequisite of acoustic density estimation using distance sampling methods (*Buckland et al.*, 2004). A detection function can be estimated empirically using measured distances to both detected and undetected calls (as in this study), statistically by fitting a function to the distribution of distances to detected calls (*Marques et al.*, 2011; *Harris et al.*, 2013), or computationally based on simulations of some or all of the call production, propagation, and detection processes (*Ksel et al.*, 2011; *Helble et al.*, 2013b; *Harris et al.*, 2018). Each method has distinct advantages and disadvantages (*Marques et al.*, 2013), but if applied correctly with valid assumptions they

can provide reliable estimates of the detection function.

The empirical approach involves measuring distances to both detected and undetected calls, then estimating the detection function based on the proportion of calls detected at each range using logistic regression (*Buckland et al.*, 2006, this study) or a generalized additive model (GAM; e.g., *Marques et al.*, 2009). This approach is desirable because it requires relatively few assumptions, but it is often impeded by the challenge of measuring the distances to undetected calls. Previous studies have overcome this difficulty using a variety of methods including deploying animal-borne acoustic tags (*Marques et al.*, 2009), combining visual and acoustic observations (*Kyhn et al.*, 2012), or conducting playback experiments (*Nuuttila et al.*, 2018). A common approach for visual surveys is to have observers with high-power binoculars set up trials for observers that are using the naked eye (*Buckland and Turnock*, 1992). Here we employ an analogous study design by using a multi-channel hydrophone array to set up trials for single sensor DMON/LFDCS platforms with the goal of assessing the range-dependent accuracy of the DMON/LFDCS for detecting right whale upcalls using a mobile (glider) and a fixed (buoy) platform.

2.3 Methods

2.3.1 Site description

From 28 Feb to 24 Mar 2017, we deployed horizontal and vertical line arrays of hydrophones forming an L-shaped array (hereafter 'array' unless otherwise specified) as well as a DMON/LFDCS Slocum glider adjacent to an extant DMON/LFDCS buoy at a nominal position of 41°8.8' N, 70°56.7' W, ∼15 km southwest of Nomans Land, a small island southwest of Martha's Vineyard, Massachusetts, USA. The water depth was ∼30 m at the buoy. The bathymetry (from the ETOPO1 Global Relief Model; *Amante and Eakins*, 2009) is relatively flat and featureless to a range of ∼15 km with the notable exception of a steep shoal near Nomans Land beginning ∼8 km northeast of the deployment site (Figure 2.1A). The glider held station within +/- 2 km of the array for the first 2-weeks of the study period before making longer (up to 10 km), roughly circular forays along a predefined course away from the array for the remainder of the mission (Figure 2.1B). The array was positioned within ∼150 m of the DMON/LFDCS buoy, with horizontal and vertical components separated by ∼120 m (Figure 2.1C). The water column was uniformly mixed for the duration of the study. Sea state during the study period was assessed using

hourly observations of significant wave height recorded at the Block Island meteorological buoy (Station 44097) ∼10 km SW of the study site (data available from NOAA National Data Buoy Center).

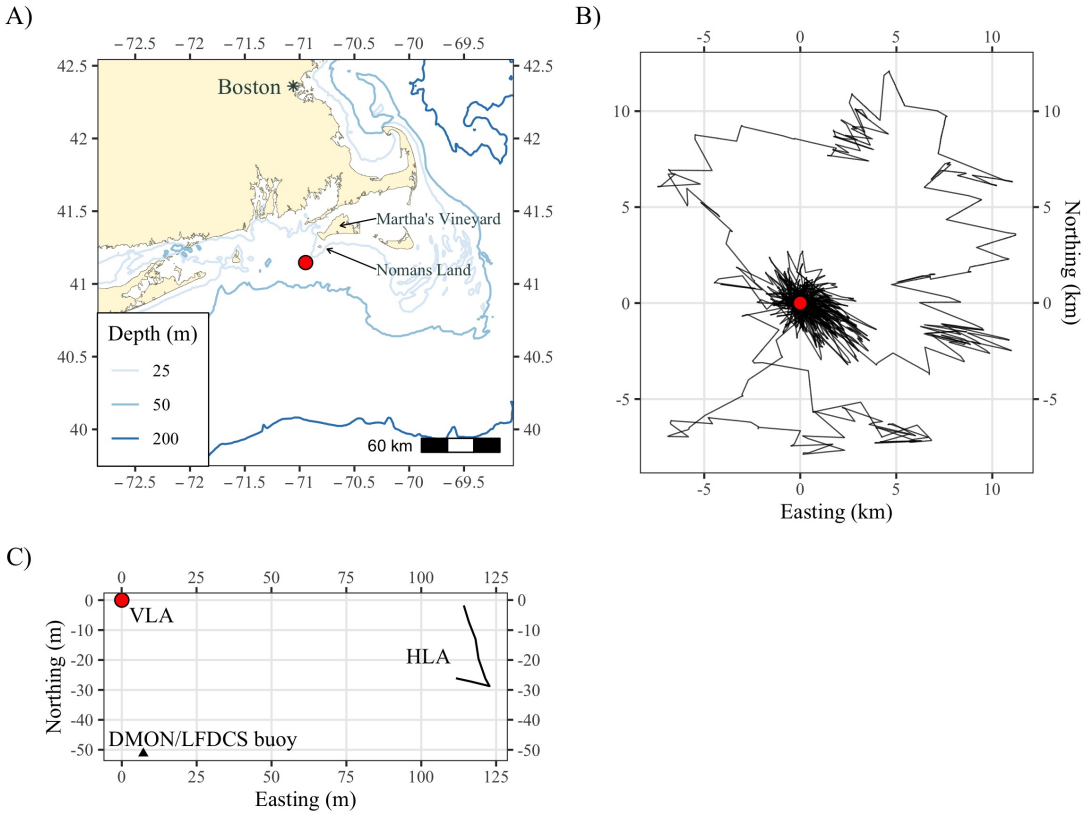

Figure 2.1: The position of the vertical line array (VLA; red circle) at A) the study site in ∼30 m water depth 15 km southwest of Nomans Land, MA, USA, B) relative to the trajectory of the glider (black line) from 28 Feb through 24 Mar, and C) relative to the positions of the horizontal line array (HLA) and DMON/LFDCS buoy.

The study site was chosen because the DMON/LFDCS buoy located there was originally deployed to monitor right whale presence in near real-time close to several US Coast Guard gunnery ranges. This area is also of particular interest because it is targeted for wind energy development in the near future. We chose to deploy the glider and array in the early spring based on historical right whale presence in the region at that time of year (*Davis et al.*, 2017).

2.3.2 System specifications

The glider and buoy were each equipped with DMON/LFDCS real-time PAM systems. In addition to generating pitch tracks in real-time, the glider DMON/LFDCS recorded audio at 2 kHz continuously while the buoy DMON/LFDCS recorded audio at 2 kHz on a 50% duty cycle (0.5 h on, 0.5 h off) due to memory constraints imposed by the year-long deployment. The audio recorded while the glider was at the surface, approximately 12% of the deployment, was contaminated by platform noise and not included in the analysis. Each system generated and classified pitch tracks of tonal signals over the full 2 kHz bandwidth and transmitted them back to shore every 2 hours. Pitch tracking was continuous on the buoy but was suspended while the glider was at the surface. The DMON hydrophone system had a sensitivity of -203 dB re 1 V μPa^{-1}, gain of 33.2 dB, zero-to-peak voltage of 1.5V, and flat frequency response between approximately 50 and 7500 Hz. Additional details on the specifications of the PAM system on the glider and buoy are available in *Baumgartner et al.* (2013, 2020) and *Baumgartner et al.* (2019), respectively.

The vertical component of the array (referred to as the vertical line array or VLA) consisted of a Several Hydrophone Receiving Unit (SHRU), 4 hydrophones, multiple environmental sensors, and a number of additional mooring components. The SHRU was suspended several meters above the anchor and acoustic release system and sampled the hydrophones continuously at a rate of 9765.625 Hz for the full deployment period. The hydrophone sensitivity was -170 dB re 1 V μPa^{-1} and recorder gain was 26 dB. The hydrophones and environmental sensors were secured to a 15 m wire rope that extended from the top of the SHRU to a steel sphere suspended $\sim$8 m below the surface. Hydrophones were positioned at approximately 27.4, 23, 18, and 13.4 m depth (nominal spacing of 5 m). The environmental sensors included two temperature loggers and a temperature-pressure logger positioned at intervals along the extent of the array to measure the temperature profile, depth, and array tilt at 0.5 Hz throughout the deployment. All environmental sensors operated without any detectable acoustic signature. The horizontal component of the array (referred to as the horizontal line array or HLA) was comprised of 8 hydrophones positioned at 7.5 m intervals along a 60 m cable coated with hairy fairing. The hydrophone sensitivity was -173 dB re 1 V μPa^{-1} and recorder gain was 23 dB. The hydrophones were sampled continuously at 4 kHz using a multichannel recorder built by Webb Research Corporation. The HLA also had a single temperature-pressure instrument

to record bottom water properties for the full deployment. Additional details on array specifications and configuration are provided in *Johnson et al.* (2020b).

2.3.3 Call detection and localization

2.3.3.1 Call detection using array

Right whale upcalls (hereafter 'upcalls') were chosen as the focal call for this analysis because they are used by the LFDCS to determine right whale presence and were amenable to localization (see Section 2.3.3.4). Upcalls are frequency modulated upsweeps from approximately 100 to 200 Hz with a duration of ∼0.75 s (see *Parks et al.* 2009 for a detailed description and discussion of upcall acoustic parameters). The full 12-channel acoustic record from the array was decimated to 2 kHz, displayed as spectrograms and visually/aurally reviewed for upcalls by an experienced analyst (HDJ) using Raven Pro 2.0 (*Bioacoustics Research Program and Program*, 2014) and consistent spectrogram parameters (512 sample DFT, 50% overlap, Hann window) which yielded a time resolution of 6.25 ms and a frequency resolution of 3.9 Hz. Only upcalls that were present on one or more channels and could be confidently scored as "detected" were included in the analysis. We assumed that the performance advantage of the array gained by the simultaneous review of multiple channels located at different depths allowed it to serve as a suitable reference to determine the probability of detection and the detection range of the DMON/LFDCS single-hydrophone platforms.

2.3.3.2 Call detection using near real-time pitch track data

Pitch tracks and automated detector output for the buoy and glider were displayed chronologically using custom-written software designed to mimic the interface used to validate near real-time detection results on the DMON/LFDCS website (robots4whales.whoi.edu). The full pitch track datasets were visually reviewed independently (i.e., without access to the archival audio data or any other detection or localization results) by the same experienced analyst performing call detection in the array data (HDJ) who was also well-versed in the review of pitch track data. Pitch tracks of upcalls were scored as "detected" or "possibly detected" depending on the confidence of the analyst following a similar protocol as described by *Baumgartner et al.* (2019)(also available at `https://dcs.whoi.edu/#procotol`). In brief, upcalls scored as "detected" convincingly adhered to the general time/frequency characteristics of upcalls (see above) and

were isolated from competing noise processes, while those scored as "possibly detected" only partially satisfied these criteria. Classification by the LFDCS was not required for a score of "detected" or "possibly detected".

2.3.3.3 Call detection using archival audio data

The complete archival audio records from the glider and buoy were displayed as spectrograms and visually/aurally reviewed chronologically for upcalls by the experienced analyst (HDJ) also using Raven Pro 2.0. The spectrogram parameters were the same as those used for the analysis of the array audio (512 sample DFT, 50% overlap, Hann window). Upcalls were given a score of "detected" or "possibly detected" depending on the confidence of the analyst. As with the pitch track analysis, the analyses of the archival audio from the glider and buoy were done independently without access to detection or localization results from any other platform.

2.3.3.4 Call localization

A normal mode back-propagation method (*Lin et al.*, 2012) using the array data was utilized to estimate range and bearing to each detected call. The method allows localization of low-frequency signals from a single array station, as opposed to the distributed arrays required for conventional arrival time difference methods (*Cato*, 1998). The technique exploits the modal dispersion of a shallow water waveguide that is well-represented by normal mode theory (*Frisk*, 1994). The vertical component of the array can be used to spatially filter modal arrivals, the arrival time differences between which can be used to make inferences about signal propagation (Figure 2.2). The general steps of the localization workflow were to (1) isolate an upcall in time and frequency space using spectrograms of the array data (see Section 2.3.3.1), (2) use a normal mode model (KRAKEN; *Porter*, 1992) and pseudo-inverse mode filtering to isolate the modal arrivals of the call (Figure 2.2), (3) use the estimated group velocities of each modal arrival to beamform to determine the arrival bearing of the call, (4) use the same mode model to estimate mode structures along the arrival path, and (5) back-propagate the received signal along the arrival path until the back-propagated modes converged (Figure 2.3). The range with the best convergence was used as the estimated range to the call. With this estimated bearing and range, the position of the calling whale was calculated. For more details on the localization methods, see *Lin et al.* (2012), and for an application to sei whale call localization, see *Newhall et al.* (2012).

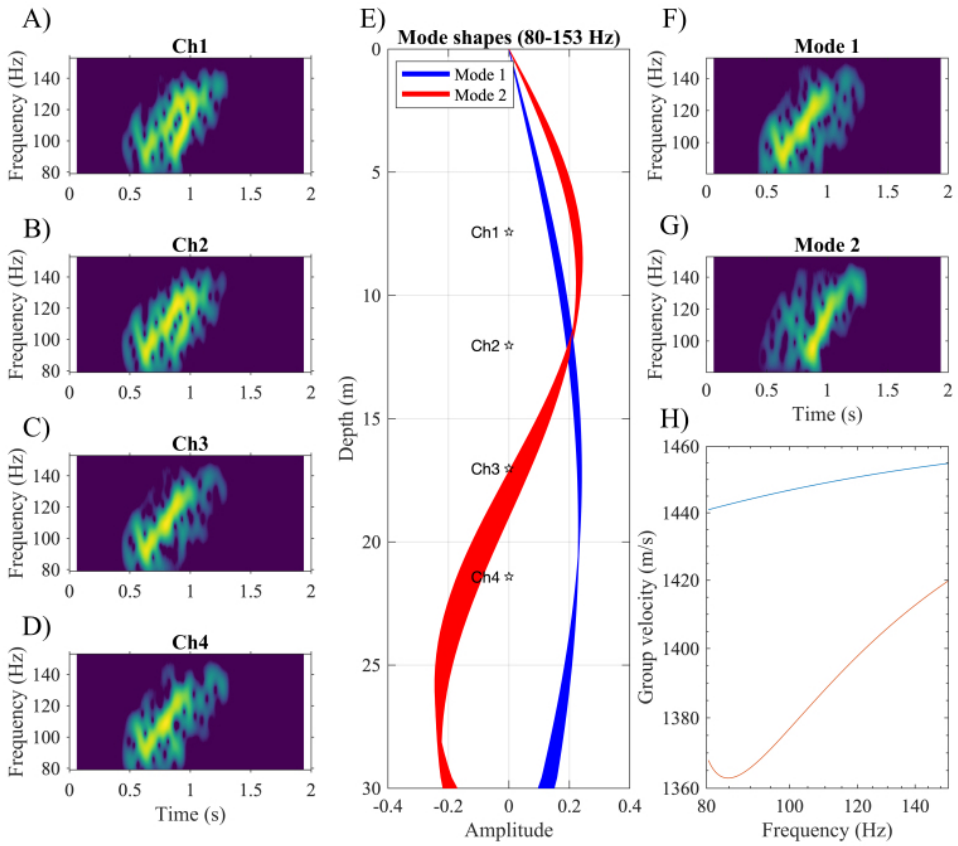

Figure 2.2: Overview of the mode filtering procedure. Panels A through D show spectrograms of a right whale upcall received on each channel of the vertical line array. Panel E shows the theoretical shapes of mode 1 (blue) and mode 2 (red) at 146 discrete frequencies within the 80-153 Hz band. These were generated using the KRAKEN normal mode model parameterized using site-specific conditions at the time of the right whale upcall. The labeled stars indicate the depth of each channel of the array. The same model produced the group velocity estimates for each mode shown in panel H. Panels F and G show spectrograms of mode 1 and mode 2, respectively, after application of the pseudo-inverse mode filter.

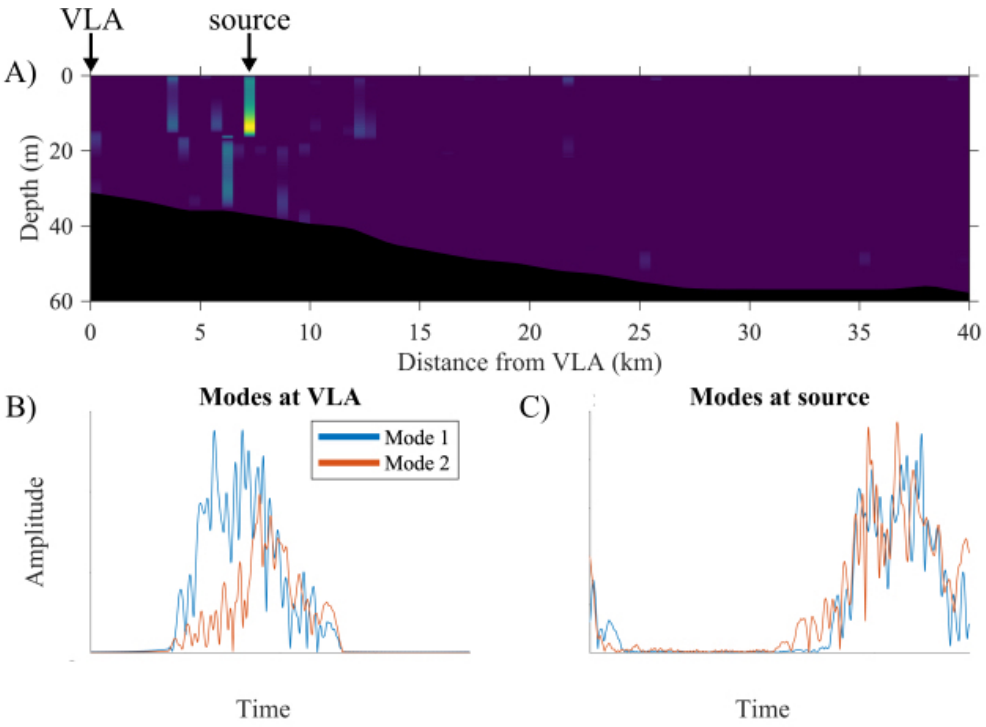

Figure 2.3: Overview of the backpropagation and ranging procedure. Panel A shows a normalized probability map of the backpropagation results with an arrow indicating the most likely range to the calling whale. Panel B shows the timing and amplitude of mode 1 (blue) and mode 2 (red) as received at the vertical line array (VLA), and panel C shows the same modes at the source after backpropagation.

The uncertainty in the range estimates was qualitatively assessed from the produced ambiguity surfaces (e.g., Figure 2.3A) and was estimated to be $\sim$1 km. The normal mode back-propagation method for localizing long distant sound sources requires the excitation of two or more propagating modes. The cut-off frequency for propagating mode 2 at the study site ($\sim$30 m water depth) was approximately 80 Hz, which prevented localization of any distant calls with substantial energy at lower frequencies. The cut-off frequency for propagating mode 3 was approximately 300 Hz. Thus, mode 3 was not reliably present in all distant upcalls and therefore not used for localization.

During the recovery of the horizontal component of the array (the HLA), it was immediately evident that it had moved from its initial deployment position. There were several storm events (2 and 15 Mar), characterized by high ambient noise levels and wave heights (Figures 2.4A, 2.4B), during which the HLA may have moved (*Johnson et al.*, 2020b). Precise estimates of the location of each HLA element were critical to our localization methodology, as errors in HLA element location prevent accurate beamforming for call bearing estimation. To correct for storm-induced movement, the HLA elements were re-localized several times using known vessel noise emitted from the WHOI coastal research vessel Tioga during cruises in the area (after *Morley et al.* 2009; details in *Johnson et al.* 2020b). These analyses provided evidence that several of the array elements moved negligible distances ($<$ 2 m) in the storm event on 2 Mar, and substantial distances (up to $\sim$15 m) in the storm event on 15 Mar. We did not correct for movement during the first storm. For the second storm on 15 Mar, we assumed that the array movement occurred at the beginning of the day, such that bearings to calls localized from 15 through 23 Mar (n = 368) were computed using the post-storm array position (Figure 2.4C). Since we were able to update the array element locations to account for storm-induced movement, the HLA beamforming results were considered reliable throughout the deployment.

2.3.4 Signal and noise level estimation

Acoustic data were calibrated using technical specifications of the recording systems as described by *Merchant et al.* (2015). Signal level, noise level and signal-to-noise ratio (SNR) were estimated for each call on the glider and buoy. The signal level was defined as the median power spectral density (PSD; dB re 1 μPa^2 Hz^{-1}) within the time-frequency "bounding box" of the call assigned during manual review of the audio data. The noise level was determined by calculating the median PSD within the same frequency and

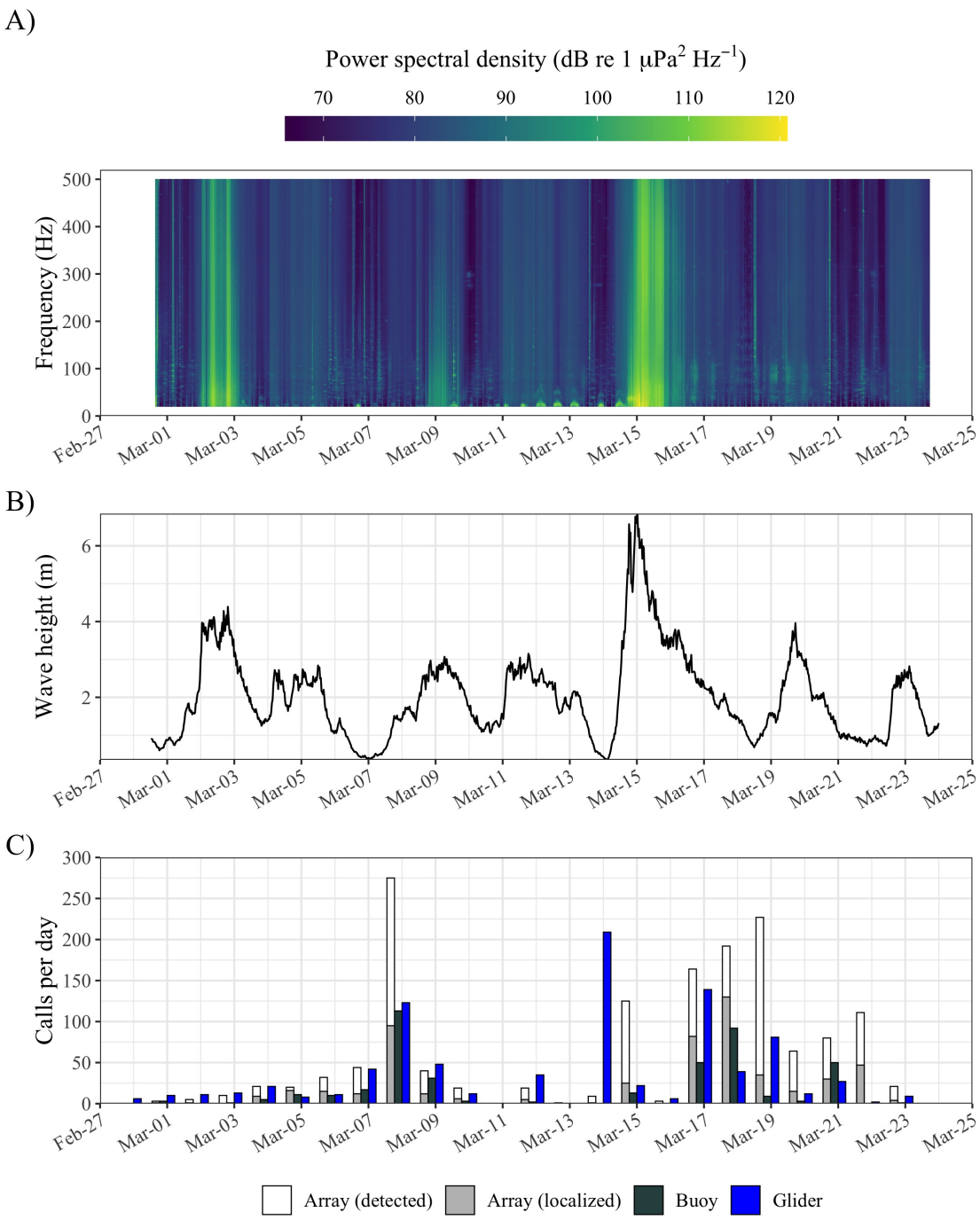

Figure 2.4: A) Power spectral density (dB re 1 μPa^2 Hz^{-1}) of channel 1 of the horizontal line array computed from 1-s time segments averaged to 1-hr resolution via the Welch method. B) Hourly observations of significant wave height from the Block Island meteorological buoy $\sim$10 km SW of the study site. C) Daily counts (calls per day) of right whale upcalls detected in the array audio (white bars; n = 1485), the buoy pitch tracks (black bars; n = 414), and the glider pitch tracks (blue bars; n = 886), as well as numbers of calls that were successfully localized (grey bars; n = 541).

duration of the call at each timestep within a 30 s audio snippet centered on each call, and then selecting the lowest median PSD of this 30-second period. This was done to avoid including transient impulsive signals in the noise level estimate. The median PSD for both the signal and noise levels was calculated by computing a spectrogram (2000 sample DFT, 50% overlap, Hann window), collating all the time-frequency cells within the bounding box, and extracting the median from the distribution. The SNR (in dB) was defined as the difference between the signal level and noise level. Signal levels that were contaminated by transient impulsive sounds were rejected and not used to calculate SNR.

2.3.5 Platform detection probability

The array was used as the reference for comparison between the DMON/LFDCS single hydrophone platforms. For each call detected and localized on the array, a score of zero was assigned if the call was not detected and one if the call was detected in the pitch track data generated by the DMON/LFDCS on the buoy. The same scoring protocol was applied to the DMON/LFDCS on the glider. This scoring protocol was used for both the pitch tracks that were available in near real-time and the archival audio that was available after platform recovery. Two separate analyses were conducted for the pitch track data to inform how the review protocol affects the probability of detection. These protocols differed in their treatment of calls scored as "possibly detected". The first used a conservative protocol in which the "possibly detected" calls were treated as if they were scored as "not detected". This protocol was designed to minimize false detections at the expense of increased missed detections. It has been extensively employed on deployments in the NW Atlantic (*Baumgartner et al.*, 2019) and is therefore the primary focus of this study. The second was a precautionary protocol in which the "possibly detected" pitch tracks were treated as if they were "detected". This protocol was designed to minimize missed detections at the expense of increased false detections. The archival audio data were only scored using the conservative protocol; there were too few calls scored as "possibly detected" in the review of the archival audio data (n = 5 for the buoy; n = 3 for the glider) to justify a protocol comparison.

The detection probability of the DMON/LFDCS single hydrophone platforms, $P_s(R)$, at range R was defined as follows:

$$P_s(R) = N_s(R)/N_a(R) \tag{2.1}$$

where $N_s(R)$ is the number of localized calls detected by the single-hydrophone platform (i.e., the buoy or the glider) at range R and $N_a(R)$ is the total number of localized calls at range R. Critically, the detection probability of the DMON/LFDCS platforms was evaluated using only calls that were first detected and localized by the array. This approach assumes that each system is analyzed independently and that the single-hydrophone platforms are not used in localization, both of which are valid here. It also assumes that the detectability of localized calls is representative of the detectability of all calls. This assumption is likely violated. Localization typically requires higher SNR than detection (e.g., *Thode et al.*, 2012), which appears to also be the case in the present study (Figure A.9). Consequently, the results presented here represent an estimate of the upper bound of the detection function of each single hydrophone system in this environment. The true detection function will likely be reduced depending on the underlying source level and depth distributions of the calls.

Detection functions for each DMON/LFDCS platform were quantified using logistic regression analysis. The series of detected/not-detected scores was used as the dependent variable. Candidate models were constructed using various combinations of detection range, noise level, and glider depth as independent variables. The glider depth term was used in the glider analysis only and was expressed in a parabolic form based on the observed relationship between glider depth and proportion of calls detected (Figure A.4). The influence of autocorrelation in detected calls was deemed minimal based on a preliminary analysis using generalized estimating equations with a first order autoregressive covariance structure implemented with the geepack package in R (*Hjsgaard et al.*, 2006). SNR was not used as a model covariate because it was correlated with both range and noise level. The most parsimonious model was selected using Akaike Information Criterion (AIC). Wald's Tests were used to evaluate the contribution of each independent variable to the overall model. Drop-in-deviance tests were used to compare among models. Separate logistic regressions were conducted for the buoy and the glider using scores from (1) pitch tracks scored using the conservative protocol (2) pitch tracks scored using the precautionary protocol, and (3) archived audio (i.e., a total of 6 logistic regressions were conducted). The fitted logistic regressions were used to estimate the probability of detecting a localized call at a given range, noise level, and glider depth, and also used to compute the effective detection radius (EDR) as described by *Buckland et al.* (2004). For all undetected calls,

we also examined the buoy and glider audio and pitch track records to determine why they were not detected by the analyst and DMON/LFDCS, respectively.

All analyses were conducted using MATLAB (The Mathworks Inc.) and R (*R Core Team*, 2019) programming languages. Analyses in R were conducted using the oce (*Kelley and Richards*, 2020), shiny (*Chang et al.*, 2020), and tidyverse (*Wickham et al.*, 2019) packages, and visualizations in R were created using the ggplot2 package (*Wickham*, 2016).

2.4 Results

2.4.1 Call detection and localization

A total of 1485 right whale upcalls were detected by the array between 28 Feb and 24 Mar. The DMON/LFDCS on the glider and buoy pitch tracked (i.e., detected) 886 and 414 right whale upcalls, respectively, during the same period. Calls occurred throughout the monitoring period but were especially abundant on 08 March and from 17 through 19 March (Figure 2.4C). Of the calls detected on the array, 36% (541 of 1485) could be confidently localized such that the back-propagated modes converged at a single range. There were several calls with potential broad-side bearing ambiguity, but range estimates using either bearing were consistent, likely owing to the relatively uniform bathymetry at the site, so these calls were retained in the analysis. The spatial distribution of localized calls was not uniform; most calls originated from the area south of the DMON/LFDCS buoy and the array (Figure 2.5). The distances to localized calls from each platform ranged from 0.4 to 30.1 km on the glider (median = 5.3 km), and from 0.3 to 29.7 km on the buoy (median = 6.2 km). Noise levels associated with calls ranged from 83.9 to 108 dB re 1 μPa^2 Hz^{-1} (median = 99.4 dB re 1 μPa^2 Hz^{-1}) on the glider and from 85.2 to 110 dB re 1 μPa^2 Hz^{-1} on the buoy (median = 98.9 dB re 1 μPa^2 Hz^{-1}). The depth of the glider at the time of call reception ranged from 0.62 to 32.0 m with a median of 13.6 m (Figure 2.6).

2.4.2 Platform detection probability

For the buoy, the proportion of localized calls detected using pitch tracks and the conservative protocol generally decreased with range (Figure 2.6A); 55.0% of localized calls within 5 km (111/202) were detected while 21.1% of localized calls between 15 and 40 km (4/19) were detected. The proportion of localized calls detected also decreased with noise (Figure 2.6C); 46.0% of localized calls received in noise levels below 100 dB re

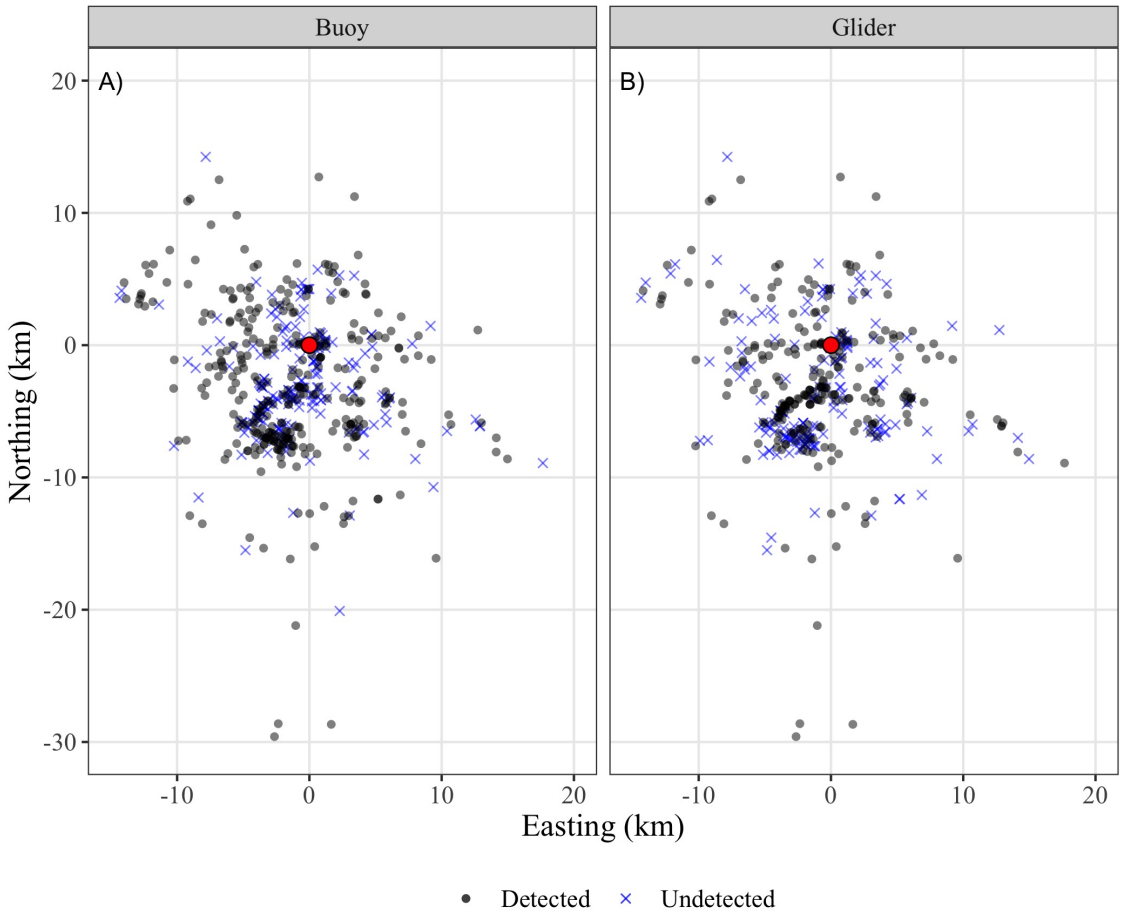

Figure 2.5: The spatial distribution of localized right whale upcalls that were either detected (grey circles) or not detected (blue crosses) by the buoy (panel A; n = 541) or the glider (panel B; n = 426) in the near real-time pitch track record using a conservative protocol. The red circle at the origin indicates the location of the array. Analogous results using a precautionary protocol or archival audio are available in Appendix A.

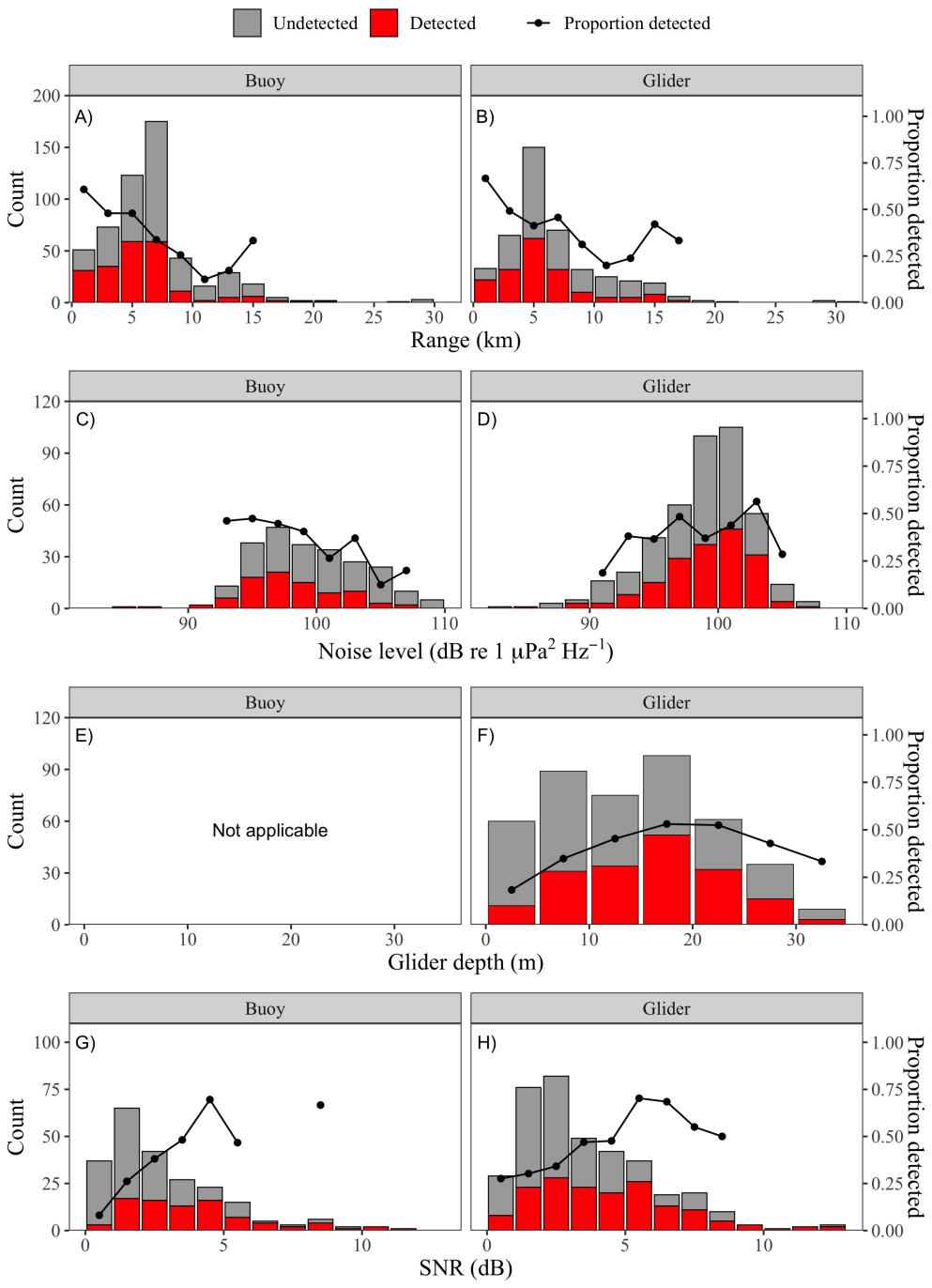

Figure 2.6: Distribution of ranges (A and B), noise levels (C and D, glider depths (E and F) and signal-to-noise ratios (SNR; G and H) from the buoy (left column) and glider (right column) of right whale upcalls localized by the array (n = 541 buoy, n = 426 glider) and detected via near real-time pitch track analysis using the conservative protocol. Total number of localized calls are shown in grey and localized calls detected in near real-time are shown in red in each bin. The black line shows the proportion of localized calls detected in bins with more than 5 calls. Analogous results using the precautionary protocol or archival audio are available in Appendix A.

1 μPa^2 Hz^{-1} (64/139) were detected, while 24.0% of localized calls received in louder noise conditions (24/100) were detected. A SNR of more than 3 dB was required to detect at least 50% of localized calls (Figure 2.6G). Calls were missed for a variety of reasons: of the 541 localized calls, 46.6% were missed due to absent or poor pitch tracks, 4.6% were missed due to interfering biological sounds (i.e., humpback whale song), 5.7% were missed due to interfering non-biological sounds (e.g., platform noise, ship noise), and 3.9% were missed due to analyst error in scoring the pitch tracks (Table 2.1; Figure 2.7A).

Table 2.1: Results from manual scoring of glider and buoy pitch track records of calls localized by the array using a conservative protocol (total number of calls = 541). Here n refers to the number of calls, while % is the percentage of total localized calls available for detection (i.e., does not consider excluded calls).

Score	Definition	Glider		Buoy	
		n	%	*n*	%
Absent	Calls were not pitch tracked at all because of low amplitude	72	16.9	102	18.9
Poor	Calls were not pitch tracked accurately/completely because of low amplitude or poor shape	84	19.7	150	27.7
Song	Uncertainty due to interfering species calls	41	9.6	25	4.6
Noise	Calls were not pitch tracked accurately/completely because of interfering sound	48	11.2	31	5.7
Missed	Human error (analyst chose wrong score erroneously)	4	0.9	21	3.9
Detected	Calls were pitch tracked and scored as detected by analyst	178	41.7	212	39.2
Exclude	Calls were not available for pitch tracking because the platform was not monitoring	114	N/A	0	N/A

The logistic regressions for the buoy were conducted using the 239 localized calls for which archival audio were available and noise levels could be calculated. The most parsimonious logistic regression model and subsequent significance testing provided evidence that the probability of detecting localized calls was negatively related to both range and noise level for all analyses (Table 2.2). In average noise conditions (100 dB re 1 μPa^2 Hz^{-1}), the fitted regression suggested that a probability of detection of 0.5 (95% CI: 0.385-0.613) occurred at 2.3 km and the effective detection radius was 8.3 km (Figure 2.8;

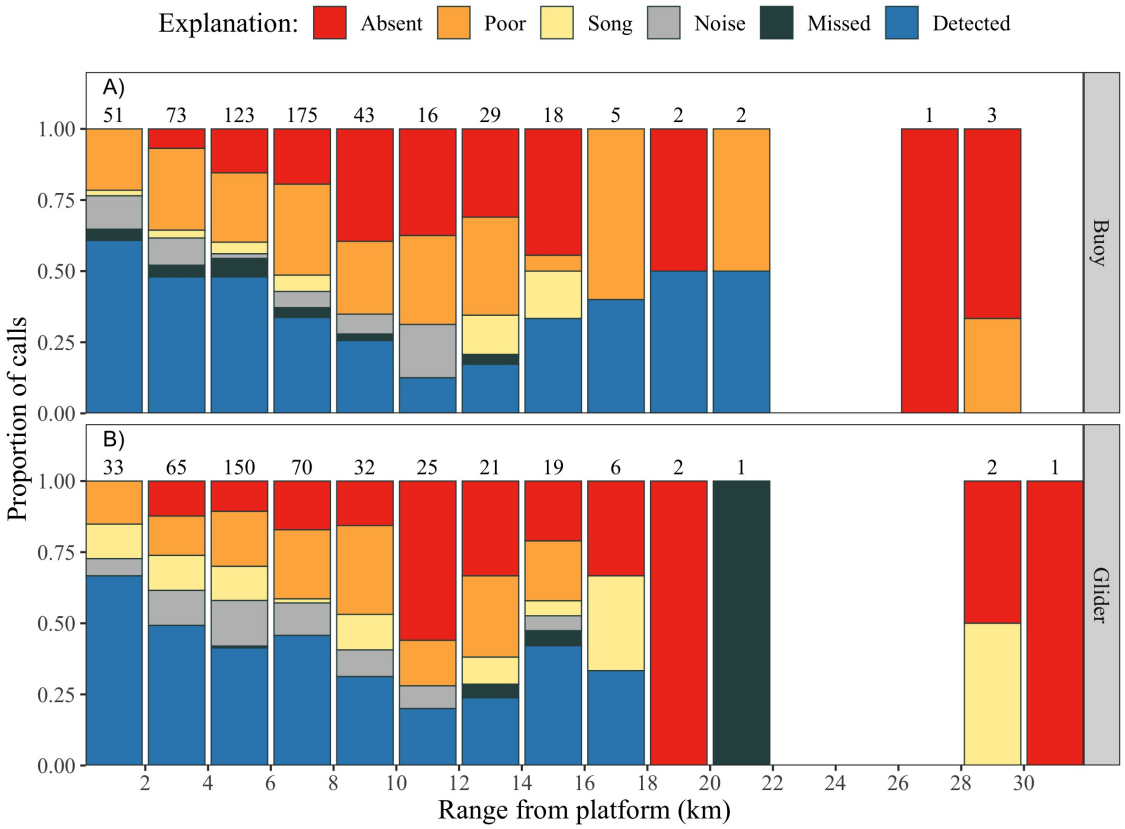

Figure 2.7: Proportion of localized calls assigned to each score category based on a conservative review of the near real-time pitch track data as a function of range from the buoy (panel A) and glider (panel B). Colors indicate the proportion of calls of a given score in 2-km range bins, while the number of calls in each bin is shown above each bar. Definitions of each category are provided in Table I. Analogous results using the precautionary protocol or archival audio are available in Appendix A.

Table 2.3). In low noise conditions (95 dB re 1 μPa^2 Hz^{-1}) the range to a probability of detection of 0.5 increased to 7.6 km. A probability of detection of 0.5 was not achieved at any range in high noise conditions (Figure 2.8).

For the glider, many localized calls (n = 115) occurred during periods when the glider produced acoustic noise during activation of the buoyancy pump during profiling inflections (typically 30 s every 3.5 min in 30-35 m depths for the glider used in this study) or electrical noise during satellite communications at the sea surface (typically 10-15 min every 2-2.25 h, or $\sim$12% of the deployment). The LFDCS recognizes these periods of noise and terminates pitch tracking during them. As calls during these periods were not available for detection and therefore not useful in determining our assessment of the effect of range on the accuracy of the DMON/LFDCS, they were excluded from the analysis. The distribution of these excluded calls was uniform with respect to range. The proportion of the remaining 426 localized calls detected using the pitch tracks and the conservative protocol decreased with range (Figure 2.6B); 51.6% of localized calls within 5 km (95/184) were detected while 18.8% of localized calls between 15 and 40 km (3/16) were detected. There was a parabolic relationship between the proportion of calls detected and glider depth, with the greatest proportion of calls detected at mid depths and lower proportion detected near the surface and bottom (Figures 2.6F, A.4). This was not explained by the proportion of time spent at depth, which was relatively uniform for 0-25 m. The influence of noise on the empirical proportion of detected calls was not obvious for the pitch track analyses (Figure 2.6D), but increasing noise was associated with a decrease in the proportion of detected calls for the archival audio analysis (Figure A.3F) and the proportion of detected calls increased with SNR in all analyses (Figures 2.6H, A.5). An SNR of more than 5 dB was required to detect at least 50% of localized calls (Figure 2.6G). Calls were missed for a variety of reasons: of the 426 available calls, 36.6% were missed due to absent or poor pitch tracks, 9.6% were missed due to interfering biological sounds, 11.2% were missed due to interfering non-biological sounds and 0.9% were missed due to analyst error in scoring the pitch tracks (Table 2.1; Figure 2.7B).

The most parsimonious logistic regression models for the glider provided evidence that the probability of detecting localized calls was related to range, noise level, and glider depth for all analyses (Table 2.2). At an average noise level (100 dB re 1 μPa^2 Hz^{-1}) and glider depth (15 m), the fitted regression suggested that a probability of detection of 0.5

Table 2.2: Selection and statistical evaluation of candidate logistic regression models describing the probability of detection of the glider and buoy. The logistic regressions used scores as the dependent variable derived from pitch track analysis with a conservative protocol, pitch track analysis with a precautionary protocol, and archival audio analysis. The full models (highlighted in grey) were the most parsimonious for all analyses. Formulae for each candidate model are provided below the table.

				Wald's Tests			Drop-in-deviance Tests	
Platform	**Analysis**	**Model***	**AIC**	**Variable**	**Coefficient**	**P-value**	**Test**	**P-value**
Glider (n = 426)	Real time pitch tracks (conservative protocol)	G1	272.5	range	-0.19	<0.001*	NA	NA
		G2	274	range	-0.19	<0.001*	G2 v G1	0.454
				noise	-0.03	0.48		
		G3	248.1	range	-0.2	<0.001*	G3 v G1	<0.001*
				glider_depth	0.35	<0.001*		
				glider_depth^2	-0.01	<0.001*		
		G4	235.7	range	-0.23	<0.001*	G4 v G2	<0.001*
				noise	-0.18	<0.001*		
				glider_depth	0.5	<0.001*	G4 v G3	<0.001*
				glider_depth^2	-0.01	<0.001*		
	Real time pitch tracks (precautionary protocol)	G1	306.6	range	-0.17	<0.001*	NA	NA
		G2	307.4	range	-0.17	<0.001*	G2 v G1	0.22
				noise	-0.04	0.29		
		G3	281.7	range	-0.19	<0.001*	G3 v G1	<0.001*
				glider_depth	0.35	<0.001*		
				glider_depth^2	-0.01	<0.001*		
		G4	268.4	range	-0.21	<0.001*	G4 v G2	<0.001*
				noise	-0.17	<0.001*		
				glider_depth	0.48	<0.001*	G4 v G3	<0.001*
				glider_depth^2	-0.01	<0.001*		
	Archival audio	G1	278.1	range	-0.15	<0.001*	NA	NA
		G2	259.7	range	-0.19	<0.001*	G2 v G1	<0.001*
				noise	-0.22	<0.001*		
		G3	262.6	range	-0.17	<0.001*	G3 v G1	<0.001*
				glider_depth	0.31	<0.001*		
				glider_depth^2	-0.01	<0.001*		
		G4	225.2	range	-0.23	<0.001*	G4 v G2	<0.001*
				noise	-0.33	<0.001*		
				glider_depth	0.45	<0.001*	G4 v G3	<0.001*
				glider_depth^2	-0.01	<0.001*		
Buoy (n = 239)	Real time pitch tracks (conservative protocol)	B1	143.7	range	-0.24	<0.001*	NA	NA
		B2	125.2	noise	-0.32	<0.001*	NA	NA
		B3	91.7	range	-0.42	<0.001*	B3 v B1	<0.001*
				noise	-0.48	<0.001*	B3 v B2	<0.001*
	Real time pitch tracks (precautionary protocol)	B1	164.7	range	-0.21	<0.001*	NA	NA
		B2	144	noise	-0.31	<0.001*	NA	NA
		B3	110.9	range	-0.37	<0.001*	B3 v B1	<0.001*
				noise	-0.43	<0.001*	B3 v B2	<0.001*
	Archival audio	B1	33.6	range	-0.16	0.23	NA	NA
		B2	21.6	noise	-0.88	0.02*	NA	NA
		B3	9.8	range	-9.25	0.46	B3 v B1	<0.001*
				noise	-10.5	0.44	B3 v B2	<0.001*

G1: score ~ range
G2: score ~ range + noise
G3: score ~ range + glider_depth + glider_depth^2
G4: score ~ range + noise + glider depth + glider depth^2

B1: score ~ range
B2: score ~ noise
B3: score ~ range + noise

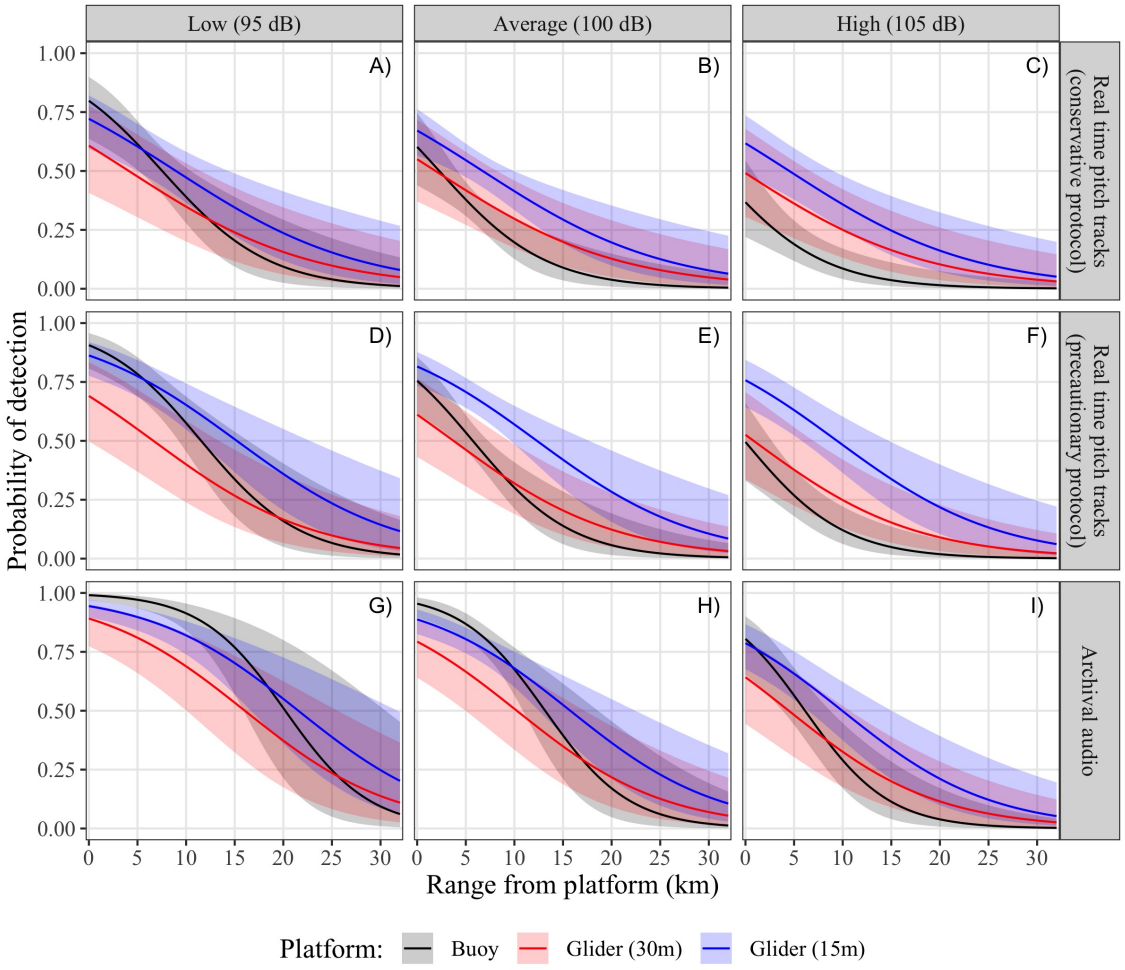

Figure 2.8: Estimated probability of detection of localized right whale upcalls as a function of range to the buoy (black lines) and glider at a depth of either 15m (blue lines) or 30m (red lines) at low (95 dB re 1 μPa^2 Hz^{-1}; left column), average (100 dB re 1 μPa^2 Hz^{-1}; middle column), and high (105 dB re 1 μPa^2 Hz^{-1}; right column) noise levels based on the conservative (top row) or the precautionary (middle row) analyses of near real-time pitch track data, or based on the manual review of archival audio (bottom row). The fitted regression models are shown as solid lines, while the 95% confidence intervals are shown as shaded regions. An alternate representation of these data showing the influence of noise levels by platform is available in Appendix A.

Table 2.3: The ranges (in km) for a given probability of detecting a right whale upcall from the glider or the buoy estimated from the most parsimonious logistic regression models (Table 2.2). Noise was fixed at an intermediate value of 100 dB re 1 μPa^2 Hz^{-1}. Glider depths were set to either 15 or 30 m. The bottom row shows the effective detection radius (EDR) computed using a 40 km truncation range.

	Range (km)								
	Real time pitch tracks (Conservative protocol)			Real time pitch tracks (Precautionary protocol)			Archival Audio		
Probability	*Glider (15m)*	*Glider (30m)*	*Buoy*	*Glider (15m)*	*Glider (30m)*	*Buoy*	*Glider (15m)*	*Glider (30m)*	*Buoy*
0.5	6.8	1.9	2.3	12.3	3.8	5.8	15.8	10.2	13.2
0.33	13.4	8.6	6.2	18.2	9.6	9.3	21.2	15.7	16.2
0.25	17.1	12.2	8.3	21.4	12.9	11.3	24.1	18.6	17.9
0.1	27.5	22.6	14.4	30.6	22	16.9	32.5	27	22.7
EDR	15.2	12.5	8.3	17.9	12.4	10.1	19.9	15.9	15.2

(95% CI: 0.430-0.569) occurred at 6.8 km and the effective detection radius was 15.2 km (Figure 2.8; Table 2.3). In low noise conditions (95 dB re 1 μPa^2 Hz^{-1}) the range to a probability of detection of 0.5 increased to 9.0 km, while in high noise conditions (100 dB re 1 μPa^2 Hz^{-1}) the range decreased to 4.5 km (Figure 2.8). Results for analogous analyses of the pitch tracks using the precautionary protocol and of the archived audio recordings from the glider and buoy are available in the supplementary material (Appendix A).

2.5 Discussion

2.5.1 Estimating and reporting detection range

Several previous efforts have succeeded in ranging and localizing baleen whale calls for purposes such as density estimation (e.g., *Harris et al.*, 2013), call attribution (e.g., *Baumgartner and Fratantoni*, 2008), or measuring noise impacts (e.g., *Thode et al.*, 2020). Few studies have attempted to quantify the probability of detecting localized calls. To our knowledge, this is the first study to empirically derive a detection function for right whales, and as such, there is a paucity of other observations available for comparison. *Laurinolli et al.* (2003) localized tonal right whale calls to a maximum range of approximately 29 km in the Bay of Fundy, and *Thode et al.* (2017) observed a maximum range to a North Pacific right whale (*Eubalaena japonica*) upcall of approximately 30 km in the Bering Sea. These

observations are similar to the maximum range of a localized call from our study ($\sim$30 km), but greater than the observed maximum detection range of the DMON/LFDCS on the glider or buoy ($\sim$20 km). The estimated probability of detection at 30 km is low, but non-zero, so it is possible that we did not have a large enough sample size to detect a call at 30 km. *Tennessen and Parks* (2016) used a modeling approach to estimate a maximum propagation distance of approximately 16 km for a right whale upcall in optimal noise conditions (85 dB re 1 μPa^2 Hz^{-1}) in the Bay of Fundy. This is lower than the maximum detection ranges observed in our study and in the *Laurinolli et al.* (2003) study. The reasons for such discrepancies are unclear, which highlights the challenges in simulating detection range.

Clark et al. (2010) conducted an excellent study of right whale upcalls in Cape Cod Bay, a shallow habitat similar to our study area, and they stated that the "acoustic detection area was reliably found to be within a range of approximately 9 km (5 nmi) from a recorder" (*Clark et al.*, 2010, p. 842). The comparability of our observations to this acoustic detection range estimate depends on the definition of "reliably". If the definition of the acoustic detection range is the range at which the probability of detecting a calling whale is 0.5 (i.e., "reliable" is defined as a 1 in 2 chance of detection), then our range estimates are shorter than those of *Clark et al.* (2010). However, if we define the detection range as the range at which the probability of detecting a calling whale is 0.33 (i.e., "reliable" is defined as a 1 in 3 chance of detection), then our detection range estimates are similar to those of *Clark et al.* (2010). Finally, if *Clark et al.* (2010) were reporting a maximum detection range, then our maximum estimated detection range of more than 30 km exceeds the detection range that they reported. We present this comparison to highlight something that is likely obvious, but perhaps underappreciated: the use of a single number for detection range is an incomplete description of the area that is effectively monitored by a passive acoustic system. From our study, we estimated that whales calling at $>$20 km can be detected in near real time by the DMON/LFDCS system carried aboard either a glider or a buoy, but the chances of a calling whale being detected at those distances are low. The detection function, or the curve describing the range-dependent probability of detection (Figure 2.8), is a near-complete description of the site-, environment- and species-specific detection range of a PAM system. Efforts should be made to estimate and report the detection function whenever possible, as it provides a vastly more accurate and appropriate

description of a system's detection range than a single number.

2.5.2 Factors influencing detection range

Our results indicate that other covariates in addition to range, such as noise level and platform depth, play an important role in the probability of detecting a call. The performance of both DMON/LFDCS platforms was significantly reduced in louder noise environments. The buoy was especially sensitive to noise, where an increase of 10 dB re 1 μPa^2 Hz^{-1} translated to a nearly 50% reduction in the probability of detecting a call at 5 km, compared to a 20% reduction on the glider. These results emphasize the importance of considering the impact of noise on the interpretation of PAM results, which, if left unaccounted for, can introduce artificial trends in detection results (e.g., *Helble et al.*, 2013a).

The improved probability of detection and reduced sensitivity to noise of the glider relative to the buoy is likely due in large part to differences in platform depth, and, by extension, transmission loss. Transmission loss refers to the decrease in acoustic intensity due to spreading or attenuation as a sound propagates. During March (i.e., prior to the onset of stratification), transmission loss generally varies parabolically with depth in this environment, with the lowest values in the middle of the water column and the highest values near the top and bottom boundaries (Figure 2.9). This agrees well with the distribution of detections versus glider depth, where a higher proportion of calls were detected when the glider was located in the middle of the water column rather than near the surface or the bottom (Figures 2.6F, A.4). When the glider depth covariate was fixed at 15m, the depth stratum with minimum transmission loss (Figure 2.9), the logistic regressions suggested the performance of the glider was consistently better than that of the buoy. In contrast, when the glider depth covariate was fixed to a value of 30 m, the same depth as the hydrophone on the buoy, the logistic regressions suggested that the performance of the platforms was nearly identical (Figure 2.8). Thus, the regular vertical profiling of the glider through regions of low transmission loss at intermediate depths confers a performance improvement relative to the buoy.

The probability of detection also varied depending on the data source (real-time pitch tracks versus archival audio), platform and detection protocol. The probability of detecting a call was lower using near real-time pitch track data compared to archival audio data. This is not surprising given that pitch tracks are an abstraction of the audio and do not possess all of the cues that an analyst would use to confidently detect and classify a call. Inspection

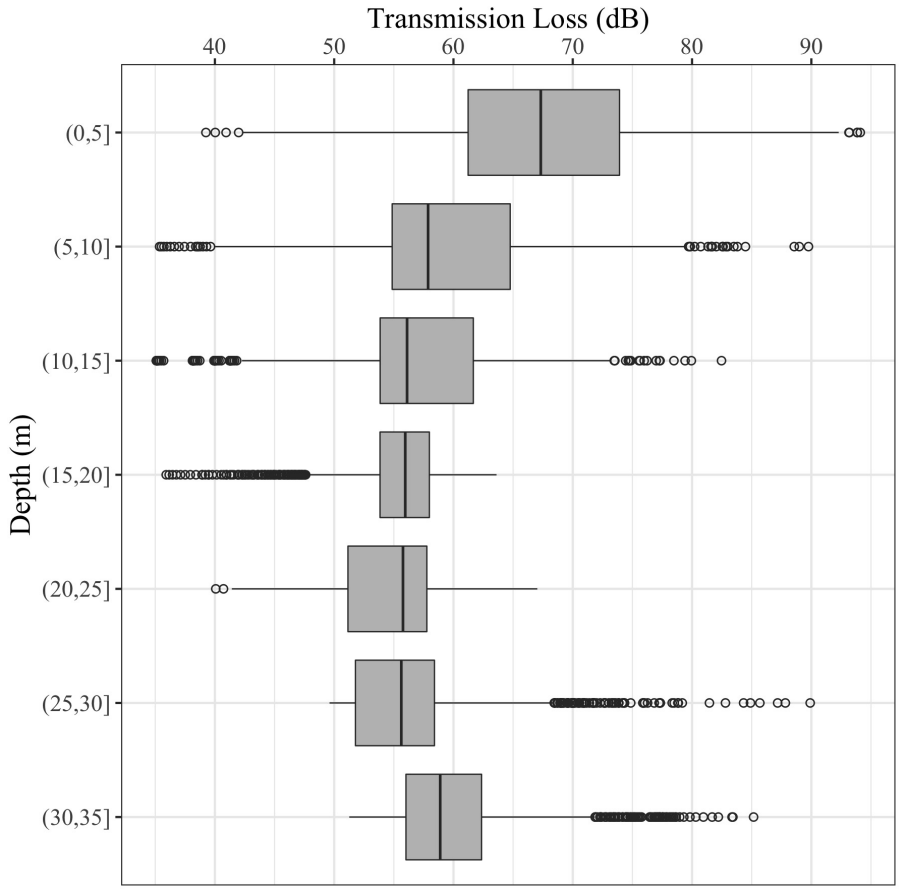

Figure 2.9: Depth distribution of transmission loss estimated using the KRAKEN normal mode model parameterized with a 100 Hz frequency source at 15m depth, two propagating modes, and environmental conditions consistent with those of the study site. Transmission loss estimates were computed at each point in a grid with 250 m range and 0.5 m depth resolution to a maximum range and depth of 35 km and 35 m, respectively, and then aggregated into 5 m depth bins.

of spectrograms and aural review of audio by an experienced analyst is considered the gold standard for detecting marine mammal calls in passive acoustic monitoring data (e.g., *Baumgartner and Mussoline*, 2011). The difference between the audio and pitch track results indicates the cost of relying on an automated detector and not directly reviewing the audio; improvements could potentially be made by either upgrading the existing detection system or using a different detector (e.g., *Simard et al.*, 2019; *Kirsebom et al.*, 2020). These differences are most pronounced at close ranges. The majority of the undetected calls within 5 km of both platforms were not detected because of poor pitch tracks, meaning that the pitch tracks were present but could not be confidently classified by the analyst because of poor shape or low amplitude. Poorly formed pitch tracks from close range calls could be due to competing biological- and platform-related noise processes, receiver depth, or variation in source levels (*Parks and Tyack*, 2005). A higher proportion of close-range calls was missed by the glider due to the presence of competing biological signals (humpback whale song). As with right whale calls, these signals may have been more detectable on the glider owing to its vertical profiling through depth strata characterized by low transmission loss.

Our results demonstrate that the detection function of a given platform changes depending on the analysis protocol. The near real-time detection protocol currently used with DMON/LFDCS gliders and buoys is conservative by design in recognition of the high costs associated with triggering a management measure based on a false-positive detection (*Baumgartner et al.*, 2019). This protocol can be relaxed to reduce missed detections at the expense of allowing false positives. This would represent a more precautionary management approach. We examined the use of a precautionary protocol where right whale calls that were scored as "possibly detected" were considered "detected" in the estimation of the detection function. We found that employing a precautionary protocol increased the real-time probability of detection by approximately 15% at close ranges ($\leq$10 km; Supplement A; Figure 2.8). In other words, the call detection protocol directly influences the detection range of a platform and thus must be designed with care and implemented with consistency.

The real-time detection rates reported here are much lower than those previously presented for the glider (*Baumgartner et al.*, 2013, 2020) or buoy (*Baumgartner et al.*, 2019) (i.e., the missed detection rates in this study are higher than previously reported). In this

study, pitch tracks were reviewed on a call-by-call basis to determine if individual localized calls were detected or not detected by the glider or buoy. In contrast, the near real-time validation protocol operates on nominal 15-minute "tally periods" to determine whale occurrence (*Baumgartner et al.*, 2013, 2019, 2020). The tally period approach is more robust to missing occasional calls when individual whales are calling repeatedly within a tally period. For example, if the probability of missing a single call is 0.5, the probability of missing 3 calls in a row is reduced to 0.125 (0.5 x 0.5 x 0.5 = 0.125) if the calls are independent. The probability of detecting at least 1 of those 3 calls is 0.875 (1 - 0.5 x 0.5 x 0.5 = 0.875). As a simple thought experiment, we can apply this logic to the per-call detection functions determined in this study to illustrate how the probability of detection may change when considering multiple calls within a given time period. The assumption of independence of calls is almost certainly violated due to correlation in a number of factors (e.g., calling behavior, background noise levels, interference from other species), so the probabilities of detection in this thought experiment are likely overestimated. However, the key concept is that the detection function of a given platform changes based on the number of calls available for detection in a given period. If the assumption of independence were not violated, for example, attempting to detect one of two available calls in average noise conditions on the buoy increases the range to the 0.5 probability of detection from 2.3 to 7.1 km, while attempting to detect one of 5 or 10 available calls increases this range to 12.8 or 16.8 km, respectively (Figure 2.10). The probability of detection of a single call in a tally period is dependent on the number of calls that are available; however, it is nearly impossible to know the number of calls that are available for detection in a tally period, particularly when calling rates likely vary widely depending on location, time of year, whale density and whale behavior. Consequently, the probability of detection results reported here for single calls (i.e., attempting to detect one of one available call; Figure 2.8) should be considered a minimum estimate that is likely improved substantially, but by an unknown amount, by using a tally period approach when the goal of monitoring is to assess right whale occurrence over time scales that are longer than instantaneous (i.e., the goal is not to detect every call at all times, but to detect occurrence over, say, daily time scales).

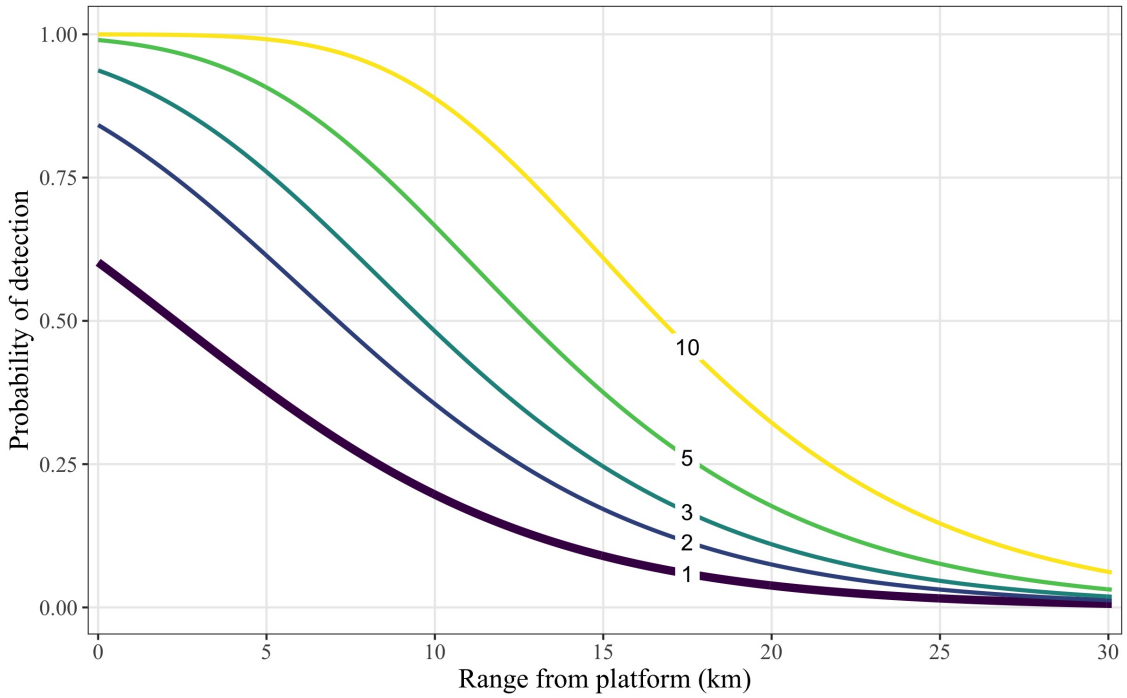

Figure 2.10: Results of a thought experiment showing the probability of detecting one of a given number of available right whale upcalls as a function of range to the buoy based on the conservative analysis of near real-time pitch track data and a fixed noise level of 100 dB re 1 μPa^2 Hz^{-1}. Each line shows the probability of detecting one call out of 1, 2, 3, 5, or 10 available calls during a fixed period of time. This analysis relies upon the unlikely assumption that calls are detected independently, so the probabilities of detection are likely overestimated (see text). Results from all combinations of platform, data source and protocol are available in Appendix A.

2.5.3 Assumptions and caveats

We chose to calculate the detection function empirically to avoid making assumptions about the source (e.g., source depth, level, frequency), environmental (e.g., ambient or platform noise level), or detector characteristics (e.g., detection threshold). A potential source of bias in our approach is that each call used to estimate the detection functions of the buoy or glider first had to be detected and localized on the array. Results from a simple simulation suggest that the methodology employed here is robust to implicit bias introduced by imperfect array detection and localization (Appendix A). We also assumed that the detection functions were logistically monotonic and thus well-represented by the logistic regression model. There was a slight increase in the proportion of calls detected beyond 10 km, but this was driven by a very small number of calls, so we do not consider this assumption to be violated (Figures 2.6A, 2.6B, A.2). We also used generalized additive models (GAMs) to estimate the probability of detection (not shown) and found that the shapes of the resulting functions were well represented with logistic functions. The detection function may take on non-monotonic shapes in more complex propagation environments (e.g., *Helble et al.*, 2013b), but this is unlikely in the relatively range-independent conditions of this study site.

Our analysis only considers calls that were available for detection by the glider or buoy, meaning they were received when each platform was actively monitoring. The buoy produced pitch tracks continuously but only recorded audio 50% of the time. In contrast, pitch track and audio data were not available approximately 12% of the time for the glider due to noise associated with surfacing or inflecting. We configured the glider to surface and inflect at this rate to facilitate shallow water navigation and the reporting of detection results every $\sim$2 h, but these parameters can be adjusted depending on the environment and monitoring objectives. We do not make an effort to correct for differences in duty cycling between platforms. Scientists or regulators seeking to employ the DMON/LFDCS on one of these platforms for a particular application should consider the relative differences in monitoring effort between platforms in mission planning.

The single-station ranging method we employed does require some assumptions to be made about signal transmission and the propagation environment. The assumptions include range-independent sound speed and bottom type, and the assumption that the propagation of the calls was well-approximated by normal mode theory. These assumptions are likely

justified, as numerous studies have demonstrated the efficacy of normal mode ranging of low-frequency signals in shallow water environments (*DSpain et al.*, 1997; *Thode et al.*, 2000; *Wiggins et al.*, 2004; *Thode et al.*, 2006; *Munger et al.*, 2011; *Abadi et al.*, 2014; *Bonnel et al.*, 2014; *Thode et al.*, 2017). We made efforts to account for variation in bathymetry by using a range- and bearing-dependent backpropagation method. The array- and glider-based environmental sensors revealed that the water column was entirely mixed throughout the study, so depth-varying sound speed was unlikely to contribute to ranging error. Conventional long-baseline array localization methods would require similar simplifying assumptions about the propagation environment (e.g., uniform bathymetry, constant sound speed).

Our analysis made no attempt to quantify the likelihood that a right whale will produce a call; the probability of detection examined here assumes a call is already available to be detected. Call types, rates, depths, and spectral characteristics (e.g., frequency, amplitude) vary depending on the time of day, season, location, environment, behavior, and individual. Some of this variability has been characterized for right whales (e.g., *Parks et al.*, 2011a,b), but small sample sizes have often precluded range-wide characterization.

Future efforts should be made to improve array detection and localization to increase sample size. We did not attempt to quantify the probability of detection for the array, but the success rate for localizing calls of 36% (541 of 1485) was similar to the success rate of *Laurinolli et al.* (2003) for loud tonal sounds in the Bay of Fundy using traditional cross-correlation and time difference of arrival methods and was substantially higher than in other studies (e.g., *Cummings and Holliday*, 1986). Many detected calls could not be localized owing to noise on one or more VLA or HLA channel(s) that prevented accurate mode filtering or beamforming, respectively. Improvements in array design and mooring configuration to reduce platform noise, as well as noise-adaptive filtering and beamforming algorithms could be pursued to increase localization success rates.

The results presented here are specific to the conditions in the area and at the time of our study. They provide an indication of how these PAM systems might perform in similar conditions, but caution is warranted when applying our results to other areas or times. Many efforts must be made to characterize variability in the source, background noise, and transmission conditions before detection probability estimates can be generalized. That said, these results have already been applied to inform dynamic management of

right whales; preliminary versions of the detection functions derived here were used to parameterize a modeling effort that suggests whale movement causes visual and acoustic detections to provide equally uncertain estimates of whale location on dynamic management timescales (Chapter 3; *Johnson et al.*, 2020a). We anticipate and hope that the results presented here will also prove useful for refining management policies in the USA and Canada as both countries have recently committed to using near real-time PAM to trigger management measures.

2.6 Conclusions

Our primary motivation for this work was to improve conservation outcomes for right whales by using an effective and reliable near real-time passive acoustic monitoring system. One such system, the DMON/LFDCS, has been operational for several years but has only recently been used to inform dynamic management measures owing partly to uncertainty in the acoustic detection range. We were able to successfully address uncertainty by conducting a dedicated study using a multi-channel reference hydrophone array to empirically quantify the probability of detecting localized right whale upcalls from autonomous DMON/LFDCS platforms in different noise conditions. Our results provide a near-complete description of both near real-time and archival performance of both monitoring platforms for a shallow water site. We quantify the impact of noise conditions and platform depth on performance and provide evidence that the profiling glider gains an advantage over the buoy by occupying depth strata characterized by low transmission loss. We also demonstrate how the detection range is influenced by the review protocol, where a more conservative protocol effectively reduces the detection range of the system. Our analysis was conducted on a call-by-call basis and therefore provides a minimum estimate of the platform detection range that can be increased by considering multiple calls. All the results presented here are specific to the conditions in the area and at the time of our study and caution is required to apply them more broadly.

Given its economy and performance, we anticipate near real-time PAM will become even more widely used in the future. We recommend that new systems quantify and report their performance (e.g., *Baumgartner et al.*, 2019, 2020) before being used operationally for management, and that the detection function should be characterized (this study) to inform mitigation applications. Furthermore, we encourage visual survey teams to conduct

and report similar analyses, as they are subject to many analogous detection challenges. Such analyses are difficult but illuminating; they can aid in the proper interpretation of the survey results, allow the standardization and inter-comparison of survey methodologies, and identify issues or sources of bias. More thorough evaluation of both acoustic and visual survey performance will help us determine which survey methodology is optimal for a particular application, how they can better complement one another, and how to best consolidate and compare these data sources for management and research purposes.

2.7 Acknowledgements

We are indebted to Ken Houtler and Ian Hanley for their skilled operation of the R/V Tioga, to John Kemp, Don Peters, Meghan Donohue, Jeff Pietro, Kris Newhall, Jim Dunn, and Nico Llanos of the WHOI Mooring Operations and Engineering Group for development, deployment, and recovery of the mooring systems, to Phil Alatalo for assistance at sea, to Ben Hodges for preparation, deployment, and recovery of the Slocum glider, to Ed O'Brien and Giorgio Caramanna of the WHOI Dive Group for assisting in mooring recovery, to Peter Koski, Julien Bonnel and Dan Zitterbart of WHOI Applied Ocean Physics & Engineering Department for guidance and advice, and to Kim Davies, Delphine Durette-Morin, Meg Carr, Marcia Pearson and Kimberly Franklin at Dalhousie University for providing helpful feedback.

Support for this study was provided by the Massachusetts Clean Energy Center (MassCEC), Bureau of Ocean and Energy Management (BOEM), and the Nova Scotia Offshore Energy Research Association (OERA). Support for HDJ was provided by the Marine Environmental Prediction and Response Network (MEOPAR) Whales Habitat and Listening Experiment (WHaLE), the Killam Foundation, Vanier Canada Graduate Scholarship program, Dalhousie University, the Nova Scotia Graduate Scholarship program, and the Canada Graduate Scholarships Michael Smith Foreign Study Supplements (CGS-MSFSS) program.

CHAPTER 3

ESTIMATING RIGHT WHALE LOCATION UNCERTAINTY FOLLOWING VISUAL OR ACOUSTIC DETECTION TO INFORM DYNAMIC MANAGEMENT

3.1 Abstract

The United States and Canada employ dynamic management strategies to improve conservation outcomes for the endangered North Atlantic right whale (*Eubalaena glacialis*). These strategies rely on near real-time knowledge of whale distribution generated from visual surveys and opportunistic sightings. Near real-time passive acoustic monitoring (PAM) systems have been operational for many years but acoustic detections of right whales have yet to be incorporated in dynamic management because of concerns over uncertainty in the location of acoustically detected whales. This rationale does not consider whale movement or its contribution to location uncertainty following either visual or acoustic detection. The goal of this study was to estimate uncertainties in right whale location following acoustic and visual detection and identify the timescale at which the uncertainties become similar owing to post-detection whale movement. We simulated whale movement using an autocorrelated random walk model parameterized to approximate three common right whale behavioral states (traveling, feeding, and socializing). We then used a Monte Carlo approach to estimate whale location over a 96-h period given the initial uncertainty from the acoustic and visual detection methods and the evolving uncertainties arising from whale movement. The results demonstrated that for both detection methods the uncertainty

in whale location increases rapidly following the initial detection and can vary by an order of magnitude after 96 h depending on the behavioral state of the whale. The uncertainties in whale location became equivalent between visual and acoustic detections within 24 to 48 h depending on whale behavior and acoustic detection-range parameterization. These results imply that using both visual and acoustic detections provides enhanced information for the dynamic management of this visually and acoustically cryptic and highly mobile species.

3.2 Introduction

United States (U.S.) and Canadian government agencies have implemented a variety of management measures in an effort to improve conservation outcomes for the endangered North Atlantic right whale (*Eubalaena glacialis*; hereafter 'right whale'). One such strategy is dynamic management, which broadly refers to risk-mitigation actions within defined areas in response to near real-time whale detections in those areas. Such actions are designed to reduce risk from the two primary sources of right whale mortality: vessel strike and fishing-gear entanglement (*Knowlton and Kraus*, 2001).

In U.S. waters, the National Oceanic and Atmospheric Administration (NOAA) can establish dynamic management areas (DMAs) on a case-by-case basis around persistent aggregations of right whales. The DMAs set a voluntary speed limit of 10 kt for vessels $\geq$20 m length that remains active for 15 d or until the risk of vessel strike is deemed reduced (*NOAA*, 2019). There are currently no mechanisms in place for dynamic fishery management to reduce right whale entanglement risk in U.S. waters.

DMAs are monitored as frequently as possible, but because they are voluntary, NOAA has no mandate to conduct regular surveillance or enforce compliance. The aerial survey team at the Northeast Fisheries Science Center typically patrols DMAs at least weekly and DMAs are kept active as long as an aggregation persists within. NOAA has also established the Right Whale Sightings Advisory System to collect, validate, and communicate opportunistic visual detection reports by others that may also be used to establish a DMA (*RWSAS*, 2019).

Canadian governmental agencies instituted dynamic management for the first time in 2018, motivated by the 2017 unusual mortality event (UME) wherein 12 right whales were found dead in the southern Gulf of St Lawrence (*Daoust et al.*, 2017; *Davies and Brillant*,

2019). Large areas of the Gulf of St Lawrence were subject to dynamic management in 2019 (*TC*, 2019). These included several zones associated with traffic separation schemes in the Honguedo Strait and Jacques-Cartier Passage wherein the visual detection of a single right whale triggered a mandatory 15 d, 10 kt speed limit for vessels 20 m length. There were also several large areas subject to dynamic and mandatory closures of fixed-gear fisheries (primarily snow crab, *Chionoecetes opilio*, and lobster, *Homarus americanus*). A single right whale visually detected in such areas triggered a 15-d closure of a number of 10'x10' grid cells in the vicinity of the detection. Affected fishers were given a predetermined period (nominally 48 h) to recover gear from these closed areas. Right whales visually detected outside these management areas also triggered fisheries closures on a case-by-case basis (*DFO*, 2019).

Transport Canada (TC) and Fisheries and Oceans Canada (DFO) are responsible for mitigating vessel-strike and gear-entanglement risk, respectively, to right whales in Canadian waters. In 2019 TC conducted weekly aerial surveys of those sections of the shipping corridors subject to dynamic management. Failure to survey within a week (e.g., due to weather, maintenance) triggered a precautionary area closure until a visual monitoring survey was completed. DFO could not guarantee any regular visual monitoring of areas subject to dynamic fisheries closures. Preliminary reports from 2018 and 2019 indicated that DFO achieved a total of 1-3 dedicated visual surveys of such areas during the 6-week snow crab fishing season (Chapter 4; *Johnson et al.*, 2021). Both DFO and TC incorporate, and act upon, validated (i.e., verified by an expert) visual detections provided by various governmental and non-governmental agencies. The collation and dissemination of all available near real-time right whale monitoring and detection data in Atlantic Canada (visual and acoustic) occurs via WhaleMap (Chapter 4; *Johnson et al.*, 2021).

Maintaining visual monitoring effort within and beyond known right whale habitats is a consistent challenge for dynamic risk-mitigation management and right whale conservation in general. Over the last several decades archival passive acoustic monitoring (PAM) has emerged as a powerful tool for efficient, safe, and persistent monitoring of right whales over time and space scales that are much greater than those achieved using conventional (aircraft and vessel) visual detection methods (e.g., *Davis et al.*, 2017). While most PAM applications are archival (meaning that all data are archived on the monitoring platform), technologies that transmit detection information in near real-time have been in use for

at least a decade (*Spaulding et al.*, 2009). For example, the Woods Hole Oceanographic Institution has developed a near real-time PAM system that has been operational in variety of ocean regions using two autonomous platforms: Slocum electric gliders (*Baumgartner et al.*, 2013, 2020, ; hereafter 'ocean gliders') and moored buoys (*Baumgartner et al.*, 2019). The performance of this system has been well characterized, and it has a false positive rate near or equal to zero for several baleen whale species, including right whales (e.g., near real-time right whale sounds are never erroneously reported as present when such sounds are not present in the acoustic record; *Baumgartner et al.*, 2019, 2020). Since 2014, ocean gliders and buoys equipped with this system in the northwest Atlantic have logged $\sim$4700 days at sea with $\sim$1500 definitive right whale acoustic detections (Chapter 4; *Johnson et al.*, 2021). Although such detections have been used on numerous occasions to inform research efforts, visual surveys and military operations, they have never been used directly to trigger dynamic management in either U.S. or Canadian waters.

These near real-time passive acoustic detection systems are currently not capable of acoustically localizing a detected call. They report the position of the acoustic platform when a call is detected, not the position of the whale. Because many low-frequency baleen whale calls can propagate long distances underwater (kms to 10s of km) there can be large uncertainty in the reported position of a near real-time acoustic detection. This uncertainty has often been cited as the primary rationale for not using near real-time acoustic detections to inform management decisions.

This rationale omits an important consideration: whale movement. There is always some delay - typically 24 h or more - between a whale detection and associated management action. The reported position of a visually detected whale is initially precise but becomes more and more uncertain as time passes and the whale moves. Thus, the whale location when first visually detected is an inaccurate estimate of where the whale will be located when the management action goes into effect. The reported location of an acoustically detected whale has low specificity (typically estimated as the location of the passive acoustic instrument +/- the acoustic detection range), yielding a similarly inaccurate estimate of where the whale will be located when the management action goes into effect. While both methods of detection have location uncertainties over management time scales, visual detections to date have been assumed, without documented foundation, to have lower uncertainty than acoustic detections for management purposes. Here we assess this

assumption by first simulating right whale movements after visual and acoustic detection and then comparing the temporal evolution of location uncertainties between the two methods.

3.3 Methods

We simulated individual whale movements using a modified version of the autocorrelated random walk model of *van der Hoop et al.* (2012). In brief, the model relied on placing a simulated whale at a given location, selecting an initial movement direction, and then simulating the movement trajectory by iteratively applying a swimming speed and turning angle at each model time step over a specified period. Initial movement direction was randomly selected from a uniform distribution between 0° and 360°. Swimming speed was randomly selected at each time step from a uniform distribution between 0 and 1.23 m s^{-1}, following *Baumgartner and Mate* (2005). The autocorrelated random walk was achieved by expressing the turning angle as the rate of change in direction (turning rate), where turning angles were constrained to a given angle per decametre (dam) travel. We used three different parameterizations of turning rate based on observations from *Mayo and Marx* (1989) to approximate movement patterns associated with three behavioral states; traveling (5.3° dam^{-1}), feeding (19.3° dam^{-1}), and socializing (52.5° dam^{-1}). A model time step of 2.5 s was chosen to simulate high resolution movements. A duration of 96 h for each model simulation was chosen to encompass the range of dynamic-management response times observed in Canadian waters. Figure 3.1 illustrates trajectories of a single simulation for a whale for each of the three behavioral states over a 24 h period.

We used a Monte Carlo approach to estimate the uncertainty in whale location over a 96 h period following visual and acoustic detection based on 100,000 realizations of each simulated whale behavior. Location uncertainty was calculated as the distance between the reported location and the true (simulated) whale location over time. The reported location, which was equivalent to the reported location of a visual detection or the location of a passive acoustic detector, was placed at the origin of a Cartesian grid. For visual detections, we assumed that the initial uncertainty in the reported position was small because most dedicated right whale visual survey protocols require the survey platform to approach the detected whale to confirm species, number, behavior, and position, as well as other information. As such, the true initial location of a visually detected whale was calculated

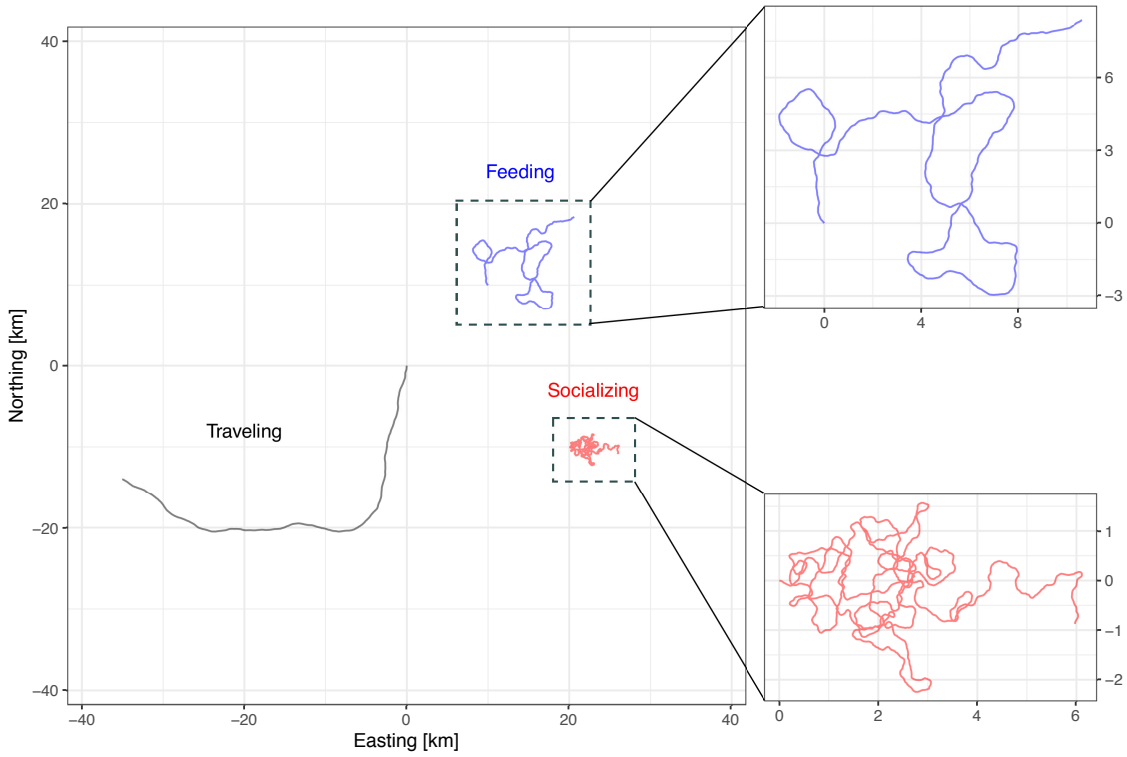

Figure 3.1: Example tracks (trajectories) of simulated right whales exhibiting traveling, feeding, and socializing behaviors over a 24 h period.

relative to the reported location with a range chosen randomly from a uniform distribution of 0 - 100 m and a bearing chosen randomly from a uniform distribution of 0° - 360°, resulting in an initial uncertainty of 0 - 100 m.

The uncertainty in the location of an acoustic detection is typically much greater than that associated with visual detections and is not well described. We used a logistic curve to model three different detection functions with a 50% probability of detection at 5, 10, and 15 km to represent short-, medium-, and long-range detection scenarios, respectively (Figure 3.2). The short- and medium-range estimates followed observations from typical coastal sites near Cape Cod (*Clark et al.*, 2010, Chapter 2) as well as model-based estimates from *Tennessen and Parks* (2016), while the long-range detection scenario was based on observations in the central Bay of Fundy (*Laurinolli et al.*, 2003) and maximum detection ranges near Cape Cod (Chapter 2). The true initial location of an acoustically detected whale was calculated relative to the reported location with a range chosen randomly from the detection range logistic curve and a bearing chosen randomly from a uniform distribution of 0° - 360°.

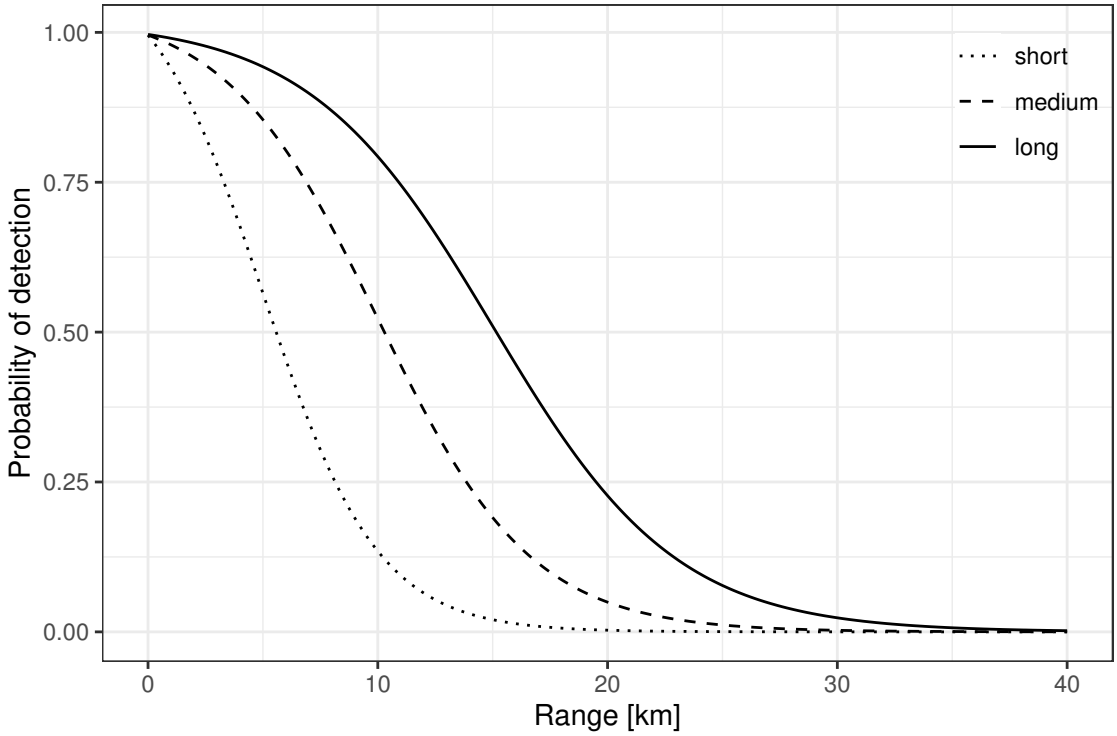

Figure 3.2: Acoustic detection functions used in the simulations to represent short (dotted line), medium (dashed line), and long (solid line) range detection scenarios.

Simulation results were based on 12 model runs, each with 100,000 realizations of a simulated whale that encompassed the combinations of the behavioral (traveling, feeding, socializing) and acoustic detection range (short, medium, and long) parameterizations. Simulated whale positions were used to calculate location uncertainties as the straight-line distance (range) from the estimated initial location at the center of the Cartesian grid at hourly intervals.

The difference in location uncertainty between visual and acoustic detections was evaluated using pairwise comparisons. We first simulated a trajectory and then defined the starting point based on either visual or acoustic detection uncertainty as described above. The difference in location uncertainty, r, at time t was calculated as follows:

$$r(t) = r_v(t) - r_a(t) \tag{3.1}$$

where r_v and r_a were the ranges from the origin to the visual and acoustic whale locations, respectively, at time t. This was applied for all trajectories and time steps. We then calculated the proportion of positive r values at each time step to estimate the probability of a visual detection providing a location estimate with an uncertainty greater than that of an acoustic detection (see Figure B.1 for a schematic). All analysis was conducted using the R programming language *R Core Team* (2019). Visualizations were produced using the ggplot2 package (*Wickham*, 2016). The R code used for this analysis is available from GitHub: `https://github.com/hansenjohnson/rw_sim`.

3.4 Results

Model results demonstrated that whale movement contributed to a rapid increase in whale location uncertainty following detection and the magnitude of this uncertainty was dependent on the movement behavior of the whale. Median uncertainty in visually detected whale location after 96 h, which was almost entirely driven by movement, was 103 km (interquartile range, IQR: 69 km) for traveling whales, 28 km (IQR: 21 km) for feeding whales, and 10 km (IQR: 8 km) for socializing whales (Figure 3.3). Location estimates derived from visual and acoustic detections for each behavior were qualitatively similar over time scales of days (Figures 3.3, B.2).

Location uncertainties for the visual and acoustic detection methods converged over

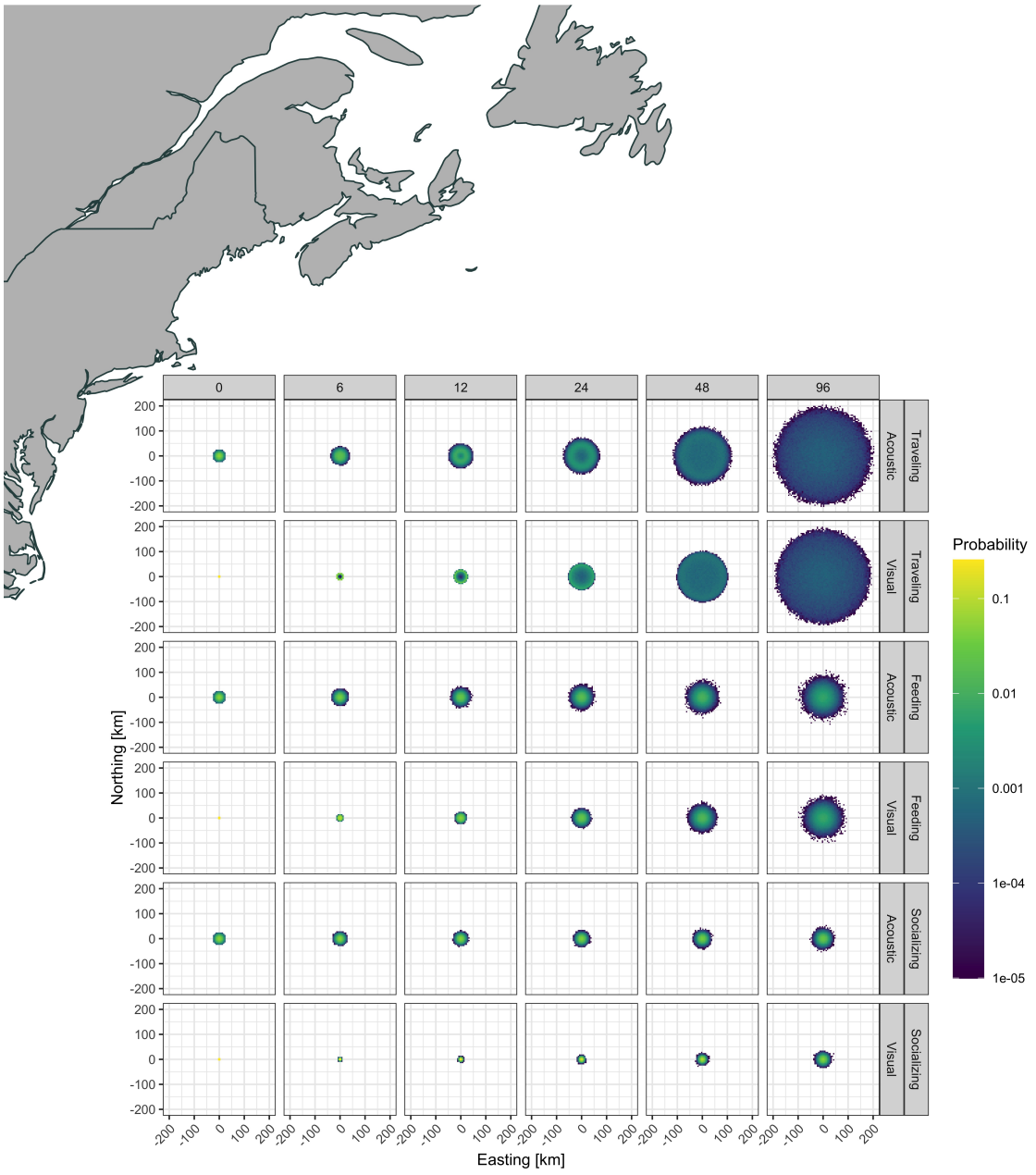

Figure 3.3: Evolution of location uncertainty after visual or acoustic detection of right whales in traveling, feeding, or socializing behavioral modes over the 96 h model period. Color indicates the location probabilities per 5 x 5 km grid cell. Columns show the time (in hours) since detection. Rows indicate the detection method (visual or acoustic) and simulated whale behavior (traveling, feeding, or socializing). The center of the domain (0,0) indicates the reported position of the detection. The acoustic data were generated using the medium detection range parameterization. Data for the other detection range parameterizations are not shown. The map provides an indication of the approximate spatial scale of the location uncertainty estimates.

time, and convergence was generally faster with higher displacement behaviors (travelling) and shorter acoustic detection range parameterizations. The differences between visual and acoustic location uncertainties never exceeded the maximum acoustic detection range, and the average difference approached zero over time (Figure 3.4A). Within 24 h there was a 10 - 47% chance that the acoustic detection provided a more accurate location estimate than a visual detection, with the larger values again associated with shorter acoustic detection ranges and higher displacement behaviors (Figure 3.4B).

Computing the probability that a simulated whale would remain within a given radius of its initial reported position provided a means of evaluating the efficacy of potential dynamic management strategies implemented on different time/space scales in habitats dominated by particular behaviors. This probability decreased with time, higher displacement movement behaviors, and smaller radii. There was a less than 10% chance of a traveling whale remaining within a $\leq$25 km radius of its reported position after 24 h, regardless of detection method. The probability of a whale remaining within 5 km of its reported position dropped below 10% in less than 24 h for traveling and feeding whales, and in approximately 96 h for socializing whales. In contrast, the probability of a feeding or socializing whale remaining within 25 km of the reported position after 24 h was 71-92% or 91-100%, respectively. This decreased slightly for socializing whales but dropped to below 50% for feeding whales after 96 h. In these cases, acoustic and visual methods produced similar estimates with better agreement in shorter detection range scenarios.

3.5 Discussion

Our results provide a reminder of the considerable mobility exhibited by North Atlantic right whales, and how their mobility contributes to a rapid expansion in location uncertainty following visual or acoustic detection. Our results also highlight the influence of the whales behavioral state on mobility and thus the post-detection uncertainty in whale location. Whales in the simulated traveling mode moved a maximum of $\sim$200 km from their initial detection location over the 96 h study period, an order of magnitude greater than whales simulated in a socializing behavior mode. *Baumgartner and Mate* (2005) observed that right whales are capable of traveling $\sim$80 km d^{-1}, nearly twice that simulated here. Conversely, there is evidence that right whales, particularly those exhibiting feeding or social behavior, may remain within a relatively small area (1 to 10 km radius) over several

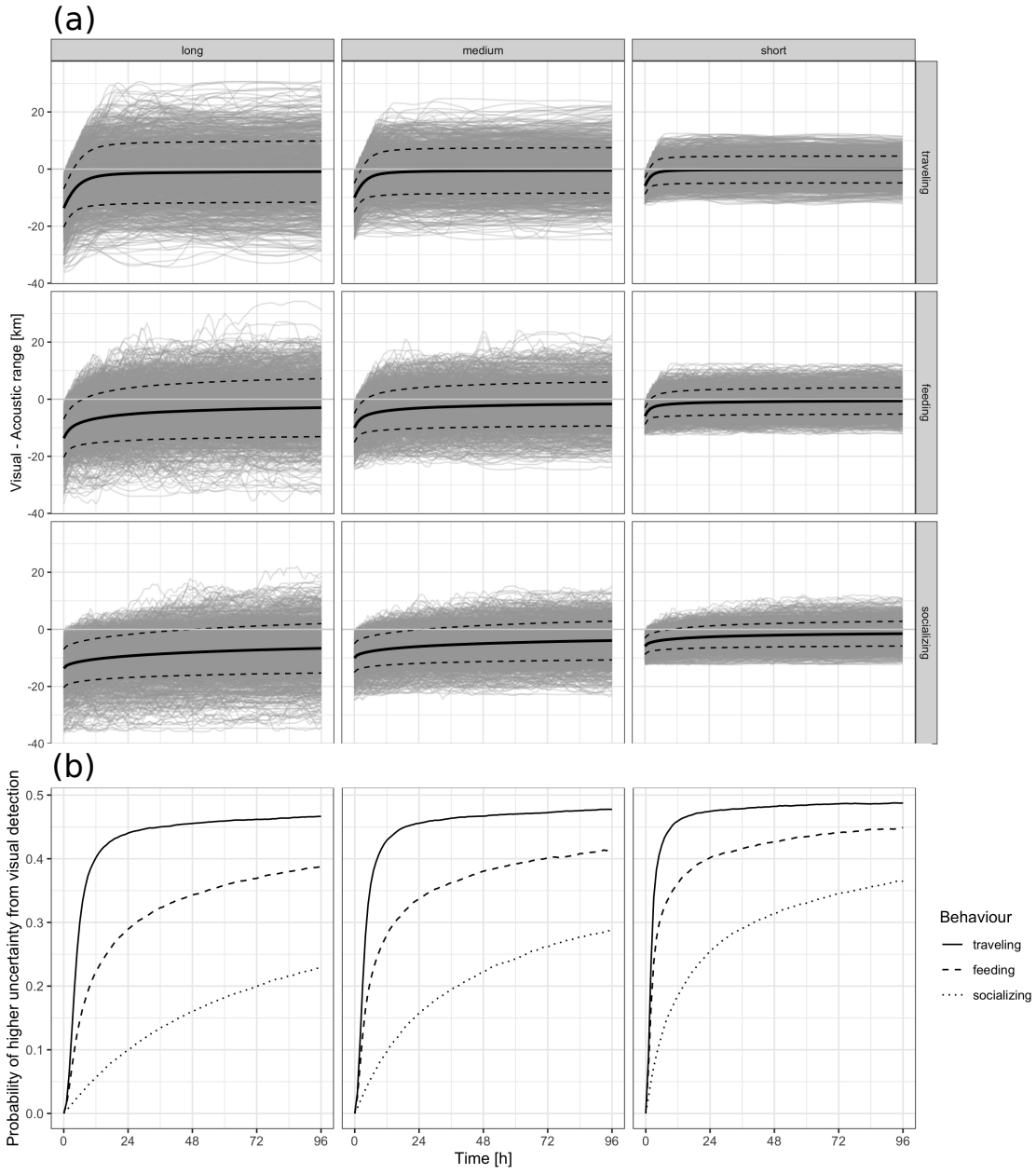

Figure 3.4: Differences in whale location uncertainties between visual and acoustic detection methods over the 96 h model period. The columns indicate acoustic detection range parameterizations (long-, medium-, and short- range). In panel (a), rows show the modeled movement behaviors (traveling, feeding, and socializing) and each dark grey solid line represents the range difference time series for a single simulated track (n=100,000). The solid and dashed black lines show the average and standard deviation of the range differences, respectively. The zero-difference line is emphasized in light grey. Panel (b) shows the probability of obtaining greater whale location uncertainty from a visual detection versus an acoustic detection.

days (e.g., *Baumgartner and Mate*, 2005).

In most cases, our study demonstrates that whale movement obfuscates the initial differences in uncertainty between visual and acoustic detection methods such that the two provide equally uncertain estimates of whale location on dynamic management timescales. This is perhaps not surprising given that the spatial extent of daily right whale movement ($\sim$80 km d^{-1}; *Baumgartner and Mate*, 2005) is of the same order as the maximum acoustic detection range ($\sim$30 km radius; *Laurinolli et al.*, 2003, Chapter 2). The rate and extent of convergence between location uncertainties from visual and acoustic detections are governed by the acoustic detection range and the type of movement behavior. Shorter detection ranges and greater displacement-movement behaviors lead to faster convergence.

A simple concept that emerges from our analyses is that an acoustically detected whale is just as likely to move toward the reported position as it is to move away. In contrast, a visually detected whale will almost certainly move away from the reported position over time. This appears to explain the more rapid expansion of location uncertainties for visually versus acoustically detected whales over the $\sim$24 h period following the initial detection. From a management perspective, it also appears to demonstrate the folly of considering right whale detections as static points on a map instead of as location estimates that have rapidly expanding uncertainty over time.

Our analysis focuses on the detection information used to trigger dynamic management strategies. The specifics of these strategies are beyond the scope of this paper, but our movement simulations provide some insights into which general strategies may be most effective. Dynamic management is only successful if the whale that triggers a response remains within the managed space over a time scale that is sufficient to allow risk mitigation to be implemented. Thus, successful risk-management strategies must incorporate the rapid expansion in location uncertainties if the elected strategy is to be effective. Focusing on small areas (e.g., $\leq$5 km radius) is demonstrably illogical. This is perhaps best illustrated in the left-most column of Figure 3.5, where there is only a maximum 50% chance that a whale will remain within the 5 km radius management area for a $\sim$24 h period. Unless there is considerable (e.g., environmental or behavioral) reason to believe the whales will remain within, or frequently revisit, a small area such as above, or management measures are implemented near-instantaneously, it is unlikely that such management measures will prove effective. Similarly, spatial dynamic management in migratory corridors where

whales are persistently traveling is unlikely to be successful when reliant on either visual or acoustic detection methods given the extent of location uncertainty that arises from whale movement. For example, one could implement a protective area of 25 km radius around a detection and have a $\sim$10% chance that a traveling whale remains within that area after $\sim$24 h (Figure 3.5). Seasonal management of larger areas would likely be more effective in such regions.

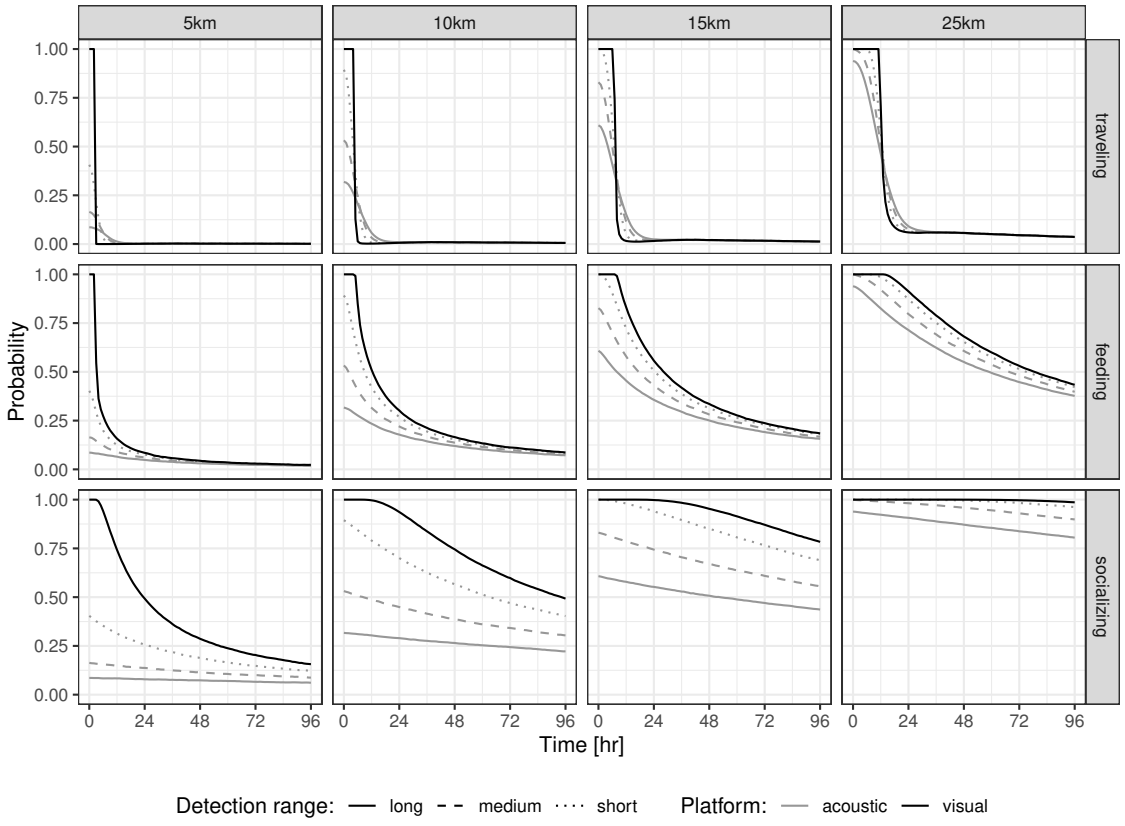

Figure 3.5: The probability a right whale detected acoustically or visually in a given behavioral state was within a given radius of the reported position over the 96 h model period. Columns indicate radii about the reported position (5, 10, 15, and 25 km) used in the probability calculation. Rows show the modeled movement behaviors (traveling, feeding, and socializing).

Dynamic management is likely to be most effective when applied to large ($>$10 km radius) areas dominated by feeding or socializing. Acoustic and visual detections provide similar information in those conditions, though acoustic detections have higher uncertainty when detection ranges are long, such as in deep waters ($>$100 m) with low ambient noise

levels (e.g., *Laurinolli et al.*, 2003). Areas that have been monitored using near real-time passive acoustics, including south of Cape Cod, the Great South Channel, the Boston shipping lanes, Roseway Basin, and the southern Gulf of St Lawrence are more likely to fall into the short- to medium-range detection scenarios (e.g., *Tennessen and Parks*, 2016).

We emphasize that this modeling study is not an attempt to faithfully depict reality. Rather, it attempts to provoke a critical reflection on dynamic management strategies and the data used to trigger them. We rely upon several simplifying assumptions to model uncertainty in reported whale position, especially for acoustically detected whales. Whale movement is a complex behavior mediated by a wide array of poorly constrained factors. The model we used here is greatly simplified. It does not, for example, attempt to include the influence of any physical (e.g., hydrodynamic conditions, water temperature, stratification, depth), biological (e.g., conspecifics, prey) or anthropogenic (e.g., shipping) factors on whale movement. However, we intentionally chose parameterizations of movement behaviors and acoustic detection ranges that would allow us to capture realistic extremes of location uncertainty; more complicated movement behaviors or the selection of a different acoustic detection range parameterization should produce location uncertainties that fall within these extremes, and therefore the conclusions of our study would remain the same.

This work only considers a whale once it has been detected; comparing acoustic versus visual detectability is beyond the scope of this study (see *Clark et al.* 2010 for such a study). This work also only applies to single whales, as near real-time acoustic density estimation of ephemerally vocalizing species from a single-hydrophone platform is not currently feasible. The thresholds used to characterize the convergence between visual and acoustic location uncertainties are somewhat subjective because there is no established method for quantifying acceptable uncertainty in data used for management purposes. We have attempted to address that subjectivity by providing multiple metrics and displaying the results in a variety of different ways and invite readers to draw their own conclusions.

We encourage further studies that focus on constraining the major sources of uncertainty mentioned here: variability in behavioral state and acoustic detection range. Whale behavior studies are limited and insufficient to construct substantiated behavioral budgets across habitats, seasons, and demographics; these budgets are essential for effective management (*Kenney et al.*, 2001). Efforts are underway to constrain acoustic detection range for near real-time PAM platforms, but this, as with movement behavior, is difficult to

constrain as it varies widely across the time and space domains within which right whales are known to occur. We also urge the research and management communities to measure compliance with dynamic management efforts and to quantify the effective risk reduction associated with these efforts. Furthermore, it is essential that management strategies be developed in a transparent, scientifically supported manner so that they can be understood, evaluated and improved upon by affected industries, researchers, and the general public.

Our analyses demonstrate the equivalence of acoustic and visual detection information in a range of conditions and provide compelling evidence that near real-time acoustic detections are relevant and useable for dynamic risk management. We suggest that the most effective dynamic management strategies would cover large areas, be fully implemented quickly, and target habitats where right whales are typically engaged in low-displacement behaviors (e.g., toward the bottom-right of Figure 3.5). In such circumstances, visual and acoustic detection methods can be used interchangeably. Many such areas are covered occasionally, at best, by visual surveys and could stand to gain tremendously from the efficiency and persistence of near real-time PAM from autonomous platforms.

3.6 Acknowledgements

We are grateful to Moira Brown, Delphine Durette-Morin, Meg Carr, Marcia Pearson, Kim Davies, Keith Thompson and Christoph Renkl for helpful feedback and discussions. HDJ was supported by a Vanier Canada Graduate Fellowship, Killam Predoctoral Scholarship, Nova Scotia Graduate Research Scholarship, and Dalhousie University Presidents Award.

CHAPTER 4

WHALEMAP: A TOOL TO COLLATE AND DISPLAY WHALE SURVEY RESULTS IN NEAR REAL-TIME

4.1 Statement of Need

Baleen whales of the Northwest Atlantic live in a highly urbanized ocean. Their recovery from commercial whaling is impeded by anthropogenic risks from ocean industry, pollution, and climate change. Effective research, conservation and risk-reduction action requires near real-time knowledge of whale distribution measured using various methods including visual surveys from vessels or planes or acoustic surveys from autonomous platforms. The rapid collation and dissemination of whale detections and survey effort is critical but challenging given the number and variety of survey organizations and methodologies at work along the east coast of the US and Canada. There are long term databases for whale survey data, such as that maintained by the North Atlantic Right Whale Consortium (narwc.org), and crowd-source reporting tools (e.g., Whale Alert) but 'WhaleMap' is the only dedicated system specifically designed to collate and display all available near real-time whale detections and survey effort. Use cases vary widely. For example, 'WhaleMap' is currently used by: government managers to design and implement risk-mitigation strategies, members of military or industry to plan safe operations, researchers to coordinate survey efforts and explore patterns in whale distribution, and members of the general public to learn about and follow along with whale conservation activities.

'WhaleMap' was designed with several specific goals:

- Incorporate whale detection and survey effort from all survey methods in near

real-time

- Allow survey teams to easily contribute and retain complete control over their data
- Provide the latest data in an accurate, user-friendly, and publicly accessible format
- Operate transparently using open-source tools and with limited supervision

Critically, 'WhaleMap' does not:

- Perform any quality-control, or take responsibility for the veracity of information contributed
- Provide a long-term database for survey results
- Allow access to raw or processed data without approval from the data originator

4.2 System

The 'WhaleMap' system workflow can be separated into data processing and visualization components (Figure 4.1). The following provides a brief overview of each. Additional details as well as specific references to all software used is available in the source code documentation (available at `https://github.com/hansenjohnson/WhaleMap`)

4.2.1 Data processing

Survey teams provide 'WhaleMap' access to a remote repository of their choice (e.g., Google Drive, Dropbox) where they upload their survey data. The 'WhaleMap' curator writes a custom script to extract the detection and effort data from each survey team and convert it to a common 'WhaleMap' format. This method eases the burden on the survey teams by allowing any team to submit data in nearly any format, provided the format is consistent and well-documented. This is essential for rapid data collection, as survey teams in the field typically lack the time and resources to reformat their data.

A scheduled job regularly clones the data from the remote repositories onto the 'WhaleMap' server and uses a makefile to dynamically and efficiently process the data from each platform and coerce it into a common format. Formatting errors in a remote data repository are automatically flagged and the contributor is notified. This ensures that any changes

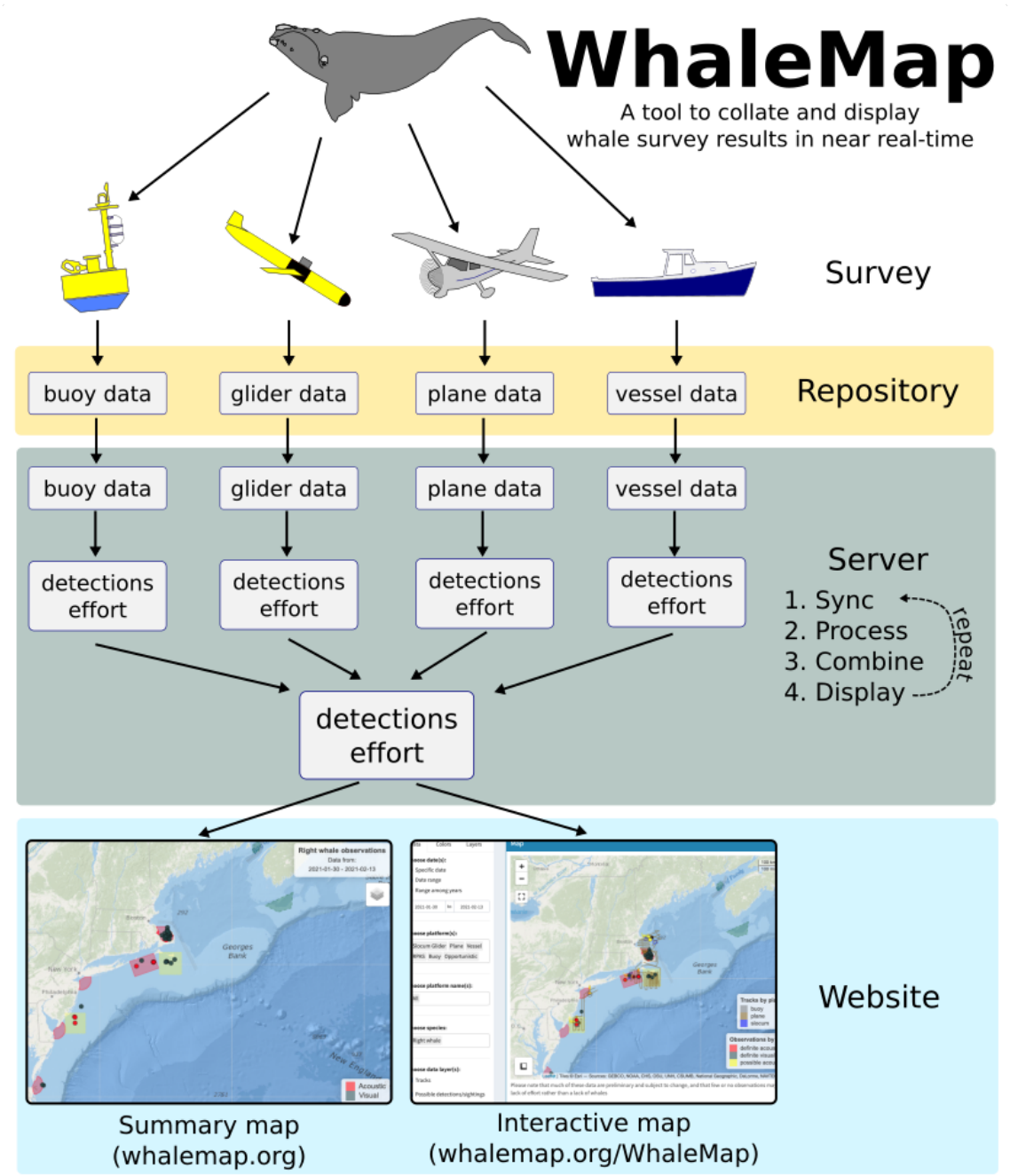

Figure 4.1: Conceptual overview of WhaleMap data processing and display

to the raw survey data quickly propagate through the entire system, which allows survey teams to retain complete control of their data and perform quality control as needed. It also guarantees that the 'WhaleMap' always contains the latest available information.

4.2.2 Visualization

Once the survey data are processed, they are visualized using two different methods. The first is the construction of self-contained HTML summary maps containing sufficient information to satisfy most casual viewers (typically the last 14-days of survey results). These can be conveniently embedded in various webpages (e.g., whalemap.org) and browsed without requiring server-side processing. These maps are dynamically regenerated as the final step in the data processing workflow, so they always contain the latest available information. The second visualization method is an interactive online application (whalemap.org/whalemap). This provides users with numerous tools with which to filter the latest processed data. The selected data are displayed in several formats including an interactive map, interactive timeseries plot, and table of summary statistics.

4.3 Conclusions

Since its launch in 2018, 'WhaleMap' has been constantly refined and optimized to better serve the overall goal of providing a common source for all near real-time whale survey data in the Northwest Atlantic. It has demonstrably improved conservation outcomes for endangered whales in this region by optimizing research activities, facilitating dynamic risk-mitigation measures, and engaging with the ocean industry and the public. 'WhaleMap' has also already been cited in several scientific publications (e.g., *Gervaise et al.*, 2021; *Koubrak et al.*, 2021; *Baumgartner et al.*, 2020; *Kowarski et al.*, 2020). We are not aware of any equivalent software in existence. It is our hope that 'WhaleMap' continues to serve the conservation community in perpetuity, and that this system can be readily adapted to benefit other regions facing similar conservation challenges.

4.4 Acknowledgements

We gratefully acknowledge the support of Pamela Emery, Stephanie Ratelle, Angelia Vanderlaan, Hilary Moors-Murphy and many other colleagues at Fisheries and Oceans

Canada, as well as Tim Cole, Elizabeth Josephson, Leah Crowe, Christin Khan, Danielle Cholewiak and others at the NOAA Northeast Fisheries Science Center. This work would not have been possible without them. We also thank Mark Baumgartner, Kim Davies, and members of the Taggart lab for advice and helpful conversations. We are indebted to the fantastic community of open source developers that constructed many of the tools on which 'WhaleMap' relies. These are referenced in detail in the system documentation. Finally, we give our most sincere thanks to the many survey teams and numerous agencies that continue to place their trust in this system and praise their tireless efforts to protect these vulnerable species. Supporting funds generously provided by Fisheries and Oceans Canada and the Natural Sciences and Engineering Research Council of Canada.

CHAPTER 5

RIGHT WHALE HABITAT IN THE SOUTHERN GULF OF ST. LAWRENCE

5.1 Abstract

The distribution of North Atlantic right whales has shifted in the last decade, perhaps best exemplified by the decreased use of several well-characterized habitats in the Gulf of Maine and Scotian Shelf and an increased occupancy of a relatively unknown habitat in the southern Gulf of St. Lawrence (GSL). The goal of this study was to characterize right whale feeding habitat in the GSL region. We conducted opportunistic oceanographic sampling during daylight hours from visual survey vessels in the presence and absence of right whales in July and August over three years (2017 - 2019). Oceanographic stations (n = 115) were typically comprised of a depth-integrated oblique ring net tow that was preceded and followed by a vertical profile with a conductivity-temperature-depth (CTD) instrument and optical plankton counter (OPC; 2018/2019 only). Small copepods (e.g., *Centropages* spp., *Psuedocalanus* spp.) were numerically dominant at all stations. Of the *Calanus* species, *C. finmarchicus* was typically most abundant but *C. hyperboreus* comprised the majority of total *Calanus* biomass based on their abundance and relative body size. Relevant physical and biological variables were derived at each station and logistic regressions were used to quantify right whale habitat associations. Results suggested a higher probability of right whale presence was associated with a thick bottom mixed layer comprised of relatively warm saline water, and abundant patches of late-stage *Calanus* near the seafloor. These results offer insights into the quantity of the prey and quality of the GSL as a right whale foraging habitat and the associated implications for right whale recovery.

5.2 Introduction

North Atlantic right whales (*Eubalaena glacialis*; hereafter 'right whales') satisfy their energetic demands by ram filter feeding on small zooplankton. Their fine baleen imposes a limit on the smallest prey items that they can ingest and is thought to have a filtration efficiency similar to a 333-micron mesh net (*Mayo et al.*, 2001). The hydrodynamic drag generated by baleen when the whale opens its mouth imposes energetic limits on swimming speed (*van der Hoop et al.*, 2019). Slow swimming speeds while foraging ($\sim$1.1 m s^{-1}; *van der Hoop et al.*, 2019) allow large, mobile zooplankton to evade capture (e.g., *Fleminger and Clutter*, 1965). Thus, right whales are optimized to feed on a narrow size range of zooplankton (nominally 0.5 - 10 mm; *Mayo et al.*, 2001) and rely entirely on external bio-physical mechanisms to aggregate these zooplankton into dense, energy-rich patches.

Zooplankton sampling in the presence of feeding right whales in numerous habitats in the Gulf of Maine and Scotian Shelf provides compelling evidence that right whales target superabundant patches (typically in excess of 103 copepods m^{-3} measured as water-column integrated abundance) of late stage (stage 4 or 5 copepodites; C4, C5) *Calanus finmarchicus* (*Murison and Gaskin*, 1989; *Beardsley et al.*, 1996; *Baumgartner et al.*, 2003b; *Baumgartner and Mate*, 2003; *Baumgartner et al.*, 2017; *Baumgartner and Mate*, 2005). These zooplankton are likely desirable prey because they contain energy-rich lipid reserves and are highly susceptible to physical aggregation mechanisms, particularly while in a dormant life-history stage known as diapause (*Baumgartner and Tarrant*, 2017). For example, process studies in the Bay of Fundy and Roseway Basin show that dense layers are formed via the interaction of copepod behavior and environmental conditions, such as tidal advection, bathymetric constraints, and the bottom mixed layer (*Baumgartner et al.*, 2003b; *Davies et al.*, 2014).

Despite their apparent proclivity for late-stage *C. finmarchicus* , right whales are capable of feeding on other taxa. They have been observed skim feeding on surface patches dominated by smaller calanoid copepods, namely *Psuedocalanus* spp. and *Centropages* spp., in Cape Cod Bay during winter (*Mayo and Marx*, 1989). Records from commercial whaling off the coast of Scotland suggest that right whales were foraging on euphausiids (*Collett*, 1909). Southern right whales (*Eubalaena australis*) have also been observed surface feeding at fast swimming speeds ($>$7 knots) on Antarctic krill (*Euphausia superba*

Hamner et al., 1988). There is anecdotal evidence of right whales feeding near abundant patches of hydrozoans and decapod larvae (in *Mayo et al.*, 2001). Though there is little direct evidence, presumably right whales could also target Arctic *Calanus* species, namely *Calanus glacialis* and *Calanus hyperboreus*. These are large energy-rich copepods that are abundant at higher latitudes within the historical right whale range (*Monsarrat et al.*, 2015) and are preyed upon by bowhead whales (*Balaena mysticetus*) using a similar foraging mechanism (e.g., *Fortune et al.*, 2020).

Right whale distribution began to shift around 2010. Occurrence declined in most of the known habitats in the Gulf of Maine (*Davis et al.*, 2017; *Davies et al.*, 2019) with the notable exception of Cape Cod Bay where occurrence has increased (*Mayo et al.*, 2018). There is evidence that these shifts broadly coincide with climate-induced changes to ocean circulation that reduced the availability of *C. finmarchicus* in the Gulf of Maine (Record et al. 2019), as well as with anomalously low climatological *Calanus* spp. abundance in most regions of the NW Atlantic (*Sorochan et al.*, 2019). The reduction in *Calanus* has been linked to low calving rates (*Meyer-Gutbrod et al.*, 2021). The shift in right whale distribution led to increased whale occurrence in regions with unmitigated risks from vessel strike and fishing gear entanglement, such as the southern Gulf of St. Lawrence (GSL). The combined effect of the reduction in calving rates and increased risk exposure has been proposed as the major barrier to species recovery (*Meyer-Gutbrod et al.*, 2021), though these issues are likely further exacerbated and complicated by additional stressors (*Moore et al.*, 2021).

Right whales have been sporadically observed in the GSL for many years (*Brown et al.*, 2009), but their occurrence in the GSL began to increase substantially beginning in about 2015 (*Simard et al.*, 2019). The increase in whale abundance and unmitigated risks from vessel strikes and fishing gear entanglements precipitated catastrophic mortality events in 2017 and 2019 in which a total of 21 right whales ($\sim$6% of the current population) were found dead in the GSL (*Pettis et al.*, 2021). These events initiated unprecedented surveillance and risk mitigation efforts in the region. From 2017 through 2019 nearly the same $\sim$40% of the population, or $\sim$140 individuals, have been documented in the GSL each summer (*Crowe et al.*, 2021). The majority of the whale detections occur in the southern portion of the GSL, specifically the section of continental shelf bounded by deep Laurentian Channel to the north, Prince Edward Island to the south, the Magdalen

islands to the east and New Brunswick/Quebec to the west. Right whale detections can occur throughout this region, though tend to concentrate in the western portion (Chapter 4; *Johnson et al.*, 2021).

Several studies have made efforts to characterize aspects of right whale foraging habitat in the GSL. *Plourde et al.* (2019) developed a spatial climatology of *Calanus* in Canadian waters that successfully identified known habitats (e.g., Roseway Basin) as well as the southern GSL as potentially suitable habitats. *Sorochan et al.* (2019) characterized interannual variation in several regional timeseries of *Calanus* abundance and discovered negative anomalies in many subregions, including in the southern GSL, over the last ten years. They also found that the climatological abundance in the southern GSL was greatest at the Shediac Valley station, in relatively close proximity to the approximate center of the distribution of right whale detections. *Brennan et al.* (2019) combined a spatial climatology with a dynamic transport model to explore mechanisms of *Calanus* transport and availability, as well as to improve estimates of *Calanus* spatial distribution. They found that advection from upstream sources in the western GSL was likely a major contributor of *Calanus* abundance in the southern GSL region. Further extension of this work contrasted *Calanus* availability in warm versus cold years, with cold years associated with circulation patterns that increased *Calanus* retention within the southern GSL (*Brennan et al.*, 2021). *Gavrilchuk et al.* (2021) improved upon the right whale bioenergetic model developed by *Plourde et al.* (2019) to show evidence of highly variable habitat suitability in the southern GSL, with generally declining habitat quality since 2014. They suggested that biomass in the southern GSL may be insufficient to support the energetic costs of reproduction, which in turn may contribute to the recent decline in calving rates.

All of these studies made use of climatological observations to inform their modeling or empirical efforts. While climatological *Calanus* abundances can be used to predict right whale presence (*Pendleton et al.*, 2009), broadscale background zooplankton sampling does not necessarily reflect prey available to right whales (*Baumgartner et al.*, 2007). Further, much of these climatological data were derived from depth integrated net samples which do not provide information on the vertical distribution of *Calanus*. Right whales are known to target thin layers of dense *Calanus*, and abundances taken in close proximity to a feeding right whale can be several orders of magnitude greater than those collected in a right whale habitat without whales present (*Baumgartner et al.*, 2003b). In this study

we conducted the first oceanographic sampling in close proximity to right whales in the southern GSL to address the following questions: 1) What is the primary prey of right whales in the Gulf of St. Lawrence?, and 2) What are the temporal and spatial relationships among right whale presence, prey, and environmental conditions?

5.3 Methods

5.3.1 Site description

Oceanographic sampling and visual survey efforts were conducted in the southern Gulf of St. Lawrence (GSL) in July and August each year from 2017 through 2019. A 15-m motor yacht, *M/V Shelagh I*, was used in 2017 and a 21-m fishing vessel, *F/V Jean-Denis Martin*, was used in 2018 and 2019. The summertime ocean circulation of the southern GSL is dominated by the Gaspé Current (GC), a buoyancy driven, unstable coastal jet that contributes to the mean eastward component of the cyclonic circulation of the GSL (*Sheng*, 2001). Upon reaching the tip of Gaspé, the GC can either remain attached to the coast and turn south into the southern GSL, or it can detach from the coast and continue along the southern margin of the Laurentian Channel. These dynamics are primarily influenced by freshwater runoff from the St. Lawrence Estuary and wind events. Typically, higher runoff and weaker winds in spring (April-June) favor the coastal attachment of the GC, which contributes to stronger southward flow into the southern GSL (*Brennan et al.*, 2021). Bathymetry in the southern GSL region is relatively shallow (75 - 150m) and uniform with the notable exception of the Shediac Valley, which begins at the shelf break and shoals southward roughly in parallel with the western coastline (*Amante and Eakins*, 2009, Figure 5.1).

5.3.2 Data collection

5.3.2.1 Right whale surveys

The primary objective of each research cruise was to conduct photographic identification (hereafter 'photo-ID') surveys of right whales in the southern GSL. Vessel-based right whale photo-ID survey methodology has been developed and refined over nearly 40 years (*Brown et al.*, 2007). Contrary to conventional line-transect sampling, right whale photo-ID surveys do not provide systematic coverage of a survey region. Instead, the survey platform seeks aggregations of right whales and attempts to photograph identifiable callosity (*Payne*

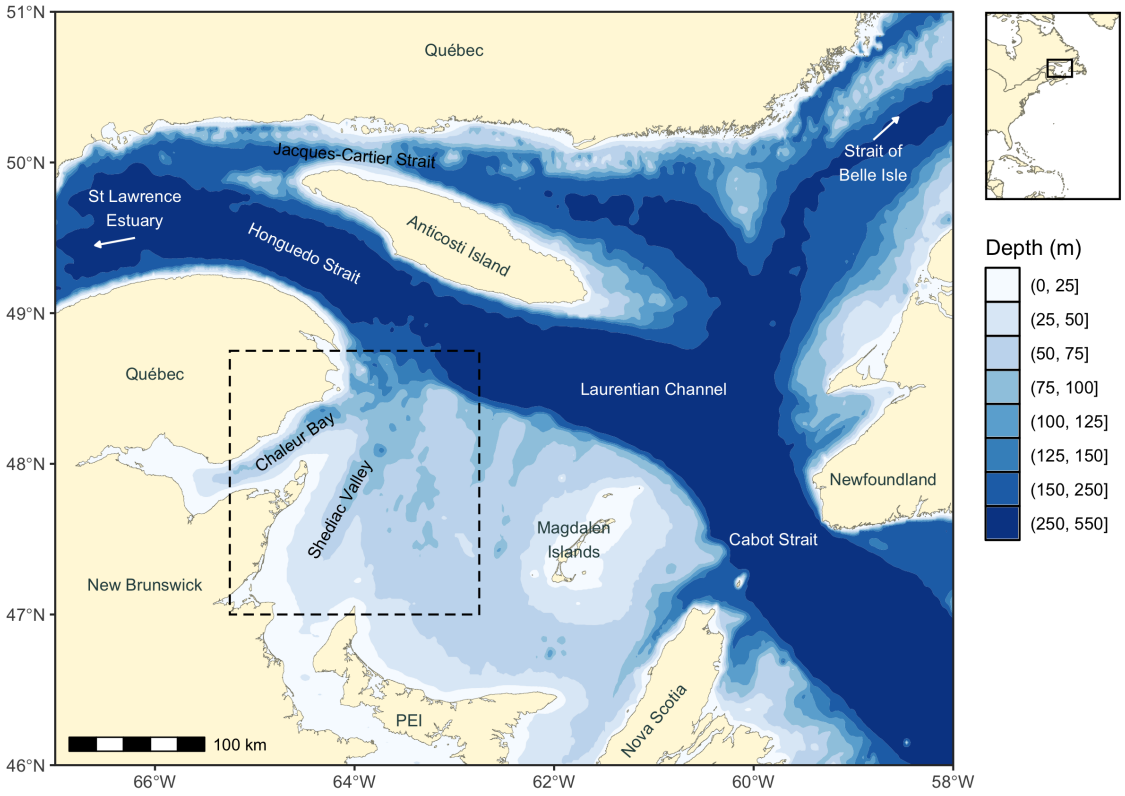

Figure 5.1: Study region (dashed line) in the southern Gulf of St. Lawrence, Canada.

and Dorsey, 1983) and/or scarring (*Kraus*, 1990) patterns of each individual. These photos are submitted into the NARWC Catalog (*Hamilton et al.*, 2007) for subsequent analyses. In addition to photographic documentation, the team also collected biological samples, such as biopsies and feces, and provided disentanglement support.

5.3.2.2 Oceanographic sampling

Oceanographic surveys were conducted on an opportunistic, non-interference basis with the visual surveys and in favorable weather conditions (less than Beaufort 7). A sampling station was conducted during morning, noon, and evening each survey day when conditions allowed. The data collected at each station changed slightly after 2017 when we began using a larger vessel with enhanced oceanographic sampling capabilities.

In 2017 a sampling station was comprised of a CTD cast to measure water column conductivity and temperature followed by a net tow to sample the depth-integrated zooplankton biomass, abundance, and community composition. The CTD casts were conducted with a Seabird SBE 37 MicroCat CTD programmed to sample at 0.5 Hz. Zooplankton were collected from vertical hauls with a 0.75-m diameter ring net with 333-micron mesh size. A depressor weight was fitted to the cod end to maintain the vertical orientation of the net during the tow. A flow meter was positioned off center of the net opening and used to record volume filtered. The CTD was also attached in-line with the net above the bridle to record the depth-time series of the haul. A Vemco V16 pressure transmitter was attached to the CTD and monitored from the vessel with a VR100 receiver to measure both the CTD and net depth in real time without the use of a conductive cable.

Sampling in 2018 and 2019 was expanded to include the use of a profiling Optical Plankton Counter (OPC; Focal Technologies Inc.) and Seabird-19 CTD housed in an aluminum cage. Each station was comprised of a full depth oblique net tow that was immediately preceded and followed by a vertical cage profile. Net tows were conducted using a 1-m diameter ring net with 200-micron mesh. A depressor weight was fitted to the net bridle to maintain the horizontal orientation of the net opening during the oblique tow. For all net tows, vertical (2017) or oblique (2018-19), efforts were made to achieve a maximum net depth within $\sim$10 m of the sea floor. The cage was lowered vertically through the water column at $\sim$0.5 m s^{-1} to a depth of $\sim$5 m above the sea floor. The same Vemco system from 2017 was used to monitor the cage and net depth in real time, as a conductive cable was not available. Either a Seabird SBE 37 or RBR Concerto was

attached in-line with the net above the bridle to record the depth-time series of the haul. Net tows were achieved at every station, but the operational limits for the cage were substantially lower than that of the net, so cage profiles were not conducted at several stations.

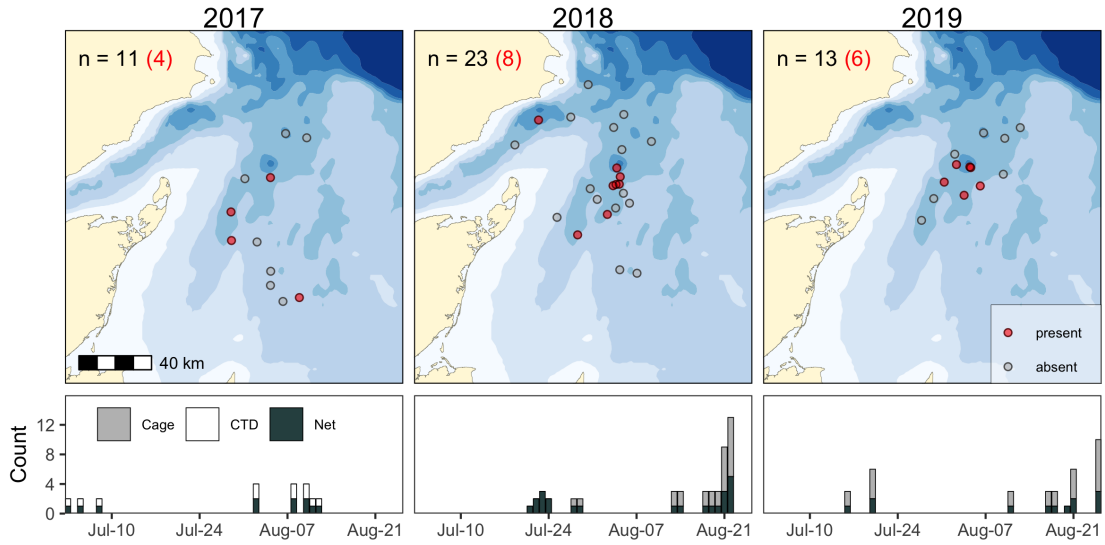

Figure 5.2: Spatial and temporal distribution of sampling effort in 2017 (left column), 2018 (center column), and 2019 (right column). The red and grey dots on the maps indicate stations where whales were present or absent, respectively. The total number of stations each year as well as the number with whale presence is indicated in the upper left of each map panel. The lower panels show the count of CTD (white), Cage (OPC/CTD; grey), and net (black) sampling events each day.

5.3.3 Data processing

5.3.3.1 Whale occurrence

Whales were considered present if at least 1 right whale was photographed within +/- 0.5 km of the average position of an oceanographic station and within +/- 1 h of the initiation of sampling. These minimum distance and time thresholds were chosen to compensate for the typical time-space mismatch between the visual and oceanographic surveys. They reflect the finest scale sampling that could be consistently achieved with our study design. Statistical analyses were repeated using several different distance and time thresholds to evaluate the sensitivity of our results to the definition of right whale presence (Appendix C). Whales were considered absent from a station if survey effort was recorded but no whales

were sighted within +/- 5 km of the station or +/- 5 h of the initiation of oceanographic sampling. These higher minimum thresholds were chosen to ensure whale absence at the time of sampling. Stations without recorded survey effort, or with whales sighted at intermediate distances and/or times, were omitted from subsequent presence/absence analyses.

5.3.3.2 Zooplankton

Zooplankton samples from all tows were removed from the net and filtered through a 333-micron sieve. In samples with sufficient biomass (more than $\sim$50 g), a subsample was collected and immediately frozen in liquid nitrogen. The total wet weight of these samples was corrected by adding the wet weight of an average subsample. The total abundance was not corrected, as we did not measure species-specific abundance or biomass of the cryovial samples. The remaining sample was preserved in 4% formalin solution buffered with calcium carbonate. After each cruise, individual zooplankton in representative aliquots of each sample were counted and identified to lowest possible taxa and life cycle stage. Samples were then filtered and weighed wet to determine bulk biomass. All zooplankton processing methods were consistent with those used for the Atlantic Zonal Monitoring Program (AZMP), which are described in greater detail in (*Mitchell et al.*, 2002). The 128 taxa that were identified from net samples were reclassified into 16 groups summarized in Table 5.1. Classifications were performed using the World Register of Marine Species (WoRMS; *Horton et al.*, 2021) and the package taxize (*Chamberlain and Szcs*, 2013) in R (*R Core Team*, 2020). Net tows that did not traverse at least 85% of the water column, as inferred from the CTD attached to the net bridle, were excluded from subsequent analyses. Biomasses of late-stage *C. finmarchicus* , *C. hyperboreus* and *C. glacialis* were estimated from net-derived abundances using average individual dry weights previously measured in the region (as in *Sorochan et al.*, 2019). A conversion factor of 297 μg ind^{-1} was used for both *C. finmarchicus* and *C. glacialis*, while 1725 μg ind^{-1} was used for *C. hyperboreus* (*Plourde et al.*, 2019).

5.3.3.3 CTD

Instrument-specific calibrations were applied to convert raw CTD data into common engineering units of pressure (decibar), temperature (Celsius) and conductivity (Siemens per meter). The downcast portion of each CTD profile was manually selected. Outliers

Table 5.1: Zooplankton classification

Group	Definition	Examples
Amphipods/Mysids	Members of the superorder *Peracarida*	*Themisto* spp., *Mysis* spp.
C finmarchicus (early)	Early stage (C1-C3) copepodites	NA
C finmarchicus (late)	Late stage (C4-C5) copepodites and adults	NA
C glacialis (early)	Early stage (C1-C3) copepodites	NA
C glacialis (late)	Late stage (C4-C5) copepodites and adults	NA
C hyperboreus (early)	Early stage (C1-C3) copepodites	NA
C hyperboreus (late)	Late stage (C4-C5) copepodites and adults	NA
Cladocerans	Members of the superorder *Cladocera*	*Evadne* spp., *Podon* spp.
Non-calanoid copepods	Members of the subclass *Copepoda*, but not of the order *Calanoida*	*Oithona* spp., *Triconia* spp.
Small calanoid copepods	Members of the order *Calanoida* (excluding *Calanus* spp.)	*Centropages* spp., *Psuedocalanus* spp.
Decapods	Members of the order *Decapoda*	*Chionoecetes opilio*, *Homarus americanus*
Fish	Members of the superclass *Pices*	*Gadus* spp., *Urophycis* spp.
Jellies	Members of the phyla *Ctenophora* and *Cnidaria*	*Aglantha digitale*, *Cyanea capillata*
Krill	Members of the family *Euphausiidae*	*Thysanoessa* spp., *Meganyctiphanes norvegica*
Molluscs	Members of the phylum *Mollusca*	*Limacina* spp.,
Worms	Members of the phyla *Chaetognatha* and *Annelida*	*Parasagitta* spp.

were removed using a median filter with a 51-point window. The data were then smoothed by fitting a Local Polynomial Regression (LOESS) curve with a span of 0.12. Smoothed downcasts were visually compared to raw data to confirm that only outliers and depth inversions were rejected. Data were averaged in 1-m depth bins. Both casts at the same station were averaged to compute a single downcast at each station. In rare cases where dedicated CTD or cage profiles could not be conducted, the same data processing was applied to compute a water column profile from the CTD attached to the net bridle. CTD casts that did not traverse at least 85% of the water column were excluded from subsequent analyses. The surface mixed layer thickness was defined as the depth to the maximum buoyancy frequency, a metric indicative of the strength of stratification. The bottom mixed layer thickness was defined as the height from the maximum CTD depth to a density change of -0.05 kg m^{-3} (as in *Baumgartner et al.*, 2003b). All oceanographic calculations, including derivation of water column practical salinity (hereafter 'salinity'), potential density (kg m^{-3}; hereafter 'density') and buoyancy frequency, were computed using the oce package in R (*Kelley and Richards*, 2020).

5.3.3.4 Optical plankton counter

OPC data were processed using similar methods as those described by Baumgartner (2003). The downcast of each OPC profile was manually selected. Records containing extreme depths, depth inversions, slow descent rates ($<$0.3 m s^{-1}), or excessive light attenuance ($>$1800 digital counts) were removed. The volume filtered in each timestep was computed as the area of the OPC tunnel (0.02 m by 0.25 m) multiplied by the change in depth. Profiles were computed by summing the particles of a given size range in 5-m depth bins. Depth bins in which the volume filtered was less than 50% of the theoretical volume of the bin (i.e., area of the OPC x 5 m) were rejected. We estimated the wet weight, W_{wet} (mg), of the OPC-filtered particles using:

$$W_{wet} = \frac{4}{3}\pi \left(\frac{ESD}{2}\right)^3 p \tag{5.1}$$

where ESD is the equivalent spherical diameter of the particle (mm) measured by the OPC, and p is the particle density (mg m^{-3}) which we assumed was equal to 1 mg mm^{-3} (*Suthers et al.*, 2006; *Fortune et al.*, 2020). Biomass profiles were computed by dividing the sum of the mass of particles in each depth bin by the volume filtered. OPC casts that did not traverse at least 85% of the water column were excluded from subsequent analyses.

All processing was conducted using the opcr package in R (*Johnson*, 2021).

5.3.4 Logistic regression

Several physical and biological variables were derived for each station (Table 5.2). Bathymetric depth, derived from the ETOPO1 dataset (*Amante and Eakins*, 2009), was selected as right whales and/or *C. finmarchicus* have been associated with deep basins in the Bay of Fundy (*Murison and Gaskin*, 1989; *Michaud and Taggart*, 2011) and Roseway Basin (*Baumgartner et al.*, 2003b; *Davies et al.*, 2013). The standard deviation in the bathymetric depth within a 5 km radius of each station was used a proxy for bathymetric slope, which has been found to play a role in forming *Calanus* aggregations in Roseway Basin (Davies et al. 2013). The water density at the surface and bottom were chosen to characterize associations with water masses, specifically the Gaspé Current at the surface or the warm, saline Atlantic water at depth. Surface and bottom mixed layer thicknesses were included to evaluate the influence of the vertical structure of the water column. Biological metrics from both the net and OPC were used to resolve several aspects of *Calanus* availability. The 1 - 2.5 mm ESD size class in 5-m depth bins were used for OPC biomass measurements, as this size class best represented *Calanus* abundance (Appendix C). Stations from all years and months were combined to increase sample size. Separate logistic regressions were fit with each habitat variable as the independent variable and the series of whale presence/absence scores as the dependent variable to characterize the relationship between each habitat variable and the probability of whale presence.

All analyses were conducted in R using the oce, shiny (*Chang et al.*, 2020), and tidyverse (*Wickham et al.*, 2019) packages unless otherwise noted. Visualizations were created using the ggplot2 (*Wickham*, 2016), ggspatial (*Dunnington*, 2021), and patchwork (*Pedersen*, 2020) packages.

5.4 Results

5.4.1 Net

Depth-integrated zooplankton abundances derived from net sampling were highly variable. The samples tended to be numerically dominated by small copepods. Small calanoid copepods (e.g., *Psuedocalanus* spp., *Centropages* spp.; Table 5.1) were the most abundant known right whale prey. Median abundance of small calanoid copepods at whale present

stations was 374 ind m^{-3} (Q1-Q3: 57-1079 ind m^{-3}), which was 43% greater than the median abundance at whale absent stations (261 ind m^{-3}; Q1-Q3: 66-710 ind m^{-3}). Late-stage *C. finmarchicus* abundances were 78 ind m^{-3} (Q1-Q3: 43-208 ind m^{-3}) and 75 ind m^{-3} (Q1-Q3: 41-126 ind m^{-3}) at whale present and absent stations, respectively. The abundances of *C. hyperboreus* were of a similar magnitude, but median abundance at whale present stations (68 ind m^{-3}; Q1-Q3: 30-101 ind m^{-3}) exceeded abundance at whale absent stations (24 ind m^{-3}; Q1-Q3: 10-51 ind m^{-3}). *C. glacialis* were relatively rare, with abundances typically less than 10 ind m^{-3} (Figure 5.3a). Median biomass (total wet weight) was 0.47 g m^{-3} (Q1-Q3: 0.22 - 0.81 g m^{-3}) at whale present stations, which was nearly double the biomass at whale absent stations (0.23 g m^{-3}; Q1-Q3: 0.14-0.35 g m^{-3}; Figure 5.3b).

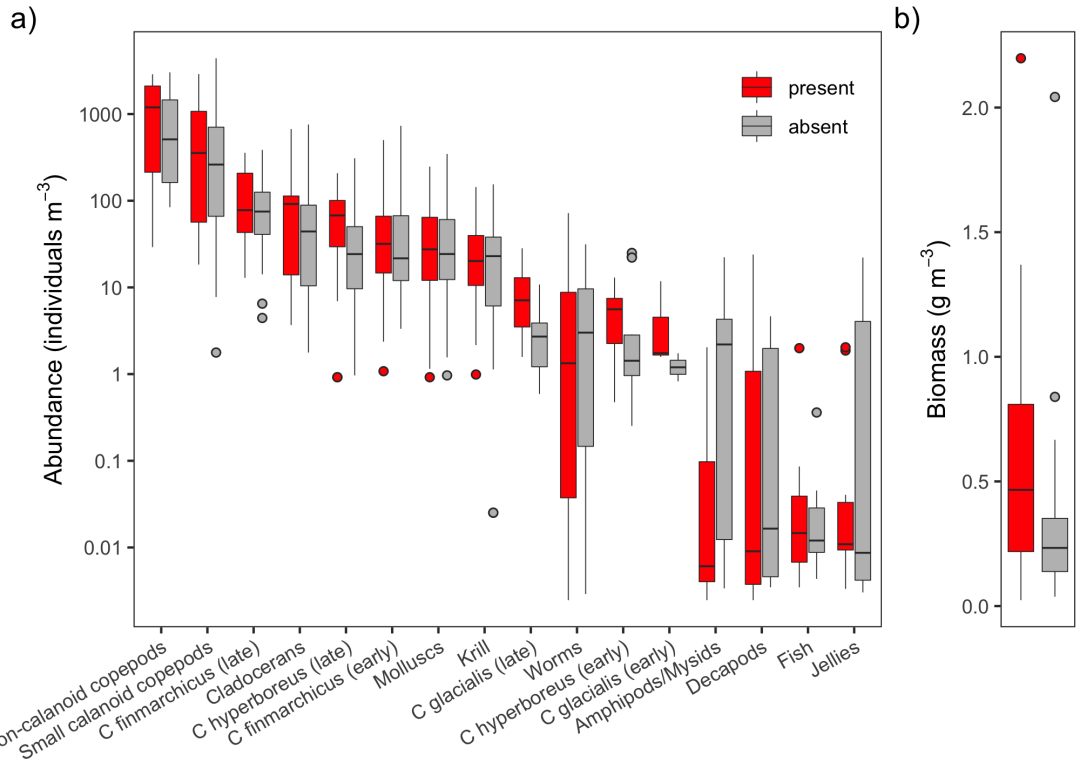

Figure 5.3: Panel a) shows the abundance of zooplankton group in the presence (red bars; n = 20) and absence (grey bars; n = 27) of right whales. Definitions of each of these zooplankton groups are provided in Table 1. Panel b) shows the biomass (total wet weight) of net contents (note that biomass was not available for one whale present station, so n = 19).

Small calanoid copepods (e.g., *Psuedocalanus* spp., *Centropages* spp.) comprised the greatest proportion of calanoid copepod abundance at all stations, followed by *C. finmarchicus*, *C. hyperboreus*, and *C. glacialis*. The proportions of each of these groups were indistinguishable between whale present and absent stations (Figure 5.4a). Conversion from abundance to biomass using individual-specific dry weights revealed that *C. hyperboreus* typically comprised the majority of calanoid biomass. The relative biomass contribution of *C. hyperboreus* was slightly ($\sim$10%) greater and substantially less variable at whale present stations than whale absent stations (Figure 5.4b). Biomass contributions by small copepods and *C. glacialis* were low ($\leq$ 5%). The contribution from *C. finmarchicus* was typically 15 - 30% at whale present stations compared to 15 - 50% at whale absent stations.

5.4.2 CTD and Optical Plankton Counter

Averaged OPC profiles revealed peaks in particle abundance near the surface (5 - 15m) and near the bottom (85 - 100m) in whale present stations (Figure 5.5a). Conversion to biomass and review of the size-frequency distribution of particles indicated that the near-surface peak was lower in biomass (Figure 5.5b) and driven by small ($<$1.5 ESD) particles (Figure 5.5c). In contrast, larger particles ($>$1.5 ESD) were much more abundant in the near-bottom peak (Figure 5.5c), which contributed to the relatively large biomass below 80m at whale present stations (Figure 5.5b). Comparison between the net and OPC revealed that the abundances of late-stage *C. finmarchicus* , *C. hyperboreus*, and *Calanus* were best represented by the 1 - 2, 1.5 - 3 and 1 - 3 mm ESD size classes, respectively (Appendix C). The CTD data revealed a three-layer system characterized by a variable and relatively warm, fresh surface layer, cold intermediate layer, and a stable warm, saline layer below $\sim$60 m. The highest OPC-derived particle biomass was associated with the deep layer (Figure 5.6).

5.4.3 Logistic regression

Depth and bottom density were significantly and positively associated with whale presence (Table 5.2). They were also highly correlated (Figure C.5). Bottom roughness was also significantly and positively associated with whale presence. Bottom mixed layer thickness was positively associated with right whales, such that whale presence was more likely with increasing thickness of the bottom mixed layer. Right whale presence was positively

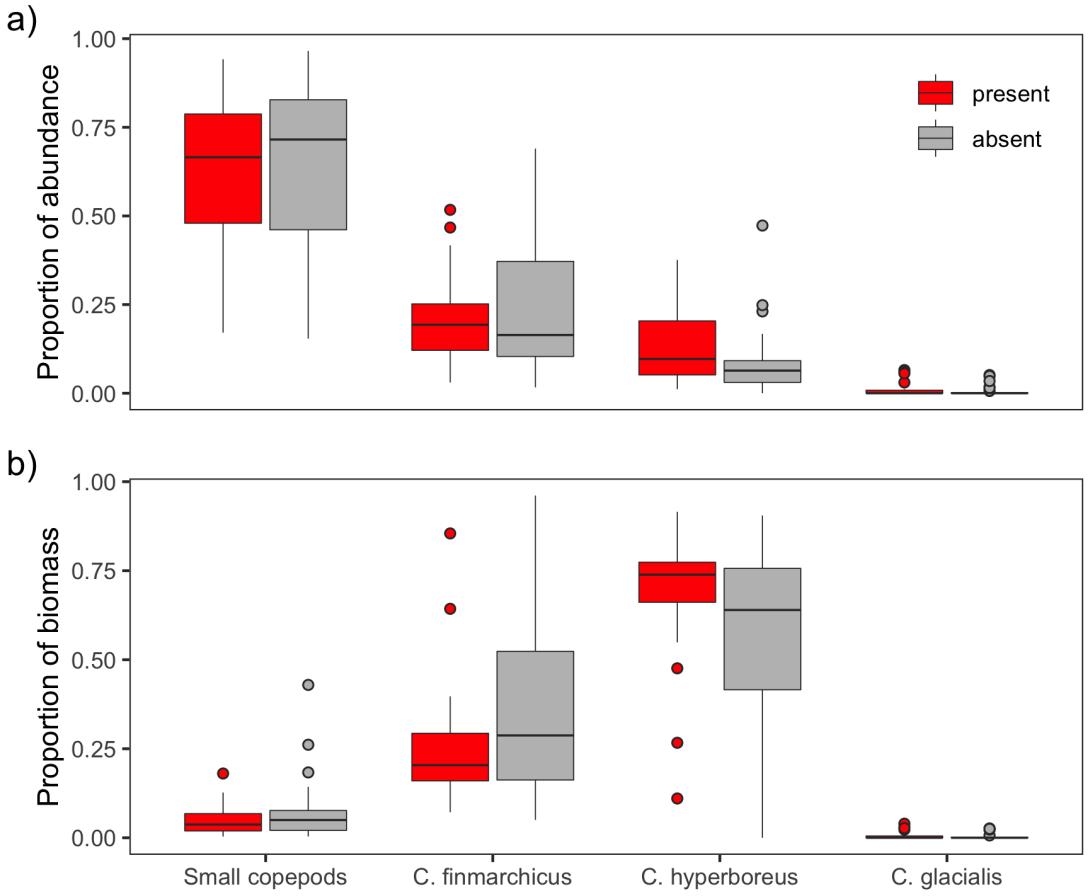

Figure 5.4: Proportion of (a) abundance and (b) biomass of calanoid copepods collected from ring net samples in the presence (red; n = 20) and absence (grey; n = 27) of right whales. Only late-stage (>C3) were considered for *Calanus* spp. Biomass (total dry weight) was estimated from abundance using individual dry weight conversions (13.3 μg ind^{-1} for small copepods; 297 μg ind^{-1} for *C. finmarchicus* and *C. glacialis*; 1725 μg ind^{-1} for *C. hyperboreus*). See Table 5.2 for a definition of small copepods.

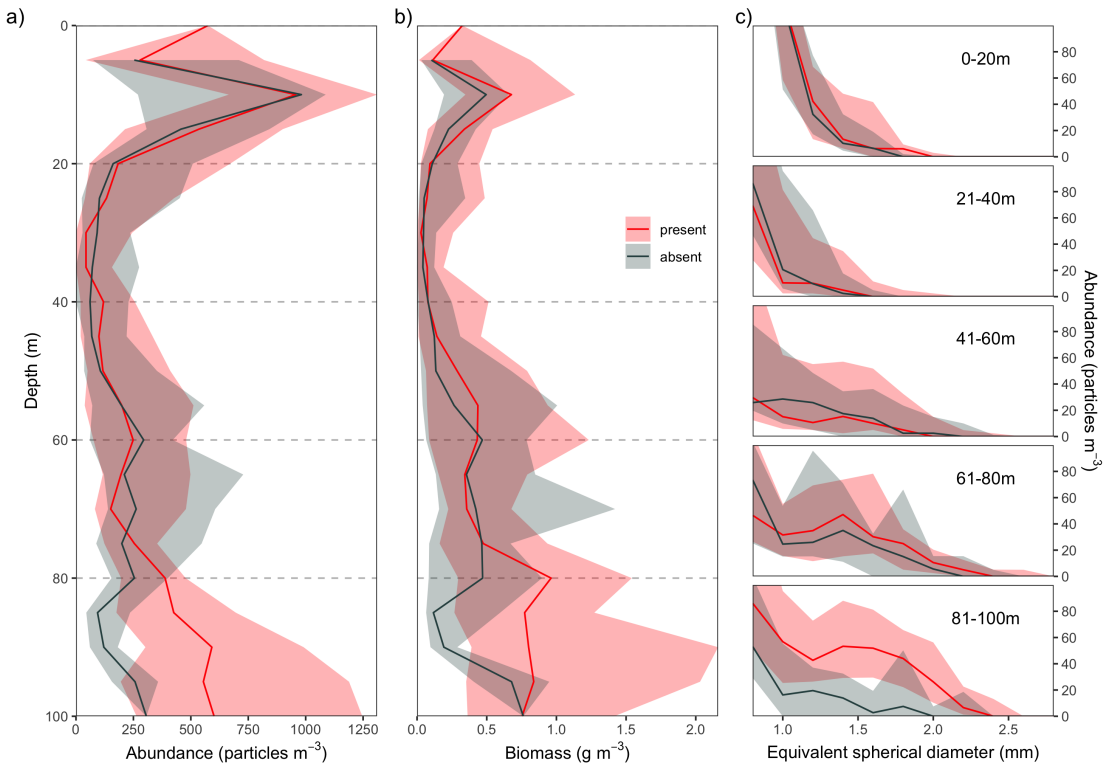

Figure 5.5: The median (solid line) and interquartile range (shaded region) of OPC-derived particle abundances from stations where whales were present (red; n = 23) or absent (grey; n = 20). Panel a) shows the vertical distribution of particles in the 0.8 - 3 mm Equivalent Spherical Diameter (ESD) size range and 5-m depth bins. Panel b) shows the estimated biomass of particles in Panel a). Panel c) shows the size distribution of particles in 20-meter depth strata and 0.2-mm ESD size bins.

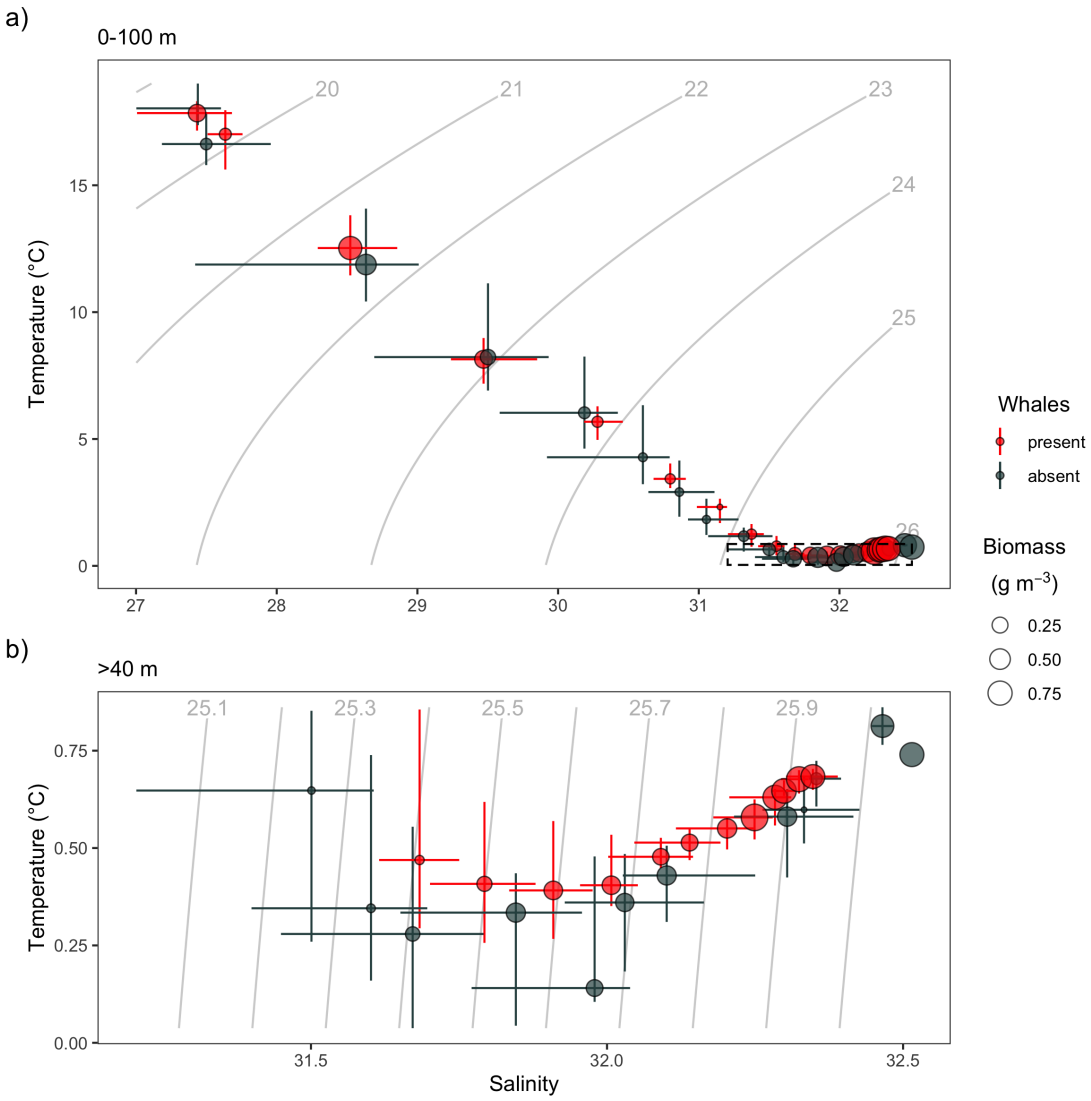

Figure 5.6: OPC-derived particle abundances in stations with whales present (red; n = 23) or absent (black; n = 20) in temperature-salinity space. The vertical and horizontal bars represent interquartile range of temperature and salinity values, respectively, and intersect at the median. The sizes of the filled circles correspond to the median particle biomass in 5-m depth bins (from Figure 5.5). Grey contour lines indicate density (kg m^{-3} - 1000) isopycnals. Panel a) shows depths from 0-100 m while panel b) provides a detailed view of depths >40 m. The plot area of panel b) is indicated with a dashed line on panel a).

associated with both the wet weight of the net tow as well as the maximum OPC biomass in the bottom 15 m. Although the regression coefficient was positive when examining right whale presence among the abundance of *C. hyperboreus* and the maximum OPC biomass, there was only modest evidence of an actual association (p = 0.078 for *C. hyperboreus*, p = 0.081 for OPC max; Table 5.2). The positive associations among whale presence and depth, bottom roughness, bottom mixed layer width, and the maximum OPC biomass in the bottom 15 m were significant regardless of the definition of whale presence. In contrast, associations among whale presence and bottom density, surface mixed layer thickness, *C. hyperboreus* abundance, net biomass, and maximum OPC biomass were more sensitive to the definition of whale presence (Appendix C).

5.5 Discussion

Our data suggest that right whales in the southern Gulf of St Lawrence in summer (July - August) are associated with a deep (80 - 100m), abundant ($> \sim$500 ind m^{-3}) layer of large zooplankton, the biomass of which is likely dominated by late-stage (primarily C4) *C. hyperboreus*. These are the first observations of right whales apparently targeting late-stage *C. hyperboreus*, which confirms what previous studies have assumed based on knowledge of right whale foraging ecology and zooplankton climatological sampling and/or simulations (*Brennan et al.*, 2019, 2021; *Plourde et al.*, 2019; *Sorochan et al.*, 2019; *Gavrilchuk et al.*, 2021). This clearly distinguishes the southern GSL from previously studied right whale feeding habitats on the Scotian Shelf (Roseway Basin; *Davies et al.*, 2014; *Baumgartner et al.*, 2003b), Bay of Fundy (*Murison and Gaskin*, 1989; *Baumgartner et al.*, 2003a,b; *Michaud and Taggart*, 2011), and Great South Channel (*Beardsley et al.*, 1996) in which stage C5 *C. finmarchicus* was the focal prey, as well as Cape Cod Bay where whales tend to feed on smaller calanoid copepods in late winter (*Mayo and Marx*, 1989). Though the opportunistic nature of our observations prevents more rigorous statistical analyses, our results provide insights into the biophysical mechanisms responsible for aggregating right whale prey in this habitat and spark numerous questions to be explored in more detail in the future.

There are several differences between *C. hyperboreus* and *C. finmarchicus* that have important implications for right whale foraging. Though their energy densities are similar (*Davies et al.*, 2012), a single adult *C. hyperboreus* is up to six times larger (by mass) than

Table 5.2: Results of single-variable logistic regressions of right whale occurrence and a given habitat variable. Sample size (n) varied as not all variables were available at all stations. The coefficient indicates the direction and magnitude of the association, while p provides the p-value of a drop-in-deviance test comparing the full and null models. The $*$ and grey highlighting indicates significance at $\alpha = 0.05$.

Variable	Units	Definition	n	Coefficient	p
depth	m	Bottom depth from shipboard echosounder	81	0.058	0*
bottom_sd	m	Standard deviation in bathymetry within 5 km radius of station	81	0.23	0.001*
ctd_bottom_density	kg m^{-3}	Density at maximum depth	66	2.09	0.021*
ctd_surface_density	kg m^{-3}	Density at minimum depth	66	-0.162	0.696
ctd_sml_depth	m	Depth of maximum buoyancy frequency	66	-0.068	0.133
ctd_bml_width	m	Height from max depth to a density change of -0.05 kg m^{-3}	66	0.2	0.012*
net_finmarchicus_conc	ind m^{-3}	Concentration of late stage (IV,V,VI) *C. finmarchicus*	47	0.005	0.145
net_hyperboreus_conc	ind m^{-3}	Concentration of late stage (IV,V,VI) *C. hyperboreus*	47	0.009	0.078
net_small_copepod_conc	ind m^{-3}	Concentration of small calanoid copepods	47	0	0.836
net_mass	g m^{-3}	Wet weight of net contents	46	1.526	0.032*
opc_max	g m^{-3}	Maximum OPC biomass	43	0	0.081
opc_avg	g m^{-3}	Average OPC biomass	43	0.001	0.304
opc_surf_max	g m^{-3}	Maximum OPC biomass within 15 m of surface	43	0	0.989
opc_deep_max	g m^{-3}	Maximum OPC biomass within 15 m of bottom	43	0.001	0.012*

an adult *C. finmarchicus*. For this reason, it is misleading to directly compare abundances of these taxa, or, for example, *Calanus* spp. abundances among the southern GSL and other right whale habitats. Using abundance to define feeding thresholds was appropriate and common practice in habitats strongly dominated by *C. finmarchicus* , but in habitats like the southern GSL with a more mixed assemblage of *Calanus* spp. it is preferable to conduct comparisons using biomass, or, ideally, energy content. To illustrate this concept, we provide a simple comparison between samples collected near right whales in the southern GSL (this study) and in the Bay of Fundy (BOF) in 1999-2001 (*Baumgartner et al.*, 2003b, Figure 5.7). *Calanus* abundances in the BOF are nearly an order of magnitude greater than those in the GSL and driven almost entirely by *C. finmarchicus* while the GSL abundance is almost equally split between *C. finmarchicus* and *C. hyperboreus*. Upon converting to biomass, the low overall abundance in the GSL is heavily compensated by the larger size of *C. hyperboreus* such that the total biomass estimates from each site are of the same order of magnitude.

Another important consideration when interpreting zooplankton data from a right whale habitat is the distinction between climatological, or baseline, abundance, such as those determined via systematic zooplankton sampling programs, versus abundance from samples collected in proximity to right whales. The thin, dense patches of *Calanus* on which right whales forage may be more likely to form when baseline zooplankton levels are high (*Pendleton et al.*, 2009), but this baseline is not necessarily representative of the prey available to right whales (*Baumgartner et al.*, 2007, 2003b). Climatological abundance estimates, such as those developed by *Sorochan et al.* (2019), are extremely valuable tools to understand long term (e.g., decadal) variability in habitat quality, but should not be used to infer absolute energy available to right whales. For example, the median biomass estimate of *Calanus* spp. in net samples we collected in the southern GSL in the absence of right whales ($\sim$5000 mg m^{-2}) was five times higher than the climatological average at the Shediac valley station ($\sim$1000 mg m^{-2}; *Sorochan et al.*, 2019), while the samples we collected in the presence of right whales ($\sim$14000 mg m^{-2}) was an order of magnitude larger than the climatological average.

Brennan et al. (2019) concluded that the accumulation of *Calanus* in the southern GSL occurs primarily through the transport of active stages via the Gaspé Current and their local transition into diapause. In all study years (2017-2019), the environmental conditions,

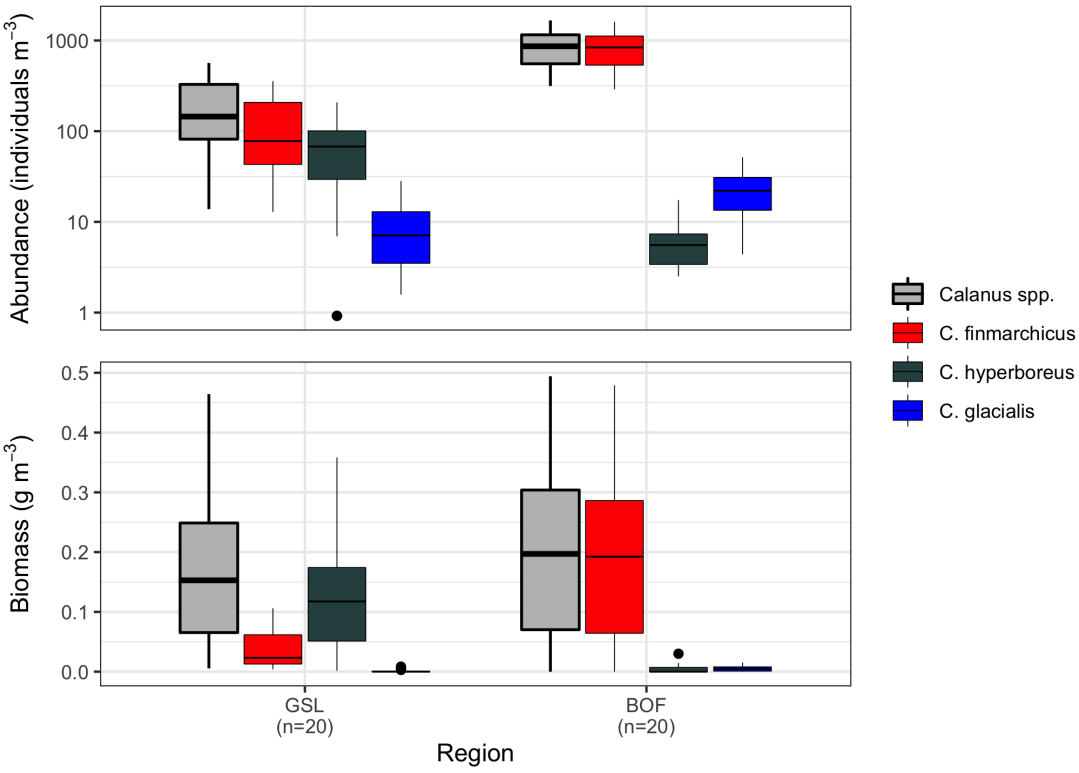

Figure 5.7: The abundance and estimated biomass of late-stage (C4-C6) *C. finmarchicus* (red), *C. hyperboreus* (black), *C. glacialis* (blue) and sum total of all three species (*Calanus* spp.; grey) collected using depth-integrated net tows near right whales in the southern Gulf of St Lawrence (GSL) in 2017-2019 (this study; n = 20) and the Bay of Fundy (BOF; n = 20) in 1999-2001 (*Baumgartner et al.*, 2003b).

namely high runoff from the St. Lawrence Estuary and relatively low wind stress, favored the coastal attachment of the GC and subsequent transport and retention of *Calanus* to and within the southern GSL (*Brennan et al.*, 2021). This suggests that the dense layer of *Calanus* near the bottom that we observed is formed via GC transport and local vertical migration, rather than by an intrusion of warm, saline water from the Laurentian Channel. The apparent association between OPC-derived biomass and the deep water mass is therefore likely not indicative of the source of *Calanus*, as has been documented in Roseway Basin (*Davies et al.*, 2014), though this hypothesis needs additional support from further study.

Bottom mixed layer depth appears to play an important role in several right whale feeding habitats, including the southern GSL, but through different mechanisms. A positive association between the thickness of the bottom mixed layer and whale presence, as we have documented in the southern GSL, has also been observed in the Bay of Fundy. *Baumgartner et al.* (2003b) proposed that a thick bottom mixed layer promotes the formation of a thin, dense layer of *C. finmarchicus* in relatively close proximity to the surface where it is more available for predation by right whales. This appears to contrast the dynamics in Roseway Basin, where a deeper 1026 isopycnal, in combination with tidal currents and the basin margin, functions to concentrate *C. finmarchicus* (*Davies et al.*, 2014). This is not a perfect comparison as the two studies did not define the bottom mixed layer in the same way and *Davies et al.* (2014) did not relate their results to whale presence, but the apparent contrast between these results highlights the complexity and habitat specificity of these aggregation mechanisms. It would seem that the dynamics in the southern GSL are more similar to those in the Bay of Fundy, where a thick bottom mixed layer makes *Calanus* more available to surface-bound right whales. If this were the case, we would expect occasional profiles where we vertically sample through the layer. This was not readily apparent in our dataset, perhaps owing to near-bottom sampling limitations described in more detail below, but has been observed by others collecting similar data in the region (K Sorochan, personal communication).

There was little evidence to support the possibility that right whales were targeting other, non-calanoid zooplankton prey. The net data did not reveal any alternative taxa in sufficient abundance and/or biomass to warrant consideration as a substantial prey resource. That said, the abundances of the small calanoid copepods is substantial, at times exceeding the

feeding threshold suggested for Cape Cod Bay (1000 individuals m^{-3}; *Mayo and Marx*, 1989). It is possible that right whales supplement their foraging on large *Calanus* spp. with consumption of these smaller copepods. Another possibility is that right whales are preying upon taxa that are large and mobile enough to evade capture by our sampling equipment. Perhaps the most likely candidate would be euphausiids, on which right whales in other regions are known to feed (*Collett*, 1909; *Hamner et al.*, 1988) and are abundant in the GSL (e.g., *McQuinn et al.*, 2015). Further study is required to explore these and other potential alternative foraging strategies in greater detail.

Our study was only possible because we were able to conduct oceanographic and prey field sampling on an opportunistic, non-interference basis with ongoing visual surveys. This resulted in a non-systematic sampling design that was unbalanced and biased towards times and places with known whale presence. This renders us unable to conduct robust temporal or spatial comparisons and warrants precautionary treatment of the p-values of the logistic regression analysis. We would consider it inappropriate to apply these statistical relationships in a predictive capacity, especially in other regions. The use of a platform of opportunity (i.e., pleasure or fishing vessel) also posed challenges for oceanographic data collection, chief among which was our inability to consistently sample in close proximity (within $\sim$10 m) to the sea floor. We sought to mitigate this limitation by only including profiles that traversed at least 85% of the water column, but in most cases the very bottom 5-10% of the water column (typically $\sim$2 - 10 m) remained unsampled. As a consequence, we are likely systematically underestimating the abundance of the deep zooplankton layer that right whales are likely feeding upon. Right whales regularly dive to the sea floor across habitats (*Baumgartner et al.*, 2017), and in some habitats are commonly observed with mud-covered heads (*Hamilton and Kraus*, 2019). This under sampling could be mitigated in future studies by using nets designed to interact with the bottom (e.g., tucker trawls), employing active acoustic sensors, and/or improving the real-time depth reporting of the profiling systems (e.g., monitor instrument depth using conductive cable).

Our results compliment numerous recent and ongoing efforts to better characterize the habitat and feeding ecology of right whales in the southern GSL. We provide evidence that right whales are targeting a mixed assemblage of late-stage *C. finmarchicus* and *C. hyperboreus* concentrated near the bottom primarily within the Shediac Valley. Our *Calanus* biomass estimates are considerably higher than those derived from systematic

sampling in the absence of right whales, which must be considered when assessing habitat suitability and the ability of right whales to meet their energetic needs. Future efforts ought to expand the temporal and spatial extent of sampling, ideally using a systematic framework that is more conducive to the development of rigorous statistical associations between oceanographic conditions and right whale presence. These efforts should employ modified sampling methods that facilitate the enumeration of the near-bottom zooplankton community, and perhaps include a biologging component to characterize right whale movement within the prey field. Such studies may allow for the development of short term (weeks to months) predictive models of right whale occurrence and distribution within the southern GSL that could be employed to better inform dynamic management measures and improve conservation outcomes.

5.6 Acknowledgements

We are indebted to Martin Noel, Guy Lanteigne, Jean-Denis Noel, the late Joe Howlett and David Anthony for their assistance, good humor, and expert operation of the research vessels used in this work, and to Sarah Haney for the use of the M/V *Shelagh I*. We are grateful for the tireless efforts and patience of those who helped conduct this fieldwork, including Pam Emery, Megan McOsker, Pete Duley, Monica Zani, Kelsey Howe, Marianna Hagbloom, Kim Franklin, and Marcia Pearson. We thank Angelia Vanderlaan, Valentina Ceballos, Gina Lonati and Kevin Sorochan for helpful discussions. Walter Judge, Daniel Morrison, Richard Cheel and Mark Merrimen provided invaluable technical support.

Support for this study was provided by the Department of Fisheries and Oceans (DFO), Natural Sciences and Engineering Research Council of Canada (NSERC), the Habitat Stewardship Program (HSP), the Marine Environmental Prediction and Response Network (MEOPAR), World Wildlife Fund (WWF), and the Canadian Whale Institute (CWI). Support for HDJ was provided by the Killam Foundation, Vanier Canada Graduate Scholarship program, Dalhousie University, the Nova Scotia Graduate Scholarship program, and the Canada Graduate Scholarships - Michael Smith Foreign Study Supplements (CGS-MSFSS) program.

We dedicate this work to the memory of our beloved colleague, friend, and captain Joe Howlett.

CHAPTER 6

USING OCEAN GLIDERS TO CHARACTERIZE BALEEN WHALE HABITAT IN THE NORTHWEST ATLANTIC

6.1 Abstract

Characterizing baleen whale habitat is challenging, in part, because of the difficulty in obtaining sufficient spatially and temporally concurrent in situ observations of the whales and local oceanographic conditions. We collected a multi-year series of concurrent acoustic whale detections and high-resolution oceanographic measurements from Slocum ocean gliders to evaluate how baleen whales associate with and partition their habitat. The focal habitat was Roseway Basin, a relatively small (30x60 km), shallow ($<$180 m) basin located $\sim$40 km seaward of SW Nova Scotia, Canada. Data were collected from 13 fall (Aug - Nov) glider surveys of the Basin over an eight-year period (2014 - 2021). Gliders were equipped to collect full-depth profiles of salinity and temperature as well as audio to detect and classify whale sounds in near real-time. Analysis of the whale detections revealed spatial, diel, and within-season patterns in detection rates that varied by species. Whale occurrence and a suite of oceanographic variables were computed in 20-km grid cells in each month and year of the study (n = 267). Descriptive and statistical (logistic regression) analyses were used to explore potential associations between the occurrence of each species and depth, topographic relief, water column stratification, current speed, and bottom mixed layer width and density. Results suggested strong, positive associations among fin, sei,

and right whale occurrence and depth. They also provided evidence that right whale occurrence in Aug-Sep was associated with well-stratified water columns overlying thick, dense bottom mixed layers, consistent with conditions previously demonstrated to have a role in aggregating their copepod prey at depth in shelf basins. Though exploratory, our results demonstrate the potential use of profiling gliders for making inferences about baleen whale habitats.

6.2 Introduction

Baleen whales filter feed on dense, ephemeral patches of low trophic level prey (*Goldbogen et al.*, 2017). Their survival depends on reliably finding and effectively exploiting these aggregations, the dynamics of which are governed by a variety of cryptic biophysical processes (*Durham and Stocker*, 2012). Characterizing the associations between baleen whales and their ocean environment can reveal insights into their ecology, improve our understanding of the physical proxies of zooplankton availability, and ultimately inform whale risk mitigation (*Baumgartner et al.*, 2017). The latter is particularly salient given the conservation status of many large baleen whale populations, coupled with intensifying risks from human activities and climate change.

Quantifying these ecological associations is challenging because of the difficulty in obtaining sufficient spatially and temporally concurrent observations of the whales and oceanographic conditions. Typical correlative habitat models rely on environmental covariates collected at different time/space scales, often restricted to the ocean surface, that may not be representative of the oceanographic process responsible for prey aggregation (*Redfern et al.*, 2006). A common example is the combination of remote-sensed dynamic variables (e.g., sea surface temperature) with results from sightings surveys. This is often because fine-scale habitat sampling is too resource-intensive to conduct over time and space scales required to develop rigorous statistical relationships. While these approaches can generate relatively accurate predictions, they are likely unable to resolve many of the processes that whales, and their prey, may be responding to (*Palacios et al.*, 2013).

Autonomous platforms have great potential for addressing this knowledge gap, as they are becoming more commonly used in oceanographic research and can often be configured to monitor both whale occurrence and oceanographic habitat persistently over large temporal and/or spatial scales. Profiling ocean gliders (hereafter ‘gliders’) are

especially desirable autonomous platforms for this application, as they are acoustically quiet and collect high resolution observations throughout the full water column. Passive acoustic monitoring (PAM) from gliders has been employed to monitor for a wide range of marine mammal species (*Baumgartner et al.*, 2014; *Kusel et al.*, 2017; *Cauchy et al.*, 2020; *Fregosi et al.*, 2020; *Verfuss et al.*, 2019; *Baumgartner and Fratantoni*, 2008; *Moore et al.*, 2007). Several systems are capable of transmitting survey results in near real-time (within a few hours) while the glider is still at sea (*Kowarski et al.*, 2020; *Klinck et al.*, 2012; *Baumgartner et al.*, 2013), facilitating the use of these platforms for dynamic planning of research and management activities. One such system, the DMON/LFDCS, is commonly deployed on Slocum gliders (Teledyne Webb Research; *Baumgartner et al.*, 2013, 2020) and moored buoys (*Baumgartner et al.*, 2019) to monitor for baleen whales, especially the endangered North Atlantic right whale (*Eubalaena glacialis*; hereafter 'right whale'). Since 2014, the DMON/LFDCS has been deployed on over 75 glider missions, amassing nearly 4000 days at sea and over 500 days with right whale detections (robots4whales.whoi.edu). These detections are relayed to managers in both the US and Canada where they are used to inform risk mitigation measures (Chapter 4; *Johnson et al.*, 2021).

To date, near real-time monitoring of right whales has been the primary motivation for many of these deployments. While achieving this, gliders are also monitoring for the presence of other species as well as collecting large quantities of hydrographic observations. These oceanographic data can provide useful ecological context for whale detections (*Aniceto et al.*, 2020; *Burnham et al.*, 2021). The primary objective of this work is to conduct an exploratory analysis using the concurrently collected environmental and whale occurrence data from glider deployments to evaluate how baleen whale species associate with oceanographic habitat.

6.3 Methods

6.3.1 Site description

The focal habitat was Roseway Basin, a relatively small (30 x 60 km), shallow ($<$180 m) basin on the Scotian Shelf located $\sim$40 km seaward of SW Nova Scotia, Canada (Figure 6.1). Variation in the hydrography is dominated by seasonal warming and cooling as well as inputs from the Nova Scotia Current (NSC) and Warm Slope Water (WSW) intrusions. The NSC, a buoyancy-driven coastal current, delivers relatively cool, fresh water from

the Gulf of St Lawrence predominately to the upper layer (30-50 m) of the water column. Intrusions of WSW contribute to relatively warm, saline water below 100m (*Dever et al.*, 2016). Studies of right whale occurrence (*Brown et al.*, 2007) habitat (*Baumgartner et al.*, 2003b) and vessel strike risk (*Vanderlaan et al.*, 2008; *Vanderlaan and Taggart*, 2009) informed the implementation of an Area to Be Avoided (ATBA) by the International Maritime Organization (IMO) in the Basin, followed shortly by the designation of the same region as a right whale critical habitat area (*DFO*, 2010). Fin (*Balaenoptera physalus*), humpback (*Megaptera novaeangliea*), sei (*Balaenoptera borealis*), and blue (*Balaenoptera musculus*) whales have also been sighted and acoustically detected in Roseway Basin (*Davis et al.*, 2020; *Johnson et al.*, 2021), though their habitat associations have not been studied in detail.

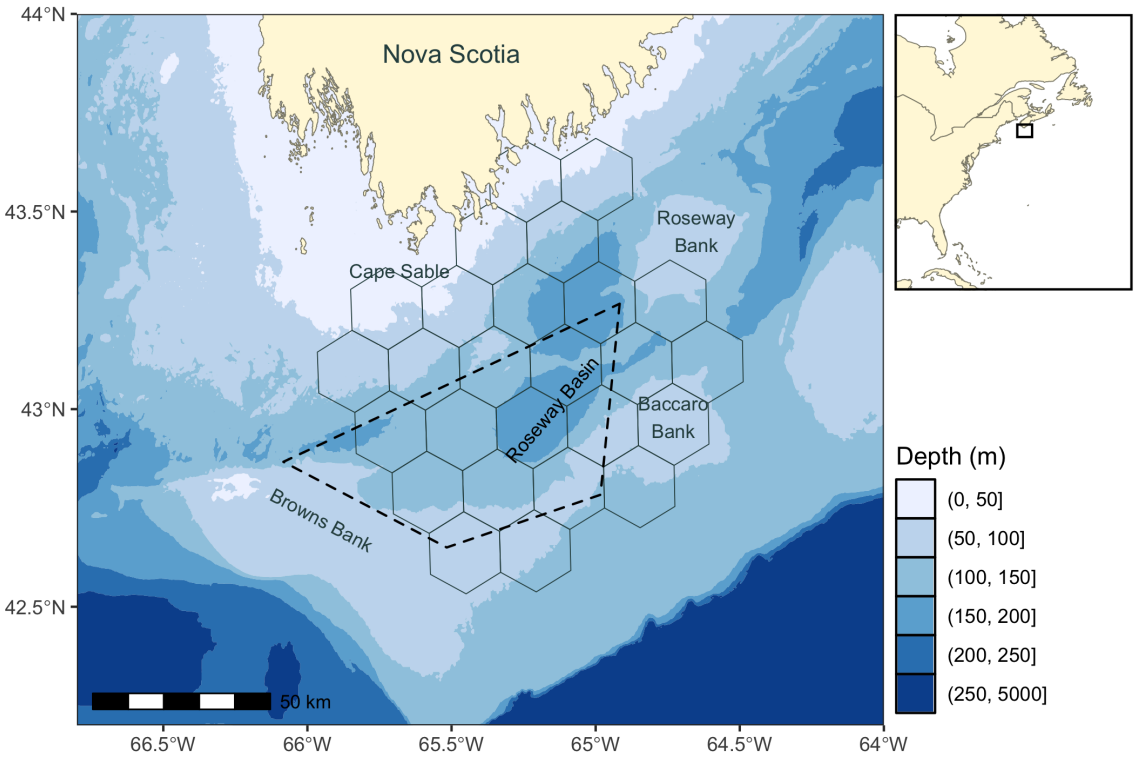

Figure 6.1: The Roseway Basin study site off Nova Scotia, Canada. Color indicates depth contours (in meters) derived from the GEBCO bathymetric dataset. The dashed line shows the Roseway Basin ATBA. The solid black lines show the grid of 20 km diameter hexagons (n = 20) used in the habitat analysis.

6.3.2 Data collection

Data were collected from 13 Slocum glider surveys of Roseway Basin in the late summer and early fall (August - November) over an eight-year period (2014 - 2021). Our study area encompassed a roughly 100 x 100 km region (42.7° to 43.6° latitude and -65.8° to -64.6° longitude) approximately centered on the ATBA. Slocum gliders are small ($\sim$1.5 meter long) battery-powered, buoyancy-driven autonomous vehicles that profile the water column at slow vertical (0.1-0.2 m s^{-1}) and horizontal (15-20 km d^{-1}) velocities for missions lasting weeks to months in duration. They surface at regular intervals (typically every 2 - 6 h) to determine their position, transmit data and receive new mission commands via satellite. The specific configuration of each glider varied by mission, but at minimum all gliders were equipped with a (either pumped or unpumped) calibrated Conductivity-Temperature-Depth (CTD) sensor to measure temperature and salinity profiles, and a PAM system to detect and classify baleen whale vocalizations. The gliders were programmed to conduct cross-basin transits of the region approximately perpendicular to the axis of the SE basin margin, but strong tidal currents introduced considerable tortuosity in the tracklines. Logistical constraints caused interannual variability in platform availability and temporal survey coverage. A CTD malfunction rendered the environmental data on the 2017 survey unusable, so this deployment was not included in the habitat analyses (Figure 6.2; Table 6.1).

6.3.3 Data processing

6.3.3.1 Whale detection data

Each glider was equipped with a PAM system comprised of the low-power digital acoustic monitoring instrument (DMON; *Johnson and Hurst*, 2007) and an on-board detection algorithm (low-frequency detection and classification system; LFDCS; *Baumgartner and Mussoline*, 2011). The DMON recorded audio at 2 kHz continuously with a hydrophone sensitivity of -203 dB re 1 V μPa^{-1}, gain of 33.2 dB, zero-to-peak voltage of 1.5V, and flat frequency response between approximately 50 and 7500 Hz. The LFDCS algorithm running on board the DMON facilitated near real-time baleen whale detection and classification. In brief, the LFDCS produces spectrograms of the audio data, removes spurious broadband noise and continuous tonal noise and then uses a contour-following algorithm to create pitch tracks of tonal sounds from the spectrogram. Each pitch track is classified by comparing attributes of the pitch track to a library of call types using quadratic discriminate

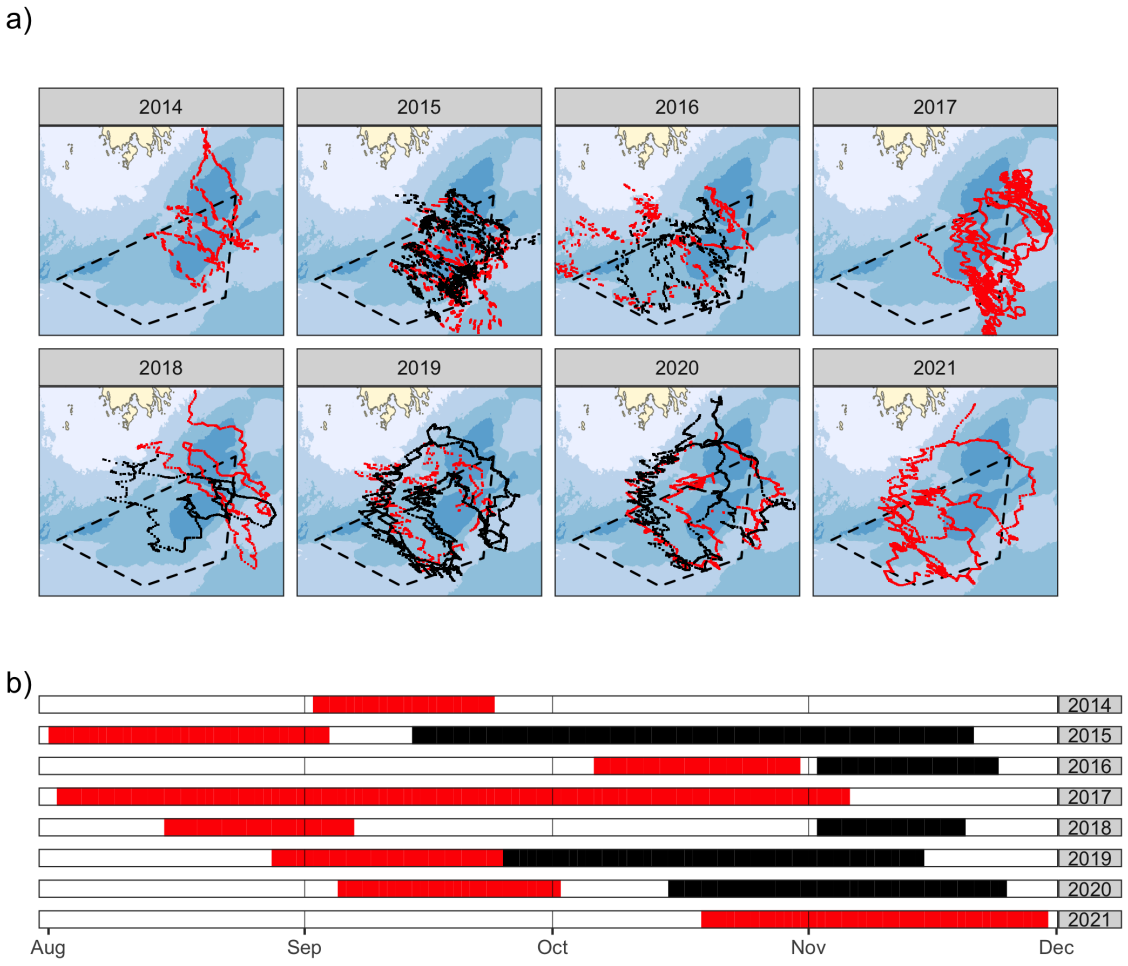

Figure 6.2: (a) Spatial and (b) temporal distributions of effort from Slocum glider surveys (n = 13) of Roseway Basin from 2014 through 2021. The colors distinguish the first (red) and second (black) surveys in a given year. The points in panel (a) show the average glider position within a ∼15 min acoustic analysis (tally) period. The bathymetric scale is consistent with that of Figure 6.1. Environmental data were not available for the 2017 mission, so it was not included in the habitat analysis.

Table 6.1: Summary of Slocum glider missions (n = 13) in Roseway Basin from 2014 through 2021. Days indicates the number of days in which both whale detection and environmental data were collected. Dist, Profiles, and Tally provide the total along-track survey distance (km), total number of glider profiles, and the total number of tally periods analyzed for whale detections, respectively. The species columns show the number of days in which each species was detected.

	Glider	Year	Start	End	Days	Dist	Profiles	Tally	Fin	Humpback	Right	Sei
1	we10	2014	02-Sep	24-Sep	23	658	1011	1408	15	3	6	11
2	we04	2015	28-Jul	04-Sep	39	1371	1516	2470	34	1	15	6
3	dal556	2015	14-Sep	30-Nov	78	2193	2777	2902	68	16	14	23
4	dal556	2016	06-Oct	31-Oct	26	981	1194	1126	16	5	5	15
5	otn200	2016	02-Nov	24-Nov	23	768	255	915	21	8	8	13
*6	otn200	2017	02-Aug	06-Nov	97	1945	-	5486	77	1	5	10
7	otn200	2018	15-Aug	07-Sep	24	467	1044	707	2	0	0	0
8	otn200	2018	01-Nov	20-Nov	20	495	769	719	16	0	0	4
9	bond	2019	28-Aug	25-Sep	29	759	673	1172	2	4	0	0
10	scotia	2019	25-Sep	15-Nov	52	1460	1388	2995	43	20	1	21
11	fundy	2020	05-Sep	02-Oct	28	668	1010	1799	22	5	11	2
12	fundy	2020	15-Oct	25-Nov	40	1111	1025	1868	29	16	4	16
13	qala1	2021	19-Oct	08-Dec	51	1398	1527	2983	44	4	2	12
				Totals	530	14274	14189	26550	389	83	71	133

*Environmental data not available for this mission

function analysis. When the glider surfaces, a subset (8 kB h^{-1}) of the pitch track and classification data are transmitted to a land station via Iridium satellite where they are divided into ∼15-minute analysis (tally) periods that are manually reviewed by a trained analyst for the acoustic presence of several species, including right, fin, sei, and humpback whales. Over daily timescales the system has a false detection rate of 0% and a missed detection rate of 17 to 24% (*Baumgartner et al.*, 2020). See *Baumgartner and Mussoline* (2011) for more information on the LFDCS and *Baumgartner et al.* (2013, 2020) for system performance from Slocum gliders.

This analysis protocol was used to determine the acoustic occurrence of four baleen whale species (fin, humpback, right, and sei whales) in near real-time for all glider deployments in this study. For each species, tally periods marked as "present" or "absent" were given a numeric score of 1 or 0, respectively. Tally periods marked "possible" were considered not detected and given a score of 0. The number of tally periods, cumulative duration of tally periods, number of tally periods with detections of each species, proportion of detected tally periods of each species, and species occurrence scores (0 = not detected, 1 = detected) were computed for each survey day and within each 20-km grid cell for the habitat analysis (see below).

6.3.3.2 Glider data

Glider science and engineering data from each deployment were extracted from the raw binary format and merged using a common timestamp. The glider CTDs were typically sampled at either 0.5 or 1 Hz. Spurious (i.e., non-physical) values for time, position, temperature, salinity, and pressure were removed. Ascending profiles were isolated based on a dive/climb state variable recorded by the glider. Profiles with fewer than 30 points, a maximum depth of less than 10 m, a minimum depth of greater than 15 m, depth intervals exceeding 5 m, or those that traversed less than 75% of the full water column, were excluded from subsequent analyses. Temperature and salinity profiles were decimated into 1-m depth bins and smoothed using a centered 9-point moving average. The potential density anomaly (kg m^{-3} - 1000; hereafter 'density') was computed for each smoothed profile. The profiles were then visually reviewed to confirm successful profile isolation and quality control. Unless otherwise noted, all oceanographic quantities were computed using the oce package (*Kelley and Richards*, 2020) in R (*R Core Team*, 2020).

6.3.3.3 Habitat data

A goal of this work was to use glider-derived environmental data and acoustic detections to make inferences about whale habitat. These data are collected over very different scales: a glider profile is usually collected over a few hundred meters (horizontally), while baleen whale calls in a continental shelf environment are commonly detected at scales of kilometers to tens of kilometers (Chapter 2). Thus, the first step towards characterizing whale-habitat associations was to define an appropriate spatial and temporal scale over which to compare the environmental and detection data. We imposed a regular hexagonal grid over the study area and aggregated whale detection and habitat data within each cell. A cell diameter of 20 km was selected based on average detection ranges of right whales (Chapter 2). This grid resolution also balanced statistical constraints, where preliminary analysis suggested models constructed using smaller cell sizes showed signs of residual autocorrelation for all species, while the use of larger cell sizes reduced sample size, spatial resolution and statistical power. In an effort to reduce potential bias arising from uneven sampling, we only included cells in the analysis that had been surveyed in at least one year in both the early (August - September) and late (October - November) months of the study (n = 20).

Several habitat variables were computed within each grid cell (Table 6.2). The average water depth (*depth*) and standard deviation of the water depth (*depth_sd*), an index of topographic relief, were calculated within each grid cell using GEBCO digital bathymetry at 30 arcsecond resolution (accessed from `https://download.gebco.net/`). Both water depth and topographic relief were included as environmental variables given their many established links to baleen whale distribution (*Redfern et al.*, 2006). Dynamic variables were computed for each profile, and the median value for all profiles within a given month and year were assigned to each cell. Surface stratification (*surf_strat*) was defined as the difference in average density between the 5-10m and 45-50m depth strata. Stratification strength was included for its potential role in zooplankton aggregation and previous associations with right whales (*Woodley and Gaskin*, 1996; *Baumgartner and Mate*, 2005). It is also highly correlated with sea surface temperature, which has been commonly related to the distribution of many cetacean species (*Redfern et al.*, 2006), as well as sea surface temperature gradient, which *Baumgartner et al.* (2003b) linked with right whale spatial distribution. The bottom mixed layer width (*bml_width*) was defined

as the height from the maximum profile depth to a density change of -0.05 kg m^{-3}, and the bottom mixed layer density (*bml_density*) was the average density within this depth stratum. We included bottom mixed layer width based on a previously documented positive association with right whale presence in Roseway, where a thicker bottom mixed layer brought dense patches of *Calanus finmarchicus* found at the top of the bottom mixed layer closer to the surface where they were more easily exploited by right whales (*Baumgartner et al.*, 2003b). Results of Chapter 5 suggest a similar mechanism in the GSL. The density of the bottom mixed layer was included to resolve hydrographic variability from flushing events or slope water intrusions. Using CTD and echosounder data from one of the Slocum glider surveys presented here (Survey 3; Table 6.1), *Ruckdeschel et al.* (2020) observed a significant fresh water flushing event throughout the basin in October 2015 which was associated with a significant reduction in zooplankton backscatter. The depth-integrated horizontal current velocity (*current_v*) was computed for each glider segment (interval between surfacings) on board the glider during the mission based on the offset between the measured glider position and the glider position predicted using dead reckoning (see Appendix of *Dever et al.*, 2016). It was considered as an environmental variable owing to previous associations between tidal current magnitude and the concentration of zooplankton along the SE margins of the basin (*Davies et al.*, 2013), and because of its apparent spatial variability as evidenced by the increasing tortuosity of glider tracks towards the western edge of the study area (Figure 6.2).

Table 6.2: Description of environmental variables used in the habitat analysis

Variable	Units	Definition
depth	m	Median seafloor depth within a grid cell (from GEBCO)
depth_sd	m	The standard deviation of seafloor depth within a grid cell (from GEBCO)
surf_strat	kg m^{-3}	The difference in average density between the 5-10 m and 45-50 m depth strata
bml_width	m	Height from the maximum profile depth to a density change of -0.05 kg m^{-3}
bml_density	kg m^{-3}	Average density within the bottom mixed layer
current_v	m s^{-1}	Magnitude of the depth-integrated horizontal current

6.3.4 Statistical analyses

6.3.4.1 Diel detection rates

Diel patterns of detection rates of each species were investigated based on previously described linkages with baleen whale foraging behavior (*Baumgartner and Fratantoni*, 2008). The sunAngle() function from the oce package was used to determine the solar altitude (in degrees above the horizon) and azimuth (in degrees eastward of north) at the time and position of each tally period from the full dataset. These fields were then used to sort detections into four light regimes: dawn (-12° $<$ altitude $<$ 0° and azimuth $<$ 180°), day (altitude $>$ 0°), dusk (-12° $<$ altitude $<$ 0° and azimuth $>$ 180°), and night (altitude $<$ -12°). The detection rate (number of tally periods with detections / total tally periods) was computed within each light regime on every day for which there were detections. To facilitate comparison among days, the detection rates for each light regime and day were adjusted by subtracting the daily average detection rate. The results were not normally distributed so Kruskal-Wallis tests followed by Dunn's multiple comparisons tests (with Bonferroni adjustment) were used to compare detection rates among light regimes for each species. These tests were implemented using the dunn.test() function in the dunn.test package (*Dinno*, 2017) in R.

6.3.4.2 Habitat associations

The association between whale presence and each environmental variable was assessed using logistic regression. Whale occurrence was expressed as 1 if whale acoustic presence was manually validated in at least one tally period within a grid cell unit, and 0 if tally periods were reviewed and no presence was detected. The general form of the logistic regression is as follows:

$$logit(\pi) = \beta_0 + \sum_{i=1}^{p} \beta_i V_i \tag{6.1}$$

where the logit of the probability of species occurrence, π, is modeled as a linear function of the predictor variables, V_i, and β_0 is the intercept, β_i are the model coefficients, and p is the number of predictor variables. There were a number of practical considerations that were also weighed during model construction. The first was the issue of overfitting, wherein an overly complex model (i.e., one that contains too many parameters) artificially conforms to the underlying data and produces inaccurate results. As a general rule, at least

10 observations of both presence and absence are necessary for each model term (*Hosmer et al.*, 2013). Right and humpback whales were less commonly detected (61 and 54 survey units), which restricted model design for these species to a maximum of five or six terms. A second consideration was the potential for correlation among independent variables, as multicollinearity can also generate unreliable model estimates (*Hosmer et al.*, 2013).

With these considerations in mind, several sets of models were constructed to evaluate the effect of a single variable on whale occurrence while attempting to control for other sources of variability. The simplest model set contained a single independent variable and a term, *effort*, containing the number of tally periods per grid cell to correct for variation in acoustic monitoring effort. It was structured as follows:

$$logit(\pi) = \beta_0 + \beta_1(effort) + \beta_2(V) \tag{6.2}$$

Several of the environmental variables were correlated with *depth* (Appendix D.5), which can confound the results. To account for the influence of depth, a second set of models including *depth* was constructed as follows:

$$logit(\pi) = \beta_0 + \beta_1(effort) + \beta_2(V) + \beta_3(depth) \tag{6.3}$$

Unconstrained temporal variation can also confound model results. To account for the influence of time on detection rates, a categorical variable was added to represent each month. These are included in the model as three dummy variables (Sep, Oct, Nov), each taking a value of 0 or 1 to represent a given month (e.g., August is represented as: Sep = 0, Oct = 0, Nov = 0). The model took the following form:

$$logit(\pi) = \beta_0 + \beta_1(effort) + \beta_2(V) + \beta_3(Sep) + \beta_4(Oct) + \beta_5(Nov) \tag{6.4}$$

Which was expanded as follows with the addition of a term for *depth*:

$$logit(\pi) = \beta_0 + \beta_1(effort) + \beta_2(V) + \beta_3(Sep) + \beta_4(Oct) + \beta_5(Nov) + \beta_6(depth) \tag{6.5}$$

The previous two models have 6 and 7 terms, respectively, which raises concern of overfitting, particularly for the less commonly detected species (right whales and humpbacks). To reduce the number of model terms while still resolving some of the temporal variability, we developed another set of models where the month terms were replaced with a single categorical variable, $late$, representing each half of the study period ($late$ = 0 for August-September, and $late$ = 1 for October-November). These terms allow comparison between the first and second halves of the study period. A set of models were formed with this new term:

$$logit(\pi) = \beta_0 + \beta_1(effort) + \beta_2(V) + \beta_3(late) \tag{6.6}$$

which were further expanded to include *depth* as follows:

$$logit(\pi) = \beta_0 + \beta_1(effort) + \beta_2(V) + \beta_3(late) + \beta_4(depth) \tag{6.7}$$

All the terms in the previous formulations are additive. This allows the strength (model intercept) of an association to change, but the direction of the association (model slope) remains constant. A set of models was developed to assess whether or not the direction of a habitat association changed between the first and second half of the study period:

$$logit(\pi) = \beta_0 + \beta_1(effort) + \beta_2(V) + \beta_3(late) + \beta_4(Vxlate) \tag{6.8}$$

where the categorical variable for time, $late$, was expressed as an interaction with the variable of interest, V. This set was expanded once again with a *depth* term as follows:

$$logit(\pi) = \beta_0 + \beta_1(effort) + \beta_2(V) + \beta_3(late) + \beta_4(Vxlate) + \beta_5(depth) \tag{6.9}$$

Monthly anomalies of environmental variables in each cell (value in each cell was subtracted from the average value of all cells in that month across all years) were computed prior to model fitting. This aided in model fitting and coefficient interpretability, though the analysis was repeated without centering and the same models emerged as significant (not shown). Models including *depth* terms (Equations 6.3, 6.5, 6.7, 6.9) produced similar results when fitted with the results of a principal components analysis of the variable of

interest and *depth*, suggesting their results are robust to multicollinearity (not shown). All models only consider temporal trends within the August - November period. We made no attempt to explicitly quantify or account for interannual variability due to the heterogeneity in annual sampling effort and relatively short timeseries; as such, we pooled data by month across years.

These models were implemented using the glm() function in the stats package in R. Model assumptions (independence of residuals, linearity of predictor variables, absence of multicollinearity, and lack of strong outliers) were assessed graphically, supplemented with computation of the variance inflation factor (using the vif() function in the car package (*Fox and Weisberg*, 2019) in R) to check for multicollinearity and Box-Pierce tests (using the Box.test() function in the stats package in R) to identify autocorrelation in the residuals at lag 1. Preliminary analyses suggested a potentially quadratic relationship between whale occurrence and *current_v*, so *current_v* was included in all models as a second order polynomial (i.e., expressed as *current_v* + *current_v*^{2}). These analyses also revealed significant autocorrelation in the residuals of models with fin whales. We successfully mitigated autocorrelation via subsampling, using only every third data point for fin whale models. This reduced sample size (number of absences = 31) substantially increased the risk of overfitting for models with more than 3 terms (i.e., model sets 2-8). The significance of each model was evaluated using drop-in-deviance (likelihood ratio) tests between the full model and a reduced version lacking the variable of interest (i.e., the term $\beta(V)$). The significance of individual model terms was assessed using Wald's tests.

Unless indicated specifically above, all analyses were conducted in R using various utility functions from tidyverse (*Wickham et al.*, 2019), lubridate (*Grolemund and Wickham*, 2011), and sf (*Pebesma*, 2018), while visualizations were implemented using ggplot2 (*Wickham*, 2016), ggspatial (*Dunnington*, 2021), and patchwork (*Pedersen*, 2020) packages.

6.4 Results

6.4.1 Whale detections

The 13 glider surveys amassed 530 days at sea, travelled over 14,000 km, and collected over 14,000 full depth profiles. They also transmitted 26,550 tally periods containing 242 days of pitch track data. Near real-time analysis of these pitch track data determined presence of fin, humpback, right and sei whales on 389, 83, 71, and 133 days, respectively

(Table 6.1).

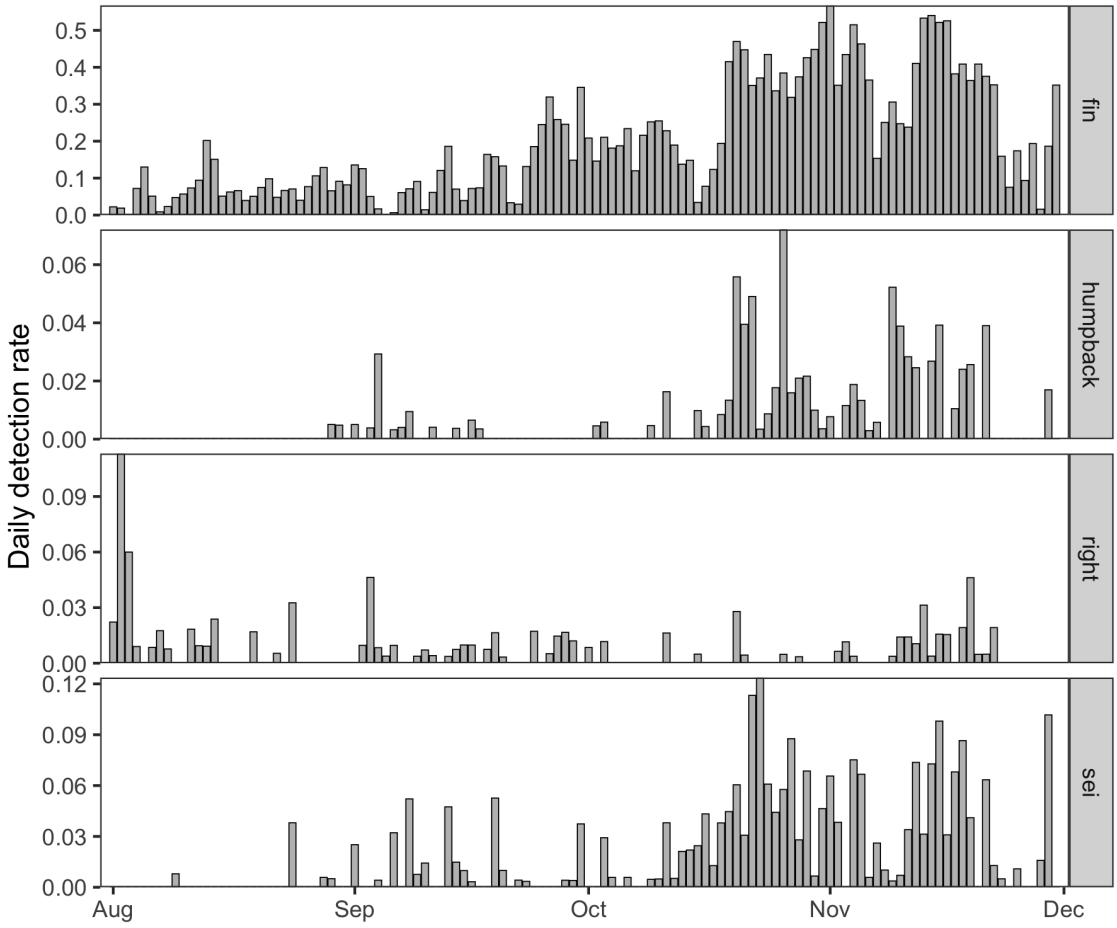

Figure 6.3: Timeseries of the daily detection rates of each species (rows) pooled across all years, computed as the number of tally periods with detections divided by the total number of tally periods for each calendar date.

6.4.1.1 Fin whales

On average, fin whales were detected on nearly every calendar day and consistently present in $>$ 20% of tally periods per day after mid-October (Figure 6.3). In some years it was not uncommon for fin whales to be detected nearly continuously (>90% daily detection rate) over multiple days (Figure D.1). Detections were spatially concentrated in the central and southern portion of the study area in August, then shifted eastward and intensified for the remainder of the period. Fin whale detections were consistently absent from the northwest coastal portion of the study area, and less commonly observed along the western

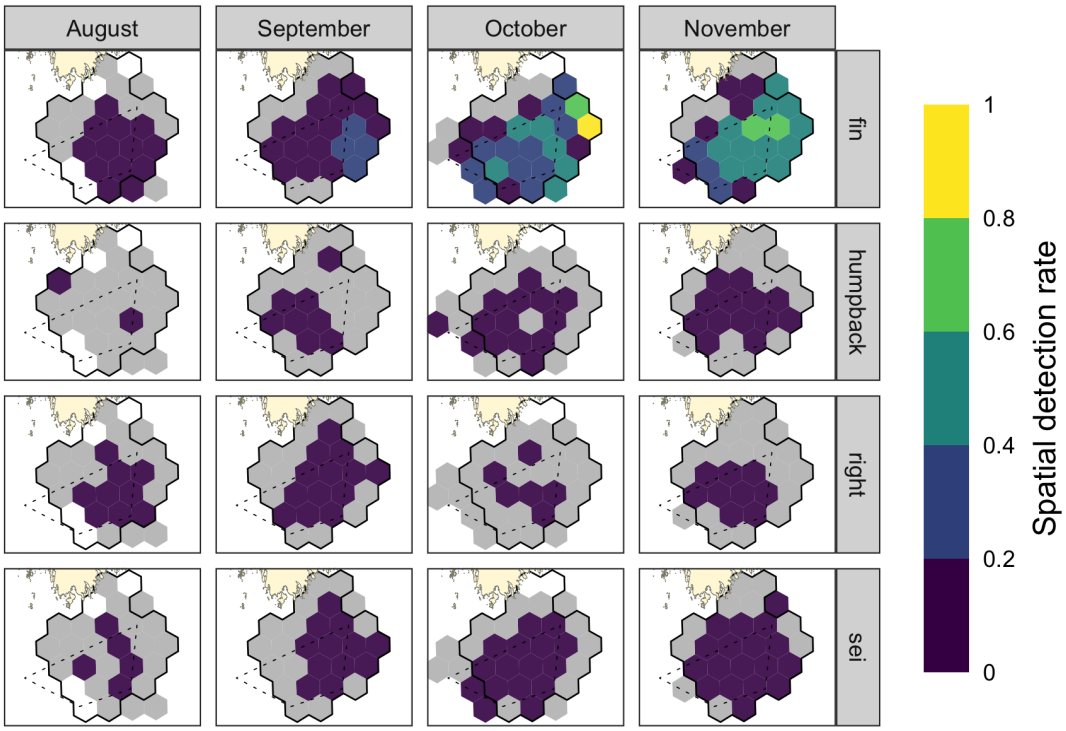

Figure 6.4: Spatial detection rates (computed as the number of detected tally periods divided by the total number of tally periods per species, grid cell, and month across years) of each species (rows) and survey month (columns) in 20 km (diameter) hexagonal grid cells. The hexagonal cells outlined in black are used for the habitat analysis. The dashed polygon denotes the Roseway Basin ATBA. Grey cells indicate areas with survey effort but no detections.

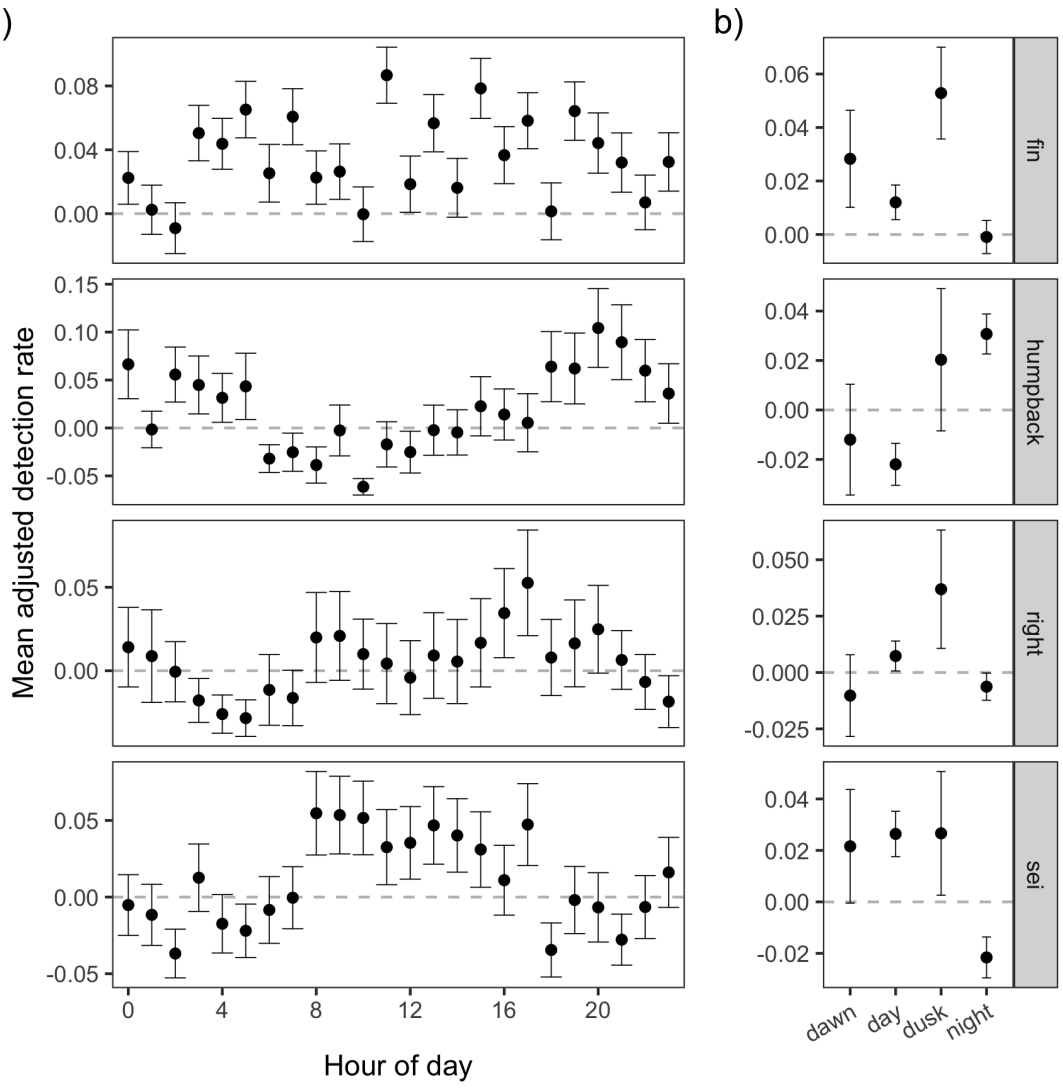

Figure 6.5: The mean (+/- standard error) adjusted detection rate (proportion of detected tally periods per hour) for each species (rows) by the (a) hour of day (local time) or (b) light regime from all glider surveys.

and southern margins of the study area later in the period (Figure 6.4). A Kruskal-Wallis rank sum test provided inconclusive evidence of variation in detection rates of fin whales among light regimes (KW = 7, p = 0.06, Figure 6.5).

6.4.1.2 Humpback whales

Humpback whales were only detected during two tally periods in late August and sporadically in September. Daily detection rates increased and became more consistent in mid-October but remained relatively low (<10%). The spatial extent of detections also increased substantially in October and November relative to the earlier months, with most detections occurring within the ATBA. Humpback detection rates varied by light regime (KW = 60.5, $p < 0.001$), with significantly higher rates at night relative to dawn, day, or dusk ($p < 0.001$; Dunn's multiple comparison test; Figure 6.5).

6.4.1.3 Right whales

Daily detection rates of right whales were highest (∼10%) in August (Figure 6.3), driven primarily by a single 2015 deployment (Figure D.3). Right whales were detected sporadically throughout the season, with lowest occurrence in October. The minimum and maximum monthly spatial extent of detections occurred in October and September, respectively. Though the spatial extent of detections varied from month to month, occurrence was most consistent along the SE margin of the deepest portion of the basin (eastern margin of the ATBA; Figure 6.4). There appears to be substantial interannual variability in detection rates, though this is difficult to characterize given temporal and spatial variation in survey effort (Figure D.4). Right whale detection rates varied by light regime (KW = 23, $p < 0.001$). Detection rates during dawn hours were significantly lower than those during day or night. Detection rates at dusk were variable, but significantly higher than those during the day ($p <= 0.001$; Dunn's multiple comparison test; Figure 6.5).

6.4.1.4 Sei whales

Sei whales were infrequently detected in August (only 4 days in 2015; Figure D.4). Daily detection rates tended to increase from September through November (Figure 6.3). Similar to fin whales, the distribution of sei whale detections encompassed the entire study area with the exception of the NW margin along the coast (Figure 6.4). Sei whale detections varied by light regime (KW = 40, $p < 0.001$). They were highest during day, low at night, and variable during dawn and dusk (Figure 6.5).

6.4.2 Habitat associations

6.4.2.1 Whale occurrence in survey units

Across all years, survey effort was conducted in 30 grid cells in August, 70 in September, 70 in October, and 97 in November (total of 267; Figure 6.6). These surveys transmitted 4,478 h (187 d) of pitch track data divided into 19,578 tally periods, all of which were analyzed in near real-time. This amounted to an average of 73 +/- 68 (mean +/- standard deviation) tally periods and 16.7 +/- 15.8 h of pitch tracks per cell. The gliders collected 12863 profiles over the same period, with an average of 48 +/- 46 profiles per cell. Spatial and temporal patterns in whale occurrence (presence/absence) in grid cells followed similar patterns to detection rate (Figure 6.4). Fin whales were detected in 68.5% of cells (183/267), humpbacks in 22.8% (61/267), right whales in 20.2%, and sei whales in 36.7% (98/267). There appeared to be interannual variability in the occurrence of some species, but this was difficult to assess given the heterogeneity in survey effort (Figure 6.6).

6.4.2.2 Environmental data

The median *depth* and *depth_sd* of each grid cell was 114.7 (Q1-Q3: 98.7-134.9) m and 16.4 (Q1-Q3: 10.4-19.7) m, respectively, with *depth* ranging from 36 - 160 m and *depth_sd* from 2 - 28 m. The distribution of *depth* and *depth_sd* was similar across months, suggesting consistent sampling with respect to bathymetry. The median stratification strength was 1.4 (Q1-Q3: 1.0-2.0) kg m^{-3} and decreased from August to November at an approximate rate of -0.4 kg m^{-3} $month^{-1}$. The median bottom mixed layer width was 18.8 (Q1-Q3: 10.9-26.8) m over the full study period and was about 6 m thicker in the first half of the period (Aug/Sep; median 21.8 m) than in the second (Oct/Nov; median 15.9 m). The median density of the bottom mixed layer was 25.9 (Q1-Q3: 25.6-26.2) kg m^{-3}, with skewed distributions in October and November driven primarily by a fresh water flushing event in 2015 (described in *Ruckdeschel et al.*, 2020). The depth integrated current ranged from 0.01 to 0.48 m s^{-1} with a median of 0.23 (Q1-Q3: 0.15-0.29) m s^{-1}.

6.4.2.3 Descriptive analysis

Qualitative comparisons of the distribution of environmental variables in grid cells where whales were acoustically detected to the distribution of all observations in a given month revealed possible associations that could inform and corroborate statistical modelling. Fin, right, and sei whales tended to occur in cells with deeper and less variable bathymetry than

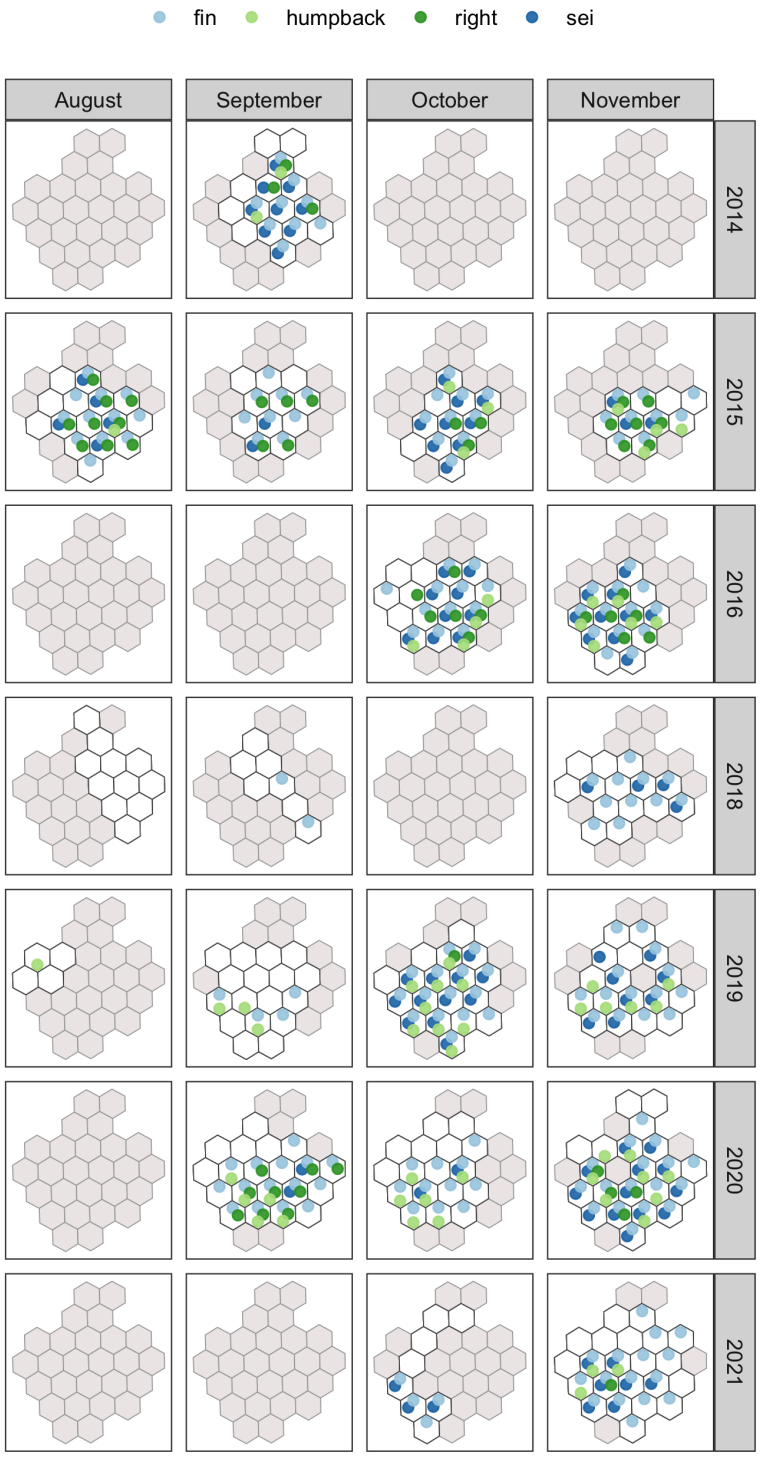

Figure 6.6: Distribution of glider survey effort and whale occurrence in each month (Aug Nov; columns) and year (2014-2021; rows) in 20 km (diameter) hexagonal grid cells in Roseway Basin. Colored points indicate the acoustic presence of a given whale species within a grid cell. Cells with survey effort (white) were included in the habitat analysis, while cells without effort (grey) were not. The extent of these grid cells within the study area is shown in Figure 6.1.

average in all months (Figure 6.7). Right whales were present in cells with higher surface stratification in each month, despite the seasonal decrease in stratification. The number of cells with humpback detections in August was low (n = 2) but occurred in shallower depths with lighter bottom densities than average. Right whale occurrence was apparently associated with a thin bottom mixed layer in September and a thick bottom mixed layer in November. The bottom mixed layer density in cells with right whale detections was well above average in August and more variable, perhaps even below average, in November. Sei whales were consistently detected in cells with below average bottom mixed layer density in August and September. Occurrence appeared to be associated with slightly elevated current speeds for each species in August, October and November, but not in September (Figure 6.7).

6.4.2.4 Logistic regression analysis

Logistic regression analysis provided evidence of associations among environmental variables and the occurrence of fin, right and sei whales (Tables 6.3, 6.4; Figure 6.8). Similarity of drop-in-deviance test results among models fit using month and two-month time intervals suggested that the coarser time resolution was successfully accounting for the major sources of temporal variability. For sei whale models, the addition of a *depth* covariate removed the significance of *bml_width*, *bml_density*, and *current_v*, suggesting that the significance of each of these terms was driven by their correlation with *depth* (Table 6.3). The significant model in set 8 showing an influence of *bml_density* on humpback occurrence is disproportionately influenced by a single detection in very light waters in August, and as such should be treated with caution. The occurrence of fin, right and sei whales was positively associated with depth such that the probability of detection was higher in above-average depths (Tables 6.3, 6.4; Figure 6.8). The effect of depth was indistinguishable between the first and second halves of the study period for right whales, but significantly stronger in the second half of the study period for sei whales. Right whale occurrence was consistently associated with above-average surface stratification in both the first and second half of the study period. In contrast, their relationship to bottom mixed layer width and density appeared to change between the first and second halves of the survey period. Occurrence in the first half of the study period was associated with a thinner, denser bottom mixed layer, and a thinner, fresher bottom mixed layer in the second half of the study period. There is evidence that the association with *bml_density*, but not

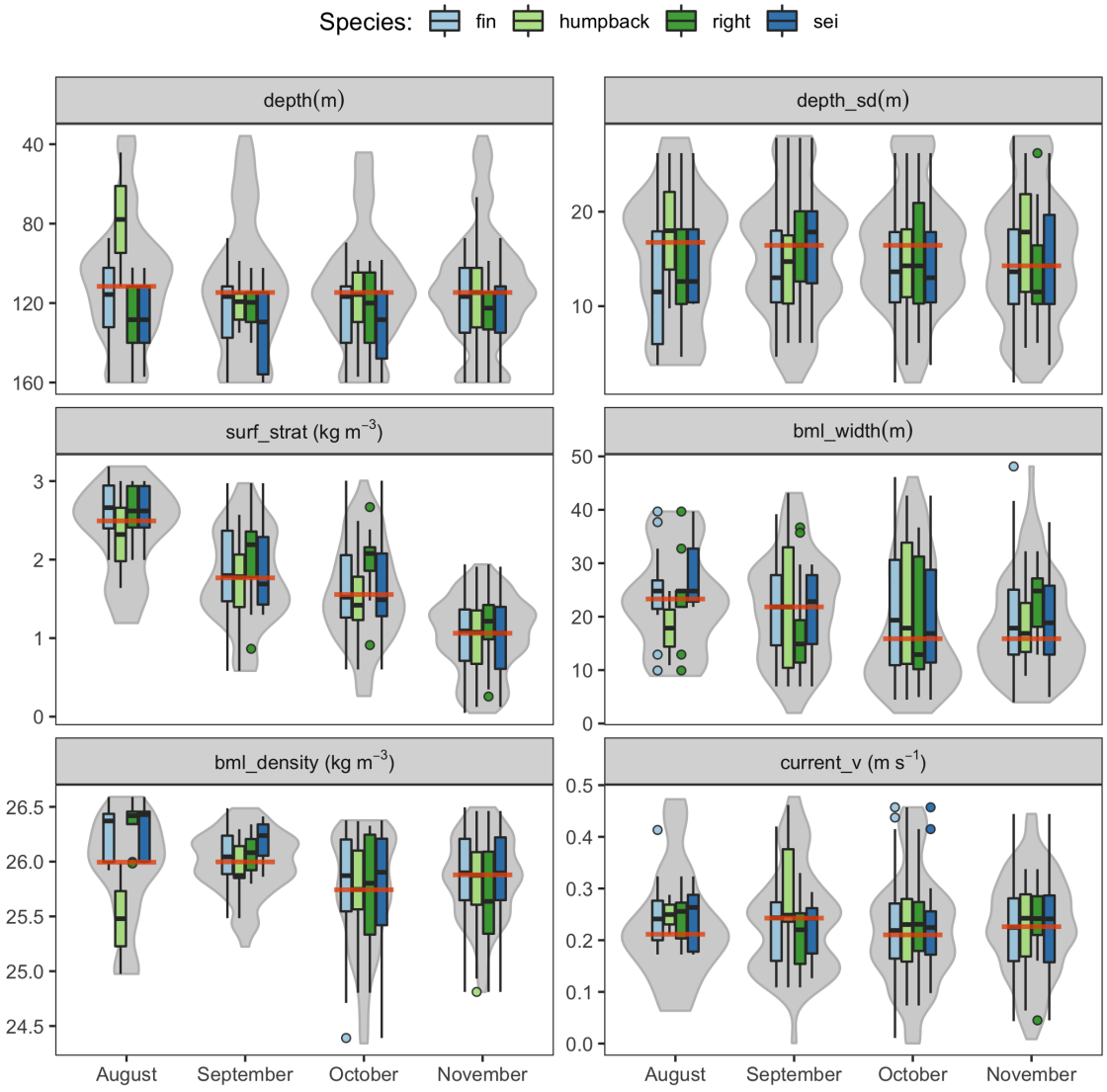

Figure 6.7: The distribution of environmental variables from grid cells in which a given whale species was detected (colored boxplots) compared to the median (red bar) and distribution (grey violin plots) of values from all grid cells in each month. The violin plots show a mirrored kernel density estimate, or essentially a smoothed histogram, of the distribution of all cells in each month. Definitions of each environmental variable are available in Table 6.2. For the boxplots, the lower, middle and upper horizontal lines provide the first, second, and third quantiles, respectively. The whiskers are drawn in either direction to a maximum of 1.5 times the interquartile range, with points outside that range plotted individually.

bml_width, was driven by the late-season flushing event in 2015 (Table D.1). There was limited evidence that *depth_sd* or *current_v* was associated with whale occurrence, though drop-in-deviance test p-values in model sets 1-6 hinted at a potentially weak relationship to sei whale occurrence (Table 6.3).

Table 6.3: Results (p-values) of drop-in-deviance tests of eight sets of logistic regression models. Model sets 1-8 were constructed with Equations 6.2-6.9 in the text, respectively, and evaluated against models of the same form but lacking the variable of interest. The number of cells with whale presence and absence are given in N_1 and N_0, respectively. Descriptive names are provided under each set to convey key differences among sets. Significance (*) was evaluated at $\alpha = 0.05$. Grey values indicate models that likely suffer from overfitting (fewer than 10 observations of presence and absence per model term). Additional information for significant models in are provided in Table 6.4.

				Set 1	Set 2	Set 3	Set 4	Set 5	Set 6	Set 7	Set 8
Species	**N_0**	**N_1**	**Variable**	***effort***	***depth***	***month***	***month+ depth***	***late***	***late+ depth***	***xlate***	***xlate+ depth***
fin	28	61	depth	0.001*	-	<0.001*	-	<0.001*	-	<0.001*	-
	28	61	depth_sd	<0.001*	<0.001*	<0.001*	<0.001*	<0.001*	<0.001*	<0.001*	<0.001*
	28	61	surf_strat	0.8	0.24	0.6	0.14	0.97	0.32	0.93	0.6
	30	59	bml_width	0.013*	0.28	0.007*	0.1	0.012*	0.16	0.002*	0.019*
	31	58	bml_density	0.001*	0.07	<0.001*	0.025*	<0.001*	0.028*	0.004*	0.031*
	26	62	current_v	0.49	0.28	0.32	0.22	0.35	0.19	0.26	0.07
humpback	206	61	depth	0.64	-	0.6	-	0.59	-	0.44	-
	206	61	depth_sd	0.68	0.57	0.73	0.61	0.69	0.58	0.81	0.75
	206	61	surf_strat	0.14	0.12	0.12	0.11	0.11	0.1	0.28	0.26
	205	61	bml_width	0.34	0.39	0.3	0.36	0.32	0.38	0.57	0.65
	205	61	bml_density	0.45	0.26	0.54	0.34	0.51	0.31	0.1	0.048*
	203	60	current_v	0.38	0.31	0.39	0.31	0.41	0.32	0.43	0.39
right	213	54	depth	0.014*	-	0.015*	-	0.015*	-	0.044*	-
	213	54	depth_sd	0.17	0.49	0.16	0.44	0.17	0.48	0.31	0.62
	213	54	surf_strat	<0.001*	0.001*	<0.001*	0.001*	<0.001*	0.002*	0.004*	0.007*
	212	54	bml_width	0.59	0.8	0.6	0.8	0.6	0.81	0.03*	0.036*
	212	54	bml_density	0.9	0.16	0.96	0.12	0.93	0.14	0.015*	0.029*
	209	54	current_v	0.08	0.11	0.08	0.1	0.07	0.09	0.09	0.09
sei	169	98	depth	<0.001*	-	<0.001*	-	<0.001*	-	<0.001*	-
	169	98	depth_sd	0.15	0.58	0.1	0.5	0.1	0.5	0.14	0.31
	169	98	surf_strat	0.69	0.99	0.7	0.87	0.71	0.89	0.93	0.98
	168	98	bml_width	0.028*	0.3	0.018*	0.26	0.019*	0.27	0.06	0.53
	168	98	bml_density	0.024*	0.77	0.015*	0.69	0.018*	0.73	0.007*	0.25
	166	97	current_v	0.06	0.05	0.047*	0.05	0.05	0.06	0.1	0.08

Table 6.4: Parameters of significant models identified from drop-in-deviance tests (see Table 6.3), where Error is the standard error of the Estimate of a given Coefficient. Model sets 1, 5, and 8 were fit using equations 6.2, 6.6, and 6.9. The p-value shows results of the Walds test of each coefficient, with significance (*) evaluated at $\alpha = 0.05$.

Species	Set	Variable	Coefficient	Estimate	Error	P
fin	1 *(effort)*	depth	(Intercept)	-0.34	0.47	0.48
			depth	0.03	0.01	0.003*
			effort	0.03	0.01	0.009*
right	5 *(late)*	depth	(Intercept)	-2.15	0.35	<0.001*
			depth	0.02	0.01	0.02*
			effort	0.01	0	<0.001*
			late	-0.4	0.34	0.24
right	5 *(late)*	surf_strat	(Intercept)	-2.23	0.35	<0.001*
			surf_strat	1.08	0.34	0.001*
			effort	0.01	0	<0.001*
			late	-0.43	0.34	0.21
right	8 *(xlate+depth)*	bml_width	(Intercept)	-2.21	0.36	<0.001*
			bml_width	-0.06	0.03	0.042*
			late	-0.41	0.35	0.24
			effort	0.01	0	<0.001*
			depth	0.02	0.01	0.023*
			bml_width:late	0.09	0.04	0.012*
right	8 *(xlate+depth)*	bml_density	(Intercept)	-2.27	0.38	<0.001*
			bml_density	1.41	1.16	0.23
			late	-0.24	0.37	0.53
			effort	0.01	0	<0.001*
			depth	0.02	0.01	0.044*
			bml_density:late	-2.47	1.18	0.037*
sei	5 *(late)*	depth	(Intercept)	-3.47	0.48	<0.001*
			depth	0.02	0.01	<0.001*
			effort	0.02	0	<0.001*
			late	2.33	0.41	<0.001*

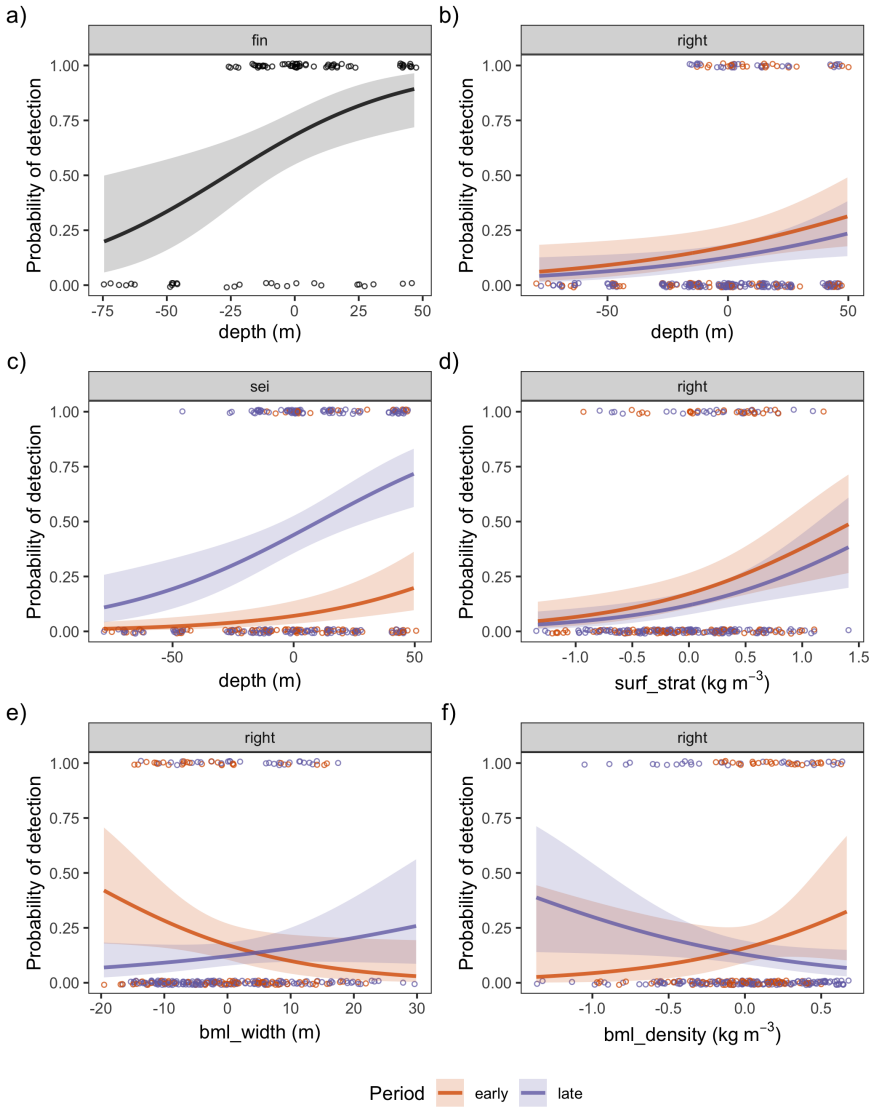

Figure 6.8: Selected results of the logistic regression analysis of whale-habitat associations over the full study period (all months; black) or in the first half (early; Aug-Sep; red) versus second half (late; Oct-Nov; blue) of the study period. Panel a shows the relationship between depth and the probability of fin whale detection over the full study period (corresponds to model set 1, fit with Equation 6.2). Panels b and c show the additive effects of survey time (early or late) and depth on the probability of right and sei whale detection, respectively. Similarly, panel d shows the additive influence of time and surface stratification on right whale detection. Models in panels b-d were from set 5 (fit with Equation 6.6). Panels e and f show the interactive effects of time and (e) bottom mixed layer width or (f) bottom mixed layer depth on right whale detections (corresponds to model set 8, fit with Equation 6.9). The solid lines show the model fit and the shaded region indicates the 95% confidence limits. The jittered points show the raw data used to construct the regressions. Values of environmental variables are expressed as anomalies from the monthly average across all years. Definitions of each environmental variable are available in Table 6.2. Model comparison results and parameters are available in Tables 6.3 and 6.4, respectively.

6.5 Discussion

6.5.1 Right whales

While a sharp decline in sightings rates in the last decade is suggestive of a change in the importance of Roseway Basin to right whales, our results indicate that right whales are sporadically present in the Basin throughout the fall. This corroborates and extends recent analyses by *Durette-Morin* (2021) and *Davis et al.* (2017) that revealed year-round right whale presence in the Basin. The occurrence of right whales in the late fall and early winter and their acoustic detection in near real-time is especially notable from a conservation perspective given the challenges (e.g., weather, visibility) of conducting regular visual surveys at that time of year, compounded with risk of entanglement and vessel strike in the region (*Vanderlaan et al.*, 2008; *van der Hoop et al.*, 2012). It further demonstrates the utility of an autonomous platform for conducting persistent surveys in adverse conditions.

Right whales were most consistently detected along the SE margin of Roseway Basin. This agrees with findings from *Davies et al.* (2014) that suggest the combined influence of slope water intrusions, tidal advection, and bathymetric constraints function to concentrate *Calanus finmarchicus* along this margin of the basin. It also aligns with the highest sighting probability derived from vessel-based surveys of the region (*Davies et al.*, 2014). These findings suggest that glider-based PAM is capable of resolving spatial associations at scales of approximately the same order of magnitude of the expected maximum detection range ($\sim$30 km; Chapter 2).

The increased detection of right whale calls in twilight hours reported here is consistent with findings from Wilkinson Basin (*Mussoline et al.*, 2012) and for periods of the year with high vocal activity in Massachusetts Bay (*Morano et al.*, 2012). In the central Gulf of Maine, *Bort et al.* (2015) documented a bimodal diel pattern of upcalls with peaks at both dawn and dusk. *Mellinger et al.* (2007) reported no diel pattern at a site located in our study area (on the SE margin of Roseway Basin), and an increase in calling during daylight hours at a site in Emerald Basin (approximately 150 km eastward of Roseway). Their analysis omitted crepuscular periods (dawn and dusk) and compared between light and dark hours. We also found no statistically significant difference between light and dark hours (Figure 6.5).

The biological significance of diel patterns in vocal behavior is unknown for right whales. There is evidence that changes in calling rates are linked to behavioral states, where calling

is higher during socializing and lower during foraging (*Parks et al.*, 2011a). In other baleen whale species, diel patterns have been associated with foraging activity (*Baumgartner and Fratantoni*, 2008, see below). The apparent spatial and temporal variation in diel patterns is perhaps indicative of specific behaviors. Improved understanding of the mechanisms behind diel periodicity may permit the use of broadscale PAM networks to elucidate behavior and inform more effective management.

Comparison of the right whale detections with local hydrography from the glider provided evidence of time-varying associations among right whale occurrence and the bottom mixed layer, where the odds of right whale presence early in the study period increased with a shallow, dense bottom mixed layer. The association with a dense bottom mixed layer early in the study period is expected based on work from *Davies et al.* (2014) showing evidence of a strong positive correlation between the water mass density and *Calanus finmarchicus* energy density in the deep Basin. Our findings conflict with those of *Baumgartner et al.* (2003b) for Roseway and the Bay of Fundy, as well as to those from Chapter 5 for the Gulf of St Lawrence, in which there was evidence of a positive association between whale occurrence and bottom mixed layer width (i.e., whale presence was more likely when the bottom mixed layer was thick). A potentially confounding factor is that the inflection depth of the glider ($\sim$8 m above the sea floor) prevented us from sampling as close to the sea floor as is typically achieved with CTD casts. A possible explanation for the discrepancy is that the zooplankton layer can be either concentrated on the interface of the bottom mixed layer, as suggested by *Baumgartner et al.* (2003b), or within it, as suggested by *Davies et al.* (2014). If above it, a thicker bottom mixed layer would aid in the formation of a discrete, dense layer close to the surface where it can be readily exploited. If within it, a thicker bottom mixed layer would dilute the zooplankton concentration. Though the dynamics of patch formation are not well-understood, the position of the *Calanus* is likely a function of their physiological state (e.g., active or in diapause), the density of the surrounding seawater (and associated impact on copepod buoyancy), and local hydrodynamic forcing (*Baumgartner and Tarrant*, 2017).

Previous studies of right whale habitat in Roseway have been restricted to the summer months. This study is the first to demonstrate changes in the strength of these associations late into the fall. The change over time may reflect a shift in the factors affecting right whale distribution and/or right whale calling behavior. It is difficult to assess the cause of

this trend as the fall is an especially dynamic period, but it was notably absent in the habitat associations of other species. It is also possible that the reason for the change is driven primarily by behavioral factors, such as a transition from foraging into travelling states, but this is speculation based loosely on observed seasonality in right whale distribution patterns (*Brown et al.*, 2007).

We also observed strong evidence that right whale presence was associated with a positive anomaly in stratification strength, and that this relationship persisted over time as the upper water column destabilized. *Baumgartner et al.* (2003b) tested for and did not find evidence of a similar relationship to stratification strength in Roseway, but *Baumgartner and Mate* (2005) observed that right whales equipped with satellite tags tended to visit areas characterized by high surface stratification. Right whales are known to feed on surface and near-surface layers of copepods in other habitats, such as Cape Cod Bay (*Mayo and Marx*, 1989). Within Roseway, perhaps right whales are associated with times and places of relatively high stratification and reduced vertical mixing because these conditions are more likely to result in the formation of dense aggregations of copepods. Though speculative, the differences in habitat associations observed here and in the early 2000's suggest that right whales are using this habitat differently than they have in the past, which may be the result of a substantial decline in the availability of late-stage Calanus across the region (*Sorochan et al.*, 2019; *Record et al.*, 2019).

6.5.2 Fin whales

Fin whale calling was extraordinarily prolific and detections were nearly constant within the deep Basin, especially later in the study period. The signal we used to detect fin whale presence, repeated sequences of the 20-Hz pulse, is considered song and suspected to be produced solely by males as part of a reproductive display (*Croll et al.*, 2002). It is highly seasonal, and some evidence suggests it is not produced in association with feeding behavior (*Romagosa et al.*, 2021). It also has the potential to propagate long distances, perhaps up to 100 km in the deep ocean (*Stafford et al.*, 2007), which is approximately the scale of our study area. The abundance of song on every deployment in this dataset suggests that Roseway Basin plays a potentially important role in fin whale reproduction. This is reinforced by findings from *Davis et al.* (2020) that show fin whales are detected year-round in Roseway Basin. Though beyond the scope of this study, detailed analysis of the song structure, namely the inter-pulse-interval, could identify the population of the

singer(s), which could prove useful for population assessment and management (*Delarue et al.*, 2009).

The same factors that likely make fin whale song an effective reproductive display impose significant barriers to using song to infer habitat associations, particularly over small spatial scales. Modelling efforts were compromised by high autocorrelation and the rarity of absences. That said, some interesting patterns emerged from our analyses. The first is the near-complete absence of fin whale detections in the coastal shallows in the NW of the study area. This absence is most pronounced in November where areas without detections were only separated by $\sim$50 km from areas where detections were nearly constant. The most likely explanation is that fin whales avoid shallow areas. It is also likely that the shoaling bathymetry increases transmission loss of fin whale calls, effectively restricting calls to deeper water (*Jensen et al.*, 2011). Perhaps both factors are at play, as fin whales seeking to advertise their reproductive status over a large range would likely avoid, or at least avoid vocalizing within, areas characterized by reduced propagation range.

6.5.3 Sei whales

The spatial and temporal patterns of sei whale detections were similar to those of fin whales. This includes the seasonal increase in detection rate and the nearly complete absence of detections in the NW portion of the study area near the coast. That said, sei whale calling was much less prolific, and, though the spatial extent of the region with detections in October / November was comparable to that of fin whales, the spatial detection rates were much lower.

The downsweep call used to identify sei whales has been linked to both foraging and song behavior. *Baumgartner and Fratantoni* (2008) documented diel patterns in call rate in close association with the diel vertical migration of zooplankton prey. One possible explanation the authors provide is that vocalizations were reduced at night while whales were foraging on zooplankton near the surface and increased during the day when the migrating layer was deep and whales engaged in social behaviors. *Tremblay et al.* (2019) observed these downsweeps produced in association with other calls in a structure consistent with that of song. Our analysis did not distinguish between potential song or non-song. That said, our observation of the same diel pattern as described by *Baumgartner and Fratantoni* (2008) provides circumstantial evidence that sei whales were engaged in

foraging behavior.

The intermediate detection rates and reduced autocorrelation also facilitated more detailed habitat analyses than was possible with fin whales. The results provided evidence of a positive association with depth that strengthened in the second half of the study period. This was consistent using time resolutions of one and two months. The cause of this trend is difficult to determine, but could be ecological (e.g., the transition to a different foraging strategy) as sei whales are perhaps the most general predators of the baleen whales considered here, capable of foraging on copepods, krill, and schooling fish (*Prieto et al.*, 2012). The shift could also be behavioral, particularly given the evidence that the same call type can be produced in association with foraging (*Baumgartner and Fratantoni*, 2008) as well as in patterned bouts consistent with song (*Tremblay et al.*, 2019). An additional confounding factor in these analyses, and perhaps a reason for the similarity between sei and fin whale associations with depth, is that their low-frequency, high amplitude vocalizations likely propagate over even greater ranges in deep areas (*Jensen et al.*, 2011).

6.5.4 Humpback whales

Humpback occurrence was determined based on the presence of song. The sparse detections in September followed by the increase in October coincides exactly with the timing of the transition from the production of song fragments to full song described by *Kowarski et al.* (2021). They attribute the timing of song onset to critical changes in photoperiod. The timeseries suggests coincident increases in sei and fin detection rates. Though speculative, the apparent synchronization of this increase could be due in part to photoperiod. It could also be a result of interannual variation in detections and/or effort, or a host of additional, unresolved factors.

Similar to *Kowarski et al.* (2018), humpback detections occurred predominately during evening and night hours. The reasons for the diel pattern are unknown. Given the relatively low numbers of humpback whale detections, as well as the potentially confounding effects of using song as a detection cue, it is perhaps not surprising that the habitat analysis did not reveal any robust associations between humpbacks and their environment. Furthermore, our model was designed to target hydrographic processes known to aggregate right whale prey. These are likely less effective prey proxies for piscivorous humpbacks, as the distribution and abundance of the schooling fish they prey upon may be decoupled from or less influenced by these physical properties and dynamics (*Hazen et al.*, 2009).

6.5.5 Challenges and caveats

Though the use of gliders for passive acoustic monitoring is well-established (*Baumgartner et al.*, 2020; *Klinck et al.*, 2012), the use of these platforms to make habitat inferences is in its infancy. We therefore consider our habitat analyses as exploratory and sought to conduct them in such a way as to overcome several of the challenges inherent to this dataset. The first potential issue is the use of acoustic detections as a measure of whale presence. Call production by baleen whales is highly variable, behaviorally mediated, and typically poorly described (e.g., *Parks et al.*, 2011a). While some calling behaviors may relate directly to foraging or habitat quality, others are likely produced in an unrelated context, serving to, for example, advertise reproductive status or maintain long range group cohesion during migration (*Payne and Webb*, 1971; *Clark and Ellison*, 2004). There is evidence that several species vocalize less frequently while foraging (*Baumgartner and Fratantoni*, 2008; *Parks et al.*, 2011a). That said, baleen whales are mobile predators with high energy demands whose distribution must at some point be correlated with that of their prey (*Palacios et al.*, 2013).

Variability in detection range poses another challenge for interpreting whale presence. Detection range varies by source (species), environment, noise level, glider depth, and analysis protocol (Chapter 2). Further, the area being monitored is almost certainly an order of magnitude larger than the area over which environmental data are being collected, leading to a time/space mismatch in occurrence and environmental data. Accounting for this mismatch of scales is not trivial. We pursued a variety of other different definitions of survey units (e.g., trackline segments, time-averaged glider position) before selecting a monthly gridding approach as the most suitable for retaining as much data and resolution as possible while addressing the temporal and spatial correlation structure and the significant heterogeneity of survey effort. A more comprehensive analysis in the future would evaluate the sensitivity of these results to the choice of grid size, and perhaps even optimize the grid sizing for each species based on the autocorrelation structure and/or estimated detection range. An alternative approach would be to apply an amplitude threshold to species detections, such that only loud calls presumably originating at close ranges from the glider would be considered in the analysis. This was not feasible in our exploratory analysis given that we determined acoustic occurrence using pitch track analysis of tally periods, rather than on a call-by-call basis. A further limitation with this approach is that the occurrence

of some species, especially humpback and right whales, was relatively rare. Rejecting additional calls under an amplitude threshold would likely further reduce sample size and statistical power. A more nuanced alternative to a threshold approach could be to include amplitude as a model covariate. All of the archived audio for these deployments is available, so such analyses could be conducted in the future.

Our overall goal was to evaluate the ecological importance of specific physical features to baleen whales, rather than develop a predictive model of whale occurrence. This is an important distinction that informed our choice of statistical approach. We chose to avoid stepwise variable selection from a large, multivariate model, as the ecological influence of a selected variables can become difficult to explain, and the resulting p-values are potentially compromised by the selection process (*Palacios et al.*, 2013). Similarly, we avoided the use of other "black box" modelling approaches in favor of the ecologically interpretable results of the logistic regression (*Redfern et al.*, 2006). We conducted preliminary analyses using Generalized Additive Models so as to avoid making any assumptions about the functional form of the relationship among the predictor and response variables. We found this approach was limited by its inability to readily resolve interactions among predictor variables. The results of our analysis demonstrate the importance of resolving these interactive effects. This makes ecological sense, as baleen whale foraging and the dynamics that aggregate their prey are almost certainly mediated by the complex interaction of multiple factors (e.g., *Hazen et al.*, 2009). The next step in our modelling procedure would be to increase the number of explanatory variables to represent additional processes/features, especially those of relevance for rorqual foraging, and to use those results to inform the careful construction of multivariate models to address specific hypotheses about whale-habitat associations.

Though we made efforts to thoroughly evaluate and address all the underlying assumptions of the logistic regression analysis, the significance levels of our tests should be interpreted with caution. Repeated hypothesis testing raises the multiple comparisons problem, wherein the likelihood of erroneous results increases with the number of tests conducted. This can be controlled by using a single, multivariate model, which would be a logical next step for this analysis (*Hosmer et al.*, 2013). Another mitigation measure is to increase the significance (i.e., α) level proportionally to the number of models run, referred to as a Bonferroni adjustment. In our case the Bonferroni adjusted significance level for

a given species and model set would be 0.008 (0.05 / 6 models). At this level, observed associations between right whales and *depth*, *bml_density*, and *bml_width* would no longer be significant. We opted to use the uncorrected p-values to avoid missing ecologically relevant relationships with small effect sizes, but suggest that precautionary treatment of these values is warranted. That said, the relationships that emerged from the statistical analyses were also evident in the raw data (Figure 6.7), instilling confidence in both the statistical approach and results.

6.6 Conclusions

We gathered a large dataset of passive acoustic and hydrographic observations using autonomous vehicles and conducted an analysis of baleen whale occurrence and potential habitat associations in Roseway Basin. Our results provide insights into the spatial and temporal distribution of each species' acoustic occurrence within the habitat and corroborate previously documented diel vocalization patterns. Though challenging to account for the mismatch of observational scales and behaviorally mediated acoustic behavior, our results identified right whale habitat associations that align with those that have been established previously. The high-resolution, fine-scale, vertical sampling of the Slocum glider provided insights into whale associations with subsurface features that would not have been possible using traditional remote-sensed data, nor feasible using shipboard methods. These platforms have great potential for helping to move the study of cetacean habitat associations beyond correlative analyses by elucidating the underlying biophysical mechanisms that influence species distribution.

6.7 Acknowledgements

We are indebted to the Coastal Environmental Observation Technology and Research (CEOTR) group and the Ocean Tracking Network (OTN) at Dalhousie University, especially Fred Whoriskey, Richard Davis, Adam Comeau, and Jude Van der Meer, for their tireless efforts to facilitate the glider surveys of Roseway Basin. We are grateful for help from Ben Hodges with glider preparations in 2014 and 2015. We thank Christoph Renkl for helpful discussions about data analysis and presentation, and Delphine Durette-Morin for assistance with the near real-time detection validation.

Support for this work was provided by the Department of Fisheries and Oceans (DFO), Natural Sciences and Engineering Research Council of Canada (NSERC), and the Marine Environmental Prediction and Response Network (MEOPAR). Support for HDJ was provided by the Killam Foundation, Vanier Canada Graduate Scholarship program, Dalhousie University, the Nova Scotia Graduate Scholarship program, and the Canada Graduate Scholarships - Michael Smith Foreign Study Supplements (CGS-MSFSS) program.

CHAPTER 7

CONCLUSIONS

The original focus of this thesis was on the use of gliders to make inferences about whale habitat and inform their conservation. In order to effectively make use of acoustic detection information from gliders, we first had to overcome one of the pervasive challenges in the field of passive acoustic monitoring: detection range. This led to the study described in Chapter 2, where we empirically derived the probability of detecting right whales from gliders and buoys as a function of range, noise level, platform depth, analysis protocol, and the number of calls considered. Including the influence of these other covariates was particularly insightful, often in ways that were not immediately obvious or intuitive. In the case of the glider, for example, platform depth exerted a stronger influence on detection range than noise level. For either platform, the use of protocols that are precautionary and/or capable of considering multiple calls can increase detection range dramatically. This has key implications for the interpretation of PAM results, especially as PAM becomes an increasingly popular tool for making inferences about marine mammal distribution.

The fieldwork for Chapter 2 concluded in the spring of 2017. Within the next few months, right whale mortalities in the Gulf of St Lawrence would skyrocket, signalling the beginning of a conservation crisis that demanded new tools to address. Dynamic risk mitigation became critical. Near real-time passive acoustic monitoring offered another source of dynamic information on whale occurrence, but interpreting these results, particularly as they relate to sightings, was not straightforward. To address this, we used preliminary detection range estimates from Chapter 2 to parameterize a simulation that quantitatively compared the uncertainty in acoustic and visual survey results on dynamic management

timescales (Chapter 3). We found that, when accounting for whale movement, the estimates of whale location derived from acoustic and visual methods become equally, and substantially, uncertain with about 1 to 2 days following a detection. The combined results of Chapters 2 and 3 were instrumental in the decision by Fisheries and Oceans Canada and Transport Canada to begin using near real-time acoustic detections interchangeably with visual survey results to trigger dynamic risk mitigation measures in Atlantic Canada.

The right whale mortality crisis and demand for dynamic management prompted a huge surge of survey effort. There was no infrastructure in place to collate and disseminate the results of these surveys in an effective way. This led to the development of WhaleMap (Chapter 4). What began as an informal, in-house tool has grown to become the definitive source of near real-time survey results for the entire east coast of the US and Canada, where it directly facilitates the implementation of nearly all dynamic management measures. Though not an academic product, per-se, WhaleMap provides another tool to advance baleen whale conservation via an improved understanding of their distribution, and in that sense is closely linked to the body of work put forward in this thesis.

In an effort to better understand the underlying mechanisms responsible for the apparent increased occupancy of the Gulf of St. Lawrence by right whales, rather than merely reporting it, we began conducting opportunistic oceanographic sampling from vessels running visual surveys (Chapter 5). Through a combination of hydrographic, net, and optical sampling, we provide evidence that right whales are feeding on a mixed assemblage of late-stage *Calanus finmarchicus* and *Calanus hyperboreus* at the bottom of the water column. The contribution of *C. hyperboreus* appears to be an especially important and distinguishing aspect of this foraging habitat, as their larger body size may compensate for the relatively low *Calanus* abundance observed in the GSL compared to other right whale habitats. This work has complimented other ongoing habitat analyses in the region by providing the first prey samples collected in close proximity to right whales and lays the groundwork for more detailed study of the dynamics that influence the distribution and abundance of right whale prey, and, by extension, right whales, within this important and high-risk habitat.

In Chapter 6, the prevailing themes of passive acoustic monitoring and habitat ecology are combined to revisit the initial goal of evaluating the use of acoustic gliders to make inferences about whale habitat. The analysis of a long (8 year) timeseries of glider

deployments in Roseway Basin revealed new insights in the temporal and spatial distribution of baleen whale acoustic occurrence. Exploratory comparisons, both descriptive and statistical, of acoustic occurrence and glider-derived environmental variables provide evidence of right whale habitat associations that have been documented previously and are ecologically interpretable. Though exploratory, these results suggest that autonomous platforms can be effective tools for studying baleen whale ecology. Given the proliferation of autonomous platforms in oceanographic research, we anticipate this will be an area of substantial growth and insight in the coming years.

In summary, the body of work put forward by this thesis advances passive acoustic monitoring, habitat ecology and conservation of baleen whales in the Northwest Atlantic. It is our hope that these efforts will contribute to the effective research and management of these species for years to come.

APPENDIX A

SUPPORTING INFORMATION FOR CHAPTER 2

A.1 Precautionary analysis of real time pitch tracks

Numerous pitch tracks resembled right whale upcalls but were not completely convincing, so they were scored as "possibly detected" (n = 79 for the buoy; n = 54 for the glider). The main text of this chapter presents results acquired using a conservative protocol in which the pitch tracks scored as "possibly detected" were treated as "not detected". This protocol is designed to minimize false detections at the expense of increased missed detections. We opted to focus on this protocol in the main text as it has been extensively employed on all previous deployments in the NW Atlantic (e.g., *Baumgartner et al.*, 2019). An alternative approach is to use a precautionary protocol that treats calls scored as "possibly detected" as "detected". This is intended for a science or mitigation application that seeks to minimize missed calls at the expense of false detections.

In our study, employing a precautionary protocol caused the probability of detecting localized calls to increase for both the buoy and the glider across all ranges, but especially at close range (Figures 2.8, A.7). For the buoy in average noise conditions (100 dB re 1 $\mu Pa^2 Hz^{-1}$), the fitted regression suggested that a probability of detection of 0.5 (95% CI: 0.427-0.571) occurred at 5.8 km. For the glider in average noise (100 dB re 1 $\mu Pa^2 Hz^{-1}$) and depth (15 m) conditions, the fitted regression suggested that a probability of detection of 0.5 (95% CI: 0.400-0.602) occurred at 12.3 km (Figures 2.8, A.7).

Pitch tracks were labeled as "possibly detected" for several reasons. The primary cause was poorly formed pitch tracks; these were responsible for 58% and 44% of pitch tracks

being scored as "possibly detected" for the buoy and glider, respectively (Table A.1). For the glider, 35% of "possibly detected" pitch tracks were missed because of humpback whale song, many of which occurred at very close ranges. In contrast, song was only implicated in 15% of the pitch tracks that were labeled as "possibly detected" for the buoy. Approximately 19% of "possibly detected" pitch tracks were caused by human error in the buoy analysis, compared to only 6% in the glider analysis (Table A.1; Figure A.6).

A.2 Analysis of archival audio

The goal of our study was to quantify the range-dependent accuracy of the DMON/LFDCS on board an ocean glider and moored buoy. The DMON/LFDCS provides near real-time acoustic presence estimates by producing an abstraction of the raw acoustic signal in the form of pitch tracks that can then be transmitted back to shore for review. The article outlines a number of analyses to evaluate the performance of the near real-time DMON/LFDCS. Here we repeat those analyses for the archival audio data recorded on the DMON. The difference in performance between the pitch track and archival audio results provides an indication of the cost, or the reduction in system performance, associated with the review of pitch tracks alone (i.e., without the aid of spectrograms or audio) in near real time.

The 541 localized calls were used to determine the probability of detection for each platform based on the manual review of archival audio data. The spatial distribution of localized calls for this analysis was non-uniform (Figure A.1). Because the DMON on the moored buoy recorded on a 50% duty cycle, audio was not available for approximately half (301/541) of all localized calls; analysis of the archival audio from the buoy was conducted using the 240 localized calls for which audio was available. The proportion of localized calls that were detected decreased with range (Figure A.2); 87% of localized calls within 5 km (67/77) were detected while 43% of localized calls between 15 and 40 km (3/7) were detected. Calls were missed for a variety of reasons: 9.1% were missed because they were faint or absent from the spectrogram, 1.7% were missed due to interfering biological sounds (i.e., humpback whale song), 0.8% were missed due to interfering non-biological sounds (e.g., other platform noise, ship noise), and 10% were missed due to human error in reviewing the audio data (Table A.1; Figure A.6). For the buoy in average noise conditions (100 dB re 1 $\mu Pa^2 Hz^{-1}$), the fitted regression suggested that a probability of detection of

0.5 (95% CI: 0.328-0.673) occurred at 13.2 km.

For the glider, the 114 localized calls that were excluded from the near real-time analysis due to platform noise were also excluded from the archival audio analysis. The proportion of the remaining 427 localized calls that were detected decreased with range (Figure A.2); 79.9% of localized calls within 5 km (147/184) were detected while 37.5% of localized calls between 15 and 40 km (6/16) were detected. Calls were missed for a variety of reasons: 15.2% were missed because they were faint or absent from the spectrogram, 1.4% were missed due to interfering biological sounds (i.e., humpback whale song), 5.4% were missed due to interfering non-biological sounds (e.g., other platform noise, ship noise), and 9.6% were missed due to human error in reviewing the audio data (Table A.1; Figure A.6). For the glider in average noise (100 dB re 1 $\mu Pa^2 Hz^{-1}$) and depth (15 m) conditions, the fitted regression suggested that a probability of detection of 0.5 (95% CI: 0.365-0.635) occurred at 15.8 km (Figure A.7).

Table A.1: Diagnostic scores associated with calls labeled as "possibly detected" during manual review of glider and buoy pitch track records of calls localized by the array. Here n refers to the number of calls, while % is the percentage of total calls labeled as "possibly detected" on each platform (54 for the glider, 79 for the buoy).

Score	Definition	Glider		Buoy	
		n	%	*n*	%
Poor	Calls were not pitch tracked accurately/completely because of low amplitude or poor shape	24	44.4	46	58.2
Song	Uncertainty due to interfering species calls	19	35.2	12	15.2
Noise	Calls were not pitch tracked accurately/completely because of interfering sound	8	14.8	6	7.6
Missed	Human error (analyst chose wrong score erroneously)	3	5.6	15	19

A.3 Simulation to evaluate methodology

A potential source of bias in our approach is that each call used to estimate the DMON/LFDCS detection function first had to be detected and localized by the array. We developed a

Table A.2: Results from manual scoring of glider and buoy archival audio records of calls localized by the array (total number of calls = 541). Here n refers to the number of calls, while % is the percentage of total localized calls available for detection (i.e., does not consider excluded calls).

Score	Definition	Glider		Buoy	
		n	*%*	*n*	*%*
Absent	Calls were not detected because of low amplitude	52	12.2	3	1.2
Poor	Calls were detected accurately/completely because of low amplitude or poor shape	13	3.0	19	7.9
Song	Uncertainty due to interfering species calls	6	1.4	4	1.7
Noise	Calls were not detected accurately/completely because of interfering sound	23	5.4	2	0.8
Missed	Human error (analyst chose wrong score erroneously)	41	9.6	25	10.4
Detected	Calls were detected by analyst	292	68.4	187	77.9
Exclude	Calls were not available for detection because the platform was not monitoring	114	N/A	301	N/A

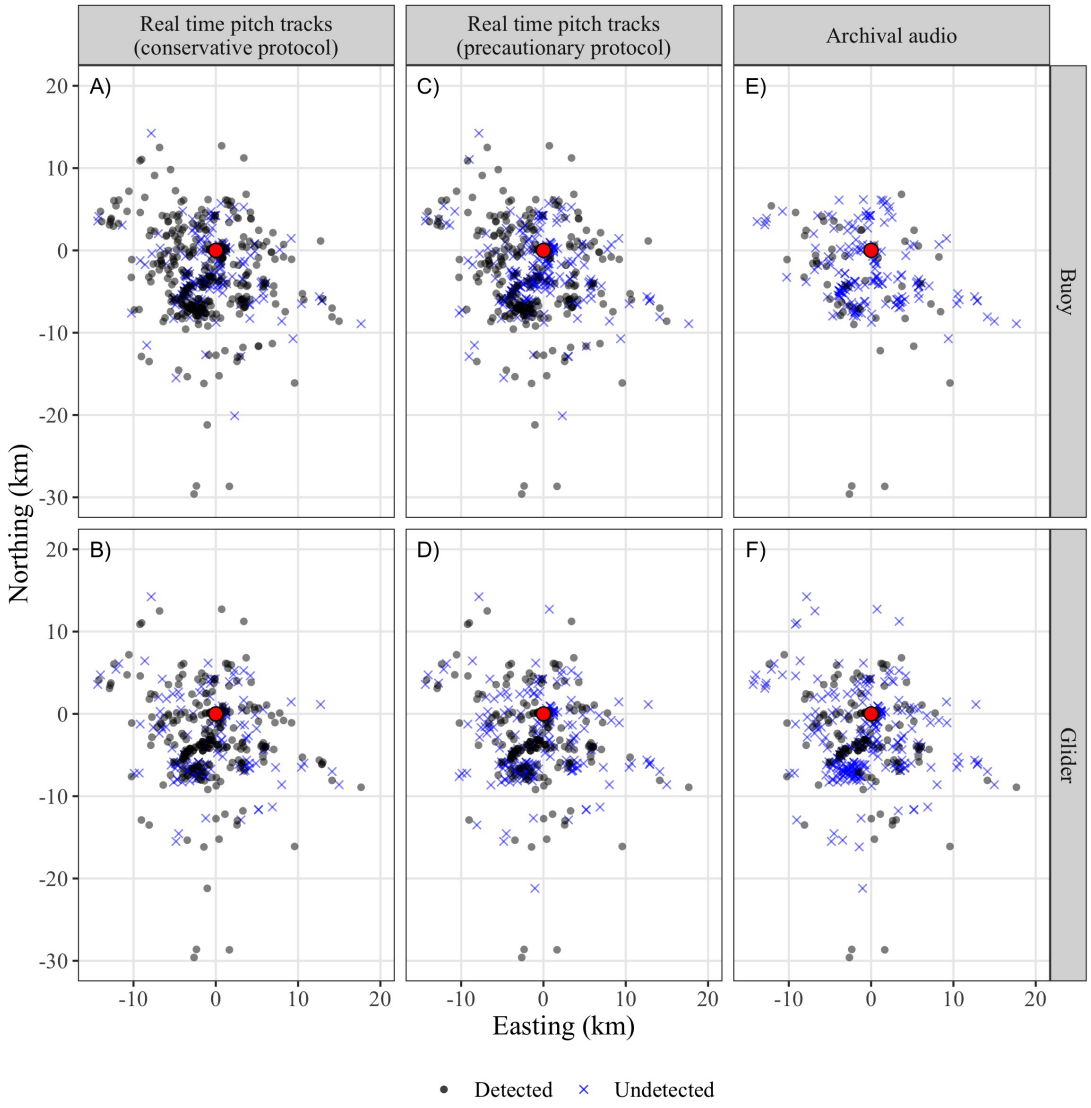

Figure A.1: The spatial distribution of localized right whale upcalls that were either detected (grey circles) or not detected (blue crosses) by the buoy (top row; n = 541) or the glider (bottom row; n = 426) in each analysis (shown in columns). The red circle at the origin indicates the location of the array. Panels A and B are shown in Figure 2.5 in the main text.

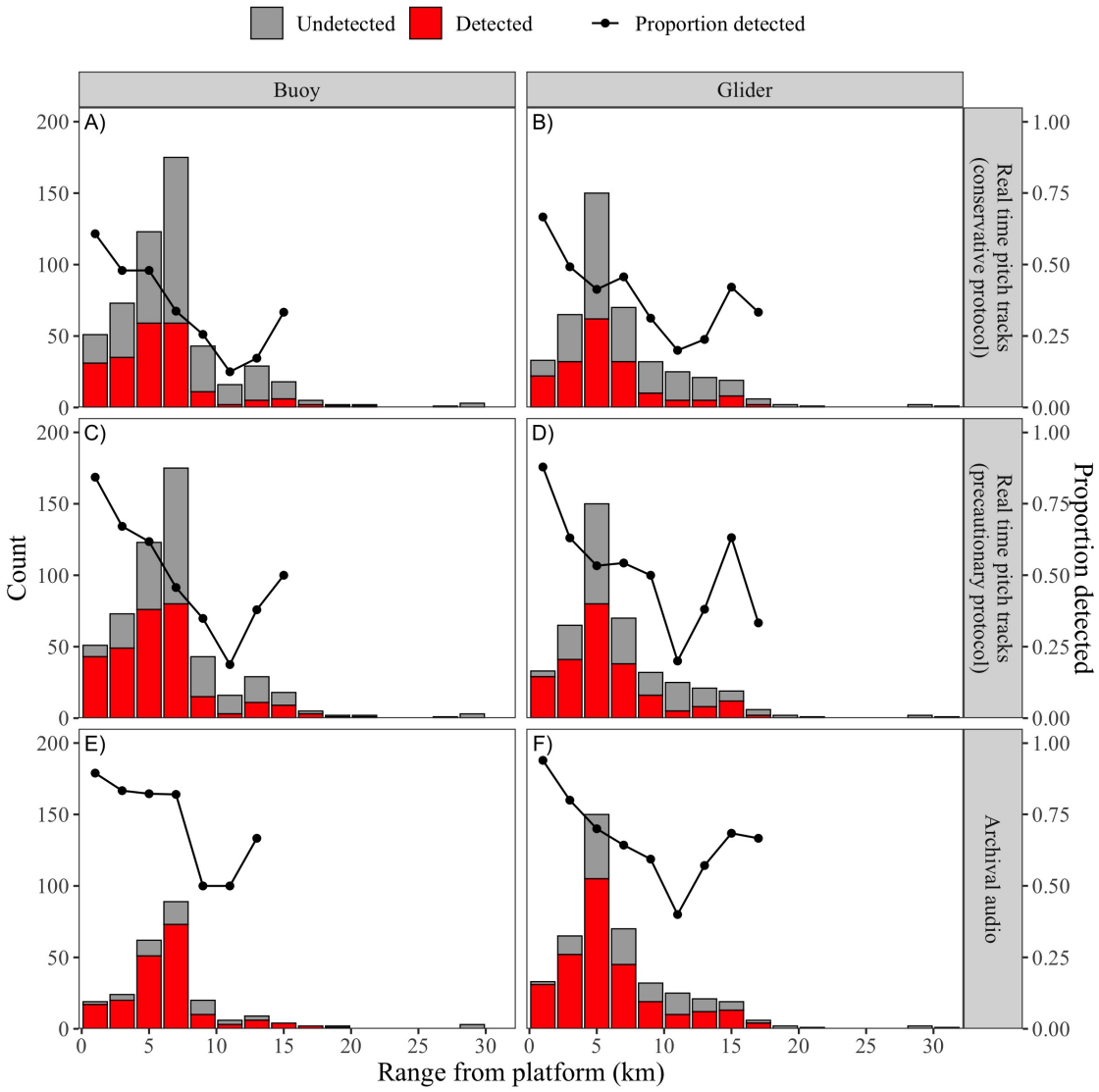

Figure A.2: Distribution of ranges from each platform (shown in columns) to right whale upcalls localized by the array and detected in a given analysis (shown in rows). Total numbers of localized calls in 2-km bins are shown in gray and localized calls detected in near real-time are shown in red. The black line shows proportions of localized calls detected in 2-km bins with more than 5 calls. Panels A and B are shown in Figure 2.6 in the main text.

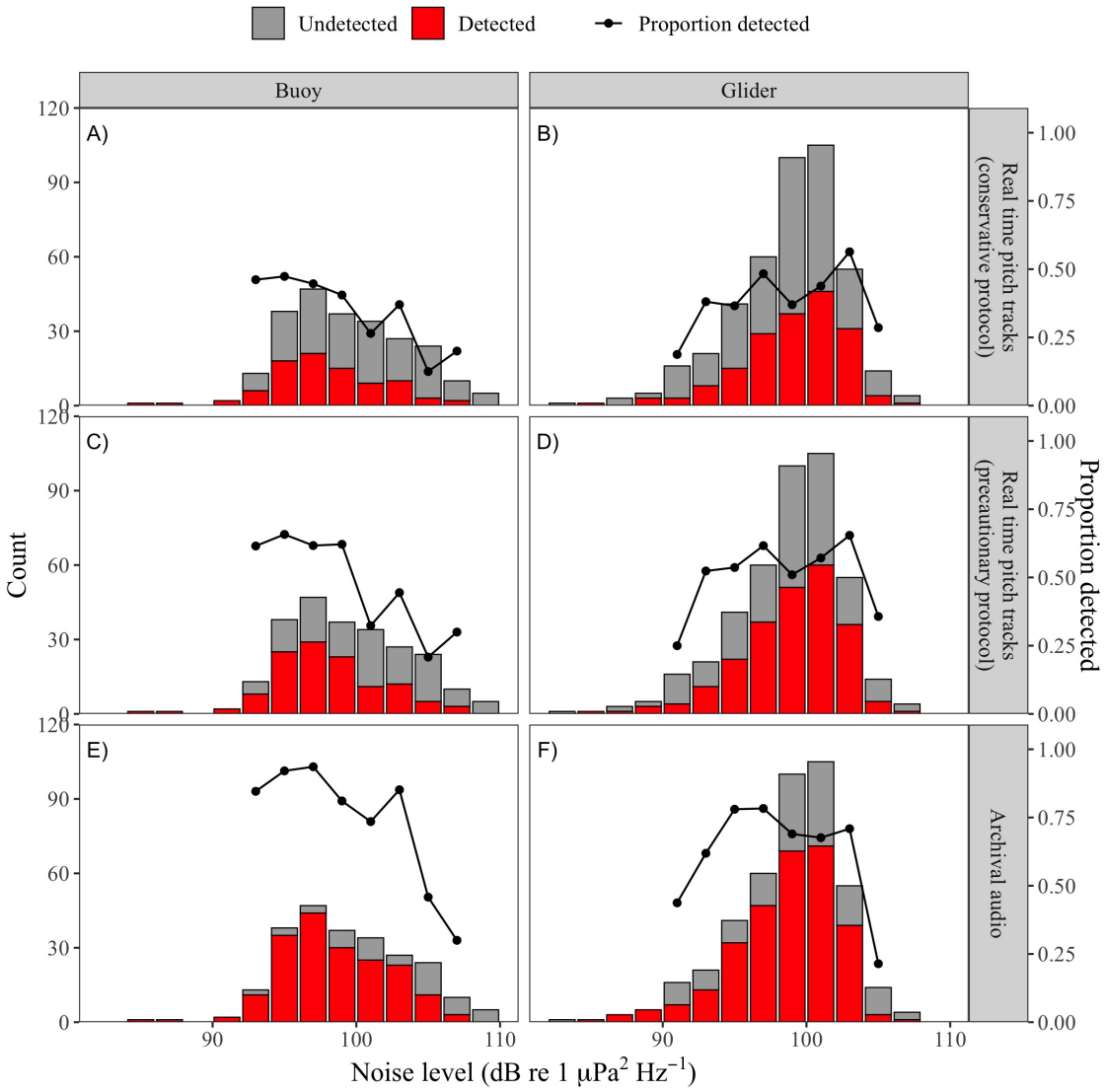

Figure A.3: Distribution of noise levels for each platform (shown in columns) associated with right whale upcalls localized by the array and detected in a given analysis (shown in rows). Total numbers of localized calls in 2-dB bins are shown in gray and localized calls detected in near real-time are shown in red. The black line shows proportions of localized calls detected in 2-dB bins with more than 5 calls. Panels A and B are shown in Figure 2.6 in the main text

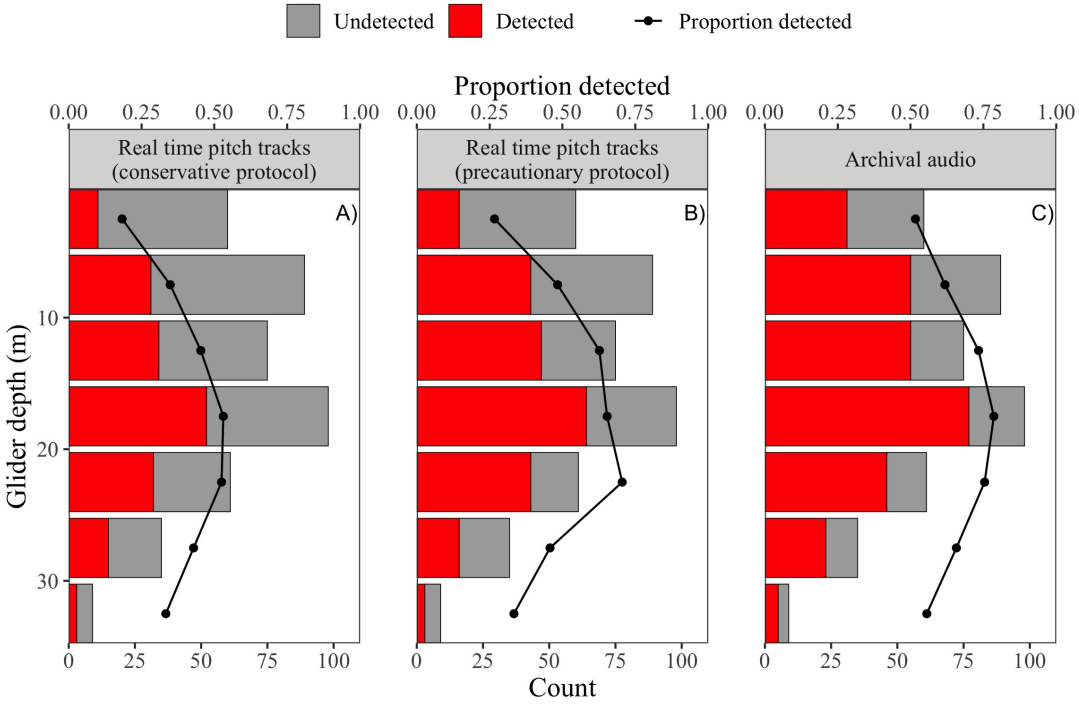

Figure A.4: Distribution of glider depths associated with right whale upcalls localized by the array and detected in a given analysis (shown in columns). Total numbers of localized calls in 5-m bins are shown in gray and localized calls detected in near real-time are shown in red. The black line shows proportions of localized calls detected in 5-m bins with more than 5 calls. Data in panel A are shown in Figure 2.6 in the main text.

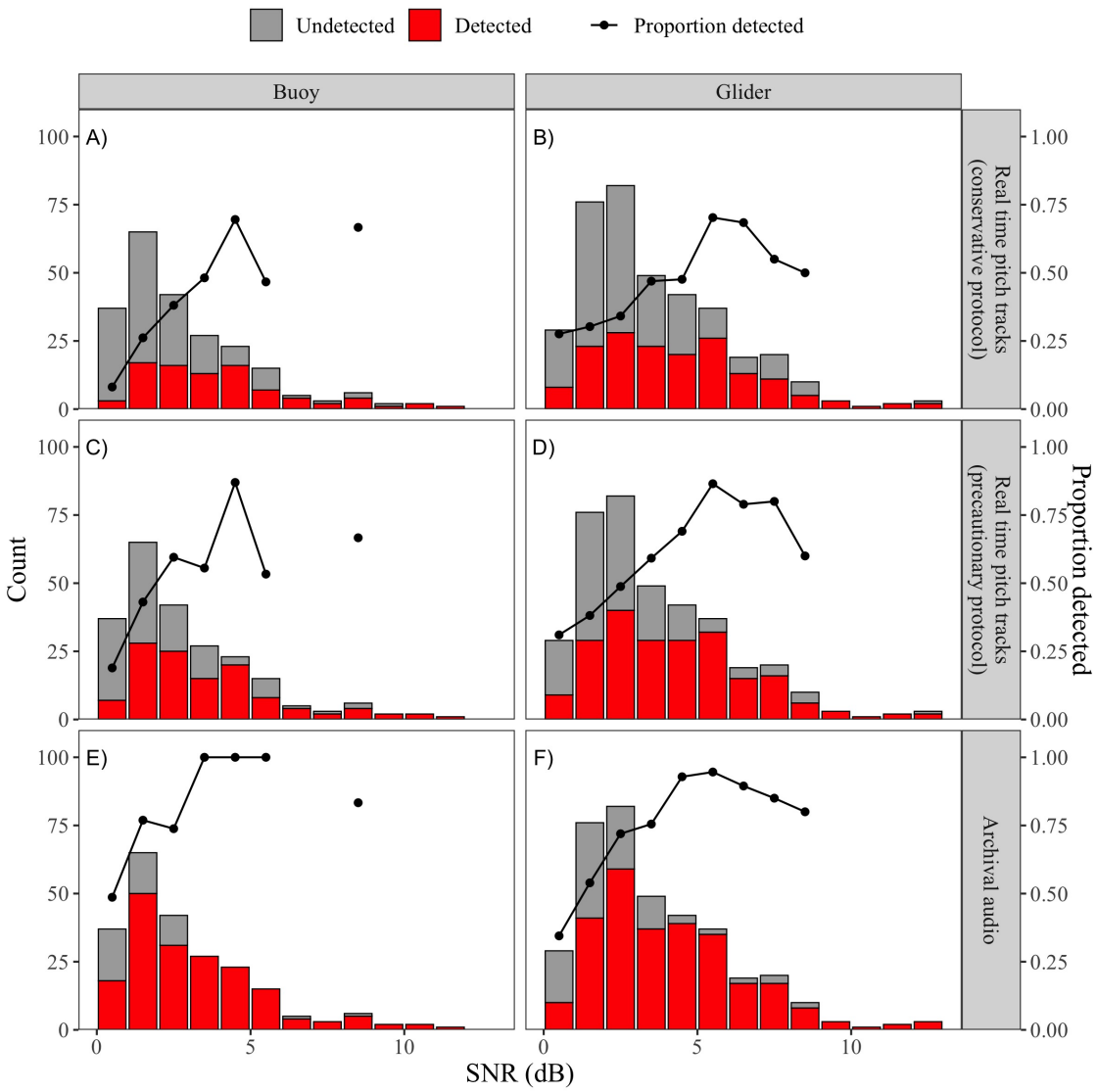

Figure A.5: Distribution of signal-to-noise ratios (SNR) for each platform (shown in columns) associated with right whale upcalls localized by the array and detected in a given analysis (shown in rows). Total numbers of localized calls in 1-dB bins are shown in gray and localized calls detected in near real-time are shown in red. The black line shows proportions of localized calls detected in 1-dB bins with more than 5 calls. Panels A and B are shown in Figure 2.6 in the main text.

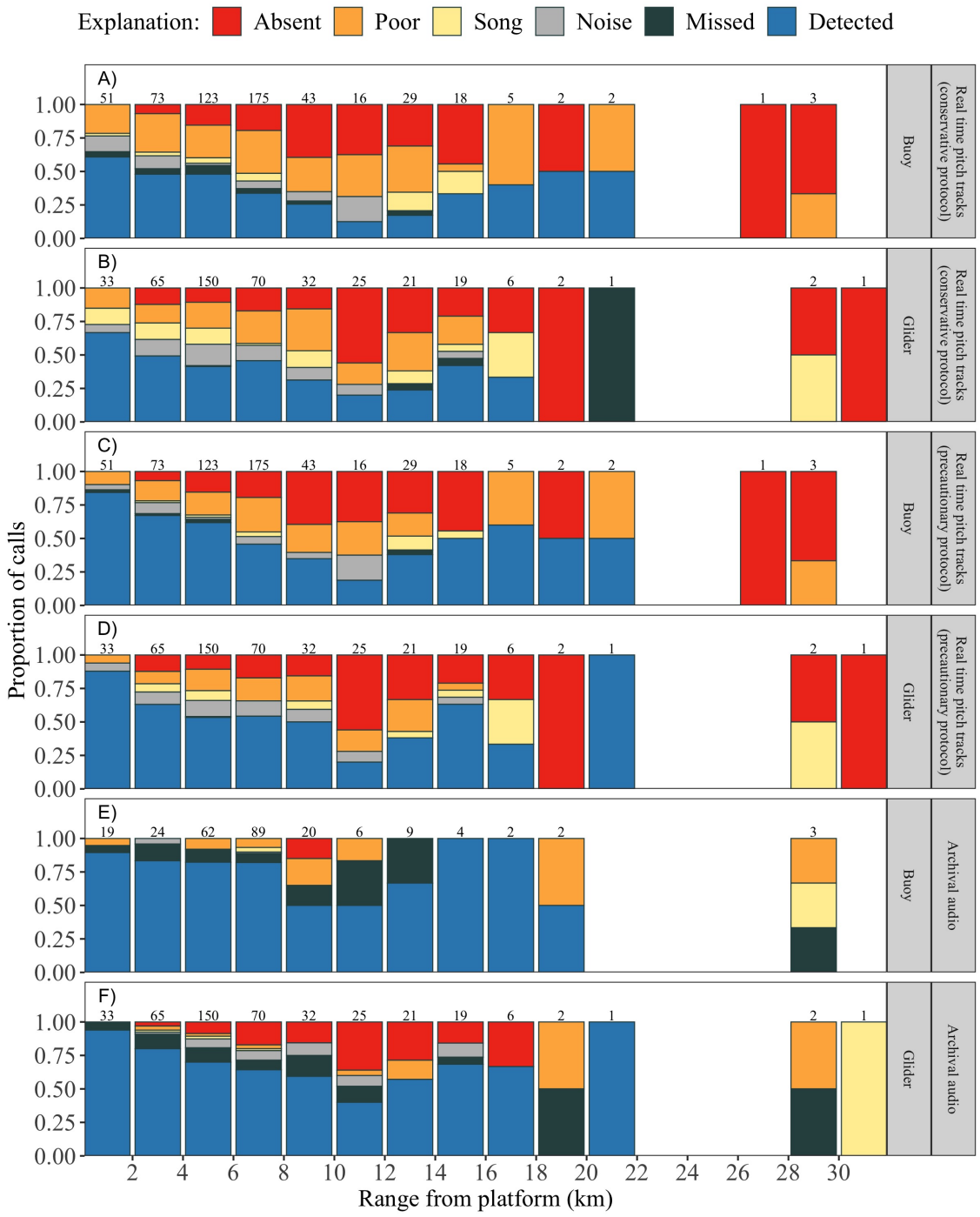

Figure A.6: Proportion of localized calls assigned to each score category based on analyses of the near real-time pitch track data or archival audio as a function of range from the platform. The platform and analysis are shown at the right of each plot. Colors indicate the proportion of calls of a given score in 2-km range bins, while the number of calls in each bin is shown above each bar. Definitions of each category are provided in Tables 2.1, A.1, and A.2. Panels A and B are shown in Figure 2.7 in the main text.

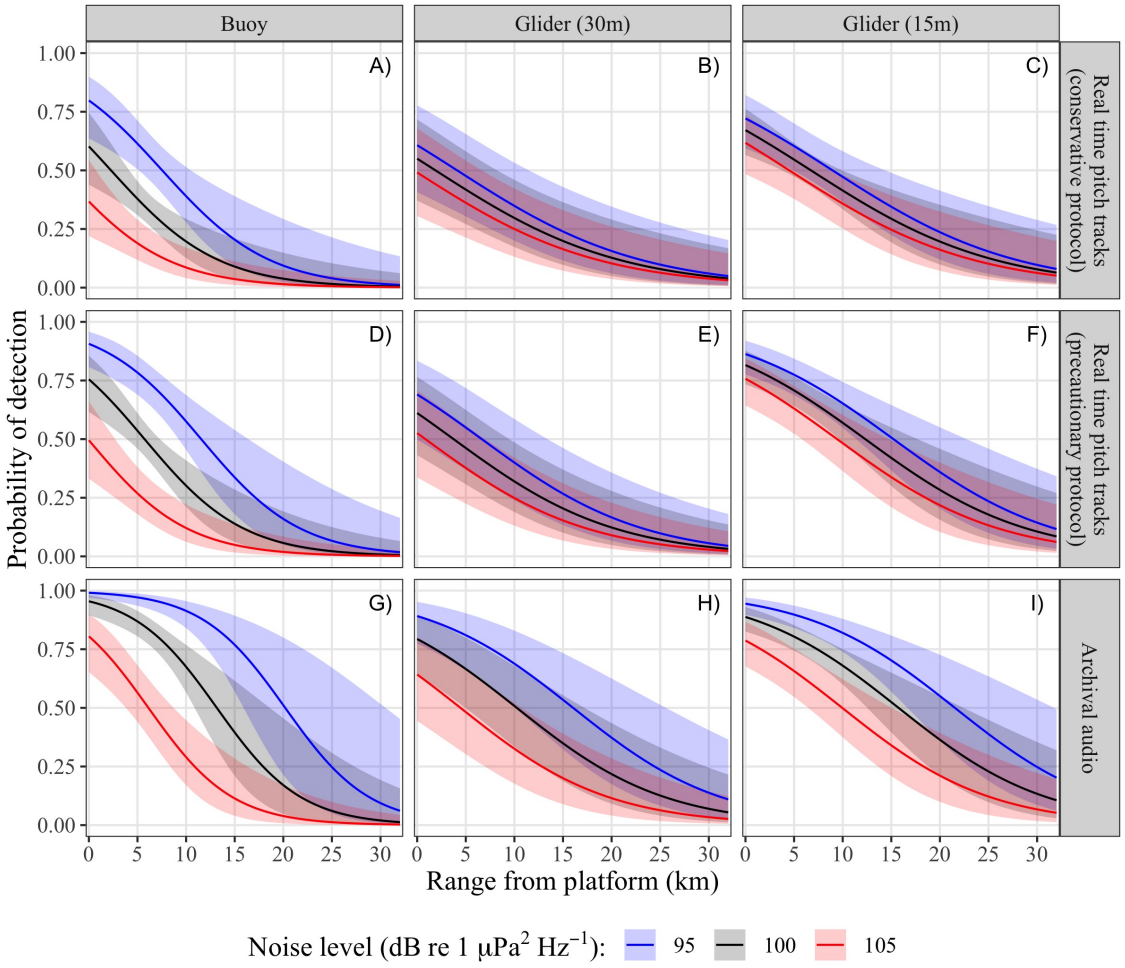

Figure A.7: Estimated probability of detection of localized right whale upcalls as a function of range to the buoy (left column) and glider at a fixed depth of 30 m (center column) or 15 m (right column) at low (blue lines), medium (black lines), and high (red lines) noise levels based on in a given analysis (rows). The fitted regression models are shown as solid lines, while the 95% confidence intervals are shown as shaded regions. An alternate representation of these data directly comparing each platform is shown in Figure 2.8 in the main text.

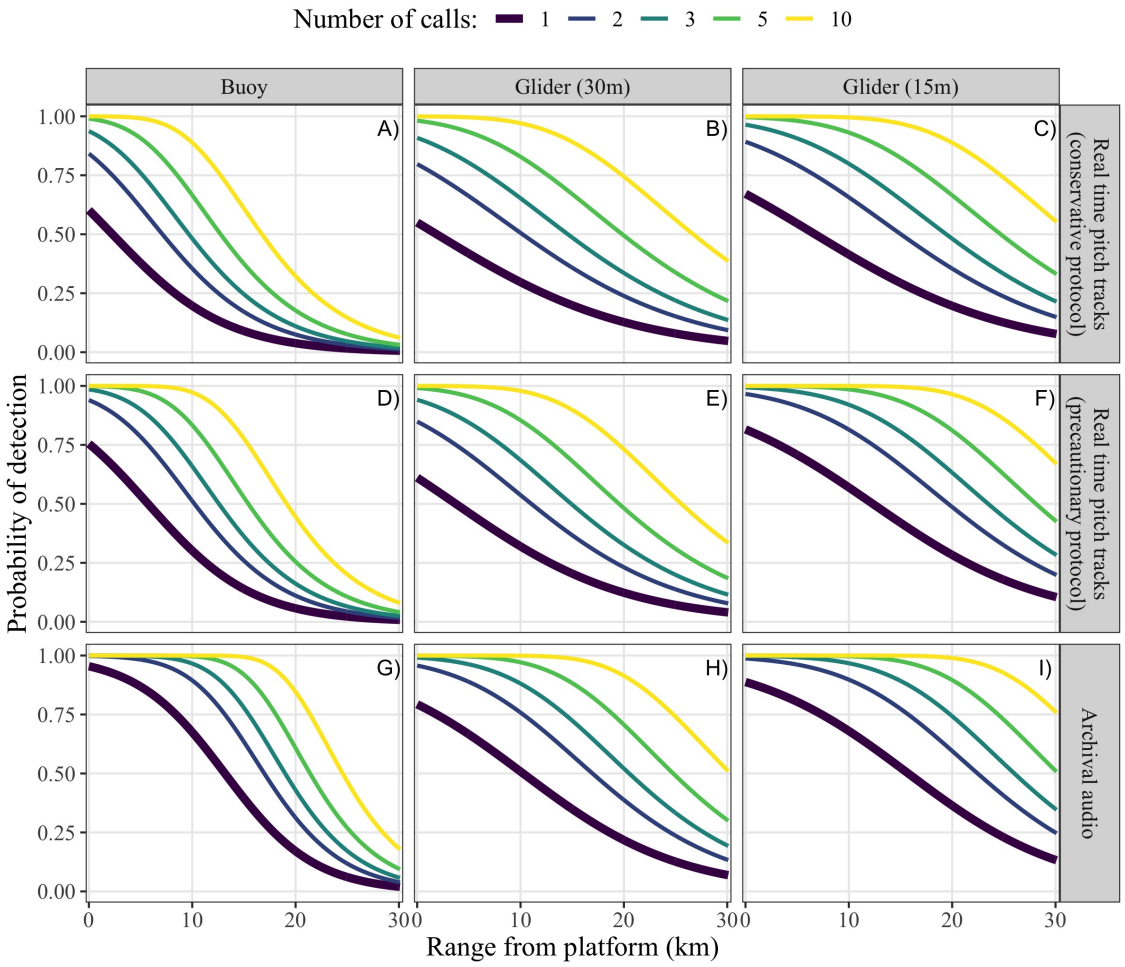

Figure A.8: Results of a thought experiment showing probability of detecting one of multiple available right whale upcalls as a function of range to the buoy (left column) and glider at a fixed depth of 30 m (center column) or 15 m (right column) based on a given analysis (shown in rows) using a fixed noise level of 100 dB re 1 m^{-2}. Each colored line shows the probability of detecting one call out of 1, 2, 3, 5, or 10 available calls during some fixed time period. This analysis relies upon the unlikely assumption that calls are detected independently, so the probabilities of detection are likely overestimated (see main text). Panel A is shown in Figure 2.9 in the main text.

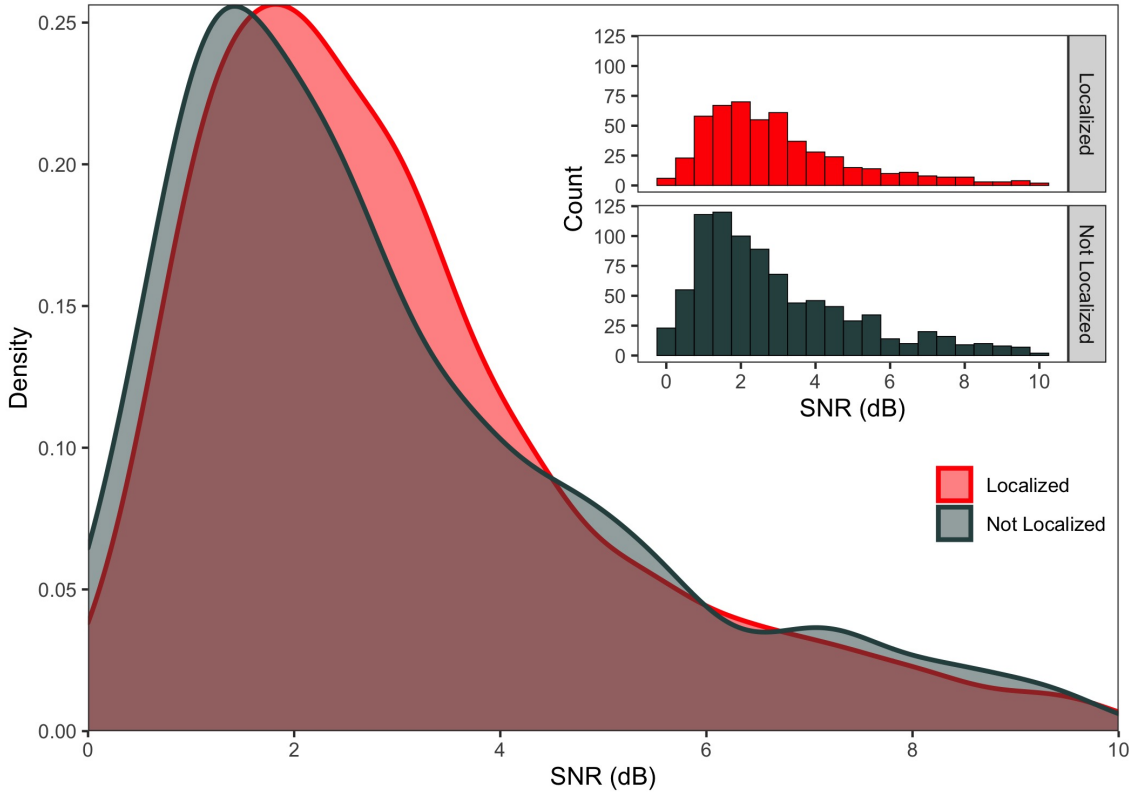

Figure A.9: The signal-to-noise (SNR) level (in dB) for calls that were detected and not localized (n = 863; black) versus those that were detected and successfully localized (n = 513; red) on the array. SNR was calculated on the array channel in which the call was detected using the method described in the main text. Calls with SNR above 10 dB (n = 101) were assumed contaminated by impulsive noise and not included. The inset shows the histogram of the raw data in 0.25 dB bins, while the main plot shows the smoothed (kernel density) estimates overlayed to facilitate comparison. The median SNR of detected calls was 2.3 dB (IQR: 2.7 dB), compared to a median of 2.6 dB (IQR: 2.3 dB) for localized calls. Results of a Mann-Whitney U test failed to reject the null hypothesis that both distributions are equal (p = 0.112)

simple simulation to determine if the empirically derived DMON/LFDCS detection function was influenced at all by the processes of array detection or array localization. The simulation was implemented in several steps. First, we specified a known array detection function, array localization function, and DMON/LFDCS detection function (Figure A.10). We assumed that the detection probabilities decreased as a logistic function with range, and that the probability of detection by the array was higher than that of the DMON/LFDCS platform. The probability of localization was fixed at 0.36 across all ranges. We also tested several range-dependent probability of localization functions but found that these had minimal effect on the end result (not shown).

Next, we generated a distribution of 10,000 calls in Cartesian space with the monitoring platforms located at the origin. The spatial distribution of calls was either uniform (e.g., Figure A.11a), or clustered (not shown). The array detection function (Figure A.10a) was applied to all 10,000 calls in the model domain to generate a distribution of array-detected calls (Figure A.11). The probability of localization (Figure A.10b) was then applied to each of these array-detected calls to determine the subset that were successfully localized (Figure A.12). The DMON/LFDCS detection function (Figure A.10c) was applied to all 10,000 calls in the model domain to generate a distribution of calls detected by the DMON/LFDCS (Figure A.13). Thus, each of the 10,000 simulated calls had 3 binary scores associated with it: (1) S_{array} was 1 if detected by the array or 0 if not detected by the array, (2) S_{loc} was 1 if detected and localized by the array, 0 if detected by the array but not localized by the array, or 0 if not detected by the array, and (3) S_{DMON} was 1 if detected by the DMON/LFDCS or 0 if not detected by the DMON/LFDCS. The localized calls that were detected (S_{array} = 1, S_{loc} = 1 and S_{DMON} = 1) or not detected (S_{array} = 1, S_{loc} = 1 and S_{DMON} = 0) by the DMON/LFDCS (Figure A.14) were used to fit a logistic regression to empirically derive the DMON/LFDCS detection function, which was then compared to the specified DMON/LFDCS detection function (Figure A.15). The specified and derived detection functions were indistinguishable in the presented simulation (Figures A.10-A.15), as well as in several other simulations (not shown; e.g., clustered distribution of 10,000 calls, increasing or decreasing probability of localization with range), suggesting that our methodology is robust to any bias introduced by imperfect detection and localization by the array.

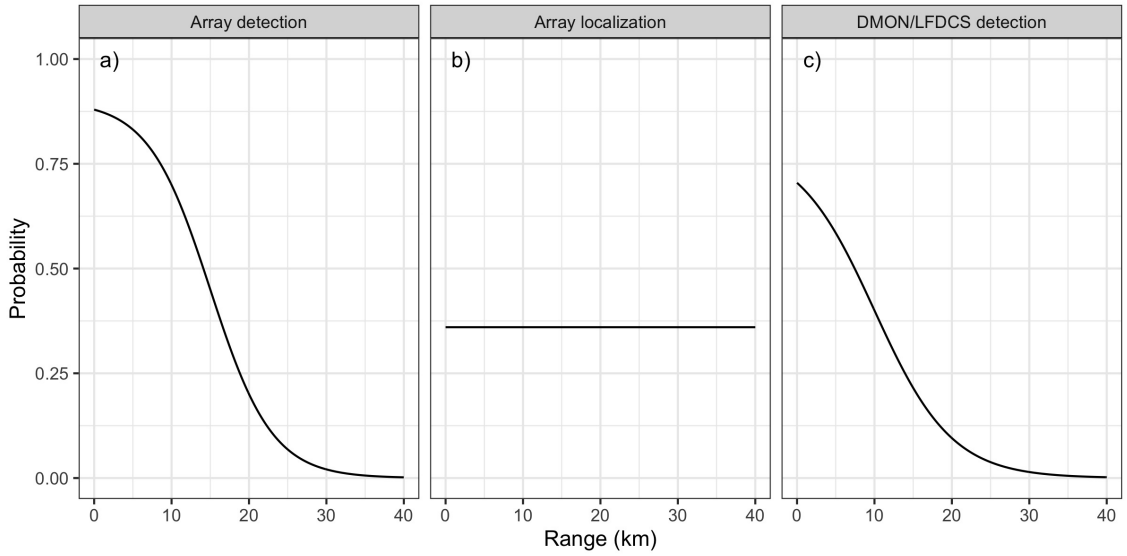

Figure A.10: The specified (a) detection function of the array, (b) localization function of the array, and (c) detection function of the DMON/LFDCS.

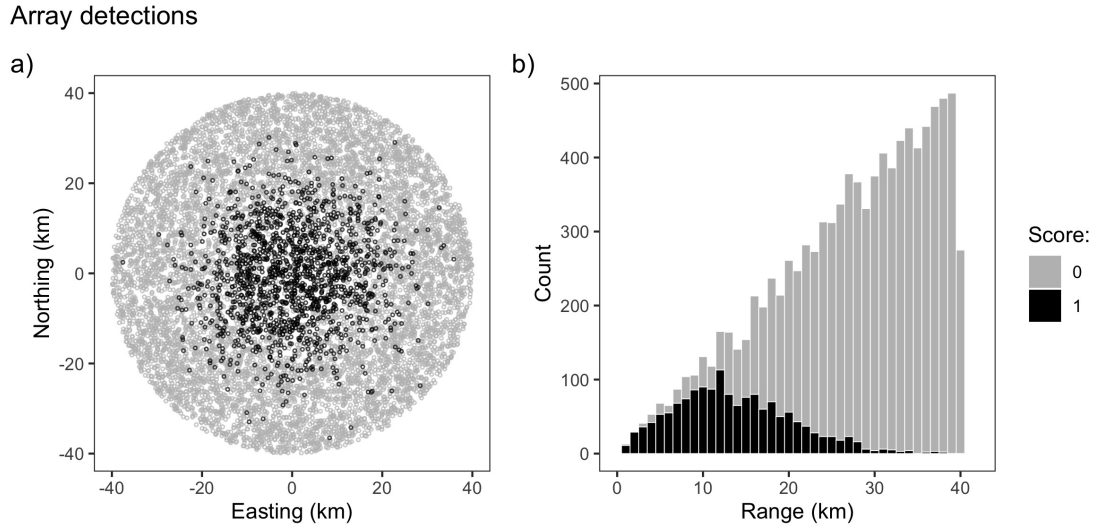

Figure A.11: A uniform distribution of simulated calls (n = 10,000) detected (black, S_{array} = 1) or not detected (grey, S_{array} = 0) by the array in (a) Cartesian space or (b) tallied in 1-km range bins. The detection function of the array is shown in Figure A.10a.

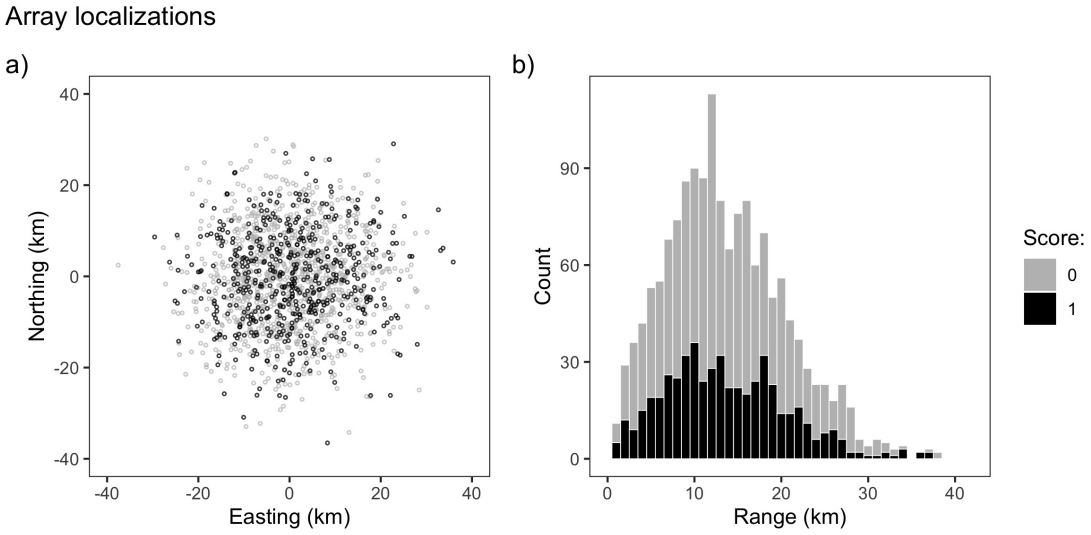

Figure A.12: The distribution of all simulated calls detected by the array (see Figure A.11), including those not successfully localized (grey, S_{array} = 1, S_{loc} = 0) and those that were successfully localized (black, S_{array} = 1, S_{loc} = 1) in (a) Cartesian space or (b) tallied in 1-km range bins. The localization function of the array is shown in Figure A.10b.

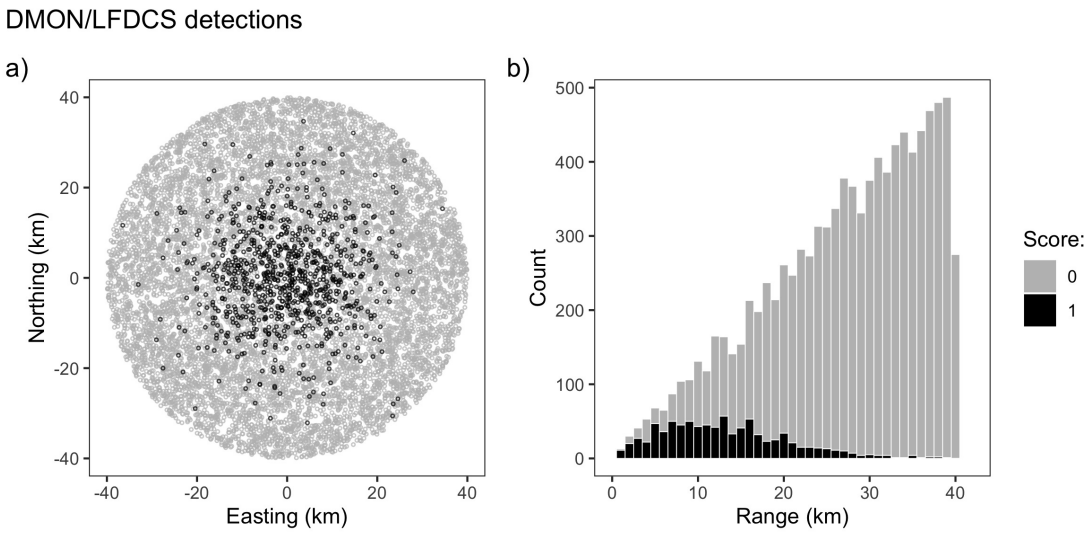

Figure A.13: The same uniform distribution of simulated calls (n = 10,000) as in Figure A.11 detected (black, S_{DMON} = 1) or not detected (grey, S_{DMON} = 0) by the DMON/LFDCS in (a) Cartesian space or (b) tallied in 1-km range bins. The detection function of the DMON/LFDCS is shown in Figure A.10c.

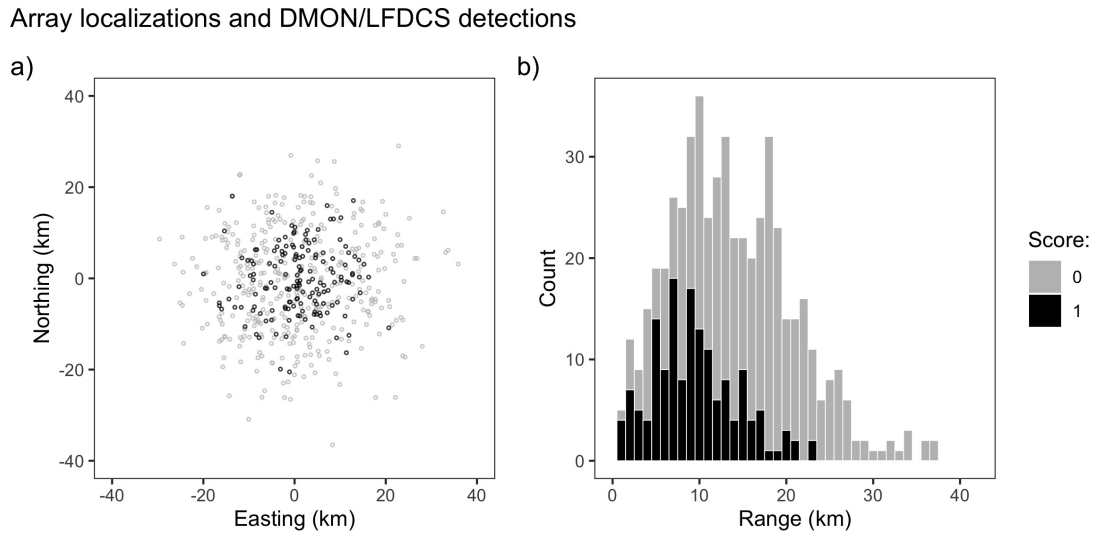

Figure A.14: The distribution of all simulated calls detected and localized by the array (see Figure A.12), including those that were not detected (grey, $S_{array} = 1$, $S_{loc} = 1$, $S_{DMON} = 0$) and those that were detected (black, $S_{array} = 1$, $S_{loc} = 1$, $S_{DMON} = 1$) by the DMON/LFDCS in (a) Cartesian space or (b) tallied in 1-km range bins.

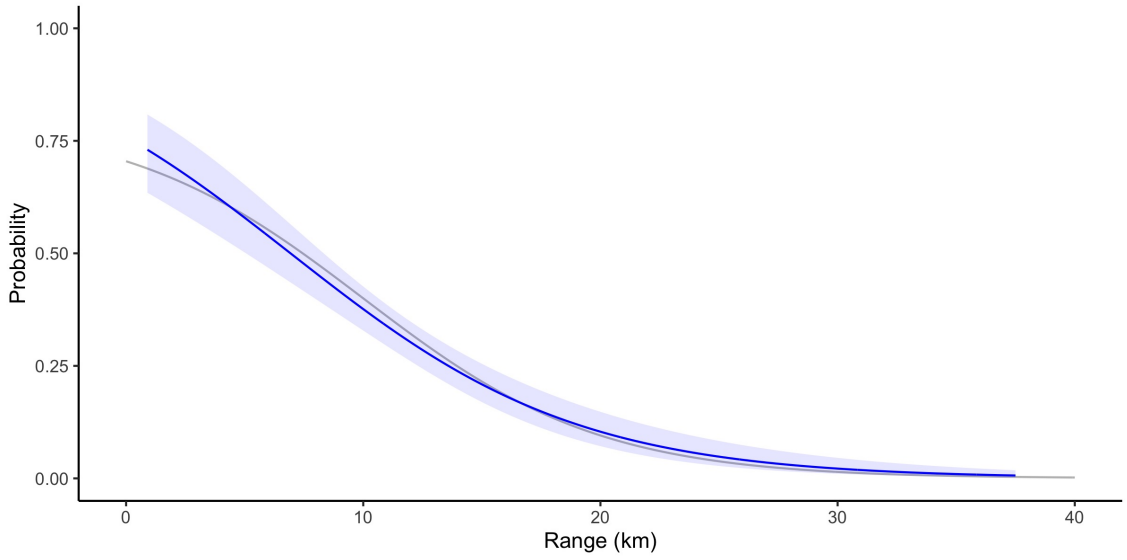

Figure A.15: The specified DMON/LFDCS detection function (grey; also in Figure A.10c) compared to the estimated detection function (blue) derived by fitting a logistic regression to the simulated data shown in Figure A.14 (i.e., $S_{array} = 1$, $S_{loc} = 1$, $S_{DMON} = 0$ or 1). The shading indicates the 95% confidence intervals of the logistic regression.

APPENDIX B

SUPPORTING INFORMATION FOR CHAPTER 3

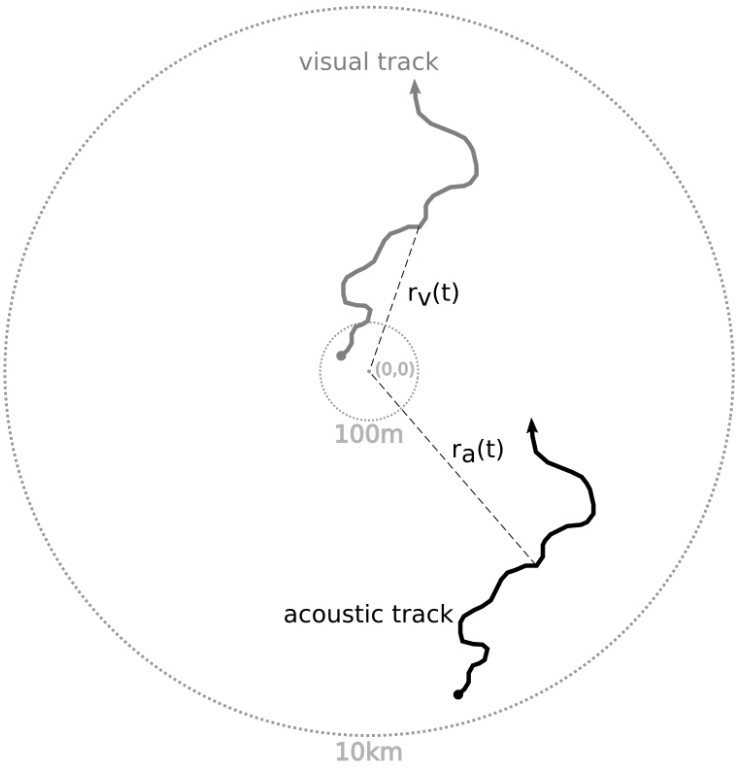

Figure B.1: Illustration of the method used to calculate the difference in visual and acoustic whale location uncertainty. The grey and black solid lines show the same track with the start point chosen according to visual or acoustic detection, respectively. Dashed lines indicated how acoustic (r_a) or visual (r_v) range was calculated between a track position at time t and the center of the Cartesian grid (0,0). Note that the schematic is not drawn to scale.

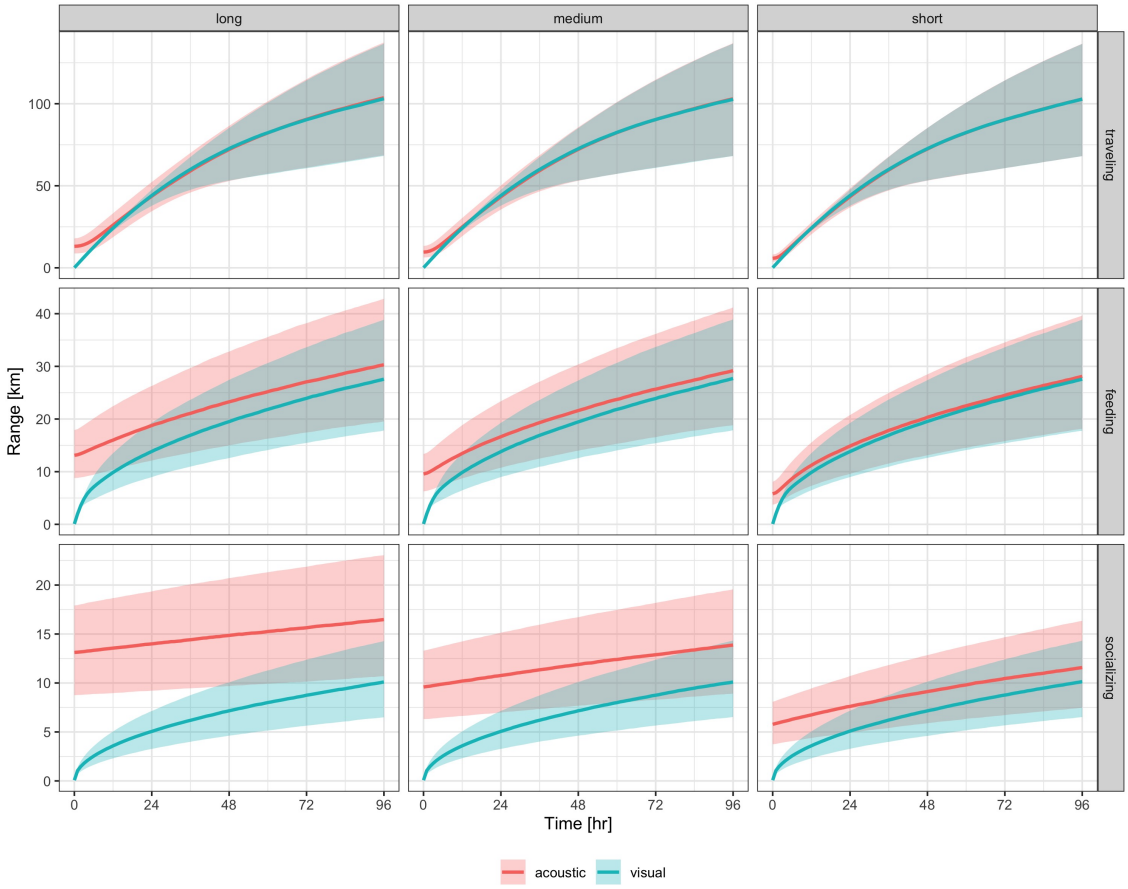

Figure B.2: Evolution of location uncertainty after visual (blue) and acoustic (red) detection for right whales in traveling, feeding, or socializing behavioral modes over the 96 h model period. Columns indicate acoustic detection range parameterizations (long-, medium-, and short- range). Rows show the modeled movement behaviors (traveling, feeding, and socializing). Solid lines indicate the median straight-line distance from the reported detection location. Shaded regions show the interquartile range. The y-axis is scaled to highlight differences between detection methods rather than among behaviors.

APPENDIX C

SUPPORTING INFORMATION FOR CHAPTER 5

C.1 Definition of right whale presence

Establishing right whale presence or absence at each station was critical to several of our analyses. This required defining appropriate time and space scales over which to associate sightings events with each station. We began by measuring the minimum distance from the average station position to a sighting (on the same day), as well as the minimum time offset from the initiation of sampling at a station to a sighting. We then defined whale presence using a range of minimum time (0.25, 0.5, 1, 2.5, 5 h) and distance (0.25, 0.5, 1, 2.5, 5 km) thresholds. We repeated the logistic regression analysis using whale presence defined using every combination of time and distance thresholds. Results indicate that some habitat associations were sensitive to the definition of presence (i.e., significant in some cases but not others; ctd_bottom_density, ctd_sml_depth, net_late_chyp_conc, net_mass, opc_mass_max) while others were not (i.e., always significant; sounder_depth, bathy_sd, ctd_bml_width, opc_mass_deep_max; Table C.1).

C.2 Comparison of net- and OPC-derived *Calanus* abundance

We compared the abundance of late-stage *C. finmarchicus*, *C. hyperboreus*, and *Calanus* spp. (*C. finmarchicus*, *C. hyperboreus*, *C. glacialis*) to OPC-derived particle abundances in ten size classes to determine which OPC size class best represented the abundance of

Table C.1: Summarized results of logistic regressions of habitat associations using different definitions of right whale occurrence. Whale presence was defined as a confirmed sighting within a minimum distance (column 1) and time (column 2) from an oceanographic station. The p-values from a drop-in-deviance test are shown below the habitat variables, with * indicating significance at 0.05. The model used in the main text and described in Table 2 is highlighted in grey.

Whale Occurrence				Habitat Variables												
Min. sighting distance (km)	Min. sighting time (h)	# whale absent stations	# whale present stations	sounder_depth	bathy_sd	ctd_bottom_density	ctd_surface_density	ctd_sml_depth	ctd_bml_width	net_late_cfin_conc	net_late_chyp_conc	net_small_copepod_conc	net_mass	opc_mass_max	opc_mass_mean	opc_mass_surf_max	opc_mass_deep_max
0.25	0.25	45	13	0*	0.02*	0.05*	0.3	0.09	0.01*	0.28	0.79	0.96	0.47	0.1	0.71	0.63	0*
0.5	0.25	45	16	0*	0.03*	0.07	0.28	0.12	0.02*	0.36	0.5	0.85	0.33	0.25	0.96	0.46	0.03*
1	0.25	45	19	0*	0.01*	0.05*	0.23	0.1	0.01*	0.51	0.56	0.82	0.32	0.12	0.46	0.98	0.01*
2.5	0.25	45	19	0*	0.01*	0.05*	0.23	0.1	0.01*	0.51	0.56	0.82	0.32	0.12	0.46	0.98	0.01*
5	0.25	45	19	0*	0.01*	0.05*	0.23	0.1	0.01*	0.51	0.56	0.82	0.32	0.12	0.46	0.98	0.01*
0.25	0.5	45	17	0*	0.01*	0.07	0.4	0.03*	0.04*	0.33	0.73	0.88	0.46	0.03*	0.26	0.96	0*
0.5	0.5	45	22	0*	0.01*	0.1	0.37	0.05*	0.05*	0.41	0.47	0.94	0.32	0.08	0.41	0.78	0.01*
1	0.5	45	29	0*	0.01*	0.24	0.22	0.03*	0.01*	0.37	0.32	0.58	0.14	0.04*	0.24	0.94	0*
2.5	0.5	45	29	0*	0.01*	0.24	0.22	0.03*	0.01*	0.37	0.32	0.58	0.14	0.04*	0.24	0.94	0*
5	0.5	45	29	0*	0.01*	0.24	0.22	0.03*	0.01*	0.37	0.32	0.58	0.14	0.04*	0.24	0.94	0*
0.25	1	45	21	0*	0.02*	0.04*	0.77	0.02*	0.04*	0.19	0.28	0.6	0.16	0.1	0.41	0.85	0.01*
0.5	1	45	36	0*	0*	0.02*	0.7	0.13	0.01*	0.14	0.08	0.84	0.03*	0.08	0.3	0.99	0.01*
1	1	45	45	0*	0*	0.05*	0.41	0.1	0*	0.15	0.06	0.53	0.02*	0.08	0.27	0.96	0.01*
2.5	1	45	50	0*	0.01*	0.04*	0.42	0.08	0*	0.2	0.07	0.54	0.03*	0.05*	0.32	0.89	0*
5	1	45	54	0*	0.01*	0.05*	0.42	0.07	0*	0.24	0.08	0.6	0.03*	0.06	0.31	0.92	0.01*
0.25	2.5	45	22	0*	0.03*	0.05*	0.8	0.03*	0.02*	0.1	0.16	0.46	0.1	0.05*	0.16	0.66	0*
0.5	2.5	45	41	0*	0*	0.02*	0.87	0.17	0.01*	0.08	0.05*	0.7	0.02*	0.03*	0.11	0.46	0*
1	2.5	45	50	0*	0.01*	0.05*	0.56	0.12	0*	0.08	0.04*	0.45	0.01*	0.04*	0.11	0.5	0*
2.5	2.5	45	61	0*	0.01*	0.06	0.57	0.07	0*	0.14	0.06	0.44	0.02*	0.02*	0.16	0.63	0*
5	2.5	45	68	0*	0.03*	0.04*	0.62	0.06	0*	0.11	0.08	0.57	0.03*	0.02*	0.16	0.63	0*
0.25	5	45	22	0*	0.03*	0.05*	0.8	0.03*	0.02*	0.1	0.16	0.46	0.1	0.05*	0.16	0.66	0*
0.5	5	45	42	0*	0.01*	0.03*	0.67	0.17	0.01*	0.06	0.05*	0.75	0.02*	0.03*	0.11	0.46	0*
1	5	45	52	0*	0.01*	0.06	0.44	0.11	0*	0.07	0.04*	0.46	0.01*	0.04*	0.12	0.54	0.01*
2.5	5	45	64	0*	0.02*	0.06	0.49	0.06	0*	0.14	0.06	0.42	0.01*	0.02*	0.17	0.69	0*
5	5	45	72	0*	0.04*	0.04*	0.54	0.06	0*	0.1	0.08	0.55	0.02*	0.02*	0.17	0.7	0*

each group. We achieved this by (1) selecting all stations with net and OPC data (n = 66), (2) restricting the OPC profile to the maximum depth achieved by the net, (3) computing the depth-integrated particle abundance in all 10 size classes (1 - 1.5, 1 - 2, 1 - 2.5, 1 - 3, 1.5 - 2, 1.5 - 2, 1.5 - 2.5, 1.5 - 3, 2 - 2.5, 2 - 3, 2.5 - 3 mm equivalent spherical diameter; ESD), (4) and comparing to the net-derived abundances of *C. finmarchicus* (Figure C.1), *C. hyperboreus* (Figure C.2), and *Calanus* spp. (Figure C.3). In addition to visualizing the agreement graphically, we also calculated Spearman's rank correlation and residual sum of squares, with the net abundance and OPC abundance treated as actual and predicted, respectively (Figure C.4). Though there was some ambiguity, results suggested that the abundances of late-stage *C. finmarchicus*, *C. hyperboreus*, and *Calanus* spp. were best represented by the 1 - 2, 1.5 - 3 and 1 - 3 mm ESD size classes, respectively.

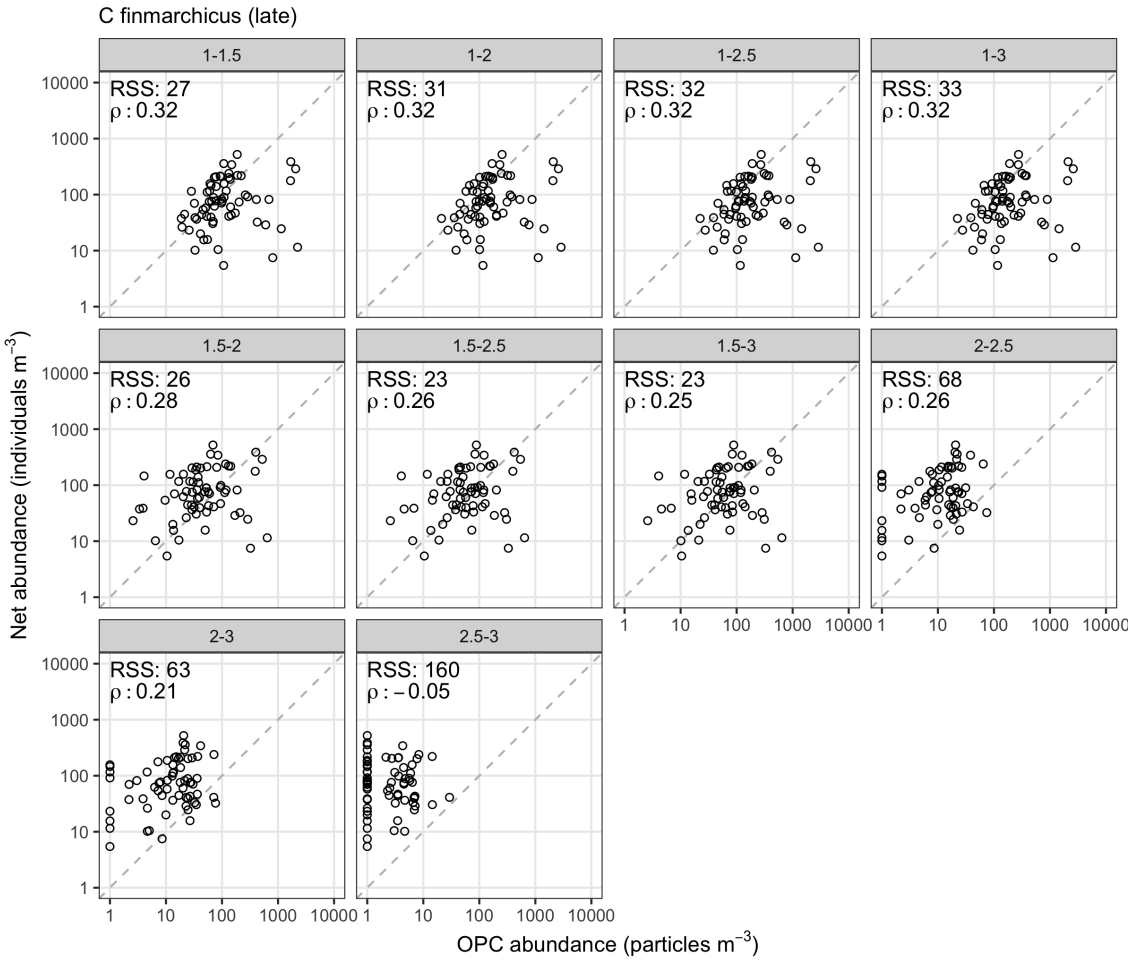

Figure C.1: Net-derived abundances of late-stage (C4, C5) *C. finmarchicus* copepodites and adults compared to OPC-derived abundances of particles from ten different size classes (in mm ESD; shown above each panel). The residual sum of squares (RSS) and Spearman's rank correlation (ρ) is indicated in each panel.

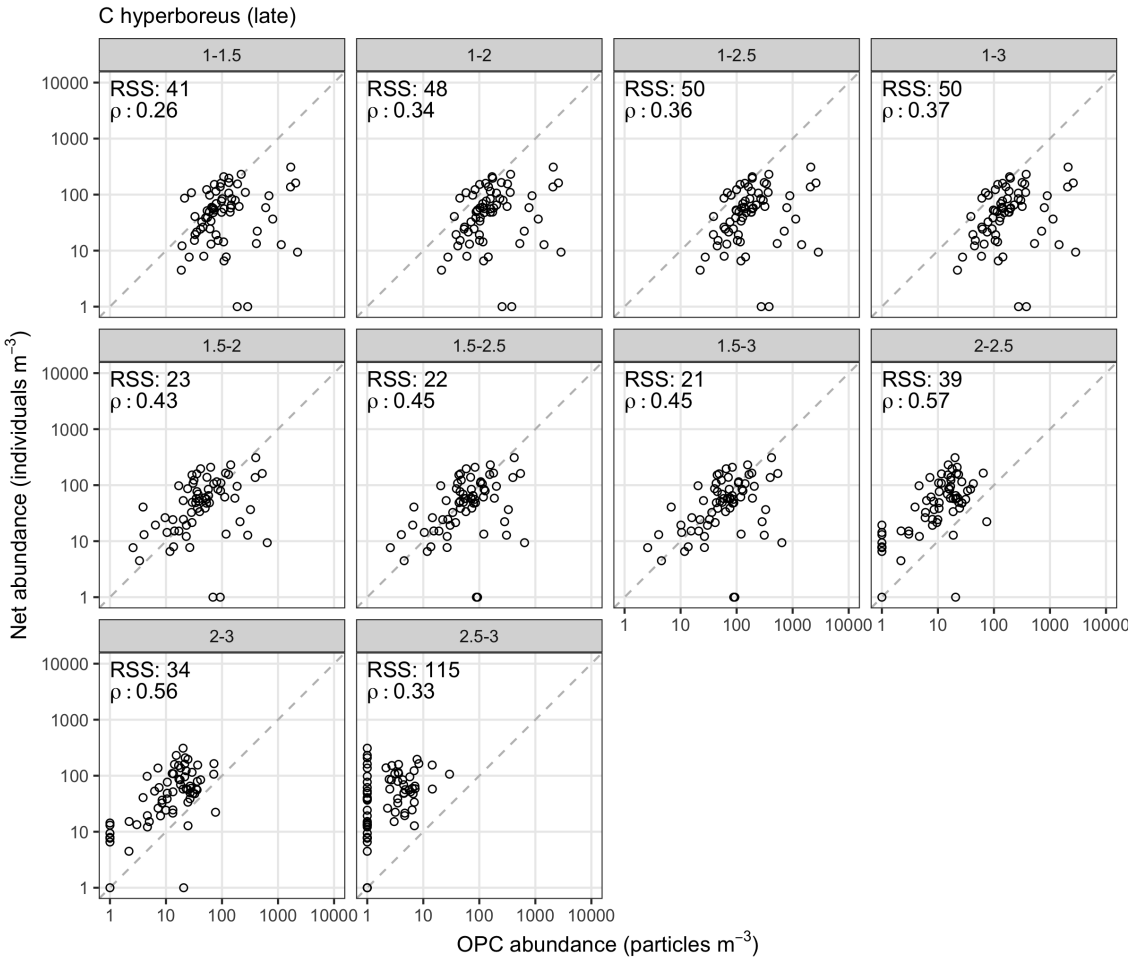

Figure C.2: Net-derived abundances of late-stage (C4, C5) *C. hyperboreus* copepodites and adults compared to OPC-derived abundances of particles from ten different size classes (in mm ESD; shown above each panel). The residual sum of squares (RSS) and Spearman's rank correlation (ρ) is indicated in each panel.

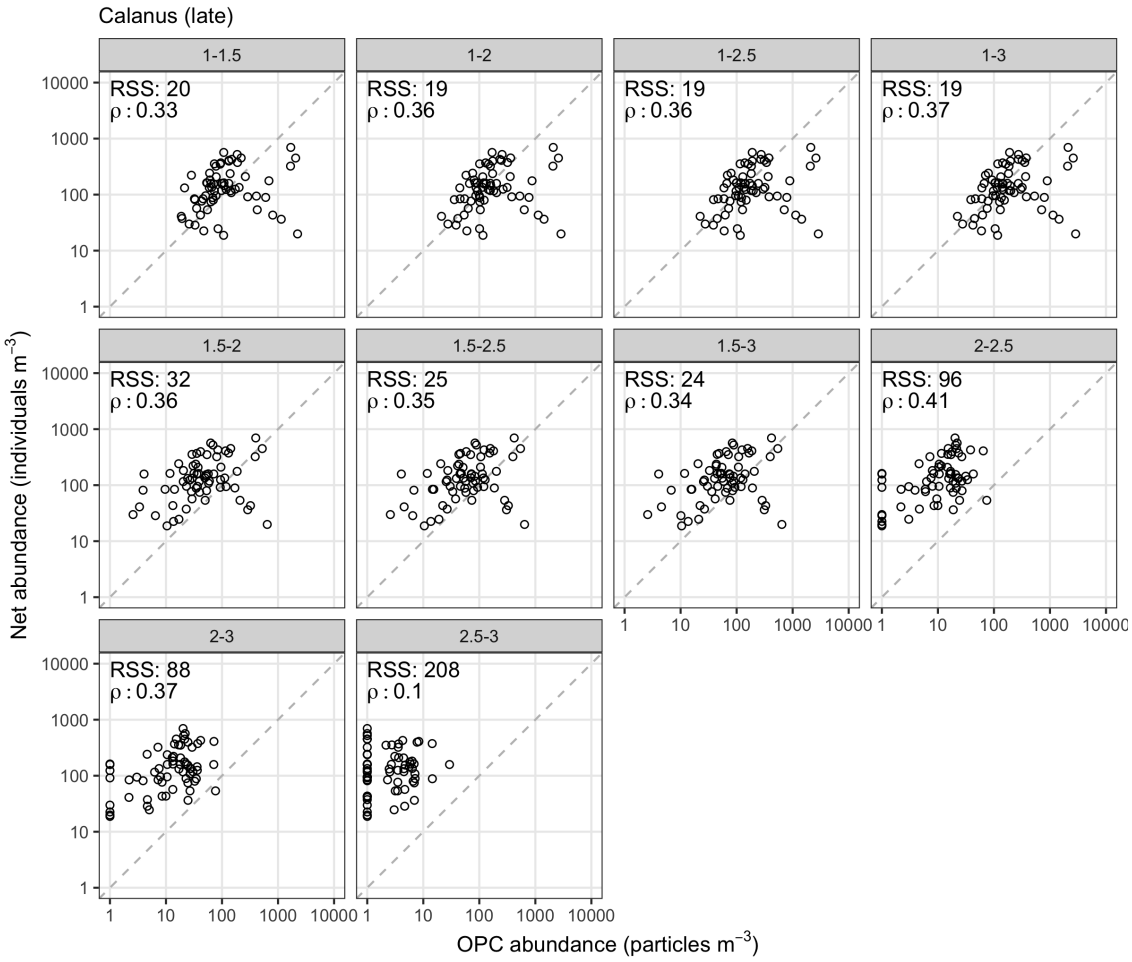

Figure C.3: Net-derived abundances of late-stage (C4, C5) *Calanus* (*C. finmarchicus* + *C. hyperboreus*) copepodites and adults compared to OPC-derived abundances of particles from ten different size classes (in mm ESD; shown above each panel). The residual sum of squares (RSS) and Spearman's rank correlation (ρ) is indicated in each panel.

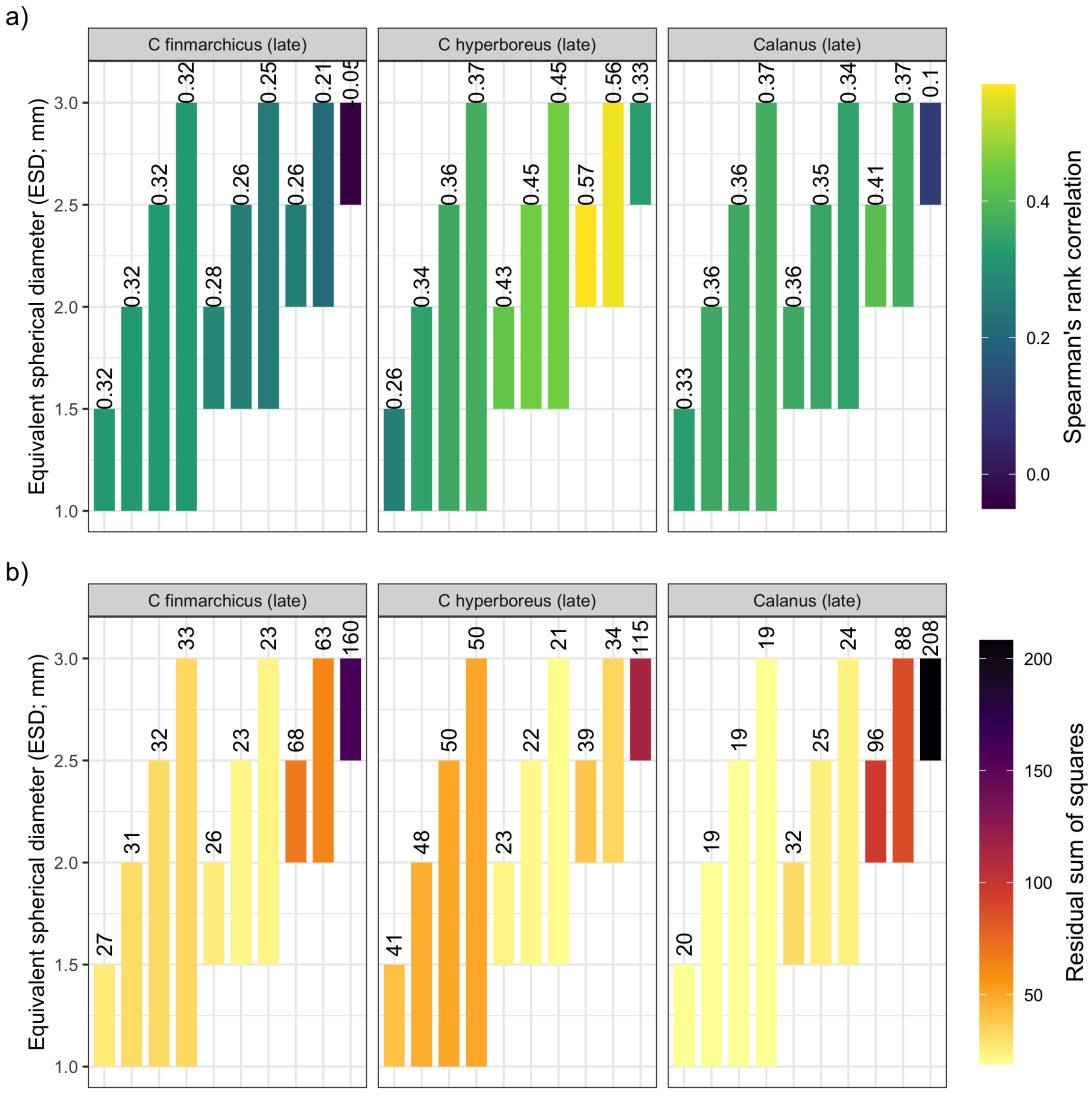

Figure C.4: The Spearman's rank correlation (a) and residual sum of squares (b) for comparisons among depth-integrated abundances derived from multiple OPC particle size classes and net tows. The correlation (in panel a) and sum of squares (in panel b) results are indicated by the color of each bar, and also shown in text above each bar. The vertical extent of each bar indicates the OPC particle size range compared to the net abundance.

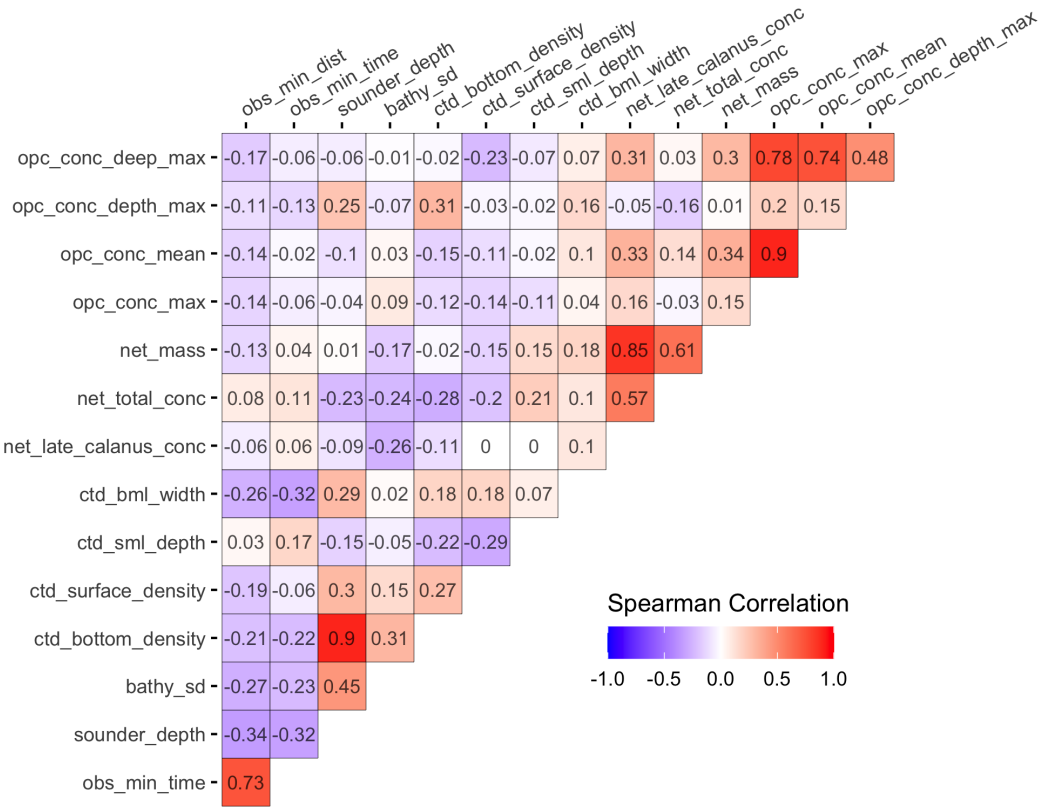

Figure C.5: Spearman's rank correlation matrix of habitat variables.

APPENDIX D

SUPPORTING INFORMATION FOR CHAPTER 6

Table D.1: Logistic regression results after removing data from Oct/Nov 2015 to evaluate the influence of that flushing event on observed whale-habitat associations. Definitions and descriptions are analogous to Table 6.3 in the main text.

				Set 1	**Set 2**	**Set 3**	**Set 4**	**Set 5**	**Set 6**	**Set 7**	**Set 8**
Species	**N_0**	**N_1**	**Variable**	***effort***	***depth***	***month***	***month+ depth***	***half***	***half+ depth***	****half***	****half+ depth***
fin	35	47	depth	<0.001*	-	<0.001*	-	<0.001*	-	<0.001*	-
	35	47	depth_sd	0.004*	0.008*	<0.001*	0.001*	<0.001*	<0.001*	0.003*	0.003*
	35	47	surf_strat	0.69	0.55	0.89	0.8	0.94	0.81	0.79	0.81
	24	58	bml_width	0.003*	0.08	0.001*	0.029*	<0.001*	0.02*	0.003*	0.05
	25	57	bml_density	0.003*	0.56	0.002*	0.4	0.002*	0.38	0.009*	0.67
	23	58	current_v	0.05	0.03*	0.08	0.036*	0.14	0.05	0.4	0.19
humpback	192	54	depth	0.33	-	0.31	-	0.31	-	0.21	-
	192	54	depth_sd	0.82	0.61	0.91	0.67	0.87	0.64	0.91	0.83
	192	54	surf_strat	0.06	0.046*	0.05	0.043*	0.049*	0.039*	0.14	0.12
	191	54	bml_width	0.29	0.44	0.27	0.42	0.29	0.44	0.52	0.69
	191	54	bml_density	0.48	0.06	0.48	0.07	0.44	0.05	0.1	0.016*
	189	53	current_v	0.43	0.27	0.4	0.24	0.42	0.25	0.47	0.36
right	202	44	depth	0.031*	-	0.033*	-	0.034*	-	0.09	-
	202	44	depth_sd	0.18	0.46	0.19	0.45	0.19	0.46	0.28	0.53
	202	44	surf_strat	0.003*	0.004*	0.003*	0.004*	0.003*	0.005*	0.01*	0.017*
	201	44	bml_width	0.47	0.95	0.46	0.92	0.46	0.92	0.007*	0.009*
	201	44	bml_density	0.02*	0.23	0.017*	0.2	0.017*	0.19	0.023*	0.18
	198	44	current_v	0.24	0.33	0.26	0.32	0.26	0.32	0.15	0.14
sei	160	86	depth	<0.001*	-	<0.001*	-	<0.001*	-	<0.001*	-
	160	86	depth_sd	0.14	0.6	0.09	0.5	0.1	0.51	0.12	0.27
	160	86	surf_strat	0.53	0.81	0.53	0.67	0.55	0.7	0.83	0.92
	159	86	bml_width	0.026*	0.28	0.017*	0.24	0.018*	0.25	0.06	0.52
	159	86	bml_density	0.002*	0.5	0.001*	0.5	0.002*	0.56	0.002*	0.24
	157	85	current_v	0.13	0.08	0.1	0.08	0.09	0.07	0.13	0.07

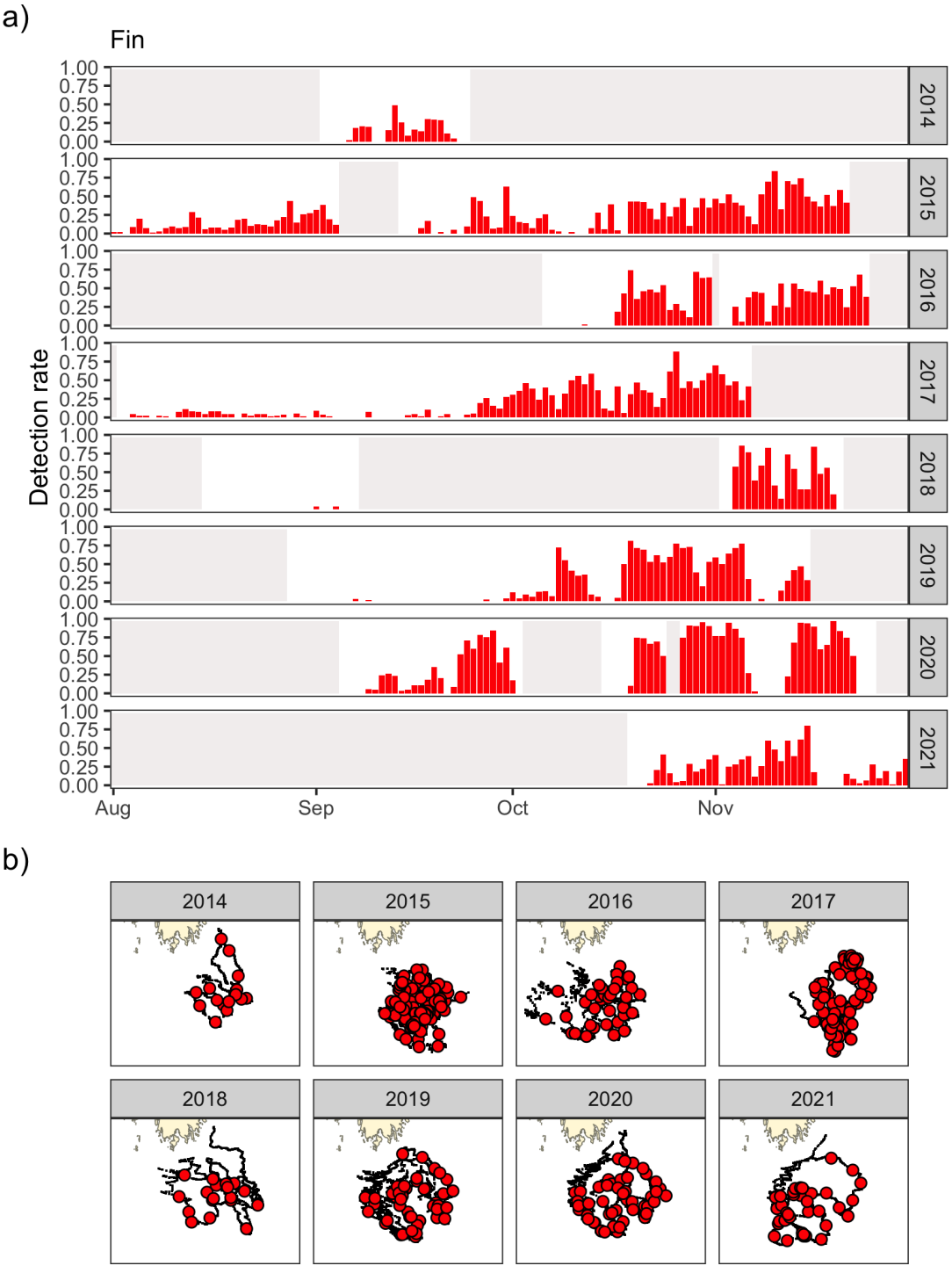

Figure D.1: Fin whale detection rates in (a) time and (b) space over the full study during the Aug - Nov period in each year from 2014-2021. Panel (a) shows the daily detection rate (proportion of detected tally periods per day) over time. Light grey shading indicates times without survey effort. The bottom panel (b) shows the location of the glider during all detected tally periods (red circles) in each year. The black line shows the path of the glider.

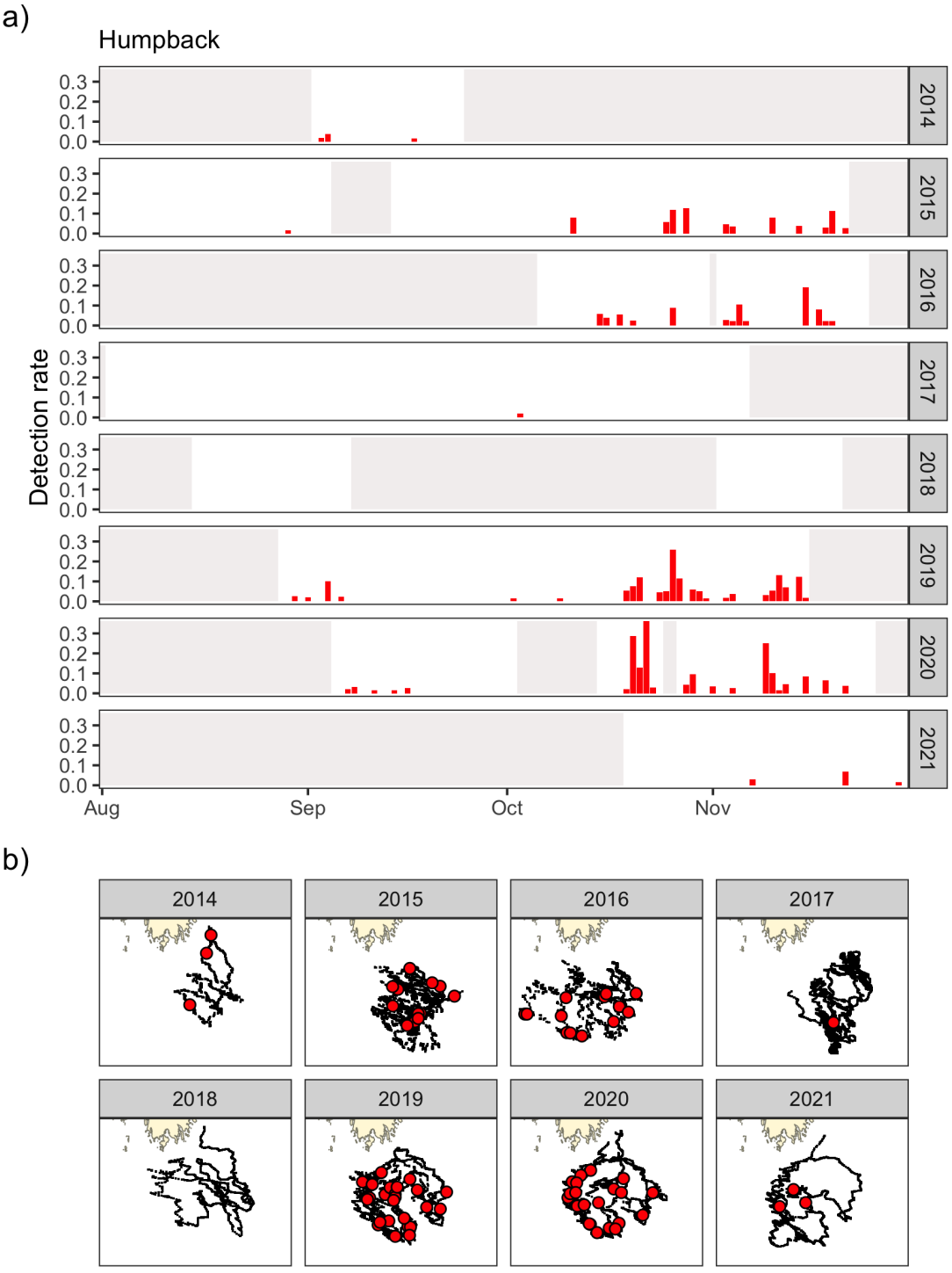

Figure D.2: Humpback whale detection rates in (a) time and (b) space over the full study during the Aug - Nov period in each year from 2014-2021. Panel (a) shows the daily detection rate (proportion of detected tally periods per day) over time. Light grey shading indicates times without survey effort. The bottom panel (b) shows the location of the glider during all detected tally periods (red circles) in each year. The black line shows the path of the glider.

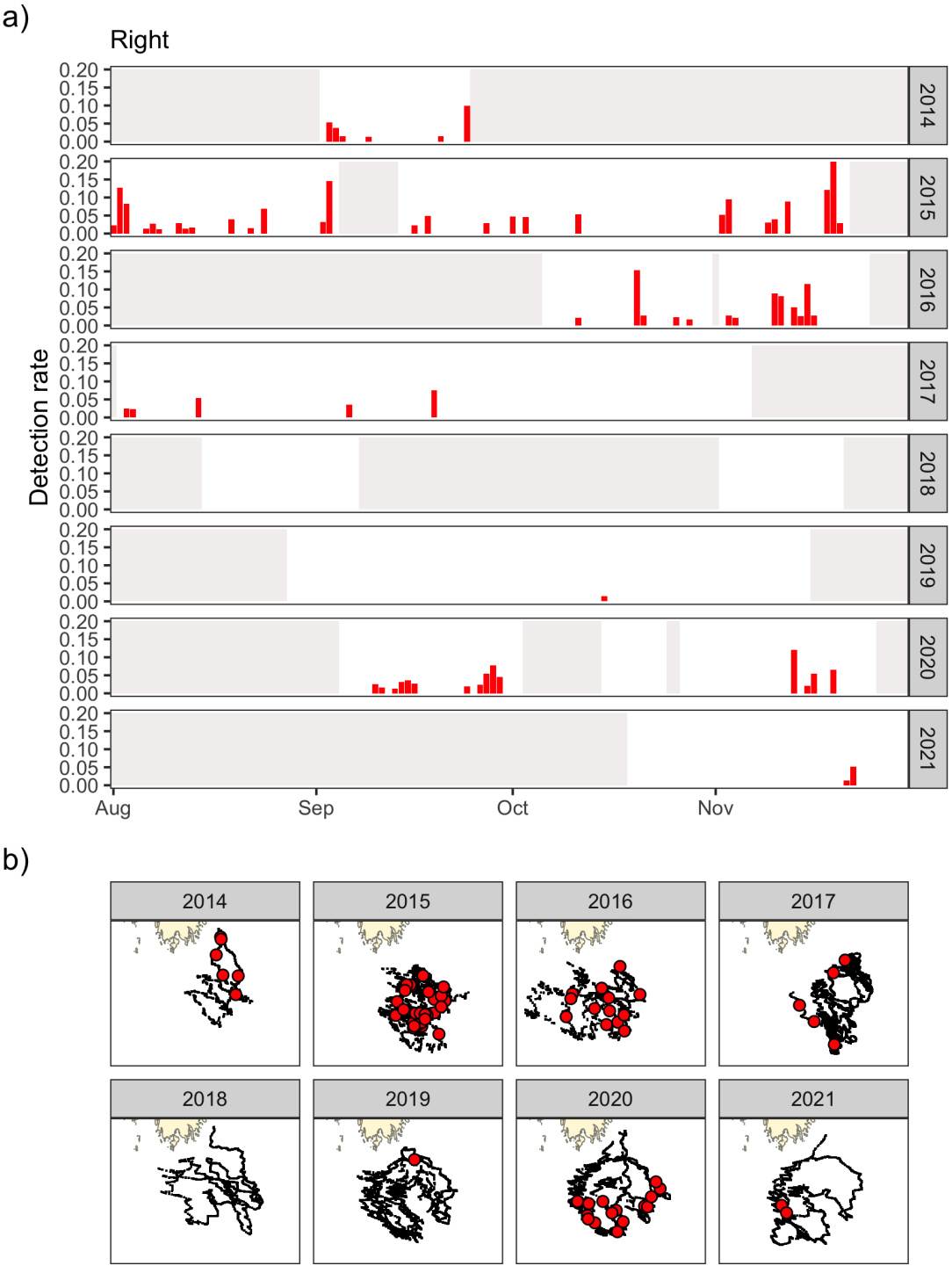

Figure D.3: Right whale detection rates in (a) time and (b) space over the full study during the Aug - Nov period in each year from 2014-2021. Panel (a) shows the daily detection rate (proportion of detected tally periods per day) over time. Light grey shading indicates times without survey effort. The bottom panel (b) shows the location of the glider during all detected tally periods (red circles) in each year. The black line shows the path of the glider.

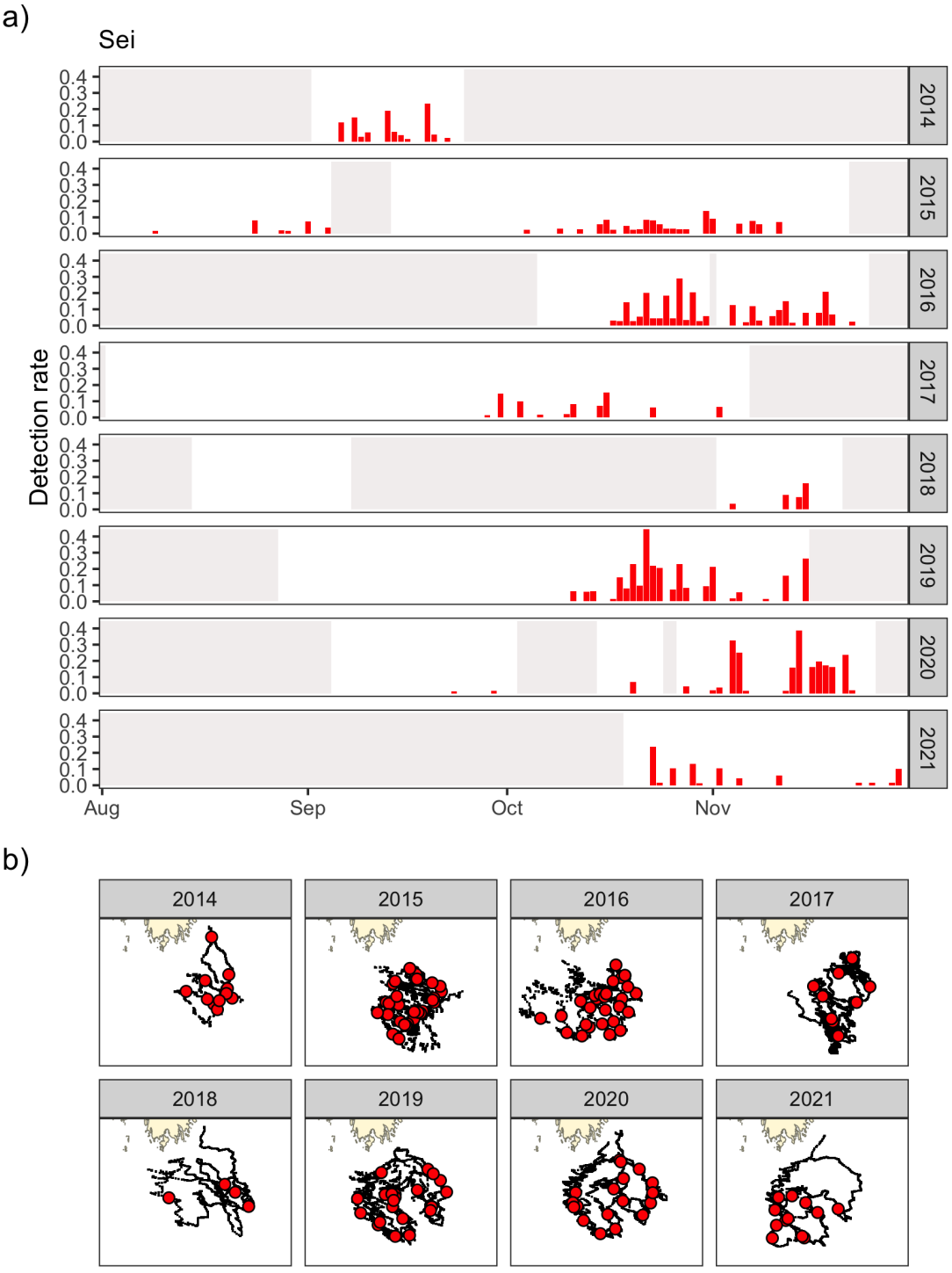

Figure D.4: Sei whale detection rates in (a) time and (b) space over the full study during the Aug - Nov period in each year from 2014-2021. Panel (a) shows the daily detection rate (proportion of detected tally periods per day) over time. Light grey shading indicates times without survey effort. The bottom panel (b) shows the location of the glider during all detected tally periods (red circles) in each year. The black line shows the path of the glider.

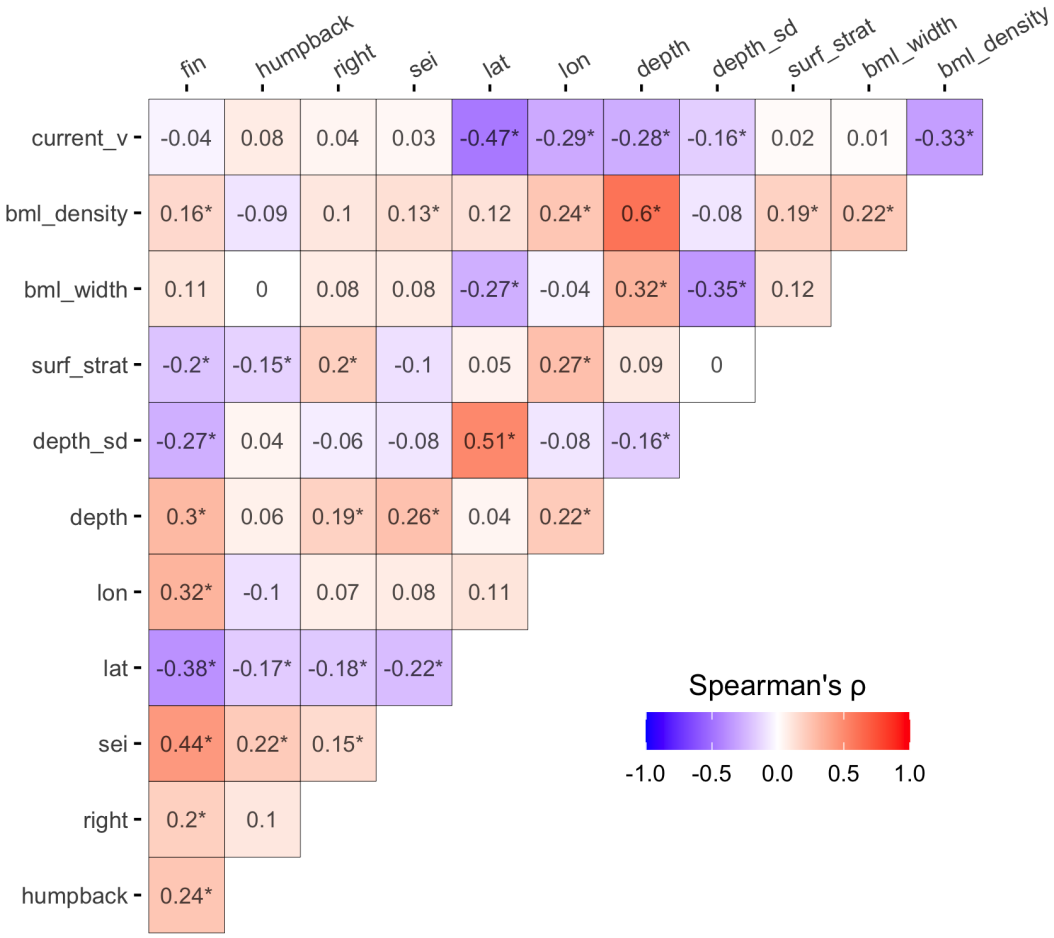

Figure D.5: Spearmans rank correlation of habitat variables, location (lat, lon), and the detection rate (number of detections / number of tally periods) of each species per grid cell. The * indicates significant correlations at a level of 0.05.

BIBLIOGRAPHY

Abadi, S. H., A. M. Thode, S. B. Blackwell, and D. R. Dowling, Ranging bowhead whale calls in a shallow-water dispersive waveguide., *The Journal of the Acoustical Society of America*, *136*, 130–130, 2014.

Amante, C., and B. W. Eakins, ETOPO1 arc-minute global relief model: procedures, data sources and analysis, 2009.

Aniceto, A. S., G. Pedersen, R. Primicerio, M. Biuw, U. Lindstrm, and L. Camus, Arctic Marine Data Collection Using Oceanic Gliders: Providing Ecological Context to Cetacean Vocalizations, *Frontiers in Marine Science*, *7*, 983, 2020.

Baumgartner, M. F., and D. M. Fratantoni, Diel periodicity in both sei whale vocalization rates and the vertical migration of their copepod prey observed from ocean gliders, *Limnology and Oceanography*, *53*, 2197–2209, 2008.

Baumgartner, M. F., and B. R. Mate, Summertime foraging ecology of North Atlantic right whales, *Marine Ecology Progress Series*, *264*, 123–135, 2003.

Baumgartner, M. F., and B. R. Mate, Summer and fall habitat of North Atlantic right whale (Eubaleana glacialis) Inferred From Satellite Telemetry, *Canadian Journal of Fisheries and Aquatic Sciences*, *62*, 527–543, 2005.

Baumgartner, M. F., and S. E. Mussoline, A generalized baleen whale call detection and classification system., *The Journal of the Acoustical Society of America*, *129*, 2889–2902, 2011.

Baumgartner, M. F., and A. M. Tarrant, The Physiology and Ecology of Diapause in Marine Copepods, *Annual Review of Marine Science*, *9*, 387–411, 2017.

Baumgartner, M. F., T. V. N. Cole, R. G. Campbell, G. J. Teegarden, and E. G. Durbin, Associations between North Atlantic right whales and their prey, Calanus finmarchicus, over diel and tidal time scales, *Marine Ecology Progress Series*, *264*, 155–166, 2003a.

Baumgartner, M. F., T. V. N. Cole, P. J. Clapham, and B. R. Mate, North Atlantic right whale habitat in the lower Bay of Fundy and on the SW Scotian Shelf during 1999-2001, *Marine Ecology Progress Series*, *264*, 137–154, 2003b.

Baumgartner, M. F., C. A. Mayo, and R. D. Kenney, Enormous Carnivores, Microscopic Food, and a Restaurant That's Hard to Find, in *The Urban Whale: North Atlantic Right Whales at the Crossroads*, pp. 138–171, Harvard University Press, Cambridge, MA, 2007.

Baumgartner, M. F., D. M. Fratantoni, T. P. Hurst, M. W. Brown, T. V. N. Cole, S. M. Van Parijs, and M. P. Johnson, Real-time reporting of baleen whale passive acoustic

detections from ocean gliders., *The Journal of the Acoustical Society of America*, *134*, 1814–23, 2013.

Baumgartner, M. F., K. M. Stafford, P. Winsor, and D. M. Fratantoni, Glider-Based Passive Acoustic Monitoring in the Arctic, *Marine Technology Society Journal*, *48*, 40–51, 2014.

Baumgartner, M. F., F. W. Wenzel, N. S. Lysiak, and M. R. Patrician, North Atlantic right whale foraging ecology and its role in human-caused mortality, *Marine Ecology Progress Series*, *581*, 165–181, 2017.

Baumgartner, M. F., J. Bonnell, P. J. Corkeron, S. M. Van Parijs, C. Hotchkin, B. A. Hodges, J. Bort Thornton, B. L. Mensi, and S. M. Bruner, Slocum Gliders Provide Accurate Near Real-Time Estimates of Baleen Whale Presence From Human-Reviewed Passive Acoustic Detection Information, *Frontiers in Marine Science*, *7*, 2020, publisher: Frontiers.

Baumgartner, M. F., J. Bonnell, S. M. V. Parijs, P. J. Corkeron, C. Hotchkin, K. Ball, L.-P. Pelletier, J. Partan, D. Peters, J. Kemp, J. Pietro, K. Newhall, A. Stokes, T. V. N. Cole, E. Quintana, and S. D. Kraus, Persistent near real-time passive acoustic monitoring for baleen whales from a moored buoy: System description and evaluation, *Methods in Ecology and Evolution*, *0*, 1–14, 2019.

Beardsley, R. C., A. W. Epstein, C. Chen, K. F. Wishner, M. C. Macaulay, and R. D. Kenney, Spatial variability in zooplankton abundance near feeding right whales in the Great South Channel, *Deep Sea Research Part II: Topical Studies in Oceanography*, *43*, 1601–1625, 1996.

Bioacoustics Research Program, and B. R. Program, Raven Pro: Interactive Sound Analysis Software, *Ithaca, NY: The Cornell Lab of Ornithology*, 2014.

Bonnel, J., A. M. Thode, S. B. Blackwell, K. Kim, A. Michael Macrander, and a. M. Macrander, Range estimation of bowhead whale (Balaena mysticetus) calls in the Arctic using a single hydrophone, *The Journal of the Acoustical Society of America*, *136*, 145–155, 2014.

Bort, J., S. M. V. Parijs, P. T. Stevick, E. Summers, and S. Todd, North Atlantic right whale Eubalaena glacialis vocalization patterns in the central Gulf of Maine from October 2009 through October 2010, *Endangered Species Research*, *26*, 271–280, 2015.

Brennan, C. E., F. Maps, W. C. Gentleman, S. Plourde, D. Lavoie, J. Chass, C. Lehoux, K. A. Krumhansl, and C. L. Johnson, How transport shapes copepod distributions in relation to whale feeding habitat: Demonstration of a new modelling framework, *Progress in Oceanography*, *171*, 1–21, 2019.

Brennan, C. E., F. Maps, W. C. Gentleman, D. Lavoie, J. Chass, S. Plourde, and C. L. Johnson, Ocean circulation changes drive shifts in Calanus abundance in North Atlantic right whale foraging habitat: A model comparison of cool and warm year scenarios, *Progress in Oceanography*, *197*, 102629, 2021.

Brown, M. W., S. D. Kraus, C. K. Slay, and L. P. Garrison, Surveying for discovery, science and management, in *The urban whale: North Atlantic right whale at the crossroads*, pp. 105–137, Harvard University Press, Cambridge, MA, 2007.

Brown, M. W., D. G. Fenton, R. K. Smedbol, C. Merrimen, K. Robichaud-Leblanc, and J. Conway, Recovery strategy for the North Atlantic right whale (Eubalaena glacialis) in Atlantic Canadian waters., *Tech. rep.*, Fisheries and Oceans Canada, Ottawa, ON, 2009.

Buckland, S. T., and B. J. Turnock, A Robust Line Transect Method, *Biometrics*, *48*, 901, 1992.

Buckland, S. T., D. R. Anderson, K. P. Burnham, J. L. Laake, D. L. Borchers, and L. Thomas, *Advanced distance sampling: estimating abundance of biological populations*, OUP Oxford, 2004.

Buckland, S. T., R. W. Summers, D. L. Borchers, and L. Thomas, Point transect sampling with traps or lures: Point transect sampling, *Journal of Applied Ecology*, *43*, 377–384, 2006.

Burnham, R. E., D. A. Duffus, and T. Ross, Remote sensing and mapping habitat features pertinent to fin whale life histories in coastal and offshore waters of Vancouver Island, British Columbia, *Journal of Experimental Marine Biology and Ecology*, *537*, 151511, 2021.

Cato, D. H., Simple methods of estimating source levels and locations of marine animal sounds., *The Journal of the Acoustical Society of America*, *104*, 1667–1678, 1998.

Cauchy, P., K. J. Heywood, D. Risch, N. D. Merchant, B. Y. Queste, and P. Testor, Sperm whale presence observed using passive acoustic monitoring from gliders of opportunity, *Endangered Species Research*, *42*, 133–149, 2020.

Chamberlain, S. A., and E. Szcs, taxize: taxonomic search and retrieval in R, *F1000Research*, *2*, 2013, publisher: Faculty of 1000 Ltd.

Chang, W., J. Cheng, J. J. Allaire, Y. Xie, and J. McPherson, *shiny: Web Application Framework for R*, 2020.

Clark, C. W., and W. T. Ellison, *Potential Use of Low-Frequency Sounds by Baleen Whales for Probing the Environment: Evidence from Models and Empirical Measurements*, Echolocation in bats and , 2004.

Clark, C. W., M. W. Brown, and P. J. Corkeron, Visual and acoustic surveys for North Atlantic right whales, Eubalaena glacialis, in Cape Cod Bay, Massachusetts, 2001-2005: Management implications, *Marine Mammal Science*, *26*, 837–854, 2010.

Collett, P. R., A few Notes on the Whale Balna glacialis and its Capture in Recent Years in the North Atlantic by Norwegian Whalers, *Proceedings of the Zoological Society of London*, *79*, 91–103, 1909,

_eprint: https://zslpublications.onlinelibrary.wiley.com/doi/pdf/10.1111/j.1096-3642.1909.tb01858.x.

Croll, D. A., C. W. Clark, A. Acevedo, B. R. Tershy, S. Flores, J. Gedamke, and J. Urban, Only male fin whales sing loud songs., *Nature*, *417*, 809–809, 2002.

Crowe, L. M., M. W. Brown, P. J. Corkeron, P. K. Hamilton, C. Ramp, S. Ratelle, A. S. M. Vanderlaan, and T. V. N. Cole, In plane sight: a mark-recapture analysis of North Atlantic right whales in the Gulf of St. Lawrence, *Endangered Species Research*, *46*, 227–251, 2021.

Cummings, W. C., and D. V. Holliday, Sounds and source levels from bowhead whales off Pt. Barrow, Alaska., *The Journal of the Acoustical Society of America*, *82*, 814–821, 1986.

Daoust, P., E. Couture, T. Wimmer, and L. Bourque, Incident Report: North Atlantic Right Whale Mortality Event in the Gulf of St. Lawrence, 2017, *Tech. rep.*, 2017.

Davies, K. T., and S. W. Brillant, Mass human-caused mortality spurs federal action to protect endangered North Atlantic right whales in Canada, *Marine Policy*, *104*, 157–162, 2019.

Davies, K. T. A., A. Ryan, and C. T. Taggart, Measured and inferred gross energy content in diapausing Calanus spp. in a Scotian shelf basin, *Journal of Plankton Research*, *34*, 614–625, 2012.

Davies, K. T. A., T. Ross, and C. T. Taggart, Tidal and subtidal currents affect deep aggregations of right whale prey, Calanus spp., along a shelf-basin margin, *Marine Ecology Progress Series*, 2013.

Davies, K. T. A., C. T. Taggart, and R. K. Smedbol, Water mass structure defines the diapausing copepod distribution in a right whale habitat on the Scotian Shelf, *Marine Ecology Progress Series*, 2014.

Davies, K. T. A., M. W. Brown, P. K. Hamilton, A. R. Knowlton, C. T. Taggart, and A. S. M. Vanderlaan, Variation in North Atlantic right whale Eubalaena glacialis occurrence in the Bay of Fundy, Canada, over three decades, *Endangered Species Research*, *39*, 159–171, 2019.

Davis, G. E., M. F. Baumgartner, J. M. Bonnell, J. Bell, C. L. Berchok, J. Bort Thornton, S. Brault, G. Buchanan, R. A. Charif, D. M. Cholewiak, C. W. Clark, P. J. Corkeron, J. Delarue, K. Dudzinski, L. T. Hatch, J. A. Hildebrand, L. Hodge, H. Klinck, S. D. Kraus, B. S. Martin, D. K. Mellinger, H. Moors-Murphy, S. Nieukirk, D. P. Nowacek, S. E. Parks, A. J. Read, A. N. Rice, D. Risch, A. irovi, M. Soldevilla, K. M. Stafford, J. E. Stanistreet, E. Summers, S. Todd, A. Warde, and S. M. Van Parijs, Long-term passive acoustic recordings track the changing distribution of North Atlantic right whales (Eubalaena glacialis) from 2004 to 2014, *Scientific Reports*, *7*, 13460–13460, 2017.

Davis, G. E., M. F. Baumgartner, P. J. Corkeron, J. Bell, C. Berchok, J. M. Bonnell, J. Bort Thornton, S. Brault, G. A. Buchanan, D. M. Cholewiak, C. W. Clark, J. Delarue, L. T. Hatch, H. Klinck, S. D. Kraus, B. Martin, D. K. Mellinger, H. Moors-Murphy, S. Nieukirk, D. P. Nowacek, S. E. Parks, D. Parry, N. Pegg, A. J. Read, A. N. Rice, D. Risch, A. Scott, M. S. Soldevilla, K. M. Stafford, J. E. Stanistreet, E. Summers, S. Todd, and S. M. Van Parijs, Exploring movement patterns and changing distributions of baleen whales in the western North Atlantic using a decade of passive acoustic data, *Global Change Biology*, *26*, 4812–4840, 2020, _eprint: https://onlinelibrary.wiley.com/doi/pdf/10.1111/gcb.15191.

Delarue, J., S. K. Todd, S. M. Van Parijs, and L. Di Iorio, Geographic variation in Northwest Atlantic fin whale (Balaenoptera physalus) song: Implications for stock structure assessment, *The Journal of the Acoustical Society of America*, *125*, 1774–1782, 2009, publisher: Acoustical Society of America.

Dever, M., D. Hebert, B. J. Greenan, J. Sheng, and P. C. Smith, Hydrography and Coastal Circulation along the Halifax Line and the Connections with the Gulf of St. Lawrence, *Atmosphere - Ocean*, *54*, 199–217, 2016.

DFO, North Atlantic right whale (Eubalaena glacialis) recovery strategy, 2010.

DFO, Fishery management measures for right whale protection, 2019.

Dinno, A., *dunn.test: Dunn's Test of Multiple Comparisons Using Rank Sums*, 2017.

Dunnington, D., *ggspatial: Spatial Data Framework for ggplot2*, 2021.

Durette-Morin, D., Measuring the Distribution of North Atlantic Right Whales (Eubalaena glacialis) Across Multiple Scales from their Vocalizations: Applications for Ecology and Management, 2021.

DuretteMorin, D., K. T. A. Davies, H. D. Johnson, M. W. Brown, H. MoorsMurphy, B. Martin, and C. T. Taggart, Passive acoustic monitoring predicts daily variation in North Atlantic right whale presence and relative abundance in Roseway Basin, Canada, *Marine Mammal Science*, *0*, 2019.

Durham, W. M., and R. Stocker, Thin Phytoplankton Layers: Characteristics, Mechanisms, and Consequences, *Annual Review of Marine Science*, *4*, 177–207, 2012, _eprint: https://doi.org/10.1146/annurev-marine-120710-100957.

DSpain, G. L., A. M. Thode, and W. A. Kuperman, Threedimensional localizations of vocalizing blue whales, *The Journal of the Acoustical Society of America*, *102*, 3212–3212, 1997, publisher: Acoustical Society of America.

Fleminger, A., and R. I. Clutter, Avoidance of Towed Nets by Zooplankton1, *Limnology and Oceanography*, *10*, 96–104, 1965, _eprint: https://aslopubs.onlinelibrary.wiley.com/doi/pdf/10.4319/lo.1965.10.1.0096.

Fortune, S. M. E., S. H. Ferguson, A. W. Trites, J. M. Hudson, and M. F. Baumgartner, Bowhead whales use two foraging strategies in response to fine-scale differences in zooplankton vertical distribution, *Scientific Reports*, *10*, 20249, 2020, number: 1 Publisher: Nature Publishing Group.

Fox, J., and S. Weisberg, *An R Companion to Applied Regression*, third ed., Sage, Thousand Oaks CA, 2019.

Fregosi, S., D. V. Harris, H. Matsumoto, D. K. Mellinger, C. Negretti, D. J. Moretti, S. W. Martin, B. Matsuyama, P. J. Dugan, and H. Klinck, Comparison of fin whale 20Hz call detections by deep-water mobile autonomous and stationary recorders, *The Journal of the Acoustical Society of America*, *147*, 961–977, 2020, publisher: Acoustical Society of America.

Frisk, G. V., *Ocean and seabed acoustics: a theory of wave propagation*, Pearson Education, 1994.

Fujiwara, M., and H. Caswell, Demography of the endangered North Atlantic right whale., *Nature*, *414*, 537–541, 2001.

Gavrilchuk, K., V. Lesage, S. Fortune, A. Trites, and S. Plourde, Foraging habitat of North Atlantic right whales has declined in the Gulf of St. Lawrence, Canada, and may be insufficient for successful reproduction, *Endangered Species Research*, *44*, 113–136, 2021.

Gervaise, C., Y. Simard, F. Aulanier, and N. Roy, Optimizing passive acoustic systems for marine mammal detection and localization: Application to real-time monitoring north Atlantic right whales in Gulf of St. Lawrence, *Applied Acoustics*, *178*, 107949, 2021.

Goldbogen, J., D. Cade, J. Calambokidis, A. Friedlaender, J. Potvin, P. Segre, and A. Werth, How Baleen Whales Feed: The Biomechanics of Engulfment and Filtration, *Annual Review of Marine Science*, *9*, 367–386, 2017, _eprint: https://doi.org/10.1146/annurev-marine-122414-033905.

Grolemund, G., and H. Wickham, Dates and Times Made Easy with lubridate, *Journal of Statistical Software*, *40*, 1–25, 2011.

Hamilton, P. K., and S. D. Kraus, Frequent encounters with the seafloor increase right whales risk of entanglement in fishing groundlines, *Endangered Species Research*, *39*, 235–246, 2019.

Hamilton, P. K., A. R. Knowlton, and M. K. Marx, Right whales tell their own stories: the photo-identification catalog., in *The Urban Whale: North Atlantic right whales at the crossroads.*, Harvard University Press, Cambridge, MA, 2007.

Hamner, W. M., G. S. Stone, and B. S. Obst, Behavior of southern right whales, Eubalaena australis, feeding on the Antarctic krill, Euphausia superba., *Fishery Bulletin*, *86*, 143–150, 1988.

Harris, D., L. Matias, L. Thomas, J. Harwood, and W. H. Geissler, Applying distance sampling to fin whale calls recorded by single seismic instruments in the northeast Atlantic., *The Journal of the Acoustical Society of America*, *134*, 3522–35, 2013.

Harris, D. V., J. L. Miksis-Olds, J. A. Vernon, and L. Thomas, Fin whale density and distribution estimation using acoustic bearings derived from sparse arrays, *The Journal of the Acoustical Society of America*, *143*, 2980–2993, 2018, publisher: Acoustical Society of America.

Hazen, E. L., A. S. Friedlaender, M. A. Thompson, C. R. Ware, M. T. Weinrich, P. N. Halpin, and D. N. Wiley, Fine-scale prey aggregations and foraging ecology of humpback whales Megaptera novaeangliae, *Marine Ecology Progress Series*, *395*, 75–89, 2009.

Helble, T. A., G. L. D'Spain, G. S. Campbell, and J. A. Hildebrand, Calibrating passive acoustic monitoring: correcting humpback whale call detections for site-specific and time-dependent environmental characteristics., *The Journal of the Acoustical Society of America*, *134*, EL400–6, 2013a.

Helble, T. A., G. L. D'Spain, J. A. Hildebrand, G. S. Campbell, R. L. Campbell, and K. D. Heaney, Site specific probability of passive acoustic detection of humpback whale calls from single fixed hydrophones., *The Journal of the Acoustical Society of America*, *134*, 2556–70, 2013b.

Horton, T., et al., World Register of Marine Species (WoRMS), 2021.

Hosmer, D. W., S. Lemeshow, and R. X. Sturdivant, *Applied logistic regression*, Wiley series in probability and statistics, 3. ed ed., Wiley, Hoboken, NJ, 2013.

Hjsgaard, S., U. Halekoh, and J. Yan, The R Package geepack for Generalized Estimating Equations, *Journal of Statistical Software*, *15*, 1–11, 2006.

Jensen, F. B., W. A. Kuperman, M. B. Porter, and H. Schmidt, *Computational Ocean Acoustics*, Springer New York, New York, NY, 2011.

Johnson, H., D. Morrison, and C. Taggart, WhaleMap: a tool to collate and display whale survey results in near real-time, *Journal of Open Source Software*, *6*, 3094, 2021.

Johnson, H. D., opcr: process and plot data from an optical plankton counter, 2021.

Johnson, H. D., M. F. Baumgartner, and C. T. Taggart, Estimating North Atlantic right whale (Eubalaena glacialis) location uncertainty following visual or acoustic detection to inform dynamic management, *Conservation Science and Practice*, *2*, e267, 2020a, _eprint: https://conbio.onlinelibrary.wiley.com/doi/pdf/10.1111/csp2.267.

Johnson, H. D., A. E. Newhall, Y.-T. Lin, and M. F. Baumgartner, Acoustic and oceanographic observations collected during the Nomans Island experiment in Spring 2017, *Technical Report*, Woods Hole Oceanographic Institution, 2020b, accepted: 2020-08-21T14:29:48Z.

Johnson, M., and T. Hurst, The DMON: an open-hardware/open-software passive acoustic detector, in *3rd International Workshop on the Detection and Classification of Marine Mammals using Passive Acoustics, Boston, Massachusetts, USA*, 2007.

Kelley, D., and C. Richards, *oce: Analysis of Oceanographic Data*, 2020.

Kenney, R. D., C. A. Mayo, and H. E. Winn, Migration and foraging strategies at varying spatial scales in western North Atlantic right whales : a review of hypotheses, *Journal of Cetacean Research and Management*, pp. 251–260, 2001.

Kirsebom, O. S., F. Frazao, Y. Simard, N. Roy, S. Matwin, and S. Giard, Performance of a deep neural network at detecting North Atlantic right whale upcalls, *The Journal of the Acoustical Society of America*, *147*, 2636–2646, 2020.

Klinck, H., D. K. Mellinger, K. Klinck, N. M. Bogue, J. C. Luby, W. A. Jump, G. B. Shilling, T. Litchendorf, A. S. Wood, G. S. Schorr, and R. W. Baird, Near-Real-Time Acoustic Monitoring of Beaked Whales and Other Cetaceans Using a Seaglider, *PLOS ONE*, *7*, e36128, 2012, publisher: Public Library of Science.

Knowlton, A. R., and S. D. Kraus, Mortality and serious injury of northern right whales (Eubalaena glacialis) in the western North Atlantic Ocean, *Journal of Cetacean Research and Management*, p. 16, 2001.

Koubrak, O., D. L. VanderZwaag, and B. Worm, Saving the North Atlantic right whale in a changing ocean: Gauging scientific and law and policy responses, *Ocean & Coastal Management*, *200*, 105109, 2021.

Kowarski, K., C. Evers, H. Moors-Murphy, B. Martin, and S. L. Denes, Singing through winter nights: Seasonal and diel occurrence of humpback whale (Megaptera novaeangliae) calls in and around the Gully MPA, offshore eastern Canada, *Marine Mammal Science*, *34*, 169–189, 2018, _eprint: https://onlinelibrary.wiley.com/doi/pdf/10.1111/mms.12447.

Kowarski, K., S. Cerchio, H. Whitehead, and H. Moors-Murphy, Where, when, and why do western North Atlantic humpback whales begin to sing?, *Bioacoustics*, pp. 1–20, 2021, publisher: Taylor & Francis.

Kowarski, K. A., B. J. Gaudet, A. J. Cole, E. E. Maxner, S. P. Turner, S. B. Martin, H. D. Johnson, and J. E. Moloney, Near real-time marine mammal monitoring from gliders: Practical challenges, system development, and management implications, *J. Acoust. Soc. Am.*, p. 16, 2020.

Kraus, S. D., RATES AND POTENTIAL CAUSES OF MORTALITY IN NORTH ATLANTIC RIGHT WHALES (EUBALAENA GLACIALIS), *Marine Mammal Science*, *6*, 278–291, 1990.

Kraus, S. D., M. W. Brown, H. Caswell, C. W. Clark, M. Fujiwara, P. K. Hamilton, R. D. Kenney, A. R. Knowlton, S. Landry, C. A. Mayo, W. A. Mclellan, M. J. Moore, D. P.

Nowacek, D. A. Pabst, A. J. Read, and R. M. Rolland, North Atlanstic Right Whales in Crisis, *Science*, 2005.

Kusel, E. T., T. Munoz, M. Siderius, D. K. Mellinger, and S. L. Heimlich, Marine mammal tracks from two-hydrophone acoustic recordings made with a glider, *Ocean Science*, *13*, 273–288, 2017.

Kyhn, L. A., J. Tougaard, L. Thomas, L. R. Duve, J. Stenback, M. Amundin, G. Desportes, and J. Teilmann, From echolocation clicks to animal densityAcoustic sampling of harbor porpoises with static dataloggers, *The Journal of the Acoustical Society of America*, *131*, 550–560, 2012.

Ksel, E. T., D. K. Mellinger, L. Thomas, T. A. Marques, D. J. Moretti, and J. Ward, Cetacean population density estimation from single fixed sensors using passive acoustics, *J Acoust Soc Am*, *129*, 3610–3622, 2011.

Laurinolli, M. H., A. E. Hay, F. Desharnais, and C. T. Taggart, Localization of North Atlantic Right Whale Sounds in the Bay of Fundy Using a Sonobuoy Array, *Marine Mammal Science*, *19*, 708–723, 2003, _eprint: https://onlinelibrary.wiley.com/doi/pdf/10.1111/j.1748-7692.2003.tb01126.x.

Lin, Y.-T., A. E. Newhall, and J. F. Lynch, Low-frequency broadband sound source localization using an adaptive normal mode back-propagation approach in a shallow-water ocean, *The Journal of the Acoustical Society of America*, *131*, 1798–1798, 2012.

Marques, T. a., L. Thomas, J. Ward, N. DiMarzio, and P. L. Tyack, Estimating cetacean population density using fixed passive acoustic sensors: an example with Blainville's beaked whales., *The Journal of the Acoustical Society of America*, *125*, 1982–1994, 2009.

Marques, T. a., L. M. Munger, L. Thomas, S. M. Wiggins, and J. A. Hildebrand, Estimating north pacific right whale Eubalaena japonica density using passive acoustic cue counting, *Endangered Species Research*, *13*, 163–172, 2011.

Marques, T. a., L. Thomas, S. W. Martin, D. K. Mellinger, J. Ward, D. J. Moretti, D. Harris, and P. L. Tyack, Estimating animal population density using passive acoustics, *Biological Reviews*, *88*, 287–309, 2013.

Mayo, C. A., and M. K. Marx, Surface foraging behaviour of the North Atlantic right whale, Eubalaena glacialis, and associated zooplankton characteristics, *Canadian Journal of Zoology*, *68*, 2214–2220, 1989.

Mayo, C. A., B. H. Letcher, and S. Scott, Zooplankton filtering efficiency of the baleen of a North Atlantic right whale, Eubalaena glacialis, *J. Cetacean Res. Manage.*, pp. 225–229, 2001.

Mayo, C. A., L. Ganley, C. A. Hudak, S. Brault, M. K. Marx, E. Burke, and M. W. Brown, Distribution, demography, and behavior of North Atlantic right whales (Eubalaena

glacialis) in Cape Cod Bay, Massachusetts, 19982013, *Marine Mammal Science*, *34*, 979–996, 2018, _eprint: https://onlinelibrary.wiley.com/doi/pdf/10.1111/mms.12511.

McQuinn, I. H., S. Plourde, J.-F. St. Pierre, and M. Dion, Spatial and temporal variations in the abundance, distribution, and aggregation of krill (Thysanoessa raschii and Meganyctiphanes norvegica) in the lower estuary and Gulf of St. Lawrence, *Progress in Oceanography*, *131*, 159–176, 2015.

Mellinger, D. K., S. L. Nieukirk, H. Matsumoto, S. L. Heimlich, R. P. Dziak, J. Haxel, M. Fowler, C. Meinig, and H. V. Miller, Seasonal occurrence of North Atlantic right whale (Eubalaena glacialis) vocalizations at two sites on the Scotian Shelf, *Marine Mammal Science*, *23*, 856–867, 2007.

Merchant, N. D., K. M. Fristrup, M. P. Johnson, P. L. Tyack, M. J. Witt, P. Blondel, and S. E. Parks, Measuring acoustic habitats, *Methods in Ecology and Evolution*, *6*, 257–265, 2015.

Meyer-Gutbrod, E. L., C. H. Greene, K. T. Davies, and D. G. Johns, OCEAN REGIME SHIFT IS DRIVING COLLAPSE OF THE NORTH ATLANTIC RIGHT WHALE POPULATION, *Oceanography*, *34*, 22–31, 2021, publisher: Oceanography Society.

Michaud, J., and C. T. Taggart, Spatial variation in right whale food, Calanus finmarchicus, in the Bay of Fundy, *Endangered Species Research*, 2011.

Mitchell, M. R., G. Harrison, K. Pauley, A. Gagn, G. Maillet, and P. Strain, *Atlantic zonal monitoring program sampling protocol*, Citeseer, 2002.

Monsarrat, S., M. G. Pennino, T. D. Smith, R. R. Reeves, and C. Umr, Historical summer distribution of the endangered North Atlantic right whale (Eubalaena glacialis): a hypothesis based on environmental preferences of a congeneric species, *Biodiversity Research*, pp. 1–13, 2015.

Moore, M. J., T. K. Rowles, D. A. Fauquier, J. D. Baker, I. Biedron, J. W. Durban, P. K. Hamilton, A. G. Henry, A. R. Knowlton, W. A. McLellan, C. A. Miller, R. M. P. Iii, H. M. Pettis, S. Raverty, R. M. Rolland, R. S. Schick, S. M. Sharp, C. R. Smith, L. Thomas, J. M. v. d. Hoop, and M. H. Ziccardi, REVIEW Assessing North Atlantic right whale health: threats, and development of tools critical for conservation of the species, *Diseases of Aquatic Organisms*, *143*, 205–226, 2021.

Moore, S. E., B. M. Howe, K. M. Stafford, and M. L. Boyd, Including Whale Call Detection in Standard Ocean Measurements: Application of Acoustic Seagliders, *Marine Technology Society Journal*, *41*, 53–57, 2007.

Morano, J. L., A. N. Rice, J. T. Tielens, B. J. Estabrook, A. Murray, B. L. Roberts, and C. W. Clark, Acoustically Detected Year-Round Presence of Right Whales in an Urbanized Migration Corridor, *Conservation Biology*, *26*, 698–707, 2012.

Morley, M. G., S. E. Dosso, and N. R. Chapman, Array element localization using ship noise, *The Journal of the Acoustical Society of America*, *125*, 1403–1409, 2009.

Munger, L. M., S. M. Wiggins, and J. A. Hildebrand, North Pacific right whale up-call source levels and propagation distance on the southeastern Bering Sea shelf, *The Journal of the Acoustical Society of America*, *129*, 4047, 2011.

Murison, L. D., and D. E. Gaskin, The distribution of right whales and Zooplankton in the Bay of Fundy, Canada, *Canadian Journal of Zoology*, *67*, 1411–1420, 1989.

Mussoline, S. E., D. Risch, L. T. Hatch, M. T. Weinrich, D. N. Wiley, M. a. Thompson, P. J. Corkeron, and S. M. Van Parijs, Seasonal and diel variation in North Atlantic right whale up-calls: Implications for management and conservation in the northwestern Atlantic ocean, *Endangered Species Research*, *17*, 17–26, 2012.

Newhall, A. E., Y.-T. Lin, J. F. Lynch, M. F. Baumgartner, and G. G. Gawarkiewicz, Long distance passive localization of vocalizing sei whales using an acoustic normal mode approach, *The Journal of the Acoustical Society of America*, *131*, 1814–1814, 2012.

NOAA, Reducing Vessel Strikes to North Atlantic Right Whales, 2019, archive Location: New England/Mid-Atlantic, Southeast.

NOAA, 20172021 North Atlantic Right Whale Unusual Mortality Event, 2021.

Nuuttila, H. K., K. Brundiers, M. Dhne, J. C. Koblitz, L. Thomas, W. CourteneJones, P. G. H. Evans, J. R. Turner, J. D. Bennell, and J. G. Hiddink, Estimating effective detection area of static passive acoustic data loggers from playback experiments with cetacean vocalisations, *Methods in Ecology and Evolution*, *9*, 2362–2371, 2018, _eprint: https://besjournals.onlinelibrary.wiley.com/doi/pdf/10.1111/2041-210X.13097.

Palacios, D. M., M. F. Baumgartner, K. L. Laidre, and E. J. Gregr, Beyond correlation: integrating environmentally and behaviourally mediated processes in models of marine mammal distributions, *Endangered Species Research*, *22*, 191–203, 2013.

Parks, S. E., and P. L. Tyack, Sound production by North Atlantic right whales (Eubalaena glacialis) in surface active groups., *The Journal of the Acoustical Society of America*, *117*, 3297–3306, 2005.

Parks, S. E., I. R. Urazghildiiev, and C. W. Clark, Variability in ambient noise levels and call parameters of North Atlantic right whales in three habitat areas., *The Journal of the Acoustical Society of America*, *125*, 1230–1239, 2009.

Parks, S. E., M. P. Johnson, D. P. Nowacek, and P. L. Tyack, Individual right whales call louder in increased environmental noise., *Biology letters*, *7*, 33–35, 2011a.

Parks, S. E., A. Searby, A. Clrier, M. P. Johnson, D. P. Nowacek, and P. L. Tyack, Sound production behavior of individual North Atlantic right whales: implications for passive acoustic monitoring, *Endangered Species Research*, *15*, 63–76, 2011b.

Payne, R., and E. Dorsey, Sexual dimorphism and aggressive use of callosities in right whales (Eubalaena australis), *Communication and behavior of whales*, pp. 295–329, 1983, publisher: Westview Press.

Payne, R. S., and D. Webb, Orientation by means of long range acoustic signaling in baleen whales, *Ann. N.Y. Acad. Sci.*, *188*, 110–141, 1971.

Pebesma, E., Simple Features for R: Standardized Support for Spatial Vector Data, *The R Journal*, *10*, 439–446, 2018.

Pedersen, T. L., *patchwork: The Composer of Plots*, 2020.

Pendleton, D. E., A. J. Pershing, M. W. Brown, C. A. Mayo, R. D. Kenney, N. R. Record, and T. V. N. Cole, Regional-scale mean copepod concentration indicates relative abundance of North Atlantic right whales, *Marine Ecology Progress Series*, *378*, 211–225, 2009.

Pettis, H. M., R. M. Pace, and P. K. Hamilton, North Atlantic Right Whale Consortium 2020 Annual Report Card, *North Atlantic Right Whale Consortium*, 2021.

Pirotta, V., A. Grech, I. D. Jonsen, W. F. Laurance, and R. G. Harcourt, Consequences of global shipping traffic for marine giants, *Frontiers in Ecology and the Environment*, *17*, 39–47, 2019, _eprint: https://onlinelibrary.wiley.com/doi/pdf/10.1002/fee.1987.

Plourde, S., C. Lehoux, C. L. Johnson, G. Perrin, and V. Lesage, North Atlantic right whale (Eubalaena glacialis) and its food: (I) a spatial climatology of Calanus biomass and potential foraging habitats in Canadian waters, *Journal of Plankton Research*, *41*, 667–685, 2019.

Porter, M. B., The KRAKEN Normal Mode Program, *Naval Research Laboratory*, pp. 1–198, 1992.

Prieto, R., D. Janiger, M. a. Silva, G. T. Waring, and J. M. Gonalves, The forgotten whale: A bibliometric analysis and literature review of the North Atlantic sei whale Balaenoptera borealis, *Mammal Review*, *42*, 235–272, 2012.

R Core Team, *R: A Language and Environment for Statistical Computing*, R Foundation for Statistical Computing, Vienna, Austria, 2019.

R Core Team, *R: A Language and Environment for Statistical Computing*, R Foundation for Statistical Computing, Vienna, Austria, 2020.

Record, N., J. Runge, D. Pendleton, W. Balch, K. Davies, A. Pershing, C. Johnson, K. Stamieszkin, R. Ji, Z. Feng, S. Kraus, R. Kenney, C. Hudak, C. Mayo, C. Chen, J. Salisbury, and C. Thompson, Rapid Climate-Driven Circulation Changes Threaten Conservation of Endangered North Atlantic Right Whales, *Oceanography*, *32*, 2019.

Redfern, J. V., M. C. Ferguson, E. A. Becker, K. D. Hyrenbach, C. P. Good, J. P. Barlow, K. Kaschner, M. F. Baumgartner, K. A. Forney, L. T. Ballance, P. Fauchald, P. N. Halpin, T. Hamazaki, A. J. Pershing, S. S. Qian, A. Read, S. Reilly, L. Torres, and F. Werner, Techniques for cetacean - habitat modeling, *Marine Ecology Progress Series*, *310*, 271–295, 2006.

Rolland, R. M., S. E. Parks, K. E. Hunt, M. Castellote, P. J. Corkeron, D. P. Nowacek, S. K. Wasser, and S. D. Kraus, Evidence that ship noise increases stress in right whales, *Proceedings of the Royal Society B: Biological Sciences*, *279*, 2363–2368, 2012.

Romagosa, M., S. Prez-Jorge, I. Casco, H. Mourio, P. Lehodey, A. Pereira, T. A. Marques, L. Matias, and M. A. Silva, Food talk: 40-Hz fin whale calls are associated with prey biomass, *Proceedings of the Royal Society B: Biological Sciences*, *288*, 20211156, 2021, publisher: Royal Society.

Ruckdeschel, G. S., K. T. A. Davies, and T. Ross, Biophysical Drivers of Zooplankton Variability on the Scotian Shelf Observed Using Profiling Electric Gliders, *Frontiers in Marine Science*, *7*, 627, 2020.

RWSAS, NOAA Right Whale Sighting Advisery System, 2019.

Sheng, J., Dynamics of a buoyancy-driven coastal jet: The Gasp Current, *Journal of Physical Oceanography*, *31*, 3146–3162, 2001.

Simard, Y., N. Roy, S. Giard, and F. Aulanier, North Atlantic right whale shift to the Gulf of St. Lawrence in 2015, revealed by long-term passive acoustics, *Endangered Species Research*, *40*, 271–284, 2019.

Sorochan, K. A., S. Plourde, R. Morse, P. Pepin, J. Runge, C. Thompson, and C. L. Johnson, North Atlantic right whale (Eubalaena glacialis) and its food: (II) interannual variations in biomass of Calanus spp. on western North Atlantic shelves, *Journal of Plankton Research*, *41*, 687–708, 2019, publisher: Oxford Academic.

Spaulding, E., M. Robbins, T. Calupca, C. W. Clark, T. Tremblay, A. Waack, A. Warde, J. Kemp, and K. Newhall, An autonomous, near-real-time buoy system for automatic detection of North Atlantic right whale calls., *The Journal of the Acoustical Society of America*, *125*, 2615–2615, 2009.

Stafford, K. M., D. K. Mellinger, S. E. Moore, and C. G. Fox, Seasonal variability and detection range modeling of baleen whale calls in the Gulf of Alaska, 1999-2002., *The Journal of the Acoustical Society of America*, *122*, 3378–3390, 2007.

Suthers, I. M., C. T. Taggart, D. Rissik, and M. E. Baird, Day and night ichthyoplankton assemblages and zooplankton biomass size spectrum in a deep ocean island wake, *Marine Ecology Progress Series*, *322*, 225–238, 2006.

TC, Protecting North Atlantic right whales from collisions with ships in the Gulf of St. Lawrence, 2019.

Tennessen, J., and S. E. Parks, Acoustic propagation modeling indicates vocal compensation in noise improves communication range for North Atlantic right whales, *Endangered Species Research*, *30*, 225–237, 2016.

Thode, A., J. Bonnel, M. Thieury, A. Fagan, C. Verlinden, D. Wright, C. Berchok, and J. Crance, Using nonlinear time warping to estimate North Pacific right whale calling depths in the Bering Sea, *The Journal of the Acoustical Society of America*, *141*, 3059–3069, 2017, publisher: Acoustical Society of America.

Thode, A. M., G. L. D'Spain, and W. a. Kuperman, Matched-field processing, geoacoustic inversion, and source signature recovery of blue whale vocalizations., *The Journal of the Acoustical Society of America*, *107*, 1286–1300, 2000.

Thode, A. M., P. Gerstoft, W. C. Burgess, K. G. Sabra, M. Guerra, M. D. Stokes, M. Noad, and D. H. Cato, A Portable Matched-Field Processing System Using Passive Acoustic Time Synchronization, *IEEE Journal of Oceanic Engineering*, *31*, 696–710, 2006, conference Name: IEEE Journal of Oceanic Engineering.

Thode, A. M., K. H. Kim, S. B. Blackwell, C. R. Greene, C. S. Nations, T. L. McDonald, and A. M. Macrander, Automated detection and localization of bowhead whale sounds in the presence of seismic airgun surveys, *The Journal of the Acoustical Society of America*, *131*, 3726–3747, 2012, publisher: Acoustical Society of America.

Thode, A. M., S. B. Blackwell, A. S. Conrad, K. H. Kim, T. Marques, L. Thomas, C. S. Oedekoven, D. Harris, and K. Brker, Roaring and repetition: How bowhead whales adjust their call density and source level (Lombard effect) in the presence of natural and seismic airgun survey noise, *The Journal of the Acoustical Society of America*, *147*, 2061–2080, 2020, publisher: Acoustical Society of America.

Tremblay, C. J., S. M. V. Parijs, and D. Cholewiak, 50 to 30-Hz triplet and singlet down sweep vocalizations produced by sei whales (Balaenoptera borealis) in the western North Atlantic Ocean, *The Journal of the Acoustical Society of America*, *145*, 3351, 2019.

van der Hoop, J. M., A. S. Vanderlaan, and C. T. Taggart, Absolute probability estimates of lethal vessel-strikes to North Atlantic right whales in Roseway Basin, Scotian Shelf, *Ecological Applications*, *22*, 2021–2033, 2012.

van der Hoop, J. M., A. E. NousekMcGregor, D. P. Nowacek, S. E. Parks, P. Tyack, and P. T. Madsen, Foraging rates of ram-filtering North Atlantic right whales, *Functional Ecology*, *33*, 1290–1306, 2019, _eprint: https://besjournals.onlinelibrary.wiley.com/doi/pdf/10.1111/1365-2435.13357.

Vanderlaan, A. S., and C. T. Taggart, Vessel collisions with whales: The probability of lethal injury based on vessel speed, *Marine Mammal Science*, *23*, 144–156, 2007.

Vanderlaan, A. S., and C. T. Taggart, Efficacy of a Voluntary Area to Be Avoided to Reduce Risk of Lethal Vessel Strikes to Endangered Whales, *Conservation Biology*, *23*, 1467–1474, 2009.

Vanderlaan, A. S., C. T. Taggart, A. R. Serdynska, R. D. Kenney, and M. W. Brown, Reducing the risk of lethal encounters: Vessels and right whales in the Bay of fundy and on the Scotian shelf, *Endangered Species Research*, *4*, 283–297, 2008.

Vanderlaan, A. S., R. K. Smedbol, and C. T. Taggart, Fishing-gear threat to right whales (Eubalaena glacialis) in Canadian waters and the risk of lethal entanglement, *Canadian Journal of Fisheries and Aquatic Sciences*, *68*, 2174–2193, 2011.

Verfuss, U. K., A. S. Aniceto, D. V. Harris, D. Gillespie, S. Fielding, G. Jimnez, P. Johnston, R. R. Sinclair, A. Sivertsen, S. A. Solb, R. Storvold, M. Biuw, and R. Wyatt, A review of unmanned vehicles for the detection and monitoring of marine fauna, *Marine Pollution Bulletin*, *140*, 17–29, 2019.

Wickham, H., *ggplot2: Elegant Graphics for Data Analysis*, Springer-Verlag New York, 2016.

Wickham, H., M. Averick, J. Bryan, W. Chang, L. D. McGowan, R. Franois, G. Grolemund, A. Hayes, L. Henry, J. Hester, M. Kuhn, T. L. Pedersen, E. Miller, S. M. Bache, K. Mller, J. Ooms, D. Robinson, D. P. Seidel, V. Spinu, K. Takahashi, D. Vaughan, C. Wilke, K. Woo, and H. Yutani, Welcome to the tidyverse, *Journal of Open Source Software*, *4*, 1686, 2019.

Wiggins, S. M., M. A. McDonald, L. M. Munger, S. E. Moore, and J. A. Hildebrand, Waveguide propagation allows range estimates for north pacific right whales in the bering sea, *Canadian Acoustics*, *32*, 146–154, 2004.

Woodley, T. H., and D. E. Gaskin, Environmental characteristics of North Atlantic right and fin whale habitat in the lower Bay of Fundy, Canada, *Canadian Journal of Zoology*, *74*, 75–84, 1996.